Title

The Design, Synthesis, and Characterization of Crystalline Molecular Machines with High Structural and Dynamic Complexities

Author

Jiang, Xing

Publication Date

2016

Peer reviewed|Thesis/dissertation

UNIVERSITY OF CALIFORNIA

Los Angeles

The Design, Synthesis, and Characterization of Crystalline Molecular Machines with High Structural and Dynamic Complexities

A dissertation submitted in partial satisfaction of the

requirements for the degree Doctor of Philosophy

in Chemistry

by

Xing Jiang

2016

ABSTRACT OF THE DISSERTATION

The Design, Synthesis, and Characterization of Crystalline Molecular Machines with High Structural and Dynamic Complexities

By

Xing Jiang

Doctor of Philosophy in Chemistry

University of California, Los Angeles, 2016

Professor Miguel A. Garcia-Garibay, Chair

Molecular machines are molecular and supramolecular entities capable of producing quasi-mechanical movements. While many examples of functional artificial molecular machines have been studied in solution, crystalline aggregates of molecular machines have been explored infrequently because of the limited freedom of motion in closely packed solids. Although previous work on amphidynamic crystals has demonstrated that rotational dynamics in crystals could be achieved and engineered by proper structural design, the existing examples are limited to simple structures and small dynamic groups. As part of the efforts to prepare artificial molecular machines capable of performing useful work, the goals of my doctoral research were to design and synthesize

crystalline molecular rotors with complex structures and explore their dynamics with solid-state NMR spectroscopy.

I have prepared two shape-persistent dendritic molecular rotors with molecular weight over 2000 Da by different synthetic strategies. The molecular rotor prepared by a convergent synthesis provided crystals with a low packing density, which allowed megahertz rotation of all aromatic groups in the rotor. The softening of local environments with temperature, resulting from the dynamics of virtually all components in the crystal, led to a new concept of crystal fluidity. The divergent strategy used in the synthesis of the other macromolecular rotor made it possible to incorporate large rotator groups in the structure. When a bulky triptycene group was used, the shape-persistent rotor was able to support its kilohertz rotation in a semicrystalline sample.

In order to realize faster triptycene rotations and to understand the structural elements required for effective solid-state gearing motions, I designed and prepared three pillared paddlewheel MOFs. I demonstrated that megahertz rotation of triptycene could be realized in a catenation-free framework, which offered a loose environment for the rotator. Since the rotator is in close contact only with the solvent molecules, its rotation is dictated solely by the hydrodynamic behavior of DMF and constitutes a diffusion-controlled process. As a result, the temperature dependence of observed rotation could shed light on the effective viscosity change of trapped solvents with temperature.

The dissertation of Xing Jiang is approved.

Selim M. Senkan

Kendall N. Houk

Miguel A. Garcia-Garibay, Committee Chair

University of California, Los Angeles

2016

To Sydney

TABLE OF CONTENTS

LIST OF FIGURES

LIST OF SCHEMES

LIST OF TABLES

LIST OF ABBREVIATIONS

A	pre-exponential factor
ADP	Adenosine diphosphate
APCI	atmospheric pressure chemical ionization
ATP	Adenosine triphosphate
BCO	bicyclo[2.2.2]octane
CD	cyclodextrin
CPMAS	cross-polarisation magic angle spinning
d	doublet (NMR)
d_n	deuterium labeled compound with n deuterons
DABCO	1,4-diazabicyclo[2.2.2]octane
DB	dibenzo
DCM	dichloromethane
DMAP	4-dimethylaminopyridine
DMF	*N*,*N*-dimethylformamide
dmit	2-thioxo-1,3-dithiole-4,5-dithiolate
DSC	differential scanning calorimetry
E_a	activation energy
e.r.	enantiomeric ratio
ESI	electrospray ionisation
GAFF	general Amber force field
GS	ground state
HATR	horizontal attenuated total reflectance

Hz	hertz
I	moment of inertia
IR	infrared
J	coupling constant
k_{rot}	rate of rotation
kcal	kilocalories
LIFDI	liquid injection field desorption/ionization
m	multiplet
MALDI	matrix-assisted laser desorption/ionization
MC	merocyanine
MD	molecular dynamics
MIM	mechanically interlocked molecule
mmol	millimole
MOF	metal-organic framework
m.p.	melting point
MS	mass spectrometry
m-FAni$^+$	*meta*-fluoroanilinium
m/z	mass to charge ratio
NMR	nuclear magnetic resonance
PMF	potentials of mean force
PMO	periodic mesoporous organosilicate
ppm	parts per million
PULSA	photoactuated unimolecular logical switching-attained reconstruction

PXRD	powder X-ray diffraction
R_f	retardation factor
s	singlet
SEM	scanning electron microscope
SP	spiropyran
SS	solid-state
t	triplet
T_1	spin-lattice relaxation time
TBAF	tetrabutylammonium fluoride
TGA	thermal gravity analysis
THF	tetrahydrofuran
TLC	thin-layer chromatography
TOF	time of flight
trityl	triphenylmethyl
TRPV	vanilloid transient receptor potential cation channel
TS	transition state
UV	ultraviolet
Vis	visible
VT	variable temperature
WHAM	weighted histogram analysis method

ACKNOWLEDGEMENT

Graduate school at UCLA is one of the best choices I have made in my life and I would like to thank all the professors, staff scientists, postdoctoral scholars, graduate and undergraduate students, for making this experience so special. I would like to first thank my supervisor Prof. Miguel Garcia-Garibay, who is an artist in both his professional and personal life. It is remarkable how good he is at being a scientist, a professor, a mentor, an editor, and a friend. He is and will continue to be my role model. Secondly I would like to thank Prof. Ken Houk for so many discussions on research and career. I am lucky to be connected in many aspects with him and the Houk research family. I also want to thank Prof. Selim Senkan and Prof. Jeffery Zink for serving on my oral exam/thesis committee.

I am also grateful for the world-class staff scientists at UCLA and their efforts to keep all the instruments running smoothly. Dr. Jane Strouse is the director of the MIC and she is in charge of virtually every single instrument. Dr. Saeed Khan is capable of solving very complex crystal structures and he has great patience refining highly disordered structures. He has obtained almost twenty new structures for me, many of them are essential for the publication of my research. Dr. Bob Taylor is an NMR specialist and is very supportive with solid-state NMR measurements despite my ignorance and unintentional mistakes.

I have made friends with many postdoctoral scholars and graduate students during my years at UCLA. They have cheered me up during the toughest times and shared my

joyful moments. These include Dr. Yong Liang, Dr. Xin Hong, Dr. Yichao Fan, Dr. Ira Staehle, Dr. Pat Commins, (Dr.) Eriko Shimada, Dr. Braulio Rodríguez-Molina, Dr. Salvador Pérez-Estrada, Dr. Lufeng Zou, Dr. Gonzalo Jiménez-Osés, (Dr.) Geeta Vadehra, (Dr.) Daniel Sun, Tim Chung, Vanessa Breslin, Jin Park, Cyndi He, Song Yang, and Morgan Howe. I would also cherish the teaching experience of mentoring two talented undergraduate students Narega Nazarian and Bing Zhang.

I would like to take this chance to thank my family members (Sujian Jiang, Qinjuan Bian, Fang Liu, Xiangyi Jiang, Xingkun Jin, Yun Jia, and Shunqiang Luo) and friends outside UCLA (Jianbo Sun, Jianlong Huo, Chenming Hong, Bo Shen, Yixin Gu, Xiangyun Shi, Shu Chen, Ruoduo Liu, and Xiuming Gu) for their unconditional support. I want to give my belated regards to my grandparents, Zhengquan Jiang and Pinhua Pan, who always had faith in me and would be thrilled if they could witness my graduation with a doctoral degree.

Finally, I am grateful for generous financial support I received to explore new possibilities in chemistry. I would like to thank the recruiting committee for offering this opportunity to join the wonderful graduate program at UCLA. The chemistry department and National Science Foundation (DMR awards granted to M.G.G.) provided research funds to synthesize and characterize new materials and travel funds to attend inspiring research meetings. I am also grateful to be selected as a recipient of 2015 UCLA Dissertation Year Fellowship to complete graduate research and thesis writing.

Associated Publications and Author Contributions

Chapter Two was previously published and adapted with permission from Jiang, X.; O'Brien, Z. J.; Yang, S.; Buenaflor, J.; Tan, C.; Khan, S. I.; Houk, K. N.; Garcia-Garibay, M. A. "Crystal Fluidity Reflected by Fast Rotational Motion at the Core, Branches and Surface Aromatic Groups of a Dendrimeric Molecular Rotor" *J. Am. Chem. Soc.* **2016**, *138*, 4650–4656. Copyright © 2016 American Chemical Society. All authors were involved in the project development. O'Brien, Buenaflor, and Tan explored the synthesis of the dendrimeric rotor under the supervision of Prof. Garcia-Garibay. I improved the reaction conditions, synthesized the different isotopologues, obtained crystalline samples, and performed solid-state NMR experiments. Prof. Garcia-Garibay and I analyzed the obtained spectra and proposed rotation models accounting for the experimental results. Dr. Khan solved the crystal structure by X-ray diffraction of single crystals I prepared. Yang and Prof. Houk performed molecular dynamics simulation and analyzed the energetic barriers of rotation. Prof. Garcia-Garibay, Prof. Houk, Yang, and I proposed mechanisms consistent with both the experimental and computational results. Prof. Garcia-Garibay and I wrote the early drafts of the manuscript and the supporting information. All authors contributed to the editing of the manuscript. This project was supported by National Science Foundation grants DMR1101934 and DMR140268 (M.A.G.-G.) and CHE1361104 (K.N.H.).

Chapter Three was previously published and adapted with permission from Jiang, X.; Rodríguez-Molina, B.; Nazarian, N.; Garcia-Garibay, M. A. "Rotation of a Bulky Triptycene in the Solid State: Toward Engineered Nanoscale Artificial Molecular Machines" *J. Am. Chem. Soc.* **2014**, *136*, 8871–8874. Copyright © 2014 American

Chemical Society. Prof. Garcia-Garibay and I designed the synthesis of the target molecule. I performed the synthesis with the assistance from Nazarian under the guidance of Prof. Garcia-Garibay. Dr. Rodríguez-Molina performed the solid-state NMR experiments. Prof. Garcia-Garibay, Dr. Rodríguez-Molina, and I analyzed the experimental data, proposed the models of dynamics, and wrote the manuscript with the supporting information. Our analysis was aided by the SEM images obtained by Dr. Stopin. All authors were involved in the editing of the manuscript. This project was supported by National Science Foundation grant DMR1101934.

Chapter Four is a manuscript under preparation and will be shortly submitted for publication as: Jiang, X.; Duan, H.; Khan, S. I.; Garcia-Garibay, M. A. "Diffusion-Controlled Rotation of a Crystalline Triptycene MOF Determined by the Hydrodynamics of a Confined Liquid" *TBD* **2016**. Prof. Duan and I designed the structure of the pillar ligand and the three MOFs under the supervision of Prof. Garcia-Garibay. Prof. Duan and I prepared the MOFs. Dr. Khan obtained crystal structures of all three frameworks. I performed the solid-state ^{2}H NMR spin-echo experiments. Prof. Garcia-Garibay and I analyzed the experimental data and performed line-shape simulation to determine the mechanism of rotation. Prof. Garcia-Garibay, Prof. Duan, and I prepared the manuscript and the corresponding supporting information. All authors contributed to the editing towards the final draft. This project was supported by National Science Foundation grant DMR140268.

VITA

2008-2010	Undergraduate Researcher, Peking University
2009-2010	Teaching Assistant, Peking University
2006-2010	Bachelor of Science, Peking University
2010-2015	Teaching Assistant/Associate, University of California, Los Angeles (UCLA)
2011-2016	Graduate Research Assistant, UCLA
2010-2016	Doctor of Philosophy, Chemistry, UCLA (expected award date: June 2016)

LIST OF PUBLICATIONS

Liang, Y.; Jiang, X.; Yu, Z.-X. "Mechanisms of Cascade Reactions in the Syntheses of Camptothecin-Family Alkaloids: Intramolecular [4^+ + 2] Reactions of *N*-Arylimidates and Alkynes" *Org. Lett.* **2009**, *11*, 5302–5305.

Liang, Y.; Jiang, X.; Yu, Z.-X. "Enantioselective Total Synthesis of (+)-Asteriscanolide via Rh(I)-Catalyzed [(5+2)+1] Reaction" *Chem. Commun.* **2011**, *47*, 6659–6661.

Liang, Y.; Jiang, X.; Fu, X.-F.; Ye, S.; Wang, T.; Yuan, J.; Wang, Y.; Yu, Z.-X. "Total Synthesis of (+)-Asteriscanolide: Further Exploration of the Rhodium(I)-Catalyzed [(5+2)+1] Reaction of Ene-Vinylcyclopropanes and CO" *Chem. Asian J.* **2012**, *7*, 593–604.

Jiang, X.; Rodríguez-Molina, B.; Nazarian, N.; Garcia-Garibay, M. A. "Rotation of a Bulky Triptycene in the Solid State: Toward Engineered Nanoscale Artificial Molecular Machines" *J. Am. Chem. Soc.* **2014**, *136*, 8871–8874.

Zhang, K.; Cai, L.; Jiang, X.; Garcia-Garibay, M. A.; Kwon, O. "Phosphine-Mediated Iterative Arene Homologation Using Allenes" *J. Am. Chem. Soc.* **2015**, *137*, 11258–11261.

Jiang, X.; O'Brien, Z. J.; Yang, S.; Buenaflor, J.; Tan, C.; Khan, S. I.; Houk, K. N.; Garcia-Garibay, M. A. "Crystal Fluidity Reflected by Fast Rotational Motion at the Core, Branches and Surface Aromatic Groups of a Dendrimeric Molecular Rotor" *J. Am. Chem. Soc.* **2016**, *138*, 4650–4656.

Jiang, X.; Duan, H.; Khan, S. I.; Garcia-Garibay, M. A. "Diffusion-Controlled Rotation of a Crystalline Triptycene MOF Determined by the Hydrodynamics of a Confined Liquid" *manuscript in preparation*.

Chapter One

Artificial Molecular Machines and Crystalline Molecular Machines

1.1. Introduction

This introductory chapter covers a brief history and recent advances in the field of artificial molecular machines with an emphasis on crystalline molecular machines. A machine is defined as "a tool containing one or more parts that uses energy to perform an intended action".[1] Scientists recognized that some molecules could also be considered as machines as they participate in the transmission of motion, force, and energy. Those molecules are named molecular machines and research of molecular machines has received increasing interests in the past decades from different realms including but not limited to physics, chemistry, biology, medicine, and material science.[2,3,4] While the concept was first conceived in 1959 by Richard Feynman in his famous lecture "there's plenty of room at the bottom",[5] it was not until the 1980s that the research of artificial molecular machines started to take off when scientists started to achieve precise control of atoms in molecules or on surfaces. One of the earliest artificial molecular machines is the molecular bevel gear prepared independently by Iwamura and Mislow (Figure 1.1).[6] Inspired by Ōki's research on rotational isomers,[7] they were able to prove that the two triptycene moieties are undergoing fast rotation and their rotational dynamics are highly correlated, similar to the macroscopic bevel gears. This landmark example was followed by many reports with complex structures to emulate macroscopic machines with stereodynamic motions under equilibrium conditions such as shuttles, brakes, and turnstiles in the 1990s.[8] With the advances of synthetic organic and inorganic chemistry, scientists are now exploring more sophisticated systems with functions that could be biased by external stimuli.

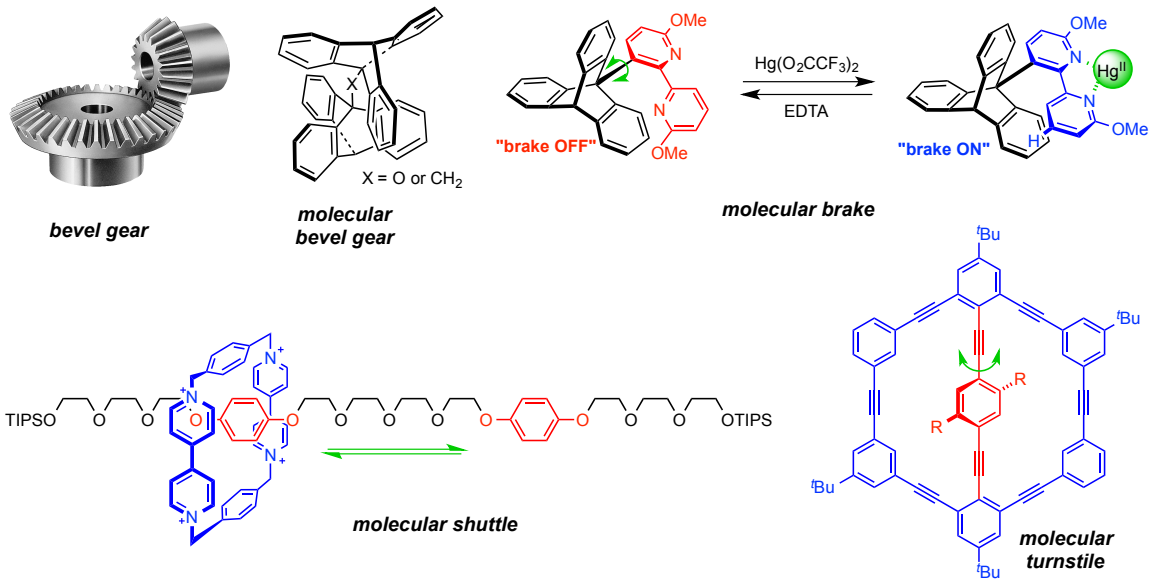

Figure 1.1. (upper left) Molecular bevel gear being a structural and functional analog of a macroscopic bevel gear and (lower left) molecular shuttle, (upper right) molecular brake, and (lower right) molecular turnstile of the same analogy.

The advancement of structural and chemical biology has also facilitated the development of artificial molecular machines. Functional biomolecular structures, such as ATP synthase, kinesin, myosin, and bacterial flagellum, are considered to be biomolecular machines, since they are also consistent with the definition of machines.[3e] Take ATP synthase as an example, it is driven by a gradient of proton concentration across the membrane to catalyze the synthesis of ATP from ADP and inorganic phosphate (Figure 1.2).[9] The complex structure of ATP synthase is composed of a water-soluble F_1 domain and a hydrophobic F_o domain embedded in the membrane. The two domains are functional by themselves when they are separated from each other after the removal of magnesium from the system. The F_1 domain independently catalyzes the hydrolysis of ATP, a reverse reaction of the ATP synthesis, and the F_o domain serves as a proton channel by itself. However, the close integration of both domains is necessary to

convert chemical energy into useful work. At the same time, the molecular behavior in the cellular environment is under the influence of complex Brownian motions, solvation, and other convoluted factors. A lot of effort is devoted to the understanding of the structure and mechanism of function of such biomolecular machines. It is now accepted that the nature of the dynamics of biomolecular machines is Brownian motion, and their task-performing capabilities are the result of biased motions controlled by the external inputs. These insights of miniature machines in nature will continue to facilitate the design and preparation of molecular machines capable of doing real work in the coming decades.

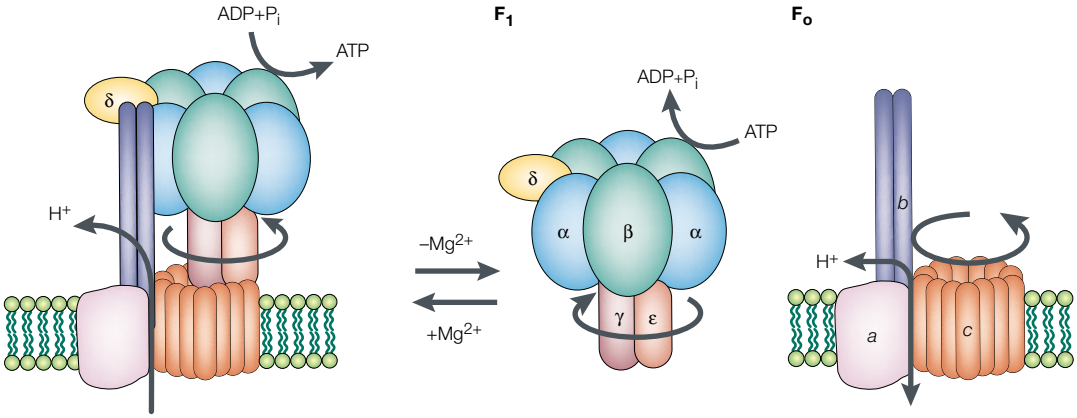

Figure 1.2. The bacterial ATP synthase has two domains, the F_1 domain of nine subunits with a stoichiometry $\alpha_3\beta_3\gamma_1\delta_1\varepsilon_1$ and the F_o domain of three kinds of transmembrane subunits with a stoichiometry $a_1b_2c_{10-14}$. Reprinted with permission from reference 9. Copyright © 2001 Nature Publishing Group.

1.2. Molecular Machines: Representative Building Blocks and Recent Examples

Much work has been done to prepare artificial molecular machines with functions similar to those of their counterparts in nature. For example, a molecular chaperone was built in 2007 by Harada and coworkers that could facilitate the ring-opening polymerization reaction of δ-valerolactone by pre-organizing the monomers and shielding the catalytic site from the back folding of the synthesized polymer.[10] In 2013, Leigh and coworkers reported a sequence-specific peptide synthesis utilizing a complex rotaxane, which is considered to be an artificial ribosome.[11] While these proof-of-concept examples are exciting and inspiring, their efficiencies are relatively low. They also failed to provide guidance about how to use molecular machines to perform meaningful tasks in real life. Currently, the research on artificial molecular machines is still at the stage of exploring different dimensions, especially the possible building blocks of future molecular machines. During the past decades, chemists have identified many functional groups that are responsive to external stimuli such as pH, temperature, humidity, mechanical stress, and light. Among other representative and widely used building blocks are azobenzene, spiropyran, and Feringa's unidirectional molecular motor. These photoresponsive groups, sometimes also referred to as photoswitches, share the advantages that changes could be introduced with precise temporal, spatial, and energetic control of input due to the virtue of light as a stimulus. In this section, a brief history of these building blocks and their unique properties and recent applications will be discussed.

1.2.1. Azobenzene and Its Application in Controlling the Assemblies of Macroscopic Gels and Biological Systems

Although azobenzene was first prepared and identified by Mitscherlich in 1843,[12] its photoisomerization was not documented until nearly a century later when Hartly noticed a new isomer was formed when a solution of azobenzene in acetone was exposed to sunlight in 1937.[13] Hartly was able to isolate *cis*-azobenzene by extraction and he proposed that azobenzene could undergo isomerization from the more stable *trans* form to a less stable *cis* form. Since then azobenzene has been the most widely explored photoswitches for the following reasons.[14,15] First, azobenzene has great photostability and it could undergo multiple photoisomerization cycles before showing significant degradation. Secondly, the UV-Vis absorption profiles of the *trans* and *cis* isomers are quite different (Figure 1.3b). The *trans* isomer has a stronger π–π^* transition at 320 nm, whereas the *cis* isomer features a relatively strong n–π^* band at 430 nm. As a result, UV light irradiation could lead to nearly quantitative isomerization from *trans*-azobenzene to *cis*-azobenzene, and visible light irradiation is effective in the reverse reaction. Finally, a fairly large change of both the shape and dipole moment is observed with isomerization. The distance between the *para*-carbons is reduced from 9.0 Å to 5.5 Å in the *cis* isomer and the dipole moment increases to 3.0 Debye. Such differences could be utilized to provide light controlled systems with the incorporation of azobenzene moieties.

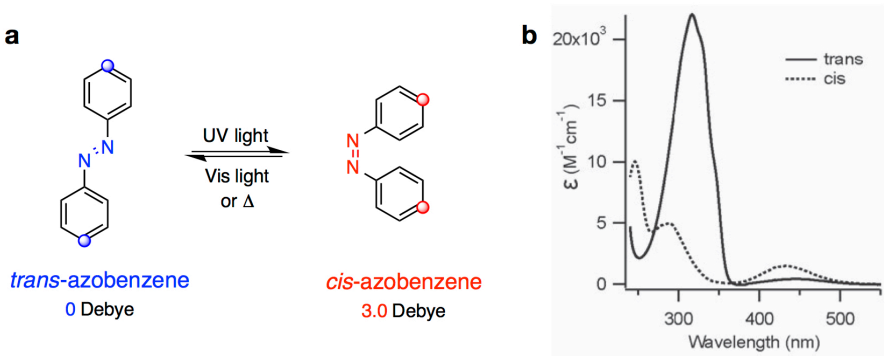

Figure 1.3. (a) The isomerization between *trans*- and *cis*-azobenzene and (b) their UV-Vis spectra in an ethanol solution. Adapted with permission from reference 15. Copyright © 2011 Royal Chemical Society.

An elegant example was reported by Harada and coworkers that takes advantage of the shape change of azobenzene in photoisomerization to control assemblies of macroscopic objects.[16] It is known that *trans*-azobenzene interacts strongly with α-cyclodextrin (αCD), while *cis*-azobenzene prefers β-cyclodextrin (βCD) with a larger cavity. Polyacrylamide-based hydrogels with azobenzene, αCD, and βCD moieties were prepared and allowed to interact with one another. Before irradiation, the azo-gel and the αCD-gel form an assembly in water because of the host-guest interaction between αCD and *trans*-azobenzene (Figure 1.4). However, upon irradiation with UV light, the azobenzene moiety undergoes a *trans* to *cis* isomerization, leading to the dissociation of the *trans*-azobenzene and αCD and the association of the *cis*-azobenzene and βCD. As a result, the assemblies of azo-gel and αCD-gel dissociated and new assemblies of azo-gel and βCD-gel were observed.

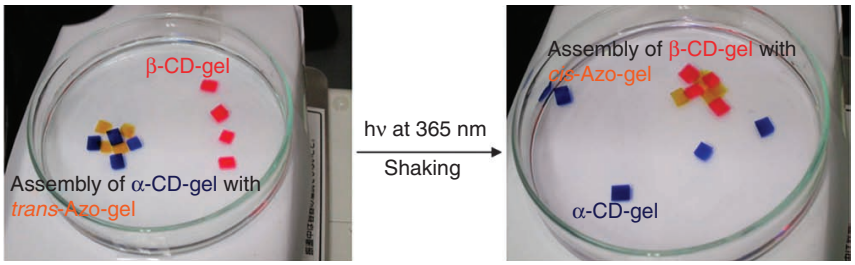

Figure 1.4. Macroscopic gel assembling controlled by light. Reprinted from reference 16 published under a Creative Commons Attribution-NonCommercial-ShareAlike 3.0 Unported License.

Recently, many scientists have explored the possibility of isomerization of azobenzene without using high energy UV light, so that the photoisomerization process could be more compatible with living cells and tissues. Longer wavelength light, such as visible and near-IR light, also has the advantage of better tissue permeability. One of the successful strategies is the preparation of tetrasubstituted azobenzenes **1** (Figure 1.5) reported by Hecht[17] and Woolley[18] independently. The steric hindrance introduced by the substituents lead to a deviation from the planar structure, and **1** could undergo photoisomerization reaction with visible light because of the destabilized ground state. Aprahamin and coworkers took a different approach to the challenge and showed that the isomerization of a BF_2-coordinated azo complex **2** could be achieved by near-infrared light irradiation at 710 nm.[19] In 2016, Trauner and coworkers confirmed that such red-shifted azobenzenes could function like the parent compound.[20] They reported a late stage functionalization for the synthesis of compound **5**, a derivative of a known photoresponsive agonist of the Vanilloid Receptor 1 (TRPV1) AzCA4.[21] As shown in Figure 1.5, coupling of vanillylamine and compound **4**, which could be readily prepared by a palladium-mediated late stage chlorination reaction from **3**, gives the desired

photochromic ligand **5**. Similar control of TRPV1 could be achieved by using **5** with irradiation of light at 560 nm, which is red-shifted by approximately 200 nm from that of the parent compound AzCA4.

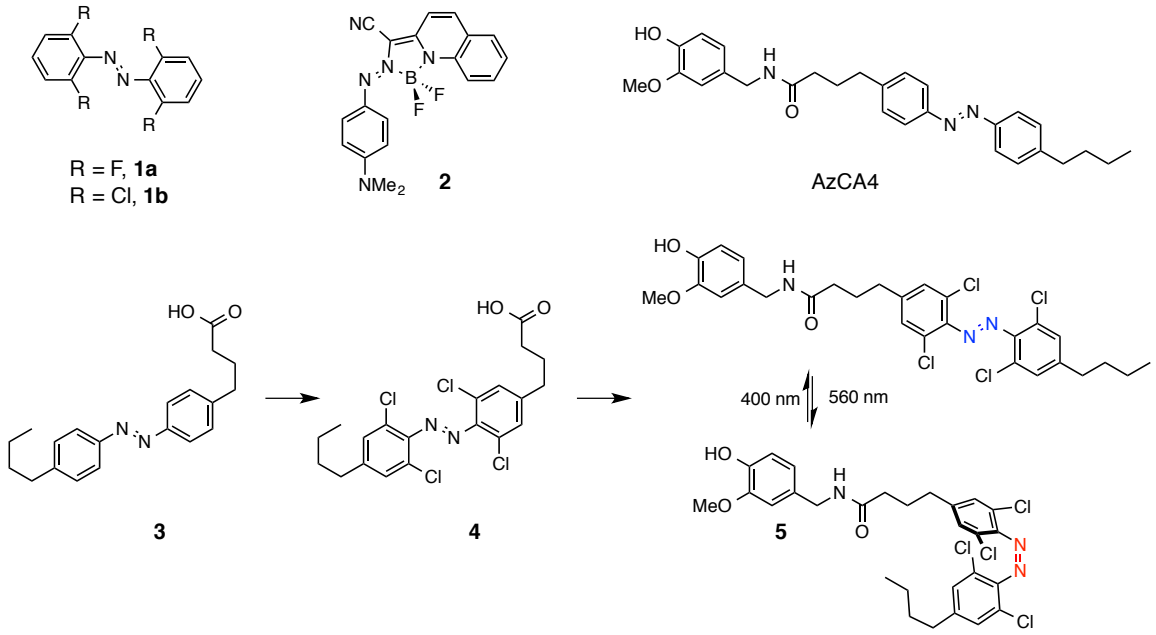

Figure 1.5. New azobenzene derivatives **1** and **2** with red-shifted photoisomerization wavelengthes and the preparation of derivative **5** and its visible light controlled isomerization.

1.2.2. Spiropyran and Its Application in Controlled Nanotube Formation and Fluorescence Imaging

Photochromism of spiropyran was first reported by Fisher and Hirshberg in 1952 who noticed that a colorless indoline spiropyran **6** solution turned red with light irradiation (Figure 1.6).[22] This was explained by an isomerization from the ring-closed spiropyran (SP) form into a charge-separated merocyanine (MC) form. The reverse reaction occured when the solution was stored in dark. It was later noted that aside from the significant color change, a very large dipole, estimated to be about 10 Debye, was

induced because of the charge separation.[23] As a result, many properties of the molecule changed drastically before and after isomerization, including hydrophilicity, affinity for charged species, redox potential, etc.

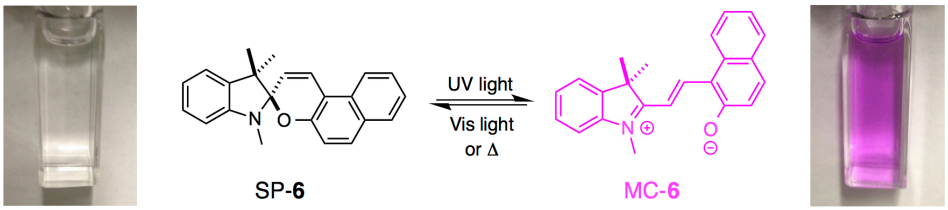

Figure 1.6. Isomerization of indoline spiropyran **6** and the associated color change in solution.

In 2013 Aida and coworkers published an excellent example of using the photoisomerization of spiropyran to control the formation of nanotubes.[24] The monomer used in their study was $GroEL_{SP}$, a mutant of molecular chaperone GroEL prepared by the coupling reaction of $GroEL_{Cys}$ and a spiropyran-appended maleimide derivative. When a solution of $GroEL_{SP}$ was exposed to UV light, ring opening of spiropyran gave $GroEL_{MC}$ with MC moieties. In the presence of Mg^{2+}, the free phenoxide of MC coordinated to Mg^{2+} and the nanotubes were formed because of multiple MC···Mg^{2+}···MC bridges between the neighboring $GroEL_{MC}$ monomers (Figure 1.7). When the nanotubes were exposed to visible light, they were cleaved into very short oligomers because the MC···Mg^{2+}···MC interactions disappeared when monomer $GroEL_{SP}$ with nonpolar SP moieties was regenerated.

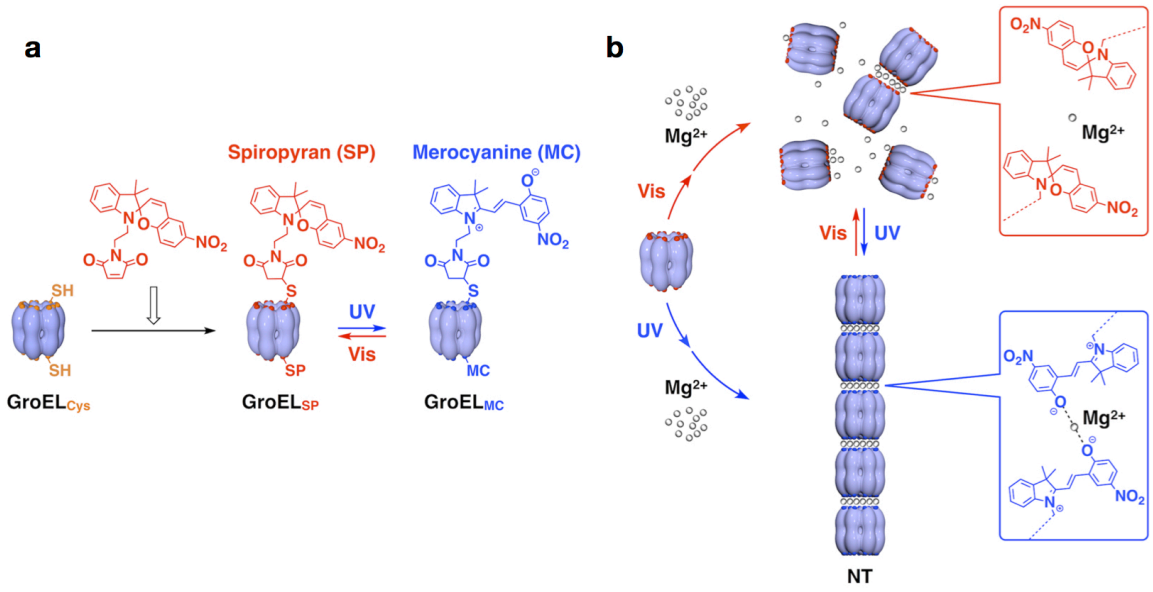

Figure 1.7. Schematic illustration of (a) the incorporation of spiropyran structure into the barrel shaped protein monomer GroEL and (b) the mechanism of light-controlled formation and dissociation of nanotubes. Reprinted with permission from reference 24. Copyright © 2013 American Chemical Society.

Since spiropyrans in the SP form have negligible visible absorption, they typically exhibit no fluorescence under visible light excitation. The ring-opened MC form, however, absorbs strongly at 570 nm and emits red fluorescence. This switchable fluorescence of spiropyran made it possible for Li and coworkers to perform photoactuated unimolecular logical switching-attained reconstruction (PULSAR) microscopy and to obtain images with resolution well below the diffraction limit.[25,26] As shown in Figure 1.8a, PULSAR employs a Gaussian mask fitting to refine the position of a single molecule of spiropyran in a traditional fluorescence image. To apply the technique to obtain high-resolution images of nanoparticles containing multiple spiropyrans, the authors applied a short pulse of irradiation to convert a small fraction of spiropyrans in the nanoparticles into the MC form and turn on their fluorescence.

Assuming the emitting MCs are distant from each other that no interaction would occur between two emitters, the positions of the nanoparticles could be determines with a Gaussian mask fitting after a few cycles of irradiation and fluorescence detection.

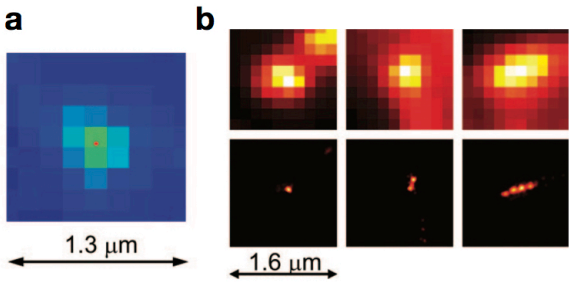

Figure 1.8. (a) The traditional fluorescence image of a spiropyran molecule with the centroid determined by a Gaussian mask fitting. (b) Comparison of images of one (left), two (middle), and four (right) spiropyran-containing nanoparticles under traditional fluorescence microscopy and PULSAR microscopy. Reprinted with permission from reference 26. Copyright © 2008 American Chemical Society.

1.2.3. Feringa's Unidirectional Molecular Motors and Their Application in Catalysis and Photoresponsive Gels

The first sterically overcrowded dissymmetric alkenes were synthesized by Feringa and Wynberg in 1977 using a McMurry coupling of ketone **7** to give two alkenes **8** and **9** with tetrasubstituted double bonds.[27] The four bulky substituents led to an out-of-plane distortion of the molecule, and both **8** and **9** were found to be optically active, although they bear no chiral center. Feringa has continued to work on the synthesis and photoisomerization of overcrowded alkenes.[28] His group reported in 1999 the unidirectional 360° rotation of an overcrowded alkene **10**, also known as Feringa's first generation molecular motor.[29] The unidirectional rotation was realized utilizing a series of four discrete photochemical and thermal isomerization steps shown in Figure 1.9b.

Irradiation (λ > 280 nm) of (3*R*,3′*R*)-(*P*,*P*)-*trans*-**10** caused a double bond isomerization from the *trans* to *cis* configuration to give (3*R*,3′*R*)-(*M*,*M*)-*cis*-**10**, which could spontaneously isomerize into a more stable *cis* isomer (3*R*,3′*R*)-(*P*,*P*)-*cis*-**10** because of the presence of the two chiral centers. Subsequent irradiation of (3*R*,3′*R*)-(*P*,*P*)-*cis*-**10** provided a fourth isomer (3*R*,3′*R*)-(*M*,*M*)-*trans*-**10**, which was converted back into the starting (3*R*,3′*R*)-(*P*,*P*)-*trans*-**10** thermally. In this work, the two stereogenic centers are the key structural elements, since they provided the access to four different stereoisomers with different thermal stabilities.

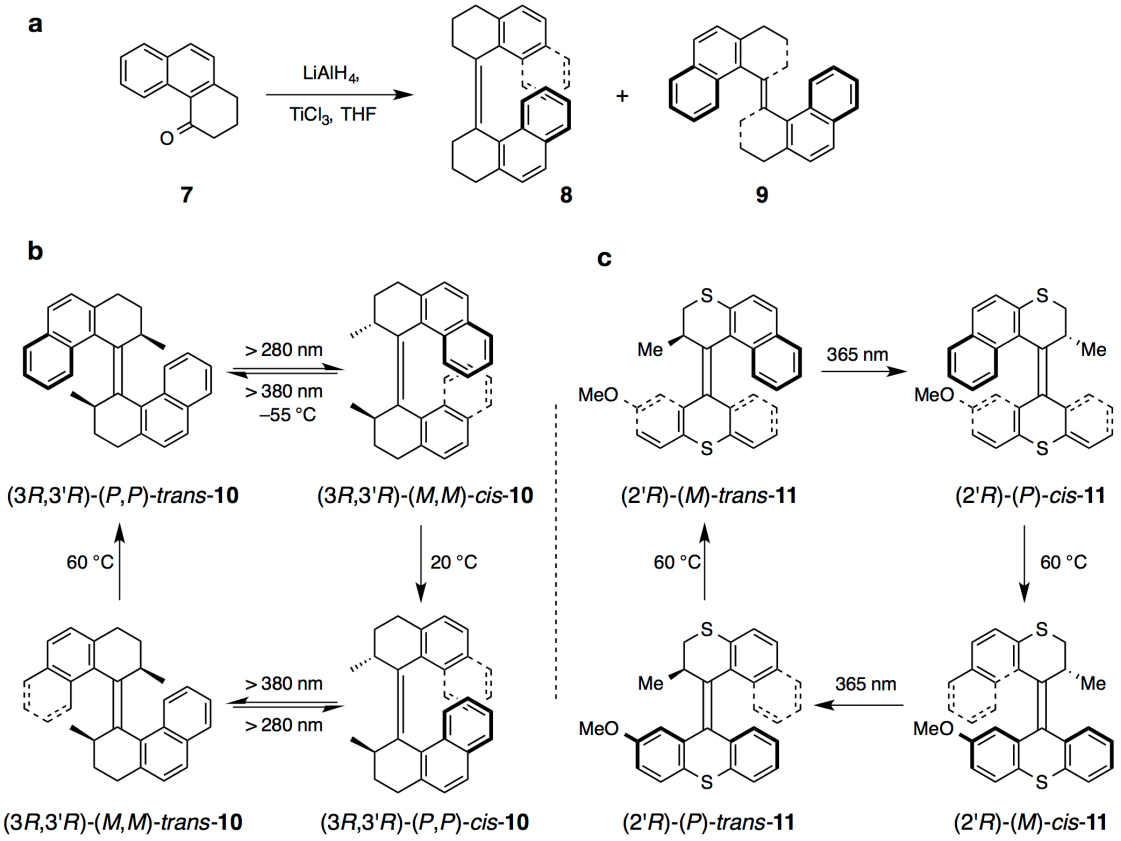

Figure 1.9. (a) The first sterically overcrowded dissymmetric alkenes prepared by the dimerization of a ketone and the 360° unidirectional rotation of Feringa's first (b) and second generation (c) molecular motors.

In 2002, Feringa and coworkers reported a second generation molecular motor **11** featuring distinct upper and lower parts, rendering it feasible for the motor to be attached to other molecules and used in different settings.[30] The were able to show that the second generation motor could undergo unidirectional rotation efficiently as the first generation with just one chiral center (Figure 1.9c).

In 2011, Wang and Feringa reported a novel photoswitchable catalyst **12** for the Michael addition of 2-methoxy thiophenol **13** to cyclohexenone **14** utilizing the first generation molecular motor.[31] The authors successfully incorporated DMAP and thiourea moieties into the two halves of the catalyst **12**, the structure of which was designed that the distances between DMAP and thiourea segments (part A and part B) would be ideal for them to cooperate in a hydrogen-bond catalyzed reaction in ***II*** and ***III*** during a cycle of 360˚ unidirectional rotation (Figure 1.10). In this reaction, part A would be used as a hydrogen bond acceptor and part B as a hydrogen bond donor. Indeed, when the isomers ***I***, ***II***, and ***III*** were subjected to the Michael addition reaction, they displayed different catalytic reactivity and selectivity. Isomer ***I*** was not an efficient catalyst and very little rate acceleration was observed. When isomer ***II*** was used, the reaction was accelerated and (*S*)-**15** was formed selectively with an *e.r.* of 75/25 (*S*/*R*). Similar rate acceleration was observed when ***III*** was used, but the stereoselectivity was inverted, and (*R*)-**15** was the major product (*S*/*R* = 23/77). This is because the change of axial chirality results in a different orientation of the DMAP moiety to the thiourea moiety, which will activate thiophenol **13** and cyclohexenone **14**, respectively. The Feringa group has recently expanded the scope of application of the molecular rotors in synthesis and prepared of a photoswitchable ligand.[32]

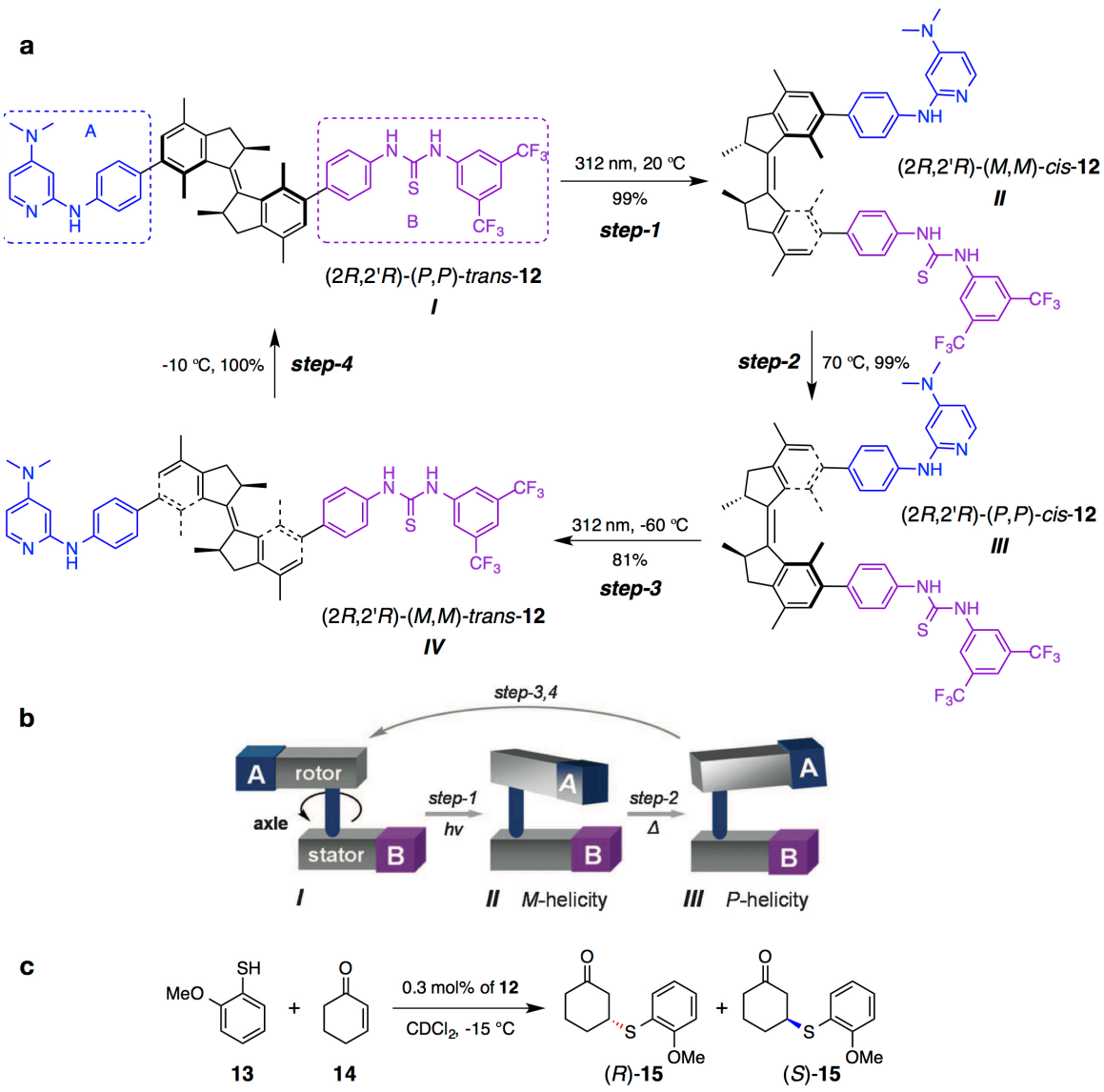

Figure 1.10. (a) Unidirectional rotation of catalyst **12** and (b) schematic representation of the isomerization processes to account for the stereoselectivity observed in (c) the Michael addition of 2-methoxy thiophenol **13** and cyclohexenone **14**. Adapted with permission from reference 31. Copyright © 2011 American Association for the Advancement of Science.

A recent example of how Feringa's overcrowded alkenes could be applied to materials were realized by a group of scientists led by Giuseppone.[33] The photoresponsive groups were cross-linked by copper catalyzed alkyne-azide cycloadditions to make gel

17. With light-activated unidirectional rotation, the volume taken up by each rotor unit was reduced, which could be visualized by the size change of the gel. As shown in Figure 1.11b, a maximum contraction of approximately 80 % was observed when the gel was irradiated for 120 min. Continued irradiation (170 min) led to rapture of the gel and a partial recovery of the gel volume.

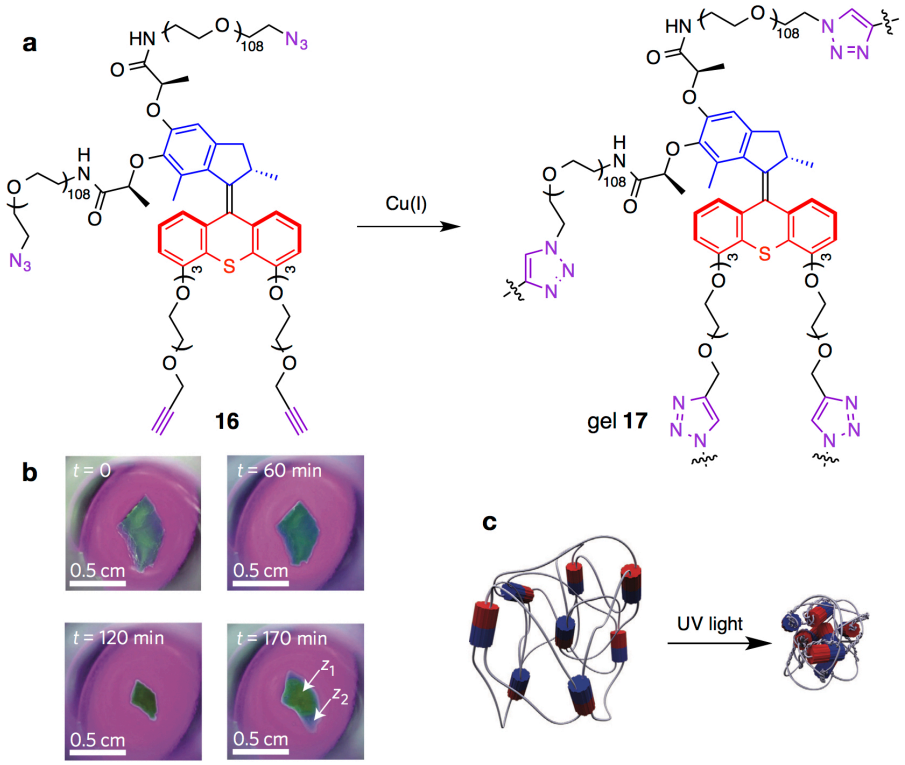

Figure 1.11. (a) The synthesis of gel **17** with molecular motors; (b) the shape change of the gel with irradiation; (c) a schematic representation of the shrinking of the gel. Adapted with permission from reference 33. Copyright © 2015 Nature Publishing Group.

1.3. Crystalline Molecular Machines

Crystalline molecular machines are appealing since they offer precise arrangement of functional components. The structural periodicity and coherency make it possible for them to respond collectively to external stimuli, which has been repeatedly demonstrated in the past decades.[34,35] In a recent example, Morimoto and Irie reported light induced mechanical change of a crystal and its potential application as an actuator.[36] The crystal cantilever, obtained from cocrystallization of photochromic diarylethene derivative **18o** and perfluoronaphthalene **19**, was able to lift a 46.77 mg lead ball with UV light irradiation while the weight of the cantilever is merely 0.17 mg (Figure 1.12).

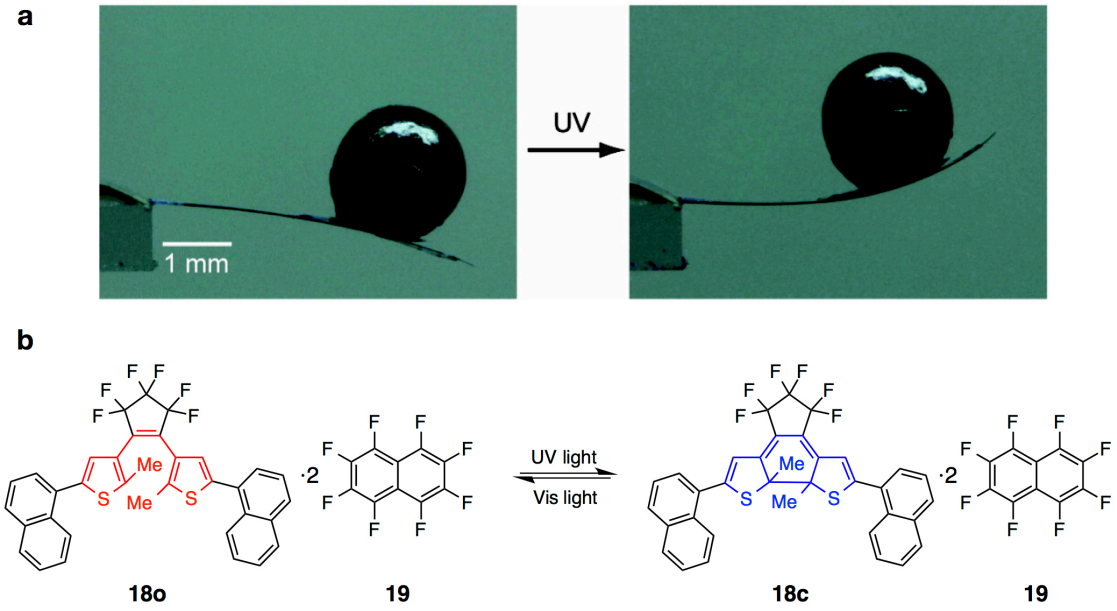

Figure 1.12. (a) A 2-mm lead ball lifted up with UV irradiation by a crystal cantilever; (b) the composition change of the crystal, resulting from the isomerization between the ring-opened isomer **18o** and the ring-closed isomer **18c**, with irradiation of light at different wavelengths. Reprinted with permission from reference 36. Copyright © 2010 American Chemical Society.

Despite the enticing features, solid-state artificial molecular machines have been

less explored as compared to molecular machines in solution largely because of the limited freedom in the solid state where molecules are closely packed. In fact, only globular molecules or functional groups such as C_{60}, admantane, methyl group, and a few others are known to exhibit relatively fast motions in the solid state. Recently, scientists started to explore general strategies to promote motion in the solid state. The Garcia-Garibay group pioneered this research with the design and engineering of *amphidynamic crystals* with both static and dynamic components. Their work, together with contribution from other research groups,[37] are discussed in the following sections.

1.3.1. Molecular Crystals of Rotors with Covalently Linked Rotators and Stators

Inspired by the structural features of macroscopic gyroscopes, Garcia-Garibay and coworkers reported the molecular gyroscope, **20**, in 2001.[38] As shown in Figure 1.13a, the central phenylene group is the rotator, and the two bulky triphenylmethyl (trityl) groups at the two ends of **20** are the stators of the molecular gyroscope. The carbon–carbon triple bonds connecting the stator and rotator constitute the rotational axis. The authors proposed that rotation would be possible for the rotators in an imagined "crystal" of macroscopic gyroscopes because their stators would protect the rotator from close contacts with others. Similarly, the central phenylene rotator of **20** was designed to be mobile in the crystals due to the steric shielding by the trityl stators. The authors were able to prove that with variable temperature (VT) solid-state nuclear magnetic resonance (SS NMR) experiments; these revealed that the phenylene groups undergo Brownian 2-fold site-exchanges with room temperature rotational frequency of about 10 kHz. The crystals obtain for gyroscope **20** were termed as *amphidynamic crystals* to highlight the

coexistence of both static and dynamic components in the crystal.

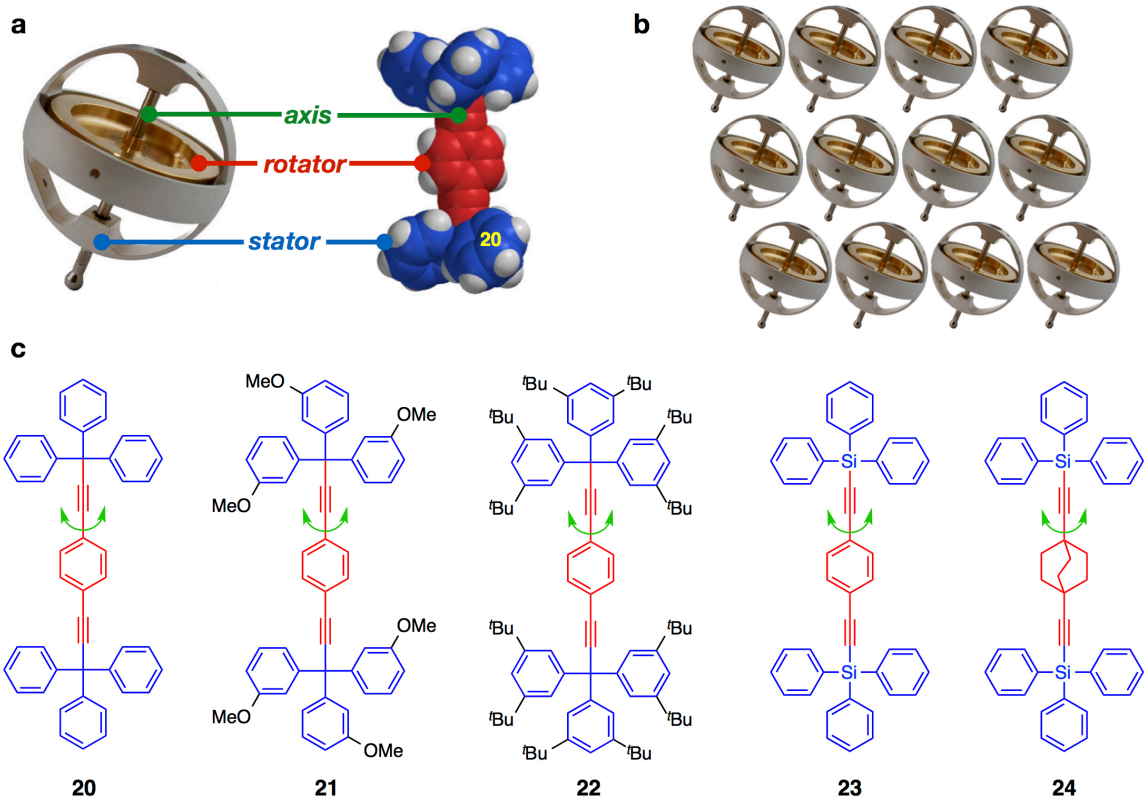

Figure 1.13. (a) A toy gyroscope and the space filling molecular gyroscopes **20** featuring their rotators, stators, and rotational axes; (b) an imagined packing structure of toy gyroscopes; (c) the chemical structure of molecular gyroscopes **20**–**24**.

The Garcia-Garibay group has explored the structure-function relationships in molecular gyroscopes and demonstrated that the frequency of rotation is partially determined by the size of the stators. They reported that the gyroscopes **21** and **22** with large tris(3-methoxylphenyl)methyl and tris(3,5-di-*tert*-butylphenyl)methyl stators displayed ambient temperature rotational rates of 108 kHz and over 100 MHz, both of them being faster than that of **20**.[39,40] The symmetry of the rotator is another factor identified to affect the rotational dynamics significantly. With the stators being the same for molecular gyroscopes **23** and **24**, the packing structures of the two are almost

identical. However, because of the higher symmetry of bicyclo[2.2.2]octane (BCO) rotator, it is able to rotate (110 MHz) more than 10 times faster than the 2-fold symmetric phenylene rotator (9 MHz).[41]

1.3.2. Metal-Organic Frameworks as Platforms for Crystalline Molecular Machines

Metal-organic frameworks (MOFs) are one of the most popular materials nowadays, and they have been widely used in gas storage, catalysis, and other applications.[42] Recently, it has been shown that MOFs and other coordination polymers are also excellent platforms to explore dynamics in the solid state because of their porous structures, exceptional crystallinity and structural versatility. In 2008, Yaghi and Garcia-Garibay explored the dynamics of phenylene groups in MOF-5.[43] They found that although there is plenty of empty space in MOF-5, the activation energy for a phenylene group to rotate is fairly high, since the conjugation between phenylene and the carboxylate groups is destroyed during the rotation.

Recently, Leob and coworker reported successful incorporation of mechanically interlocked molecules (MIMs) into MOFs. They realized of rotational and translational dynamics of interlocked macrocyles, both have been systematically studied for MIMs in solution, by taking advantage of the empty space of MOFs.[44] Unlike previous attempts, Leob and coworkers used the interlocked complexes, such as **25** and **26**, as the building blocks for the synthesis of MOF **UWDM-1** and **UWDM-4**, respectively (Figure 1.14). They were able to verify the inclusion of interlocked macrocycles in the crystals. The porous structures of the MOFs made it possible for the macrocycles to display relatively fast rotational motion in **UWDM-1** and translational motion in **UWDM-4**.

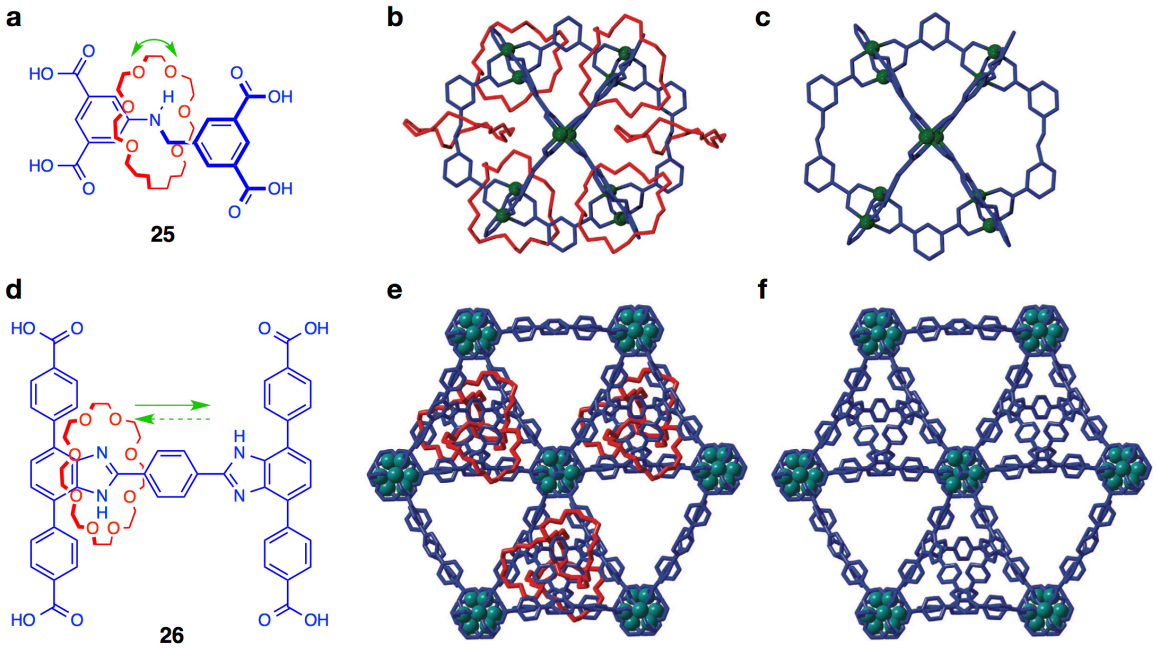

Figure 1.14. (a,d) Ligands for the synthesis of MOFs **UWDM-1** and **UWDM-4** and the crystal structure of the frameworks (b,e) with the macrocycles shown in red, and (c,f) omitted for clarity. Adapted with permission from: (b,c) reference 44a, copyright © 2015 Nature Publishing Group, and (e,f) reference 44b, copyright © 2012 Nature Publishing Group.

1.3.3. Crystalline Molecular Machine and Supramolecular Crystals

While crystalline molecular gyroscopes and MOFs provide access to various solid-state dynamic phenomena, there are drawbacks associated with these systems, because of the difficulties of synthesis. Since it is also challenging to predict their function beforehand, the tedious preparation might lead only to materials with no intended function. By contrast, multiple-component crystals could be obtained in a more convenient way, making it possible to evaluate and re-engineer those supramolecular crystals in a relatively short period of time. Among the successful examples of dynamic supramolecular crystals, three recent ones are presented here.

In 2015, Metrangolo and Garcia-Garibay reported cocrystals of 1,4-diazabicyclo[2.2.2]octane (DABCO) and fluoro-substituted iodobenzenes.[45] As shown in Figure 1.15a, a trimer was formed with DABCO as a bidentate halogen-bond acceptor and pentafluoroiodobenzene **27** as the donor. An analysis of the crystal structure revealed that DABCO resides loosely in a cavity surrounded by **27**. The dynamic properties of DABCO were analyzed using multiple techniques, and the authors concluded that it experiences ultrafast 3-fold rotations at a frequency of approximately 5.2 GHz at 297 K. In 2009, a group of scientist led by Akutagawa and Nakamura reported a three-component crystal with *m*-fluoroanilinium (*m*-$FAni^+$) forming a hydrogen-bonding assembly with dibenzo[18]crown-6 (DB[18]crown-6) in the presence of a $[Ni(dmit)_2]^-$ (dmit = 2-thioxo-1,3-dithiole-4,5-dithiolate) counterion.[46] The major interactions among the three components are the electrostatic interactions. Two different layered structures consisting of the hydrogen-bonding assemblies and $[Ni(dmit)_2]^-$ counterions, respectively, were formed in the crystal. The former layer was less densely packed because of the irregular shape of the assemblies. As a result, *m*-$FAni^+$ experiences dipole reorientation under an electric field and the crystal exhibits ferroelectric features with a transition temperature at 346 K. An earlier example reported in 2005 showed that weak van de Waals interactions and geometrical matching could also be used to engineer solid-state dynamics.[47] As mentioned before, C_{60} undergoes rotational motion in the crystalline state; however, such rotation also experiences hindrances from neighboring C_{60} molecules despite their globular shape. In a cocrystal of C_{60} and cubane, the smaller cubane molecule could perfectly fit into the octahedral void formed by C_{60} molecules, because of its concave van de Waals surfaces (Figure 1.15e). The inclusion of cubane increased the

distance between neighboring C_{60} molecules and led to faster C_{60} rotation with a lower activation energy.

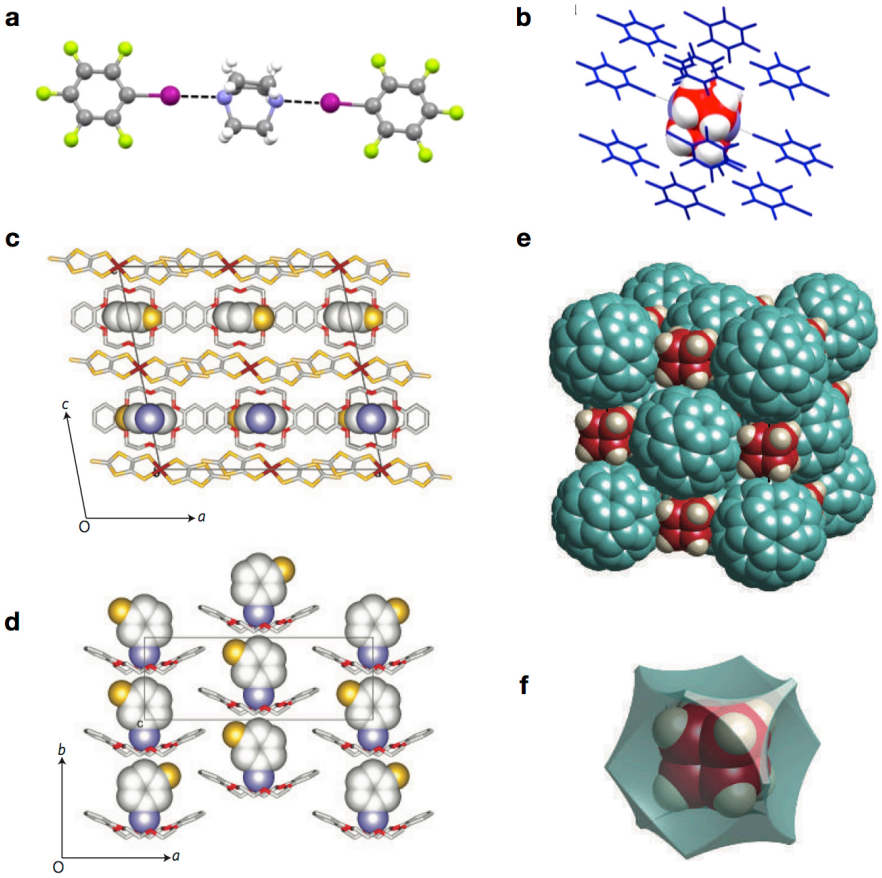

Figure 1.15. (a) A halogen-bonded trimer of pentafluoroiodobenzene **27** and DABCO in their cocrystal; (b) the crystal structure featuring the DABCO rotator surrounded by **27**. (c) Crystal structure of (*m*-FAni$^+$)(DB[18]crown-6)[Ni(dmit)$_2$]$^-$ view along the *b* axis; (d) the supramolecular rotator layer viewed along the *c* axis. (e) The packing structure of C_{60}-cubane cocrystal formed because of the complementary convex shape of C_{60} and (f) the concave surface of cubane. Reprinted with permission from: (a,b) reference 45, copyright © 2015 American Chemical Society, (c,d) reference 46, copyright © 2009 Nature Publishing Group, and (e,f) referece 47, copyright © 2005 Nature Publishing Group.

1.4. Summary

Research on artificial molecular machines has advanced greatly in the past few decades, focusing on stereodynamic behaviors under equilibrium conditions and stimuli-controlled properties. Although many inspiring examples of molecular machines in the solution phase have been reported, they are unlikely to do useful work because of their random positions and orientations. Crystalline molecular machines could respond to external stimuli collectively, since they offer coherent and periodically orientated 3D structures. However, only a limited number of functional crystalline molecular machines have been reported. My thesis is devoted to the design, synthesis, and characterization of solid-state molecular machines with complex structures and dynamic properties.

1.5. References

1. https://en.wikipedia.org/wiki/Machine

2. (a) Credi, A.; Silvi, S.; Venturi, M. *Molecular Machines and Motors: Recent Advances and Perspectives*; Springer International Publishing: Switzerland, **2014**. (b) Feringa, B. L.; Brwone, W. R. *Molecular Switches*; Wiley-VCH: Weinheim, Germany, **2011**.

3. (a) Abendroth, J. M.; Bushuyev, O. S.; Weiss, P. S.; Barrett, C. J. *ACS Nano* **2015**, *9*, 7746. (b) Erbas-Cakmak, S.; Leigh, D. A.; McTernan, C. T.; Nussbaumer, A. L. *Chem. Rev.* **2015**, *115*, 10081. (c) Coskun, A.; Banaszak, M.; Astumian, R. D.; Stoddart, J. F.; Grzybowski, B. A. *Chem. Soc. Rev.* **2012**, *41*, 19. (d) Kay, E.; Leigh, D.; Zerbetto, F. *Angew. Chem., Int. Ed.* **2007**, *46*, 72. (e) Browne, W. R.; Feringa, B. L. *Nat. Nanotechnol.* **2006**, *1*, 25. (f) Kinbara, K.; Aida, T. *Chem. Rev.* **2005**, *105*, 1377. (g) Kottas, G. S.; Clarke, L. I.; Horinek, D.; Michl, J. *Chem. Rev.* **2005**, *105*, 1281. (h) Balzani, V.; Credi, A.; Raymo, F.; Stoddart, J. *Angew. Chem., Int. Ed.* **2000**, *39*, 3348.

4. (a) Zhao, Y.; Chen, L.; Swager, T. M. *Angew. Chem., Int. Ed.* **2016**, *55*, 917. (b) Ragazzon, G.; Baroncini, M.; Silvi, S.; Venturi, M.; Credi, A. *Nat. Nanotechnol.* **2015**, *10*, 70. (d) De, S.; Pramanik, S.; Schmittel, M. *Angew. Chem., Int. Ed.* **2014**, *53*, 14255. Schönberger, M.; Althaus, M.; Fronius, M.; Clauss, W.; Trauner, D. *Nat. Chem.* **2014**, *6*, 712. (e) Velema, W. A.; van der Berg, J. P.; Hansen, M. J.; Szymanski, W.; Driessen, A. J. M.; Feringa, B. L. *Nat. Chem.* **2013**, *5*, 924. (f) Nguyen, T.-T.-T.; Türp, D.; Wagner, M.; Müllen, K. *Angew. Chem., Int. Ed.* **2013**, *52*, 669. (g) Perera, U. G. E.; Ample, F.; Kersell, H.; Zhang, Y.; Vives, G.; Echeverria, J.; Grisolia, M.; Rapenne, G.; Joachim, C.; Hla, S.-W. *Nat. Nanotechnol.* **2013**, *8*, 46. (h) Thies, S.; Sell, H.; Schütt, C.; Bornholdt, C.; Näther, C.; Tuczek, F.; Herges, R. *J. Am. Chem. Soc.* **2011**, *133*, 16243. (i) Silvi, S.;

Arduini, A.; Pochini, A.; Secchi, A.; Tomasulo, M.; Raymo, F. M.; Baroncini, M.; Credi, A. *J. Am. Chem. Soc.* **2007**, *129*, 13378. (j) Muraoka, T.; Kinbara, K.; Aida, T. *Nature* **2006**, *440*, 512. (k) Hernandez, R.; Tseng, H.-R.; Wong, J. W.; Stoddart, J. F.; Zink, J. I. *J. Am. Chem. Soc.* **2004**, *126*, 3370.

5. Feynman, R. P. *Eng. Sci.* **1960**, *23*, 22.

6. (a) Iwamura, H.; Mislow, K. *Acc. Chem. Res.* **1988**, *21*, 175. (b) Kawada, Y.; Iwamura, H. *J. Am. Chem. Soc.* **1981**, *103*, 958. (c) Cozzi, F.; Guenzi, A.; Johnson, C. A.; Mislow, K. *J. Am. Chem. Soc.* **1981**, *103*, 957. (d) Kawada, Y.; Iwamura, H. *J. Org. Chem.* **1980**, *45*, 2547.

7. Ōki, M. *Angew. Chem., Int. Ed. Engl.* **1976**, *15*, 87.

8. (a) Bedard, T. C.; Moore, J. S. *J. Am. Chem. Soc.* **1995**, *117*, 10662. (b) Kelly, T. R.; Bowyer, M. C.; Bhaskar, K. V.; Bebbington, D.; Garcia, A.; Lang, F.; Kim, M. H.; Jette, M. P. *J. Am. Chem. Soc.* **1994**, *116*, 3657. (c) Anelli, P. L.; Spencer, N.; Stoddart, J. F. *J. Am. Chem. Soc.* **1991**, *113*, 5131.

9. Yoshida, M.; Muneyuki, E.; Hisabori, T. *Nat. Rev. Mol. Cell Biol.* **2001**, *2*, 669.

10. Osaki, M.; Takashima, Y.; Yamaguchi, H.; Harada, A. *J. Am. Chem. Soc.* **2007**, *129*, 14452.

11. Lewandowski, B.; De Bo, G.; Ward, J. W.; Papmeyer, M.; Kuschel, S.; Aldegunde, M. J.; Gramlich, P. M. E.; Heckmann, D.; Goldup, S. M.; D'Souza, D. M.; Fernandes, A. E.; Leigh, D. A. *Science* **2013**, *339*, 189.

12. Mitscherlich, E. *Ann. Pharm.* **1834**, *12*, 311.

13. Hartley, G. S. *Nature* **1937**, *140*, 281.

14. Griffiths, J. *Chem. Soc. Rev.* **1972**, *1*, 481.

15. Beharry, A. A.; Woolley, G. A. *Chem. Soc. Rev.* **2011**, *40*, 4422.

16. Yamaguchi, H.; Kobayashi, Y.; Kobayashi, R.; Takashima, Y.; Hashidzume, A.; Harada, A. *Nat. Commun.* **2012**, *3*, 603.

17. Bléger, D.; Schwarz, J.; Brouwer, A. M.; Hecht, S. *J. Am. Chem. Soc.* **2012**, *134*, 20597.

18. Samanta, S.; Beharry, A. A.; Sadovski, O.; McCormick, T. M.; Babalhavaeji, A.; Tropepe, V.; Woolley, G. A. *J. Am. Chem. Soc.* **2013**, *135*, 9777.

19. (a) Yang, Y.; Hughes, R. P.; Aprahamian, I. *J. Am. Chem. Soc.* **2014**, *136*, 13190. (b) Yang, Y.; Hughes, R. P.; Aprahamian, I. *J. Am. Chem. Soc.* **2012**, *134*, 15221.

20. Konrad, D. B.; Frank, J. A.; Trauner, D. *Chem. Eur. J.* **2016**, *22*, 4364.

21. Frank, J. A.; Moroni, M.; Moshourab, R.; Sumser, M.; Lewin, G. R.; Trauner, D. *Nat. Commun.* **2015**, *6*, 7118.

22. Fischer, E.; Hirshberg, Y. *J. Chem. Soc.* **1952**, 4522.

23. Klajn, R. *Chem. Soc. Rev.* **2014**, *43*, 148.

24. Sendai, T.; Biswas, S.; Aida, T. *J. Am. Chem. Soc.* **2013**, *135*, 11509.

25. Tian, Z.; Li, A. D. Q. *Acc. Chem. Res.* **2013**, *46*, 269.

26. Hu, D.; Tian, Z.; Wu, W.; Wan, W.; Li, A. D. Q. *J. Am. Chem. Soc.* **2008**, *130*, 15279.

27. Feringa, B.; Wynberg, H. *J. Am. Chem. Soc.* **1977**, *99*, 602.

28. Feringa, B. L. *Acc. Chem. Res.* **2001**, *34*, 504.

29. Koumura, N.; Zijlstra, R.; van Delden, R. A.; Harada, N.; Feringa, B. L. *Nature* **1999**, *401*, 152.

30. Koumura, N.; Geertsema, E. M.; van Gelder, M. B.; Meetsma, A.; Feringa, B. L. *J. Am. Chem. Soc.* **2002**, *124*, 5037.

31. Wang, J.; Feringa, B. L. *Science* **2011**, *331*, 1429.

32. Zhao, D.; Neubauer, T. M.; Feringa, B. L. *Nat. Commun.* **2015**, *6*, 6652.

33. Li, Q.; Fuks, G.; Moulin, E.; Maaloum, M.; Rawiso, M.; Kulic, I.; Foy, J. T.; Giuseppone, N. *Nat. Nanotechnol.* **2015**, *10*, 161.

34. Irie, M.; Fukaminato, T.; Matsuda, K.; Kobatake, S. *Chem. Rev.* **2014**, *114*, 12174.

35. Al-Kaysi, R. O.; Müller, A. M.; Bardeen, C. J. *J. Am. Chem. Soc.* **2006**, *128*, 15938.

36. Morimoto, M.; Irie, M. *J. Am. Chem. Soc.* **2010**, *132*, 14172.

37. (a) Ichikawa, J. I.; Hoshino, N.; Takeda, T.; Akutagawa, T. *J. Am. Chem. Soc.* **2015**, *137*, 13155. (b) Comotti, A.; Bracco, S.; Yamamoto, A.; Beretta, M.; Hirukawa, T.; Tohnai, N.; Miyata, M.; Sozzani, P. *J. Am. Chem. Soc.* **2014**, *136*, 618. (c) Zhang, Q.-C.; Wu, F.-T.; Hao, H.-M.; Xu, H.; Zhao, H.-X.; Long, L.-S.; Huang, R.-B.; Zheng, L.-S. *Angew. Chem., Int. Ed.* **2013**, *52*, 12602. (d) Setaka, W.; Yamaguchi, K. *J. Am. Chem. Soc.* **2013**, *135*, 14560. (e) Lemouchi, C.; Iliopoulos, K.; Zorina, L.; Simonov, S.; Wzietek, P.; Cauchy, T.; Rodríguez-Fortea, A.; Canadell, E.; Kaleta, J.; Michl, J.; Gindre, D.; Chrysos, M.; Batail, P. *J. Am. Chem. Soc.* **2013**, *135*, 9366. (f) Zhang, W.; Ye, H.-Y.; Graf, R.; Spiess, H. W.; Yao, Y.-F.; Zhu, R.-Q.; Xiong, R.-G. *J. Am. Chem. Soc.* **2013**, *135*, 5230.

38. (a) Dominguez, Z.; Dang, H.; Strouse, M. J.; Garcia-Garibay, M. A. *J. Am. Chem. Soc.* **2002**, *124*, 7719. (b) Dominguez, Z.; Dang, H.; Strouse, M. J.; Garcia-Garibay, M. A. *J. Am. Chem. Soc.* **2002**, *124*, 2398.

39. Khuong, T.-A. V.; Dang, H.; Jarowski, P. D.; Maverick, E. F.; Garcia-Garibay, M. A. *J. Am. Chem. Soc.* **2007**, *129*, 839.

40. Khuong, T.-A. V.; Zepeda, G.; Ruiz, R.; Khan, S. I.; Garcia-Garibay, M. A. *Cryst. Growth Des.* **2004**, *4*, 15.

41. Karlen, S. D.; Reyes, H.; Taylor, R. E.; Khan, S. I.; Hawthorne, M. F.; Garcia-Garibay, M. A. *Proc. Natl. Acad. Sci. U. S. A.* **2010**, *107*, 14973.

42. Furukawa, H.; Cordova, K. E.; O'Keeffe, M.; Yaghi, O. M. *Science* **2013**, *341*, 1230444.

43. Gould, S. L.; Tranchemontagne, D.; Yaghi, O. M.; Garcia-Garibay, M. A. *J. Am. Chem. Soc.* **2008**, *130*, 3246.

44. (a) Zhu, K.; O'Keefe, C. A.; Vukotic, V. N.; Schurko, R. W.; Loeb, S. J. *Nat. Chem.* **2015**, *7*, 514. (b) Vukotic, V. N.; Harris, K. J.; Zhu, K.; Schurko, R. W.; Loeb, S. J. *Nat. Chem.* **2012**, *4*, 456.

45. Catalano, L.; Pérez-Estrada, S.; Terraneo, G.; Pilati, T.; Resnati, G.; Metrangolo, P.; Garcia-Garibay, M. A. *J. Am. Chem. Soc.* **2015**, *137*, 15386.

46. Akutagawa, T.; Koshinaka, H.; Sato, D.; Takeda, S.; Noro, S.-I.; Takahashi, H.; Kumai, R.; Tokura, Y.; Nakamura, T. *Nat. Mater.* **2009**, *8*, 342.

47. Pekker, S.; Kováts, E.; Oszlányi, G.; Bényei, G.; Klupp, G.; Bortel, G.; Jalsovszky, I.; Jakab, E.; Borondics, F.; Kamarás, K.; Bokor, M.; Kriza, G.; Tompa, K.; Faigel, G. *Nat. Mater.* **2005**, *4*, 764.

Chapter Two

Crystal Fluidity Reflected by Fast Rotation of All Aromatic Groups in a Dendritic Molecular Rotor

2.1. Introduction

While exploring the design of structures capable of supporting the functions of molecular machines,[1,2] our group has proposed the use of *amphidynamic crystals* featuring molecular gyroscopes and other molecular rotors with static frames and dynamic components.[3,4,5] Compound **1** is one of the simplest molecular gyroscopes with an open topology that we have analyzed in some detail[5f,g] (Figure 2.1). It consists of a phenylene rotator at the center linked by a double alkyne axle to a stator comprised of two triphenylmethyl (trityl) groups. The dumbbell shape of **1** makes it difficult for it to pack efficiently and generates a low-density region in the middle of the structure that, along with local volume fluctuations,[4e] allows for rotation of the central phenylene. Using variable temperature (VT) solid-state quadrupolar echo ^{2}H NMR spectroscopy (SS ^{2}H NMR), cross-polarization magic angle spinning (CPMAS) ^{13}C NMR spectroscopy, and computational analysis we showed that the trityl stators engaged in a relatively tight 6-fold edge-to-face phenyl embrace are static, while the central rotator experiences a thermally activated 180° site exchange with a frequency of *ca*. 15 kHz at 297 K.[5f] More recently, we and others have described new examples of amphidynamic crystals with a range of internal dynamics.[4,6] Some of them have promising applications as novel materials with dielectric[4f,6a,d] and ferroelectric[6g,i,j] functions.

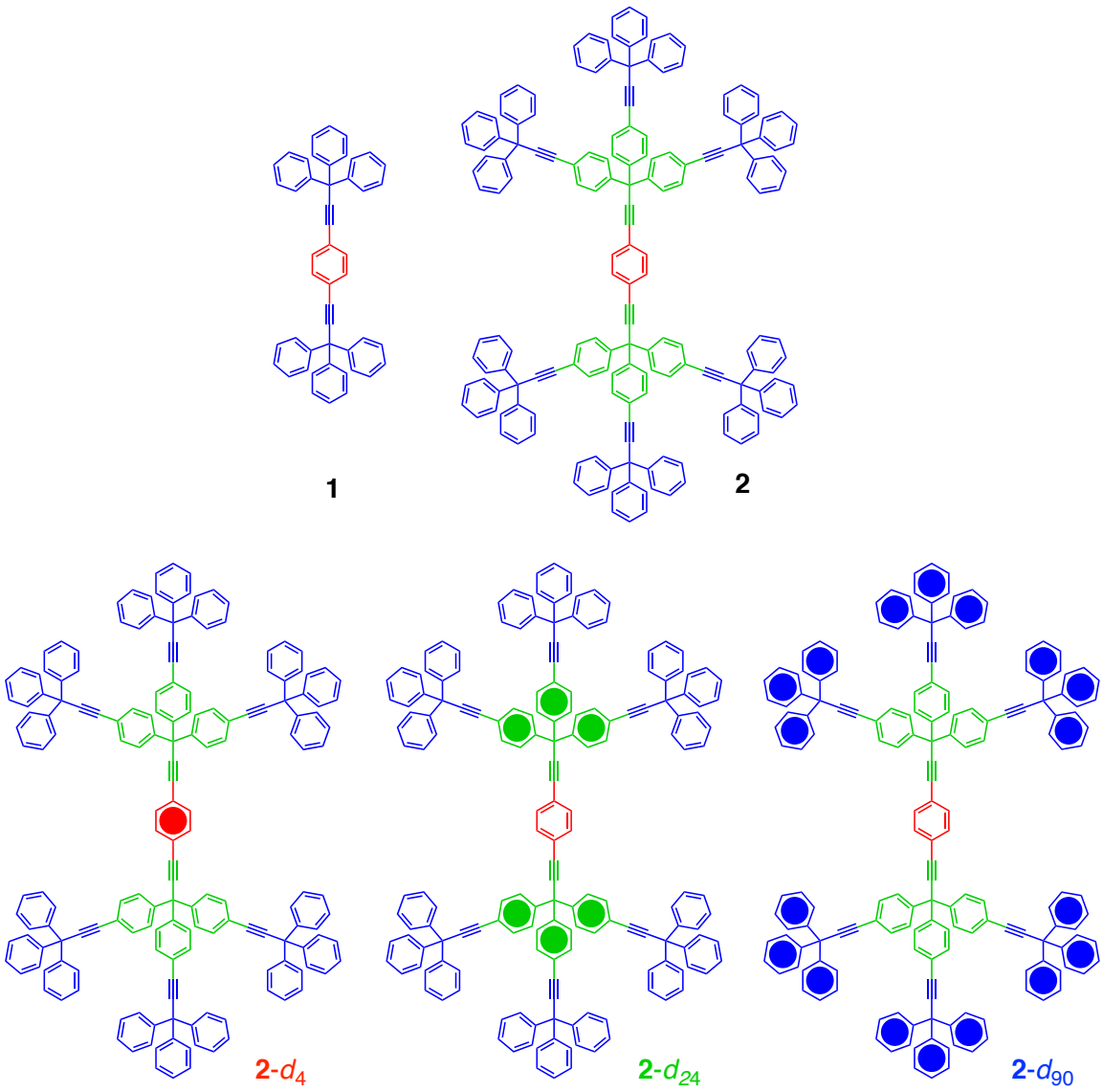

Figure 2.1. Structures of molecular rotor **1**, dendrimeric molecular rotor **2**, and its isotopologues **2**-d_4, **2**-d_{24} and **2**-d_{90} with filled circles indicating perdeuterated phenylene and phenyl groups.

Considering strategies to increase the size of molecular gyroscopes to the range of biomolecular machines,[7] we decided to explore strategies to expand the architecture of **1** in a self-similar, radially growing manner. We viewed compound **2** as a promising target to obtain a well-ordered amphidynamic crystal based on its highly symmetric, shape-

persistent, hyperbranched structure, and its many shape-conserving conformational degrees of freedom. We report here the synthesis, structure, and dynamic processes in **2**, a unique type of amphidynamic crystal. Crystals of this high molecular weight organic substance were obtained only from unconventional solvent mixtures. The crystal structure of **2** confirms the formation of a low-density crystal with a large amount of solvent molecules and intermolecular contacts reminiscent of a protein crystal. A close look at the structure suggested that motion might not be restricted to the central phenylene rotator (shown in red in Figure 2.1), but extended to the phenylene branches (shown in green), and into the peripheral phenyl groups (shown in blue). With that in mind, and taking advantage of a very efficient modular synthesis, we prepared deuterated isotopologues **2**-d_4, **2**-d_{24} and **2**-d_{90} to analyze their rotational dynamics. SS ^{2}H NMR measurements described here reveal ambient temperature rotational motion in the megahertz regime, indicating a crystal structure where every aromatic group displays fast rotational dynamics, whether it is the central phenylene rotator, phenylene groups in the trityl branches, or phenyl groups in the peripheral trityl groups. Crystals of dendritic rotor **2** represent a new type of amphidynamic crystals in which the frame of reference is solely determined by the C–C single bond framework and the quaternary carbons, which retain their equilibrium positions in the lattice while everything else rotates. Rotational dynamics as a function of temperature indicate that this unusually mobile environment is characterized by relatively high activation energies ($E_a \approx 15$ kcal/mol) and very large pre-exponential factors ($A \approx 10^{18}$ s^{-1}). In a structure where every aromatic group undergoes thermally activated rotations, an unusually large pre-exponential factors suggests that those dynamic processes are influenced by changes in the internal fluidity of the crystal

lattice, rather than a static potential energy hypersurface of a simple site-exchange process.

2.2. Synthesis and Characterization

Dendrimeric molecular rotor **2** was synthesized by taking advantage of the convergent strategy illustrated in Scheme 2.1. Sonagashira reaction between 3,3,3-triphenylpropyne **3**[5g] and 4-bromo-iodobenzene occurred selectively at the iodine site to give aryl bromide **4**. Treatment of **4** with *n*-butyllithium provided an aryl lithium species, which was trapped with diethyl carbonate to give triarylmethanol **5**. When refluxed in a mixture of acetyl chloride and toluene, triarylmethanol **5** was converted to a triarylmethyl chloride intermediate, which was further reacted with ethynyl magnesium bromide to yield triarylpropyne **6**. Although palladium catalyzed coupling reactions of two large components are generally difficult,[8] we were able to achieve a double Sonagashira coupling reaction between terminal alkyne **6** and 1,4-diiodobenzene. Under optimized reaction conditions, rotor **2** could be obtained in 70 % isolated yield and the homocoupling side reaction of **6** (not shown) was suppressed.

Scheme 2.1. Synthesis of Rotor **2**.[#]

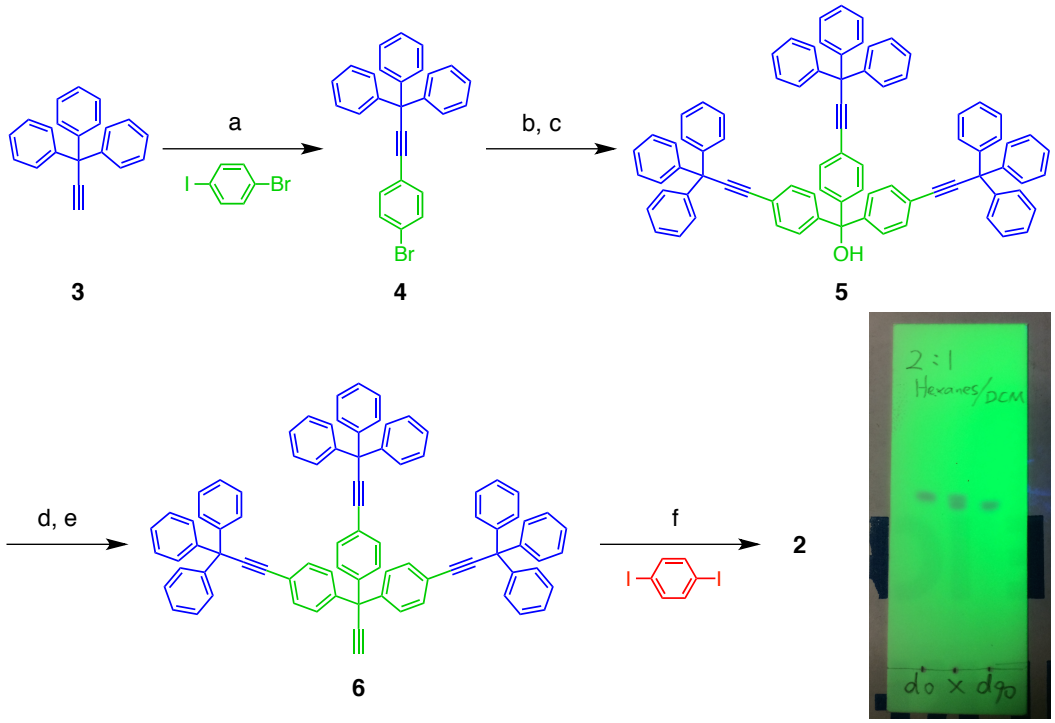

[#]Reagents and conditions: (a) $PdCl_2(PPh_3)_2$, CuI, THF, *i*-Pr_2NH, reflux, 91 %; (b) *n*-BuLi, THF; then (c) diethyl carbonate, –78 °C to r.t., 85 %; (d) AcCl, Tol, reflux; (e) THF, ethynylmagnesium bromide, Tol, reflux, 63 % over 2 steps; (f) $Pd(PPh_3)_4$, CuI, NEt_3, PPh_3, DMF, 70 °C, 70 %. TLC plate illustrating the separation of **2** and **2**-d_{90} in the middle lane.

Isotopologues **2**-d_4, **2**-d_{24}, and **2**-d_{90} were prepared employing similar reactions with deuterated starting materials, 1,4-dibromobenzene-d_4 and **3**-d_{15}[9] to establish the desired isotopic labels. The details of the synthesis are included in the experimental section. Rotors **2**, **2**-d_4, **2**-d_{24} and **2**-d_{90} were all fully characterized by solution ^{1}H and ^{13}C NMR, IR, and MALDI-TOF MS. Splitting of corresponding carbon signals could be observed in the ^{13}C NMR for rotors **2**-d_4, **2**-d_{24} and **2**-d_{90} due to the C–D couplings (J = 22–25 Hz). The intensities of C–H stretching peaks (3000–3100 cm^{-1}) and C–H out-of-

plane bending peaks (650–850 cm^{-1}) in IR of isotopologues **2**-d_{24} and **2**-d_{90} were significantly reduced resulting from the deuterium substitutions. To our surprise, the retention value (R_f) of isotopologue **2**-d_{90} (0.47) on a thin-layer chromatography (TLC) plate is different from those of rotors **2,** **2**-d_4, and **2**-d_{24} (0.49). This is a rather rare example of TLC separation of isotopologues,[10] and it could be explained by a reduced hydrodynamic radius of the molecule due to the collective effects of polydeuteration at the periphery.[11]

2.3. Crystallization and X-Ray Structure of Dendrimeric Molecular Rotor 2

Crystallization of large organic molecules has always been a daunting challenge. To date, there are only a handful of crystal structures of compounds with molecular weight over 2,000 Da in literature.[8b,12] Fortunately, we obtained good quality crystals from warm supersaturated solutions of **2** and its isotopologues in a non-conventional solvent mixture containing 2,4,6-trimethylpyridine and 2,2,4-trimethylpentane.[13] X-ray diffraction data was collected at 100 K and the crystal structure was solved in the triclinic space group, P-1. The asymmetric unit consists of one half of the rotor molecule together with about four solvent molecules, most of them being 2,4,6-trimethylpyridine. Since some of the solvent molecules are highly disordered and could not be modeled accurately, they were removed using the SQUEEZE algorithm.[14] As shown in Figure 2.2, the three C–Ph bond vectors of the inner trityl groups on the sides of the structure adopt *anti* conformations, as is commonly seen in crystals of molecular gyroscopes of this

type.[5] A similar disposition can be observed for the peripheral trityls. Interestingly, all four trityl groups in the upper half of the rotor (Figure 2.2, left) have *P* or *PPP* helicity, while the other four related by an inversion center have *M* or *MMM* helicity. The inner alkyne axles display a slight deviation from linearity as measured by an angle of 175° measured from the *ipso* carbon of the central phenylene rotator to the center of the alkyne bond to the trityl quaternary carbon.

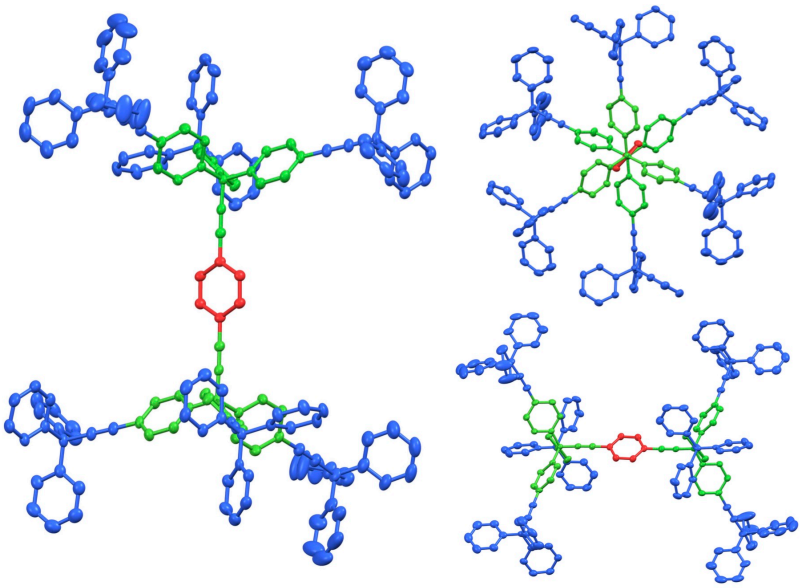

Figure 2.2. (left) Crystal structure of dendritic rotor **2** with thermal ellipsoids showing 50% probability. Solvent molecules and hydrogen atoms are omitted for clarity. (top right) View down the principal molecular axis and (bottom right) side view of **2** showing the *anti* conformations, respectively, between branch (green) trityls and the branch (green) and the peripheral (blue) trityls.

Further analysis of the crystal structure shows the packing coefficient is only 0.46 without including the solvent molecules,[15] which is very low compared with the typical range (from 0.64 to 0.77) for organic molecules.[16] As a result, very few rotor–rotor close contacts were observed, mostly describable in terms of edge-to-face aromatic

interactions. For example, the two faces of the central phenylene (**C** in Figure 2.3) are in close proximity to the edges of trityl branch phenylenes from two neighbors (**B**—**C**—**B**), and its two edges are directed toward the face of peripheral phenyl rings from neighboring molecules (**P**—**C**—**P**). Each of the branch phenylenes has only one close contact either with the central phenylene (**B**—**C**) or with one of the peripheral phenyl rings (not shown). The peripheral phenyl rings have less than two close contacts on average with other phenyl/phenylene rings. These observations support our hypothesis that the hyperbranched structure would lead to less interaction in the crystals, which is imperative to the realization of fast dynamics. It should be also noted that solvent molecules are also dynamic while they support the crystal structure, just like water molecules in protein crystals.[17] While attempting to obtain a crystal structure at 200 K, we noticed that all solvent molecules were disordered and none of them could be properly refined.

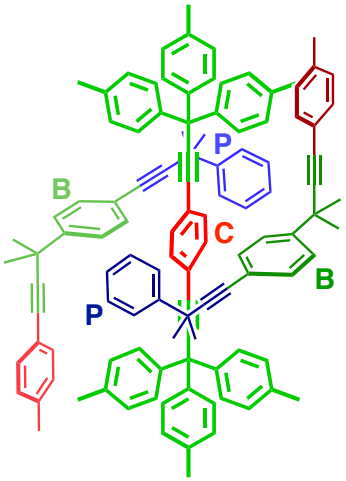

Figure 2.3. Schematic representation of the packing environment of the central phenylene (C) engaged in edge-to-face interactions acting as an acceptor with a branch phenylene (B) and as a donor with a peripheral (P) phenyl group.

2.4. Variable Temperature Solid-State ^{2}H NMR Experiments

^{2}H NMR spectroscopy is a widely used technique to analyze the internal dynamics of deuterium-enriched groups in the 10^3–10^8 Hz regime in the solid state.[18] The method relies on static sample measurements acquired with the quadrupolar spin echo pulse sequence, and is based on the changes in line shape that result from the dynamic narrowing of the broad powder pattern in the static spectra. Since the line shape is sensitive to both the trajectory and frequency of the site exchange dynamics, simulation of the experimental spectra usually provides sufficient information to characterize motions in solids in great detail.[19] The ^{2}H NMR spin-echo experiments were performed on crystalline and amorphous samples of **2**-d_4, **2**-d_{24}, and **2**-d_{90} to explore the dynamics of the central phenylene, branch phenylenes, and peripheral phenyls selectively.[20] Spectra with good signal to noise ratios could be obtained for all the crystalline samples and the amorphous samples of **2**-d_{24} and **2**-d_{90} (Figure 2.4). To our satisfaction, spectra obtained for all crystalline samples of **2**-d_4, **2**-d_{24}, and **2**-d_{90} indicated the presence of fast dynamic processes of the corresponding moieties that could be slowed (to a few kilohertz) when the samples were cooled. Those components were mostly static in amorphous samples, but they could be rendered mobile with sufficient thermal energy.

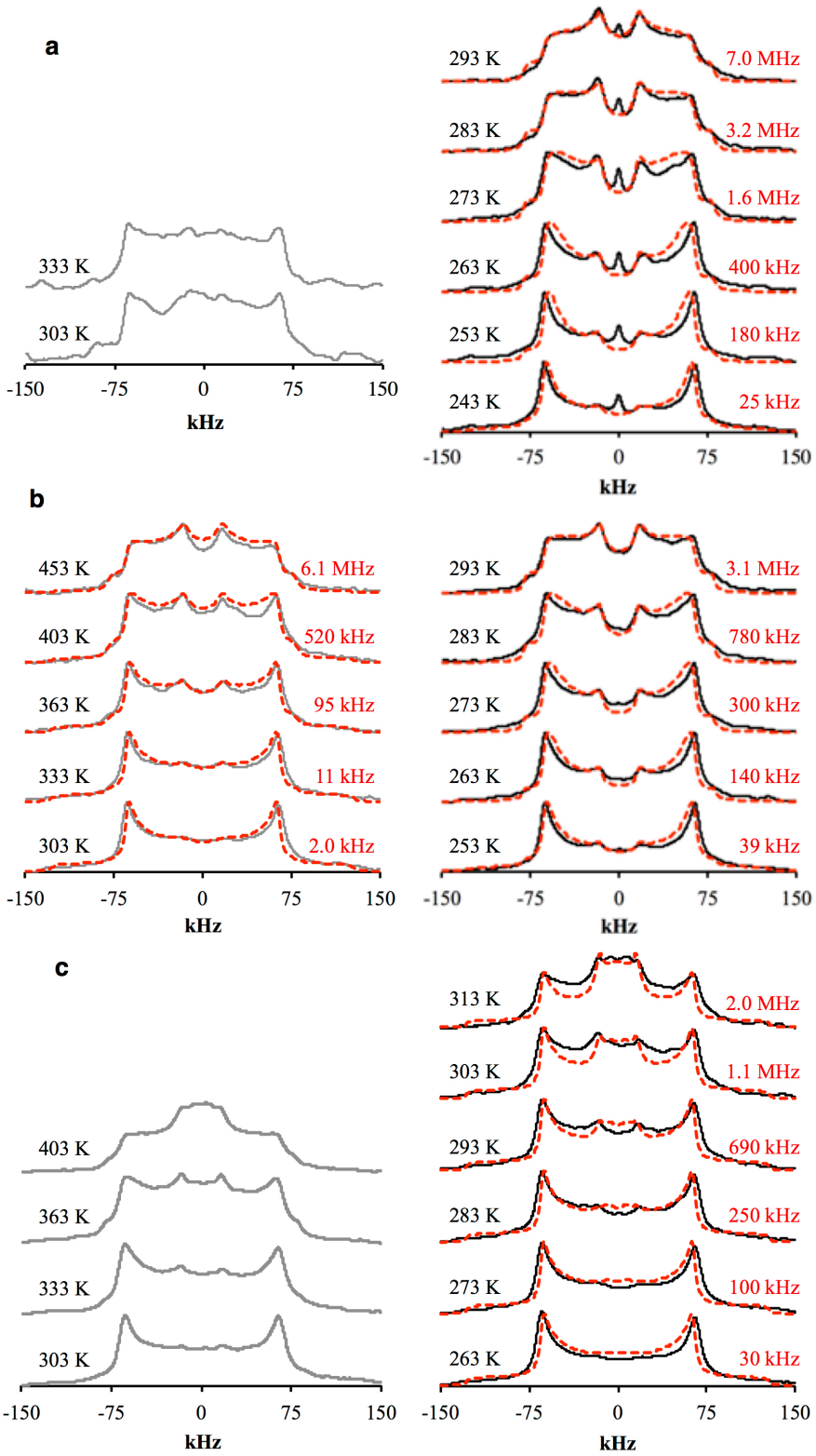

Figure 2.4. Experimental (grey solid spectra for the amorphous samples and black solid spectra for the crystalline samples) and simulated (red dashed spectra) SS ^{2}H NMR spectra of (a) rotor **2**-d_4, (b) rotor **2**-d_{24}, and (c) rotor **2**-d_{90} at variable temperatures.

The sharp peak at the center of the spectrum of the crystalline samples of **2**-d_4 (Figure 2.4a) is the isotropic peak resulting from a small fraction of **2**-d_4 dissolved in residual solvent. The line shape of rest of the spectra could be simulated with a model that considers a 2-fold flip for the phenylene group. The best simulation at 293 K suggested a rotational frequency of 7.0 MHz. Rotational frequencies estimated in a similar manner for spectra measured at 283, 273, 263, 253, and 243 K indicated closest matches at 3.2 MHz, 1.6 MHz, 400 kHz, 180 kHz, and 25 kHz, respectively. The spectra obtained for the amorphous sample of **2**-d_4 turned out to be very noisy, even after over 48 h of acquisition time, due to the combined effects of the low deuterium content (only 4 deuterium atoms in one molecule) and the lower sensitivity of SS ^{2}H NMR in amorphous samples. Next we examined the ^{2}H NMR spectra of **2**-d_{24} at various temperatures. The spectra obtained for the crystalline sample could be simulated well by considering a 2-fold-flip model with a log-Gaussian distribution[21] of the rotational frequencies having a width σ = 0.5. Rates of rotation at 293 K, 283 K, 273 K, 263 K, and 253 K were estimated to be 3.1 MHz, 780 kHz, 300 kHz, 140 kHz, and 39 kHz, respectively. The need for a Gaussian distribution may be attributed to the coexistence of three crystallographically nonequivalent branch phenylenes in the sample. The ^{2}H NMR spectra for amorphous sample of **2**-d_{24} measured at 303 K showed a static powder pattern, indicating that motions in a glassy state are slower. As the amorphous sample was heated, line shape changes were also consistent with a 2-fold flipping process, just like the crystalline sample, but with a larger distribution of exchange rates (σ = 2). Rotational exchange frequencies for experimental spectra measured at 453 K, 403 K, 363 K, 333 K, and 303 K corresponded to 6.1 MHz, 520 kHz, 95 kHz, 11 kHz, and 2.0 kHz.

The ^{2}H NMR spectra of the peripheral phenyl groups measured with samples of **2**-d_{90} is characterized by a rather complex superposition of a static signal, corresponding to the deuterium atom at the *para*-position, plus the signal of the other four deuterium atoms that are *ortho*- and *meta*- to the point of attachment of the phenyl ring. Since the C–D bond vector of the *para*-deuterium is aligned with the rotational axis (C–Ph bonds), its orientation does not change with rotation and its signal remains constant. By contrast, the other four C–D bonds have a cone angle of ± 60° with respect to the rotational axis, such that any angular displacement can cause changes in the lineshape of the spectrum. As shown in the right column in Figure 2.4, the spectral data of **2**-d_{90} started with a spectrum approaching the slow exchange regime at 263 K, and displayed spectral changes characteristic of increasing motion as the sample temperature reaches 313 K. Notably, a simple 180° site exchange model could not provide a reasonable simulation for the experimental spectra (Figure A.2.45), Instead, the experimental data could be reproduced reasonably well with a 4-fold rotation model and a 2:1 population distribution (Figure A.2.46) on non-equivalent sites related by 90°. This model led to site exchange rates of 2.0 MHz, 1.1 MHz, 690 kHz, 250 kHz, 100 kHz, and 30 kHz at 313 K, 303 K, 293 K, 283 K, 273 K, and 263 K, respectively.

This model is an approximation as the real system has nine non-crystallographically equivalent peripheral phenyl groups, each with a potentially different site exchange rate. It is not surprising that the same 4-fold rotation model with a 2:1 population could only provide a qualitative simulation for the spectra of the amorphous **2**-d_{90} samples with all phenyl groups rotating independently. This also suggests that

rotational trajectories are dictated by molecular structures while rotational frequencies and their temperature dependence are determined by the crystallinity of the samples.

While it would be very insightful to document and understand the dynamics of the solvent, we were not able to observe them directly using NMR spectroscopy. As crystals are fragile and tend to desolvate, all measurements had to be carried out in the presence of excess of solvent supernatant. As a result, the signals corresponding to solvent molecules in the crystal lattice could not be properly identified.

2.5. Mechanisms of Rotation of Branch Phenylene and Peripheral Phenyl Groups: Correlated Trityl Group Rotations

While the rotational dynamics of the central phenylene in **2**-d_4 are well accounted for by a two fold-site exchange involving 180° rotations between degenerate sites, the branch phenylenes in **2**-d_{24} and the peripheral phenyl groups is **2**-d_{90} are part of trityl groups and could be expected to undergo correlated (gearing) motions. The fact that suitable simulations for **2**-d_{24} required only a 2-fold site exchange model while those for **2**-d_{90} required a 4-fold site exchange with unequal populations was investigated. We examined the rotational mechanisms for compound **2** with molecular dynamics (MD) simulations using the AMBER14 program.[22] Parameters were generated with the antechamber module using the general Amber force field (GAFF), and atomic partial charges assigned using the AM1-BCC method. Activation free energies in vacuum were obtained for different rotational mechanisms using umbrella sampling, and potentials of mean force (PMF) were constructed using the weighted histogram analysis method (WHAM), with the dihedral angles extracted every 50 fs.[23] As suggested by the space-

filling model (Figure 2.5a), a 2-fold rotation of one phenylene while the other two are completely static is an energetically demanding process because of the proximity of the three phenylene groups. With a calculated barrier of ca. 19 kcal/mol in the vacuum, it is unlikely to occur in the solid state. However, it is possible to have independent rotation of one ring while the other two are oscillating, and the corresponding activation energy was estimated to be only 3–5 kcal/mol in vacuum. Alternatively, the three rings could rotate synchronously to change the absolute configuration of the chiral propeller conformation of the trityl group, a process extensively studied by Mislow and others.[24] In vacuum, this enantiomerization process is associated with angular displacements of ca. 90° and energy barriers of about 1 kcal/mol (Figure 2.5b, dashed curves). Analysis of the lowest energy trajectory suggests a "2-ring flip" mechanism, as proposed by Mislow for trityl isomerization in solution. In the crystal, however, the two enantiomers (*P* and *M*) are in a chiral environment and have different energies. Consequently, if one enantiomer is much higher in energy in the crystal (Figure 2.5b, blue curve), an effective 2-fold rotation (from one *P*-enantiomer to a transient *M*-enantiomer to the next *P*-enantiomer) would be observed, instead of a 4-fold rotation. Under the most extreme circumstances, one enantiomer could be a local maximum (transition state of rotation), and the correlated motion of three phenylenes would also appear to be 2-fold rotations (Figure 2.5b, green curve). As a result, while the experimental data and MD simulation are both consistent with an effective 2-fold rotation in the case of **2**-d_{24}, it is not possible to distinguish between correlated motion of three phenylenes and the independent rotation of one phenylene while the other two oscillate.

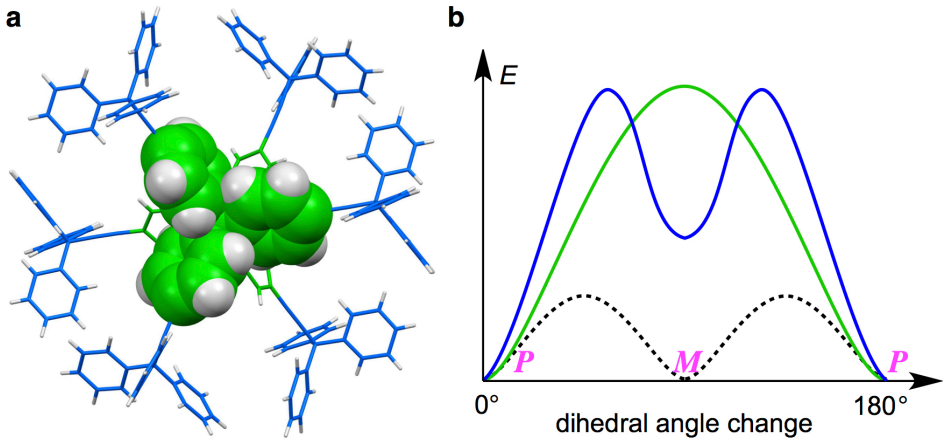

Figure 2.5. (a) Space filling representation of a branch phenylene trityl group indicating the necessity of a correlated process to allow for 2-fold 180˚ rotations. (b) Energy changes of correlated phenylene rotation in a trityl group in vacuum corresponding for apparent 2-fold (green solid curve) and 4-fold (blue solid curve and black dashed curve) rotation modes.

The mechanisms of rotation for the peripheral phenyl groups in **2**-d_{90} samples can also be analyzed as discussed above and considering the potentials shown in Figure 2.5. In fact, the experimentally observed 4-fold rotational model can be understood in terms of a trityl enantiomerization process where the crystallographically observed enantiomer is lower in energy but the second enantiomer is thermally accessible. Thus, a ca. 2:1 population distribution suggested that the two enantiomers (*P* and *M*) are both local minima and the energy difference between them is small. This is also consistent with the crystal structure, where the periphery phenyls displayed larger thermal ellipsoid than the rest of the rotor structure.

2.6. Activation Parameters

The Arrhenius plots constructed from the rotational exchange frequencies observed at each of the experimental temperatures for the central phenylene (**2**-d_4), branch phenylenes (**2**-d_{24}) and peripheral phenyls (**2**-d_{90}) are shown in Figure 2.6. The most significant result is that all the aromatic groups in the structure in the crystals undergo rapid site exchange dynamics near ambient temperature. For the crystalline samples (Table 2.1), the corresponding activation energies (E_a) and pre-exponential factors (A) are 15.7 kcal/mol and 3.5×10^{18} s^{-1} for **2**-d_4, 15.5 kcal/mol and 7.8×10^{17} s^{-1} for **2**-d_{24}, and 13.7 kcal/mol and 7.8×10^{15} s^{-1} for **2**-d_{90}. Similar activation parameters obtained for different aromatic segments in the molecule are consistent with the fact that all of them share contacts (Figure 2.3), and thus a shared potential.

It is important to note that pre-exponential factors on the order of 10^{16}–10^{18} s^{-1} cannot be associated with an elementary process, such as the torsional mode that becomes an internal rotation when provided with sufficient thermal energy. In fact, elementary rotations involving phenylenes groups are limited to values on the order of ca. 10^{12} s^{-1}, as shown by quantum mechanical calculations of the corresponding torsional mode or by classical mechanics calculations based on its moment of inertia.[25] Numerous previous studies with crystalline phenylene rotors have also revealed pre-exponential values of this magnitude, with exception encountered when non-crystalline samples are analyzed.[26] We have previously suggested that abnormally high pre-exponential factors in the solid state can be associated with changes in the fluidity of the structure, rather than with a static potential of the corresponding motions. For example, when exploring the temperature-dependence of the rotational dynamics of a *p*-phenylene group in a periodic mesoporous

organosilicate (PMO), we obtained non-linear data within a temperature region indicating an apparent activation energy of 47 kcal/mol and an apparent pre-exponential value of 4.0 × 10^{41} s^{-1}, both of which are, of course, nonsensical.[26] Further analysis based on differential scanning calorimetry (DSC) supported a reasonable interpretation for the observed results. It was shown that the steep slope of the rotational frequency vs. inverse temperature in the corresponding Arrhenius plot was the result of the structural softening that occurs when the 2D rigid glass becomes a 2D rotational fluid, during a second order glass transition. In a similar manner, we propose that a large slope and intercept in the Arrhenius plot of crystalline dendrimeric molecular rotor **2** is the result of a crystal structure that becomes increasingly soft, or more "fluid-like" as the temperature increases. We would like to suggest the term *crystal fluidity* to convey the softening of the local environment in crystals that results from the temperature-dependent conformational motions, librations, group rotations, and presumably solvent dynamics.

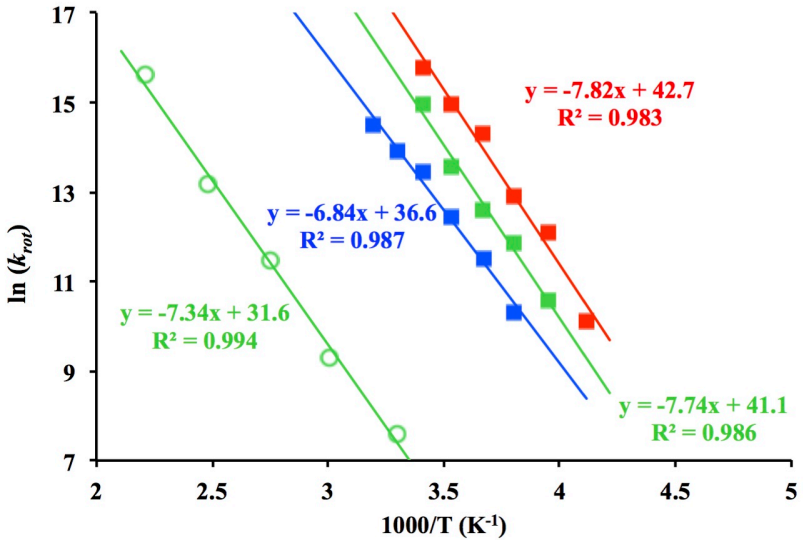

Figure 2.6. Arrhenius plots for crystalline (filled squares) and amorphous samples (open circles) of isotopologues of **2**-d_4 (red), **2**-d_{24} (green), and **2**-d_{90} (blue).

Table 2.1. Summary of apparent activation parameters.

Sample	E_a (kcal/mol)	A (s^{-1})
2-d_4, crystalline	15.7	3.5×10^{18}
2-d_{24}, crystalline	15.5	7.8×10^{17}
2-d_{24}, amorphous	14.7	5.3×10^{13}
2-d_{90}, crystalline	13.7	7.8×10^{15}

If we assume that the correct pre-exponential factor for any given potential is dictated by the torsional motion of a phenylene with a constant value of ca. 1.0×10^{12} s^{-1}, we can estimate a "corrected" activation energy for every temperature. In the case of **2**-d_4 the experimental data would be consistent with an energy barrier that changes from 7.9 kcal/mol at 253 K, when the structure is relatively rigid, to a barrier of 6.9 kcal/mol at 293 K as the structure becomes more fluid. A similar analysis for the data obtained in the case of **2**-d_{24} gives what would be "corrected" activation energies of 8.6 and 7.4 kcal/mol at 253 and 293 K, respectively. Thus, it is reasonable to conclude that the dynamic behavior observed with crystals of **2**-d_4 and **2**-d_{24} is the result of a barrier change of ca. 1 kcal/mol over a rather modest temperature range of only 40 K. A similar analysis with samples of amorphous **2**-d_{24} showed that variations in the "corrected" activation energy over a similar temperature interval are much smaller (Table A.2.1). Furthermore, an interpretation based on a decreasing barrier is also consistent with the fact that all aromatic groups are undergoing temperature-activated, fast rotational dynamics, such that their local potential becomes increasingly fluid.

2.7. Conclusions

A highly efficient convergent synthesis was developed for the synthesis of a macromolecular dendritic rotor in its natural abundance and selectively deuterated forms to carry out quadrupolar echo ^{2}H NMR line shape analysis. Amphidynamic crystals obtained from a mixture of 2,4,6-trimethylpyridine and 2,2,4-trimethylpentane showed a low-density structure that allows for the fast rotation of all the aromatic groups, including one located at the core, six located at the branches, and 18 at the periphery. It is notable that the rotational frequencies of the three segments of the structures reach the megahertz regime near ambient temperatures and exhibit similar activation parameters. While close activation energies are consistent with rotational potentials based on interactions between the three parts of the structure, pre-exponential factors that are up to 6 orders of magnitude larger than those expected for elementary processes are interpreted in terms of a temperature-induced softening of the packing structure. These observations indicate that rotational dynamics in this hyperbranched structure depend more on the fluidity of the crystal than on the contacts and interactions that would make up a static potential derived from the equilibrium position of the atoms in the structure.

2.8. Experimental

2.8.1. General Methods

Unless otherwise notified all commercially available compounds were purchased and used as received without further purification. 3,3,3-Triphenylpropyne **3**[5g] and 3,3,3-triphenylpropyne-**3**-d_{15}[9] were prepared as previously reported in the literature. Thin-layer chromatography (TLC) plates pre-coated with silica gel 60 F_{254} were purchased and they were visualized using a UV lamp. Flash column chromatography was performed using silica gel (230–400 mesh) as the stationary phase. Anhydrous tetrahydrofuran (THF) and benzene (PhH) were distilled from sodium-benzophenone in a continuous still under an atmosphere of argon. Anhydrous toluene (Tol) was distilled from calcium hydride under argon. Triethylamine (NEt_3) was dried over potassium hydroxide (KOH) overnight before used. Melting points of solids were measured without calibration of the apparatus. ^{1}H NMR and ^{13}C NMR spectra in solution were recorded at 500 MHz and 125 MHz, respectively. Chemical shifts are reported in ppm and the (residual) solvent signals of $CDCl_3$ (^{1}H NMR: δ 7.26 ppm; ^{13}C NMR: δ 77.0 ppm) were used as reference. Multiplicities of the peaks are reported as singlet (s), doublet (d), triplet (t), or multiplet (m). The coupling constants J are reported in Hz. Infrared spectra (IR) were obtained with a HATR-FTIR instrument. Mass spectra were acquired on MALDI-TOF (low-res), LIFDI-TOF (high-res), and ESI/APCI-TOF (high-res) instruments.

2.8.2. Synthesis and Characterization

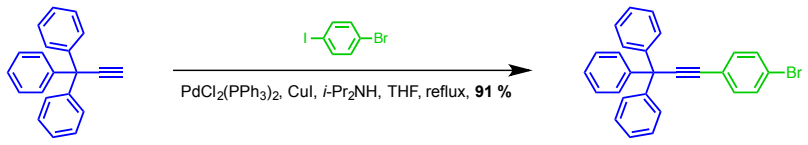

3 **4**

To a 250 mL 3-neck flask with stir bar and condenser were added 3,3,3-triphenylpropyne **3** (2.007 g, 7.48 mmol), 4-bromo-1-iodobenzene (2.116 g, 7.48 mmol), anhydrous THF (80 mL), and di-*iso*-propylamine (40 mL) under argon. The resulting mixture was degased for 60 min before palladium bis(triphenylphosphine) dichloride (524 mg, 0.748 mmol) and copper iodide (0.142 g, 0.748 mmol) were added into the flask. The reaction mixture was refluxed for 6 hours and then cooled down to room temperature. Saturated NH_4Cl solution (100 mL) was added in to quench the reaction, and the compound was extracted with DCM (100 mL) twice. The combined organic layers were washed with brine, dried over anhydrous $MgSO_4$, and concentrated to give a crude. Flash column chromatography of the crude product using hexanes as the eluent provided the desired compound **4** (2.890 g, 91 %).

4: White solid, m.p. 139–140 °C; ^{1}H NMR (500 MHz, $CDCl_3$, ppm): δ 7.27–7.32 (m, 15H), 7.36–7.37 (m, 2H), 7.44–7.46 (m, 2H); ^{13}C NMR (125 MHz, $CDCl_3$, ppm): δ 56.1, 84.0, 96.9, 122.2, 122.5, 126.9, 128.1, 129.1, 131.5, 133.1, 145.1; IR (powder, cm^{-1}): ν 695(s), 743(s), 757(s), 827(s), 890(w), 1009(m), 1032(m), 1069(m), 1178(w), 1261(w), 1394(w), 1445(m), 1487(s), 1597(m), 1728(w), 3031(w), 3056(w); HRMS (ESI/APCI, TOF): m/z calculated for $C_{27}H_{20}Br$ (MH^+): 420.0743, found: 420.0738.

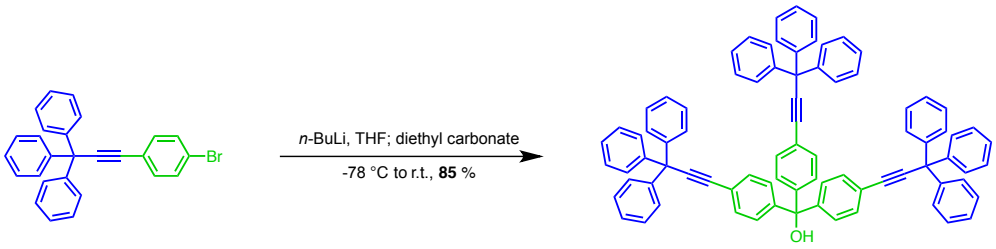

4 **5**

To a solution of arylbromide **4** (1.009 g, 2.38 mmol) in anhydrous THF (10 mL) in a round bottom flask was add *n*-BuLi (1.09 M solution in hexane, 2.83 mL, 3.08 mmol) dropwise under argon at –78 °C. The reaction mixture was stirred in the cooling bath for 1 hour before an excess of diethyl carbonate (0.58 mL, 4.79 mmol) was added into the flask and it was stirred for another hour before it was allowed to warm up to room temperature. Saturated NH_4Cl solution (50 mL) was added in to quench the reaction, and the product was extracted with diethyl ether (50 mL) twice. The combined organic layers were washed consecutively with water and brine, dried over anhydrous $MgSO_4$, and concentrated to give a brownish crude. Flash column chromatography of the crude product (dry loading) using a hexanes-ether mixture (4:1, v/v) as the eluent provided the desired compound **5** (715 mg, 85 %).

5: White solid, m.p. 286–287 °C; ^{1}H NMR (500 MHz, $CDCl_3$, ppm): δ 2.75 (s, 1H), 7.24 (app. d, J = 9.0 Hz, 6H), 7.27–7.36 (m, 45H), 7.48 (app. d, J = 9.0 Hz, 6H); ^{13}C NMR (125 MHz, $CDCl_3$, ppm): δ 56.1, 81.6, 84.7, 96.2, 122.8, 126.8, 127.7, 128.0, 129.1, 131.3, 145.2, 145.9; IR (powder, cm^{-1}): ν 695(s), 744(s), 830(s), 890(w), 907(w), 1024(m), 1184(m), 1319(w), 1403(w), 1446(m), 1490(s), 1596(m), 3026(w), 3058(w), 3569(w); HRMS (LIFDI, TOF): m/z calculated for $C_{82}H_{58}O$ (M^+): 1058.4482, found: 1058.4448.

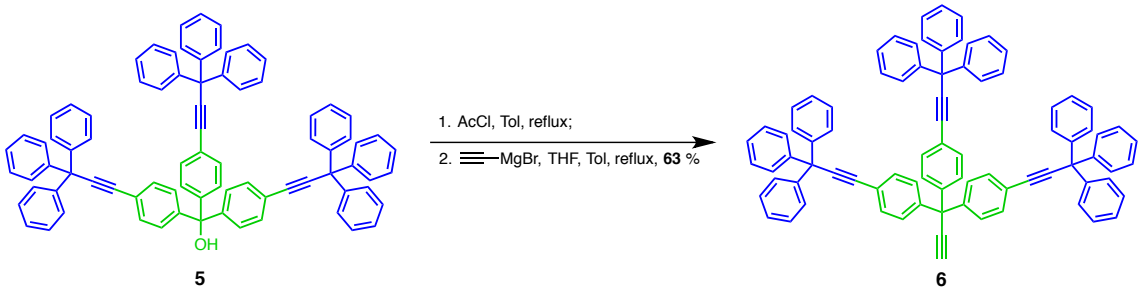

Triarylmethanol **5** (1126 mg, 1.063 mmol), anhydrous toluene (5 mL), and acetyl chloride (5 mL) were added to a round bottom flask equipped with a condenser, and the resulting mixture was heated up to reflux for 5 hours. The solvents were removed by evaporation under reduced pressure. Anhydrous toluene (10 mL) was added into the flask and the solvent was removed again. The residue was taken up in 100 mL anhydrous toluene. The toluene solution was heated to reflux under Ar before ethynylmagnesium bromide (0.5 M solution in THF, 10 mL, 5.0 mmol) was added to the flask, and the reaction mixture was heated to reflux overnight before it was allowed to cool down to room temperature. Saturated NH_4Cl solution (50 mL) was added in to quench the reaction, and the compound was extracted with DCM (200 mL). The organic layer was washed with brine, dried over anhydrous Na_2SO_4, and concentrated to give a dark brown crude. Flash column chromatography (dry loading) of the crude product using a mixture of hexanes and DCM (4:1, v/v) as the eluent yielded the desired compound **6** (720 mg, 63 %).

6: White solid, m.p. 254–255 °C; ^{1}H NMR (500 MHz, $CDCl_3$, ppm): δ 2.77 (s, 1H), 7.27 (app. d, J = 8.5 Hz, 6H), 7.29–7.40 (m, 45H), 7.50 (app. d, J = 8.5 Hz, 6H); ^{13}C NMR (125 MHz, $CDCl_3$, ppm): δ 55.1, 56.1, 74.3, 84.7, 88.4, 96.2, 122.5, 126.8, 128.0, 128.9, 129.1, 131.4, 144.0, 145.2; IR (powder, cm^{-1}): ν 696(s), 743(s), 827(s), 890(w), 1025(m), 1026(m), 1079(w), 1183(m), 1283(w), 1406(w), 1446(m), 1490(s),

1596(m), 3026(w), 3058(w), 3298(w); HRMS (ESI/APCI, TOF): m/z calculated for $C_{84}H_{59}$ (MH^+): 1067.4611, found: 1067.4620.

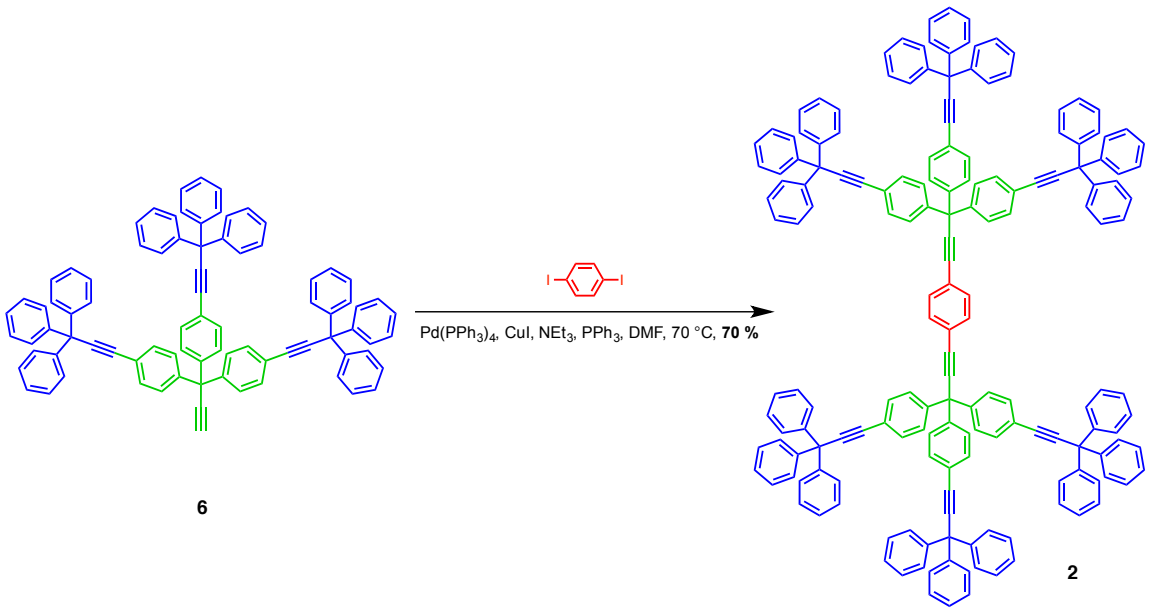

To a 10 mL round bottom flask was added **6** (73 mg, 0.068 mmol), 1,4-diiodobenzene (12.3 mg, 0.037 mmol), triphenylphosphine (5.2 mg, 0.020 mmol), and triethylamine (0.3 mL) in anhydrous DMF (2.5 mL), and the resulting mixture was cooled down to –78 °C before it was connected to vacuum for 30 min to remove residual oxygen dissolved in the solvent. Then palladium tetrakis(triphenylphosphine) (11.6 mg, 0.010 mmol) and copper iodide (1.9 mg, 0.010 mmol) were added to the flask under argon. The reaction mixture was stirred at 70 °C overnight and it was then poured into saturated NH_4Cl solution (20 mL). The mixture was extracted with DCM (20 mL) twice and the combined organic layers were washed with H_2O and brine consecutively, and dried over Na_2SO_4. The solvent was removed *in vacuo* and a light brown crude was obtained. Flash column chromatography (dry loading) using a mixture of hexanes and DCM (3:1, v/v) removed most of the impurities in the crude. Further purification by

crystallizations from a hexanes-benzene mixture (2:1, v/v) yielded the pure product **2** (52 mg, 70 %).

2: White solid, m.p. 401–403 °C; ^{1}H NMR (500 MHz, $CDCl_3$, ppm): δ 7.26–7.36 (m, 102H), 7.43 (s, 4H), 7.48 (app. d, J = 9.0 Hz, 12H); ^{13}C NMR (125 MHz, $CDCl_3$, ppm): δ 55.8, 56.1, 84.7, 85.5, 96.0, 96.2, 122.5, 122.9, 126.8, 128.0, 128.9, 129.1, 131.5, 131.5, 144.4, 145.2; IR (powder, cm^{-1}): ν 696(s), 743(s), 830(m), 890(w), 1025(m), 1184(m), 1261(w), 1405(w), 1447(m), 1490(s), 1596(m), 3028(w), 3058(w); MS (MALDI, TOF): m/z calculated for $C_{174}H_{118}Na$ (MNa^+): 2231 (100 %), 2232 (94 %), 2233 (58 %), 2230 (53 %), 2234 (18 %), found: 2231(100 %), 2232 (89 %), 2233 (60 %), 2230 (58 %), 2234 (28 %).

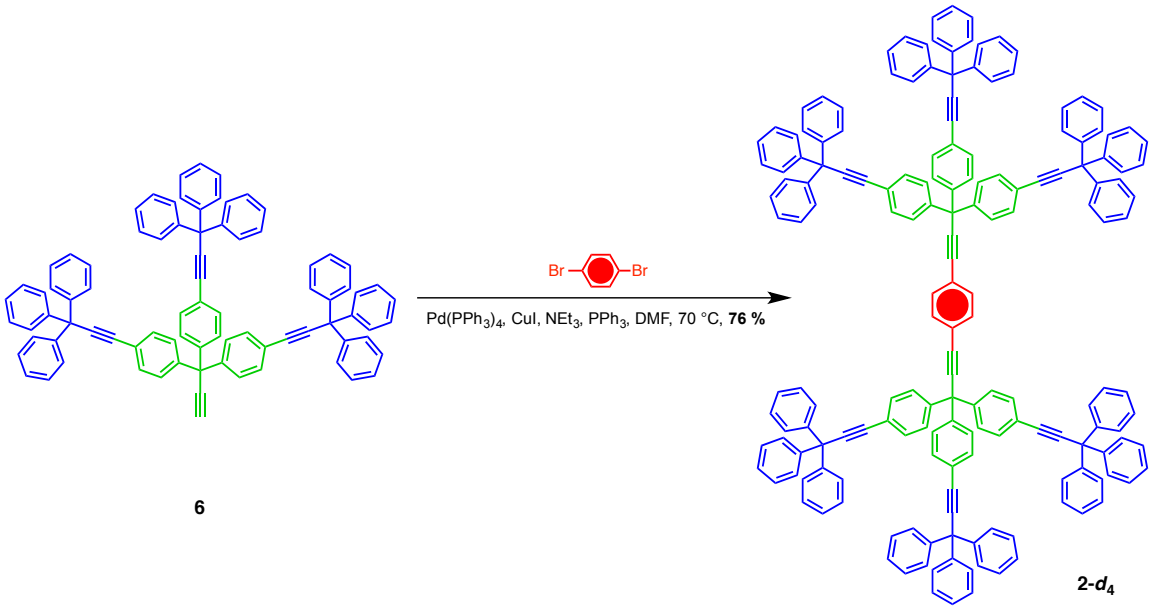

To a 25 mL round bottom flask was added **6** (300 mg, 0.281 mmol), 1,4-dibromobenzene-d_4 (33.7 mg, 0.140 mmol), triphenylphosphine (14.7 mg, 0.056 mmol), and triethylamine (0.5 mL) in anhydrous DMF (3 mL), and the resulting mixture was cooled down to –78 °C before it was connected to vacuum for 30 min to remove oxygen

dissolved in the solvent. Then palladium tetrakis(triphenylphosphine) (32 mg, 0.028 mmol) and copper iodide (5.3 mg, 0.028 mmol) were added into the flask under argon atmosphere. The reaction mixture was stirred at 70 °C overnight before it was poured into saturated NH_4Cl solution (50 mL). The compound was extracted with DCM (30 mL) twice and the combined organic layers were washed with H_2O and brine consecutively, and dried over anhydrous Na_2SO_4. The solvent was removed *in vacuo* and a light brown crude was obtained. Flash column chromatography (dry loading) using a mixture of hexanes and DCM (3:1, v/v) removed most of the impurities in the crude. Further purification by crystallizations from a hexanes-benzene mixture (1:1, v/v) yielded the pure product **2**-d_4 (237 mg, 76 %).

2-d_4: White solid, m.p. 400–401 °C; ^{1}H NMR (500 MHz, $CDCl_3$, ppm): δ 7.24–7.33 (m, 102H), 7.46 (app. d, J = 8.5 Hz, 12H); ^{13}C NMR (125 MHz, $CDCl_3$, ppm): δ 55.8, 56.1, 84.7, 85.5, 96.1, 96.2, 122.5, 122.7, 126.8, 128.0, 128.9, 129.1, 131.1 (t, J = 25.0 Hz), 131.5, 144.4, 145.2; IR (powder, cm^{-1}): ν 695(s), 744(s), 829(m), 891(w), 1026(m), 1079(w), 1184(w), 1446(m), 1490(m), 1596(w), 3026(w), 3058(w); MS (MALDI, TOF): m/z calculated for $C_{174}H_{114}D_4Na$ (MNa^+): 2235 (100 %), 2236 (95%), 2237 (59 %), 2234 (53 %), 2238 (27 %), found: 2235 (100 %), 2236 (85%), 2237 (61 %), 2234 (52 %), 2238 (32 %).

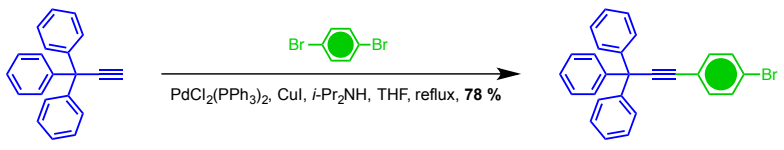

3 **4**-d_4

To a 3-neck flask with stir bar, additional funnel, and condenser were added 1,4-dibromobenzene-d_4 (5.001 g, 20.8 mmol), anhydrous THF (20 mL), and di-*iso*-propylamine (20 mL) under argon. 3,3,3-Triphenylpropyne **3** (1.000 g, 3.73 mmol) was dissolved in anhydrous THF (20 mL) in the additional funnel. Both the solutions were degased for 30 min before palladium bis(triphenylphosphine) dichloride (78 mg, 0.11 mmol) and copper iodide (21 mg, 0.11 mmol) were added into the flask. The reaction mixture in the 3-neck flask was heated to reflux and then the solution of **3** in the additional funnel was added into the flask slowly over 30 min. The reaction mixture was reflux for 2 hours before it was allowed to cool down to room temperature. Saturated NH_4Cl solution (100 mL) was added in to quench the reaction, and the compound was extracted with ether (100 mL) twice. The combined organic layers were washed with water and brine, dried over Na_2SO_4. The solvent was evaporated *in vacuo* and flash column chromatography of the residue using hexanes as the eluent provided the desired compound **4**-d_4 (1.241 g, 78 %).

4-d_4: White solid, m.p. 139–140 °C; ^{1}H NMR (500 MHz, $CDCl_3$, ppm): δ 7.30–7.41 (m, 15H); ^{13}C NMR (125 MHz, $CDCl_3$, ppm): δ 56.1, 84.0, 96.9, 121.9, 122.2, 126.9, 128.0, 129.1, 131.0 (t, J = 25.5 Hz), 132.6 (t, J = 25.2 Hz), 145.0; IR (powder, cm^{-1}): ν 696(s), 735(s), 754(s), 818(w), 890(w), 1017(m), 1032(m), 1079(w), 1180 (w), 1307(w), 1386(m), 1445(m), 1490(m), 1596(w), 1954(w), 3023(w), 3057(w); HRMS (ESI/APCI, TOF): m/z calculated for $C_{27}H_{16}D_4Br$ (MH^+): 427.0994, found: 427.0996.

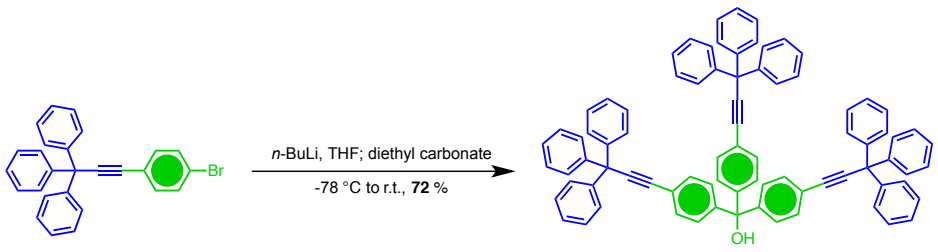

4-d_4 **5**-d_{12}

To a solution of arylbromide **4**-d_4 (1628 mg, 3.81 mmol) in THF (20 mL) in a 100 mL round bottom flask in an acetone-dry ice bath was added *n*-BuLi (1.6 M solution in hexane, 2.40 mL, 3.84 mmol) under argon atmosphere. The reaction mixture was stirred in the chilling bath for 1 hour before an excess of diethyl carbonate (1.0 mL, 8.3 mmol) was added into the flask. The reaction mixture was stirred at –78 °C for another hour and it was allowed to gradually warm up to room temperature. Saturated NH_4Cl solution (50 mL) was added in to quench the reaction, and the compound was extracted with DCM (50 mL) twice. The combined organic layers were washed consecutively with water and brine, dried over Na_2SO_4, and concentrated to give a yellow crude. Flash column chromatography of the crude product (dry loading) using a hexanes-ether mixture (4:1, v/v) as the eluent provided the desired compound **5**-d_{12} (976 mg, 72 %).

5-d_{12}: Yellow Solid, m.p. 285–286 °C; ^{1}H NMR (500 MHz, $CDCl_3$, ppm): δ 2.78 (s, 1H), 7.30–7.33 (m, 9H), 7.35–7.38 (m, 18H), 7.40–7.41 (m, 18H); ^{13}C NMR (125 MHz, $CDCl_3$, ppm): δ 56.1, 81.5, 84.6, 96.2, 122.6, 126.8, 127.3 (t, J = 24.1 Hz), 128.0, 129.1, 130.9 (t, J = 24.3 Hz), 145.2, 145.8; IR (powder, cm^{-1}): ν 680(m), 696(s), 740(m), 756(m), 828(w), 900(m), 1000(w), 1032(m), 1102(w), 1185(w), 1322(w), 1417(w), 1447(m), 1490(m), 1596(w), 3026(w), 3058(w), 3563(w); HRMS (LIFDI, TOF): m/z calculated for $C_{82}H_{46}D_{12}O$ (M^+): 1070.5235, found: 1070.5280.

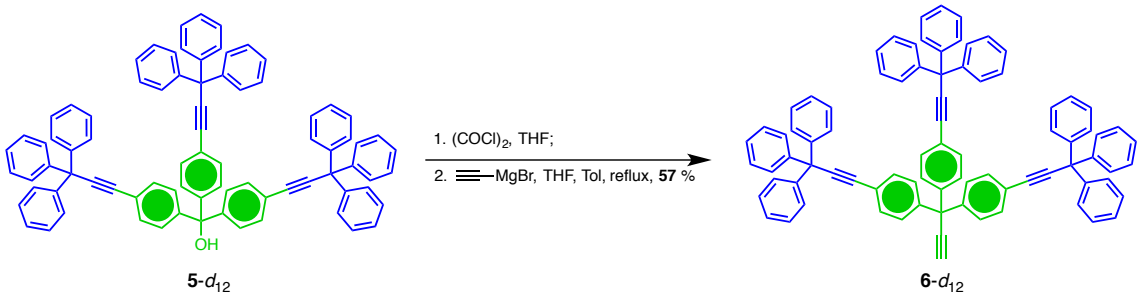

5-d_{12} **6**-d_{12}

Triarylmethanol **5**-d_{12} (976 mg, 0.91 mmol), anhydrous THF (5 mL), and oxalyl chloride (2.0 mL) were added to a round bottom flask and the resulting mixture was stirred at room temperature overnight. The solvents were then removed by evaporation *in vacuo*. The residue was taken up in anhydrous toluene (10 mL) and the solvent was removed again. The residue was dissolved in anhydrous toluene (50 mL) and the resulting solution was heated up to reflux under argon. Ethynylmagnesium bromide (0.5 M solution in THF, 10.0 mL, 5.0 mmol) was added to the flask, and the reaction mixture was refluxed for 4h before it was allowed to cool down to room temperature. Saturated NH_4Cl solution (30 mL) was added in to quench the reaction, and the mixture was extracted with DCM (50 mL) twice. The combined organic layers were washed with brine, dried over Na_2SO_4, and concentrated to give a brown crude. Flash column chromatography (dry loading) of the crude product using a mixture of hexanes and DCM (4:1, v/v) as the eluent yielded the desired compound **6**-d_{12} (565 mg, 57 %).

6-d_{12}: White solid, m.p. 285–286 °C; ^{1}H NMR (500 MHz, $CDCl_3$, ppm): δ 2.72 (s, 1H), 7.23–7.33 (m, 45H); ^{13}C NMR (125 MHz, $CDCl_3$, ppm): δ 55.0, 56.1, 74.2, 84.6, 88.4, 96.2, 122.3, 126.8, 128.0, 128.4 (t, J = 24.2 Hz), 129.1, 131.0 (t, J = 24.2 Hz), 143.8, 145.2; IR (powder, cm^{-1}): ν 680(m), 696(s), 722(w), 756(s), 871(w), 902(w), 1002(w), 1033(m), 1080(w), 1158(w), 1183(w), 1322(w), 1411(m), 1447(s), 1490(s),

1596(m), 1952(w), 3022(w), 3059(w), 3284(w); HRMS (ESI/APCI, TOF): m/z calculated for $C_{84}H_{47}D_{12}$ (MH^+): 1079.5365, found: 1079.5374.

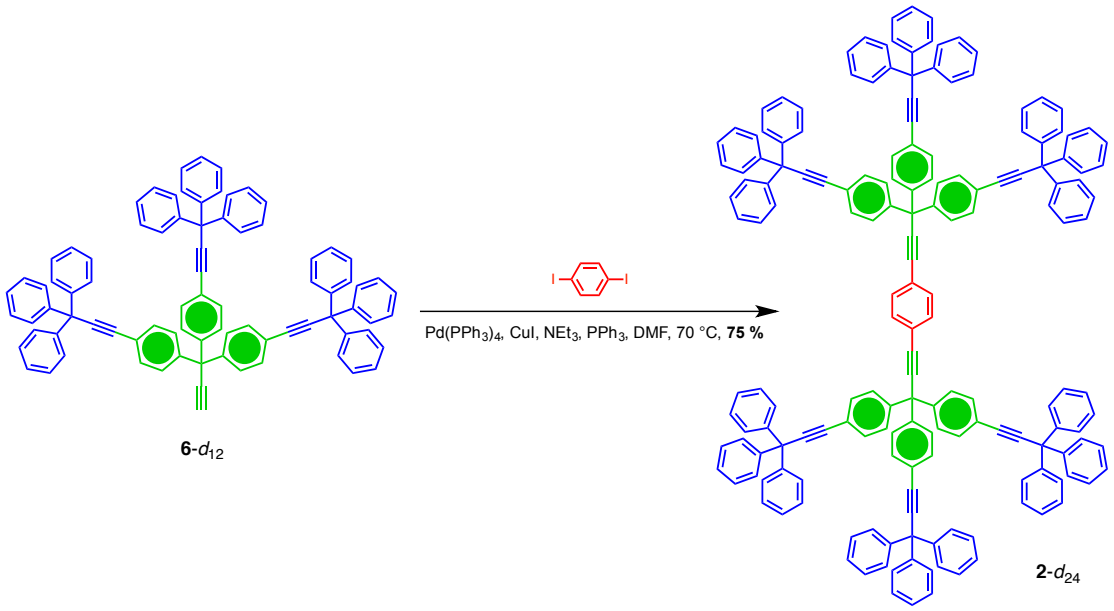

To a round bottom flask was added **6**-d_{12} (565 mg, 0.523 mmol), 1,4-diiodobenzene (86.3 mg, 0.261 mmol), triphenylphosphine (27 mg, 0.10 mmol), and triethylamine (1 mL) in anhydrous DMF (5 mL) under argon. The flask was placed in an acetone-dry ice bath and connected to vacuum for 30 min to remove residual oxygen. Then palladium tetrakis(triphenylphosphine) (60 mg, 0.052 mmol) and copper iodide (10 mg, 0.053 mmol) were then added into the flask. The reaction mixture was stirred at 70 °C overnight before it was cooled back to room temperature and poured into saturated NH_4Cl solution (50 mL). The compound was extracted with DCM (30 mL) twice and the combined organic layers were washed with H_2O and brine, and dried over anhydrous Na_2SO_4. The solvent was removed *in vacuo* and a light brown crude was obtained. Flash column chromatography (dry loading) using a mixture of hexanes and DCM (3:1, v/v)

removed most of the impurities in the crude. Further purification by crystallizations from a hexanes-benzene mixture (1:1, v/v) yielded the pure product **2**-d_{24} (440 mg, 75 %).

2-d_{24}: white solid, m.p. 401–402 °C; ^{1}H NMR (500 MHz, $CDCl_3$, ppm): δ 7.26–7.36 (m, 90H), 7.43 (s, 4H); ^{13}C NMR (125 MHz, $CDCl_3$, ppm): δ 55.7, 56.1, 84.7, 85.5, 96.0, 96.2, 122.3, 122.9, 126.8, 128.0, 128.5 (t, J = 22.8 Hz), 129.1, 131.1 (t, J = 22.8 Hz), 131.5, 144.2, 145.2; IR (powder, cm^{-1}): ν 677(s), 696(s), 723(w), 739(w), 758(m), 840(w), 870(w), 902(w), 1033(w), 1079(w), 1182(w), 1323(w), 1410(w), 1446(m), 1490(m), 1596(w), 3027(w), 3059(w); MS (MALDI, TOF): m/z calculated for $C_{174}H_{94}D_{24}Na$ (MNa^+): 2255 (100 %), 2256 (95 %), 2257 (59 %), 2254 (53.1 %), 2258 (27 %), found: 2255 (100 %), 2256 (80 %), 2257 (40 %), 2254 (60 %), 2258 (28 %).

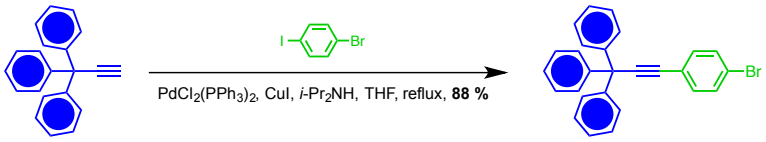

3-d_{15} **4**-d_{15}

To a 100 mL round bottom flask with stir bar and condenser were added 3,3,3-triphenylpropyne **3**-d_{15} (283 mg, 1.00 mmol), 4-bromo-1-iodobenzene (425 mg, 1.50 mmol), THF (10 mL), and di-*iso*-propylamine (10 mL) under Ar. The resulting mixture was purged with argon for 20 min before palladium bis(triphenylphosphine) dichloride (14 mg, 0.02 mmol) and copper iodide (4 mg, 0.02 mmol) were added into the flask. The reaction mixture was heated to reflux for 1h before it was cooled down to room temperature. Saturated NH_4Cl solution (50 mL) was added in to quench the reaction, and the compound was extracted with ether (50 mL) twice. The combined organic layers were washed with brine, dried over Na_2SO_4, and concentrated under

vacuum to give a dark brown crude. Flash column chromatography of the crude product using a mixture of hexanes and DCM (10:1, v/v) as the eluent provided the desired compound **4**-d_{15} (385 mg, 88 %).

4-d_{15}: White solid, m.p. 131–132 °C; ^{1}H NMR (500 MHz, $CDCl_3$, ppm): δ 7.36 (app. d, J = 8.5 Hz, 2H), 7.45 (app. d, J = 8.5 Hz, 2H); ^{13}C NMR (125 MHz, $CDCl_3$, ppm): δ 55.9 (weak signal due to lack of efficient relaxation), 83.9, 96.9, 122.2, 122.5, 126.4 (t, J = 24.0 Hz), 127.5 (t, J = 24.1 Hz), 128.7 (t, J = 24.5 Hz), 131.5, 133.1, 144.9; IR (powder, cm^{-1}): ν 661(w), 750(w), 789(m), 821(s), 836(m), 865(m), 905(m), 961(w), 1012(m), 1071(m), 1095(w), 1261(w), 1330(m), 1362(m), 1393(w), 1486(s), 1560(w), 2274(w); HRMS (ESI/APCI, TOF): m/z calculated for $C_{27}H_5D_{15}Br$ (MH^+): 438.1684, found: 438.1687.

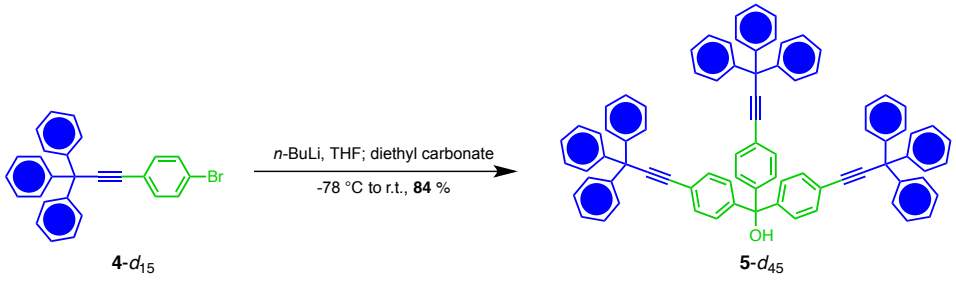

4-d_{15} **5**-d_{45}

To a solution of arylbromide **4**-d_{15} (801 mg, 1.83 mmol) in THF (20 mL) in a round bottom flask was add *n*-BuLi (1.6 M solution in hexane, 1.4 mL, 2.24 mmol) under argon at –78 °C. The reaction mixture was stirred for 1 hour before an excess of diethyl carbonate (0.08 mL, 0.66 mmol) was added into the flask. The reaction mixture was stirred for another hour before it was allowed to warm up to room temperature. Saturated NH_4Cl solution (50 mL) was added in to quench the reaction, and the product was extracted with DCM (50 mL) twice. The combined organic layers were washed with

water and brine, dried over Na_2SO_4, and then concentrated to give a crude. Flash column chromatography of the crude product (dry loading) using a hexanes-ether mixture (4:1, v/v) as the eluent provided the desired compound **5**-d_{45} (563 mg, 84 %).

5-d_{45}: White solid, m.p. 286–287 °C; ^{1}H NMR (500 MHz, $CDCl_3$, ppm): δ 2.73 (s, 1H), 7.25 (app. d, J = 8.5 Hz, 6H), 7.49 (app. d, J = 8.5 Hz, 6H); ^{13}C NMR (125 MHz, $CDCl_3$, ppm): δ 55.9, 81.6, 84.6, 96.2, 122.8, 126.3 (t, J = 22.2 Hz), 127.5 (t, J = 24.0 Hz), 127.7, 128.7 (t, J = 24.0 Hz), 131.3, 145.1, 145.9; IR (powder, cm^{-1}): ν 749(w), 786(m), 827(s), 866(m), 904(m), 961(w), 1014(m), 1154(w), 1327(m), 1362(m), 1403(w), 1502(m), 1560(w), 2275(w), 3559(w); HRMS (LIFDI, TOF): m/z calculated for $C_{82}H_{13}D_{45}O$ (M^+): 1103.7307, found: 1103.7301.

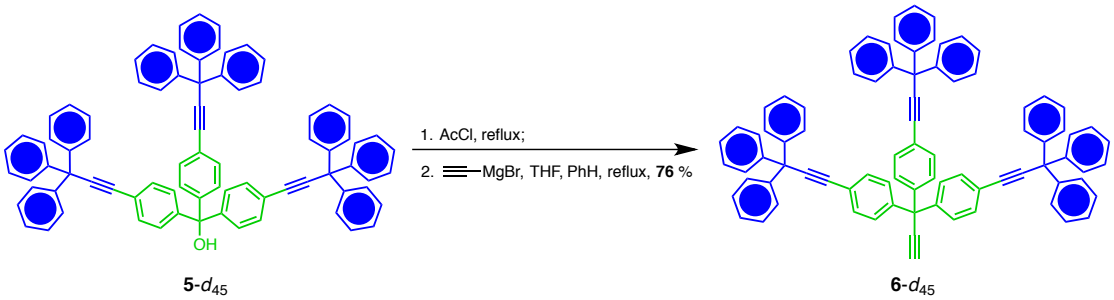

5-d_{45} **6**-d_{45}

Triarylmethanol **5**-d_{45} (563 mg, 0.510 mmol) and acetyl chloride (20 mL) were added to a round bottom flask equipped with a condenser, and the resulting mixture was heated up to reflux for 2 hours before the excess of acetyl chloride were removed by evaporation under reduced pressure. The residue was dissolved in anhydrous benzene (50 mL) and ethynylmagnesium bromide (0.5 M solution in THF, 6.0 mL, 3.0 mmol) was added to the flask, and the reaction mixture was heated to reflux overnight under argon. Saturated NH_4Cl solution (50 mL) was added in to quench the reaction, and the compound was extracted with DCM (50 mL) twice. The combined organic layers were

washed with brine, dried over Na_2SO_4, and concentrated to give a pale yellow crude. Flash column chromatography of the crude product using a mixture of hexanes and ether (4:1, v/v) as the eluent yielded the desired compound **6**-d_{45} (430 mg, 76 %).

6-d_{45}: White Solid, m.p. 252–254 °C; ^{1}H NMR (500 MHz, $CDCl_3$, ppm): δ 2.83 (s, 1H), 7.38 (app. d, J = 8.5 Hz, 6H), 7.60 (app. d, J = 8.5 Hz, 6H); ^{13}C NMR (125 MHz, $CDCl_3$, ppm): δ 55.1, 55.9, 74.3, 84.6, 88.4, 96.2, 122.5, 126.3 (t, J = 21.7 Hz), 127.5 (t, J = 23.8 Hz), 128.7 (t, J = 23.7 Hz), 128.9, 131.4, 143.9, 145.0; IR (powder, cm^{-1}): ν 657(w), 748(w), 787(m), 826(s), 866(m), 904(m), 961(w), 1020(w), 1185(w), 1328(m), 1362(m), 1405(w), 1499(m), 1560(w), 2276(w), 3293(w); HRMS (ESI/APCI, TOF): m/z calculated for $C_{84}H_{14}D_{45}$ (MH^+): 1112.7436, found: 1112.7449.

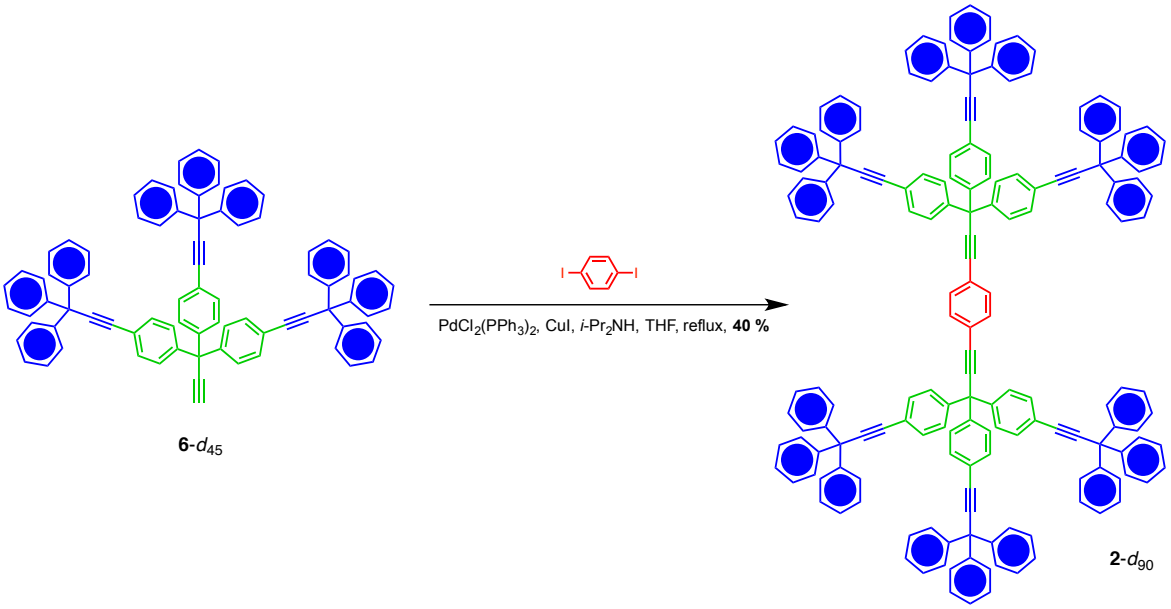

To a 50 mL 3-neck flask was added **6**-d_{45} (550 mg, 0.494 mmol), 1,4-diiodobenzene (74 mg, 0.22 mmol), THF (20 mL), and di-*iso*-propylamine (5 mL), and the resulting mixture was degased for 30 min before palladium bis(triphenylphosphine) dichloride (31 mg, 0.044 mmol) and copper iodide (8.4 mg, 0.044 mmol) were added to

the flask under argon atmosphere. The reaction mixture was refluxed overnight before it was poured into saturated NH_4Cl solution (50 mL). The mixture was extracted with DCM (50 mL) twice and the combined organic layers were washed with brine, and dried over anhydrous Na_2SO_4. The solvent was removed *in vacuo* and a light brown crude was obtained. Flash column chromatography (dry loading) using a hexanes-DCM mixture (3:1, v/v) as the eluent removed most of the impurities in the crude, but a significant amount of Further purification by fractional crystallization from a benzene and hexanes mixture (1:1, v/v) provided the desired product **2**-d_{90} (208 mg, 40 %).

2-d_{90}: White solid, m.p. 405–406 °C; ^{1}H NMR (500 MHz, $CDCl_3$, ppm): δ 7.25 (app. d, J = 8.5 Hz, 6H), 7.40 (s, 4H), 7.46 (app. d, J = 8.5 Hz, 6H); ^{13}C NMR (125 MHz, $CDCl_3$, ppm): δ 55.8, 55.9, 84.6, 85.5, 96.0, 96.2, 122.5, 122.9, 126.3 (t, J = 23.1 Hz), 127.5 (t, J = 23.9 Hz), 128.7 (t, J = 24.1 Hz), 128.9, 131.5, 144.4, 145.1; IR (powder, cm^{-1}): ν 657(w), 695(w), 748(w), 787(m), 827(s), 865(m), 904(m), 961(w), 1020(m), 1185(w), 1328(m), 1362(m), 1404(w), 1500(m), 1560(w), 2276(w); MS (MALDI, TOF): m/z calculated for $C_{174}H_{28}D_{90}Na$ (MNa^+): 2321 (100 %), 2322 (93 %), 2323 (58 %), 2320 (53 %), 2324 (27 %), found: 2321 (100 %), 2322 (60%), 2323 (50 %), 2320 (80 %), 2324 (23 %).

2.8.3. Crystallization Conditions and X-Ray Diffraction of Single Crystals

Colorless prisms of compound **2** could be obtained by addition of 2,2,4-trimethylpentane to a hot solution of **2** in 2,4,6-trimethylpyridine followed by slowly cooling down the mixture to room temperature. Similar crystals could be obtained from a mixture of 2,2,4-trimethylpentane and *o*-xylene in the same manner. For both cases, the volume percentage of 2,2,4-trimethylpentane in the solvent mixture was about 30 %. The prisms were immediately subjected to diffraction after they were removed from the mother liquor to avoid solvent loss. The diffraction data was obtained at 100 K on an X-ray diffractometer system with Mo-Kα radiation (λ = 0.71073 Å) and an area detector. The structure was solved and refined using the SHELXTL software package. All atoms were refined anisotropically, and hydrogen atoms were placed at calculated positions. The disordered solvent molecules were removed using the SQUEEZE algorithm.

2.8.4. Powder X-Ray Diffraction

PXRD Analyses were carried out using Cu-$K_{\alpha 1}$ = 1.5406 Å radiation. Data were collected at room temperature in the range of 2theta = 5–50°. The measurements were done with a thin layer of the sample on a zero-background plate. To prevent the solvent loss of the crystalline sample during the measurement, a drop of 2,2,4-trimethylpentane/2,4,6-trimethylpyridine solvent mixture was added onto the plate.

2.8.5. Solid-State ^{2}H NMR Quadrupolar Echo Experiment

Solid-state ^{2}H NMR spectra were acquired on a Bruker DRX 300 instrument at ^{2}H frequency of 46.07 MHz. In the spin-echo experiments, a quadrupolar-echo sequence with phase cycling was used to suppress undesired single- and double-quantum coherence-transfer artifacts. A pulse of 50 μs with a refocusing delay of 42 μs was used in the sequence. The spectrometer produced 2.5-μs ^{2}H 90-degree pulses (46.07 MHz) with recycle delays of 20 s between pulses inside the coil. Variable temperature experiments were performed between 243 K and 453 K. For all these experiments, 45 mg to 100 mg solid sample was placed inside a borosilicate glass NMR tube between two glass rods and sealed with Teflon tape. For the crystalline samples, small cotton balls saturated with 2,2,4-trimethylpentane/2,4,6-trimethylpyridine solvent mixture were placed at both ends of the tubes to prevent the solvent loss. After any high temperature or low temperature experiments, the samples were cooled/warmed back to the starting temperature and ^{2}H NMR spectra were taken again to ensure that no irreversible transition occurred during the VT experiments. The number of scans to obtain spectra with decent signal to noise ratio ranges from a few hundred to a few thousand. The data was processed with a line broadening of 5 kHz.

2.8.6. Simulation of the Experimental Spectra

All simulation was performed utilizing the online program offered by professor H. W. Spiess.[19] The spectra obtained for **2**-d_4 (crystalline sample) and **2**-d_{24} (crystalline and amorphous samples) were quickly identified to be the result of simple 2-fold rotations (Figure 2.4). For the samples of **2**-d_{90}, the line-shape of the spectra could not be

reproduced with a simple 2-fold rotation model (Figure A.2.45a). Next we considered a 4-fold flips since the intrinsic symmetry of phenyls (C_{2v}) limits their possible dynamics to 2n-fold (n = 1, 2, 3, 4…) flips. It was not surprising that simulations using a simple 4-fold rotation model with even distribution of occupation at all 4 sites also failed to reproduce the experimental line-shapes given that not much disorder was observed crystallographically (Figure A.2.45b). To our delight, the 4-fold rotational model together with a 2:1:2:1 ratio of occupation at the four sites led to simulated spectra matching the experimental ones. Other ratios (3:1:3:1 and 4:1:4:1) were also explored but they offered spectra with line-shapes different from the experimental ones (Figure A.2.46). Including a distribution of rotational frequencies or jump angles did not improve the simulation at all, nor did the complex combination of 2-fold and 4-fold rotation modes. Spectra from those simulations were thus not presented here.

2.8.7. Molecular Dynamics Simulation

Molecular dynamics simulation of rotor **2** was performed using Amber 14. The parameters were generated with the antechamber module using the general Amber force field (GAFF), and the atomic partial charges were assigned using the AM1-BCC method. In the simulation, the structure of **2** was first minimized in vacuum with no solvent model. The system then was heated from 0 to 300 K under constant pressure of 1 atm in 2 ns before it was then equilibrated for 0.5 ns with 1 fs time step at a constant volume. Production trajectories were then run for additional 1 ns under the same simulation conditions. The dihedral angle change of each phenylene groups in one branch trityl unit was tracked and shown in Figure A.2.47. Although much less frequent compared to the

correlated motions, isolated rotation of one aromatic ring is indeed possible even in vacuum.

The activation energies of branch phenylenes rotation in vacuum were studied using umbrella sampling and potentials of mean force (PMF) were constructed using Weighted Histogram Analysis Method (WHAM) with the dihedral angles extracted every 50 fs. At each window, 1ns MD was performed with harmonic potential applied on the dihedral at 300 K under 1 atm pressure. When one phenylene explored 180-degree dihedral angle change from the lowest-energy-state with a 5° step width, the other two phenylene rings was allowed to relax to mimic correlated rotation (Figure A.2.48, red circles). Umbrella constraint of 200 kcal/(mol·Å^2) was applied to the chosen phenylene ring. The free energy change of rotation was found to be less than 1 kcal/mol in vacuum. Since the independent rotation of one phenylene is a higher energy process in vacuum, we could only estimate the activation energy by restraining a second phenylene while the chosen phenylene group was experiencing the 180° dihedral angle change as described above. The obtained energy diagram (Figure A.2.48, green triangles) matched well with a 2-fold rotation model with activation energy of *ca*. 5 kcal/mol. If we restrain both of the second and the third phenylenes, the energetic change would reflect the activation barrier to rotate one phenylene with the other two being completely static (Figure A.2.48, black squares). The activation energy of this process in vacuum (*ca*. 19 kcal/mol) was already higher than the experimental data (no more than 15 kcal/mol).

2.9. Appendix

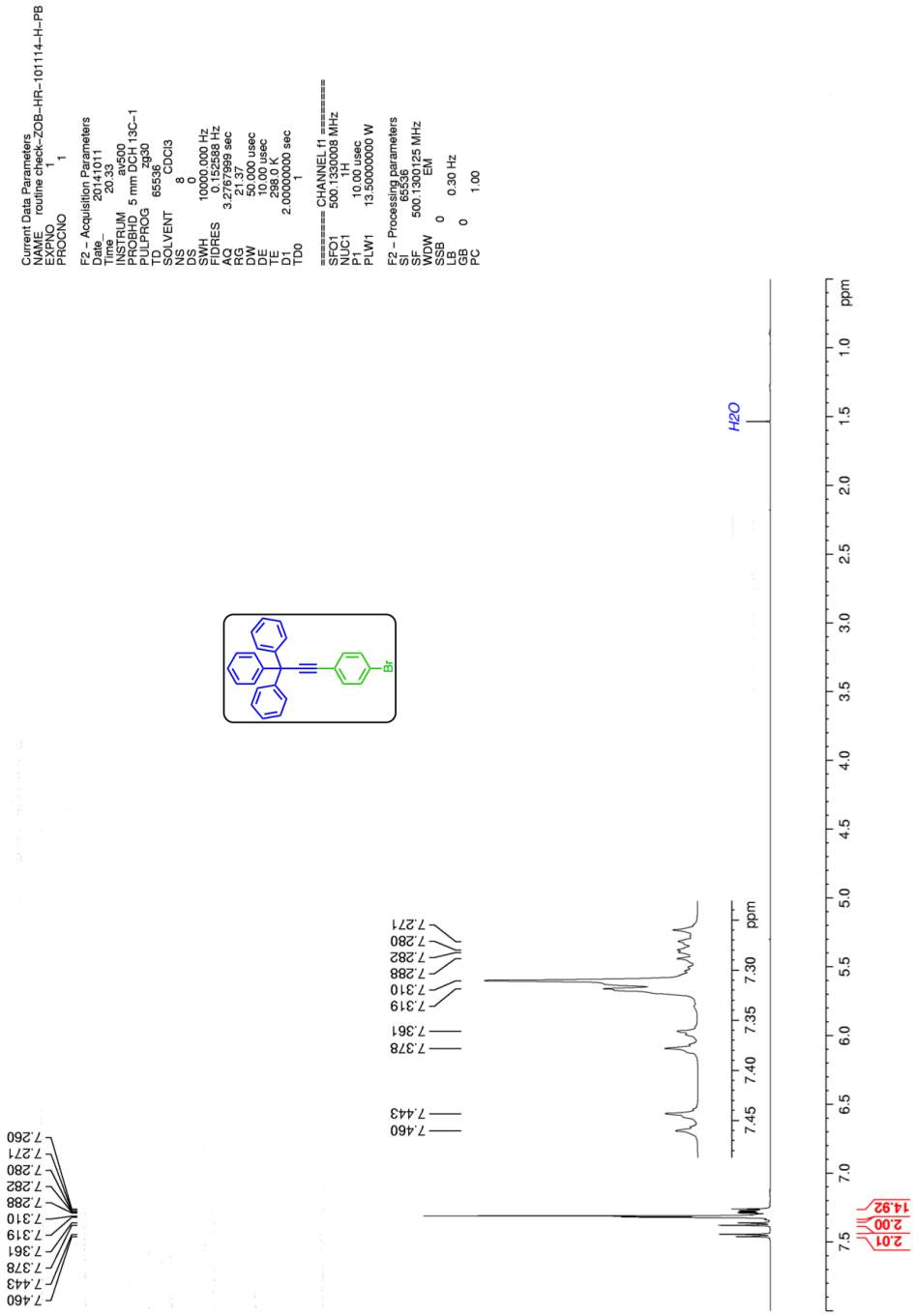

Figure A.2.1. ^{1}H NMR of compound **4** at 500 MHz in $CDCl_3$.

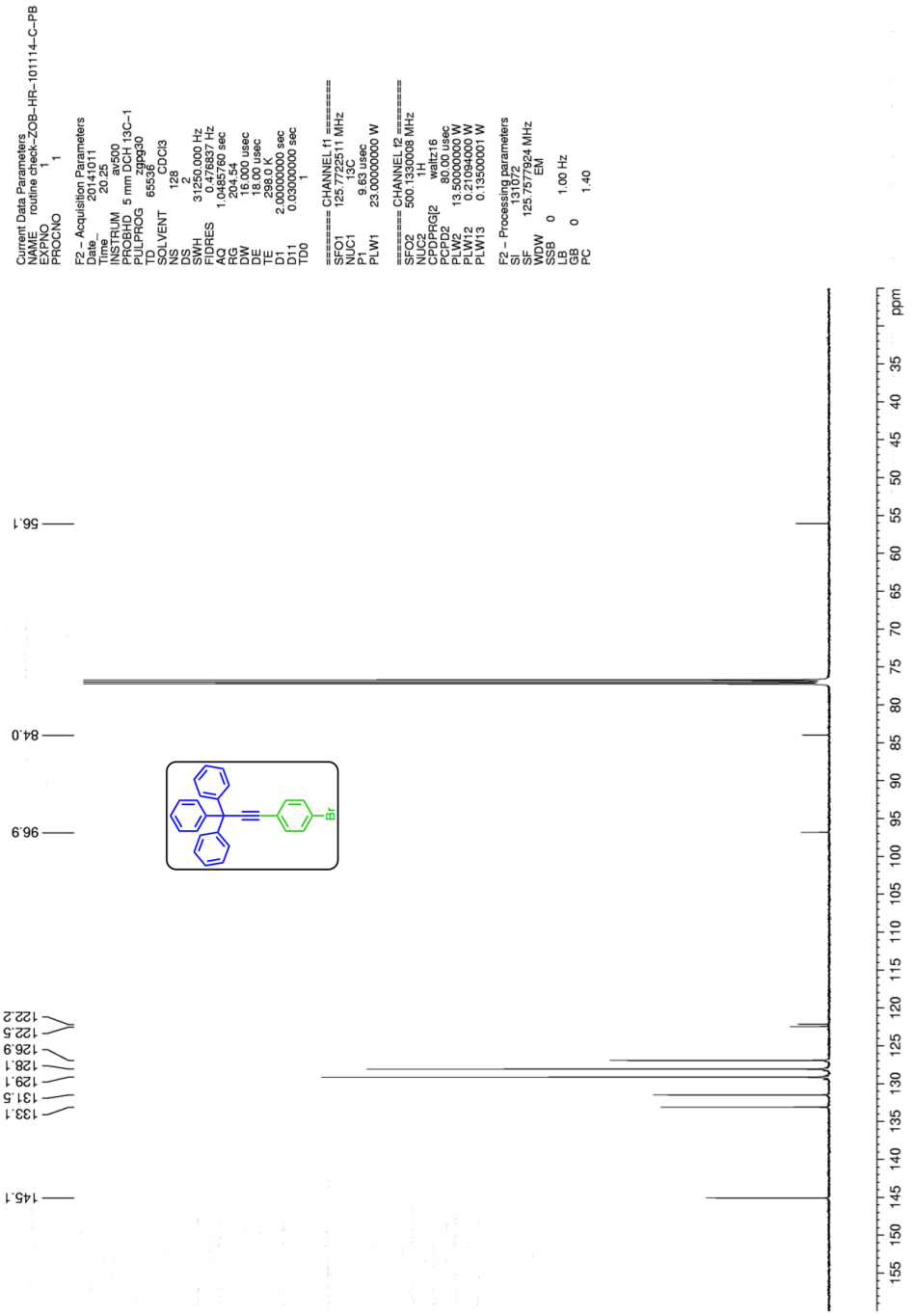

Figure A.2.2. ^{13}C NMR of compound **4** at 125 MHz in $CDCl_3$.

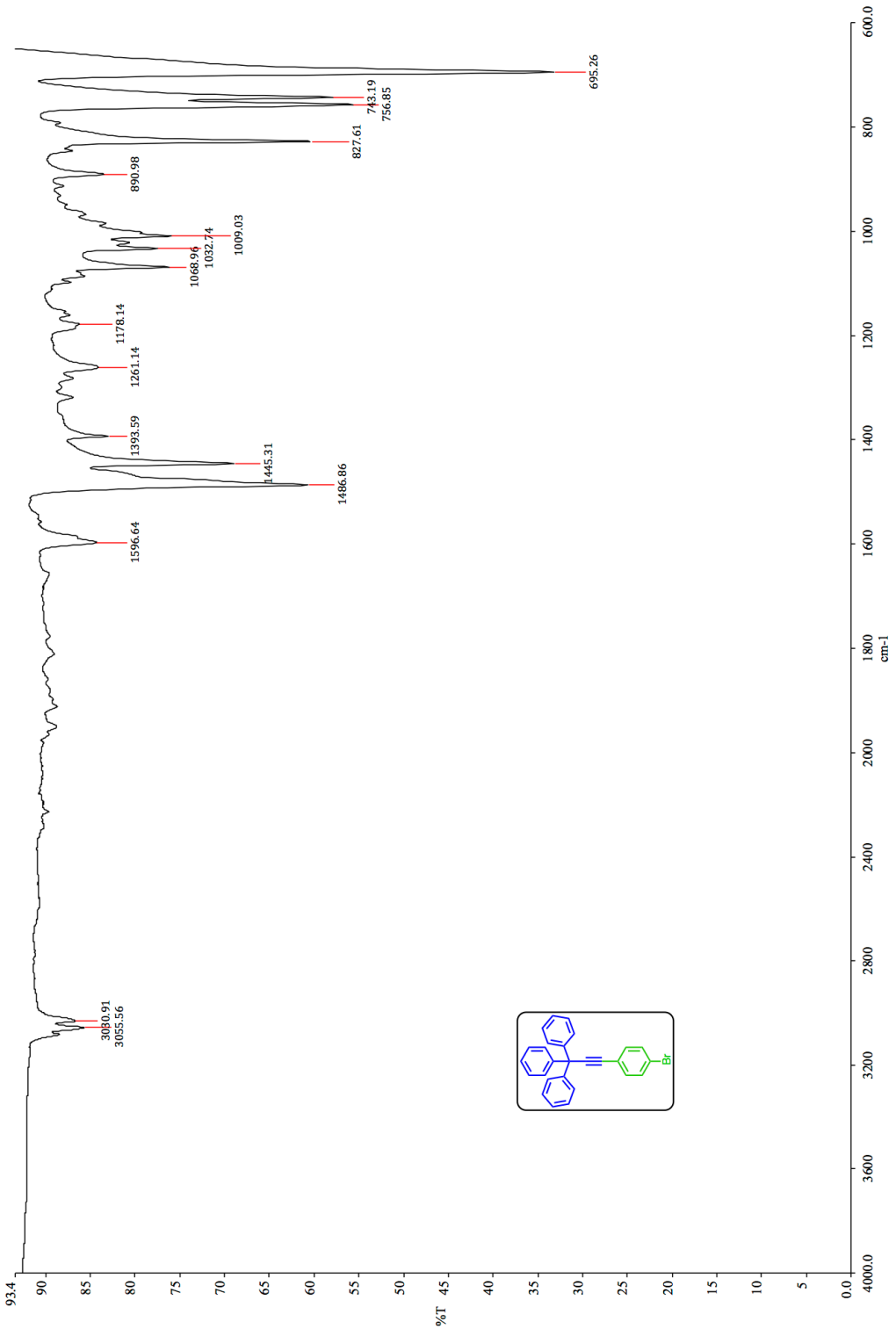

Figure A.2.3. IR of compound **4**.

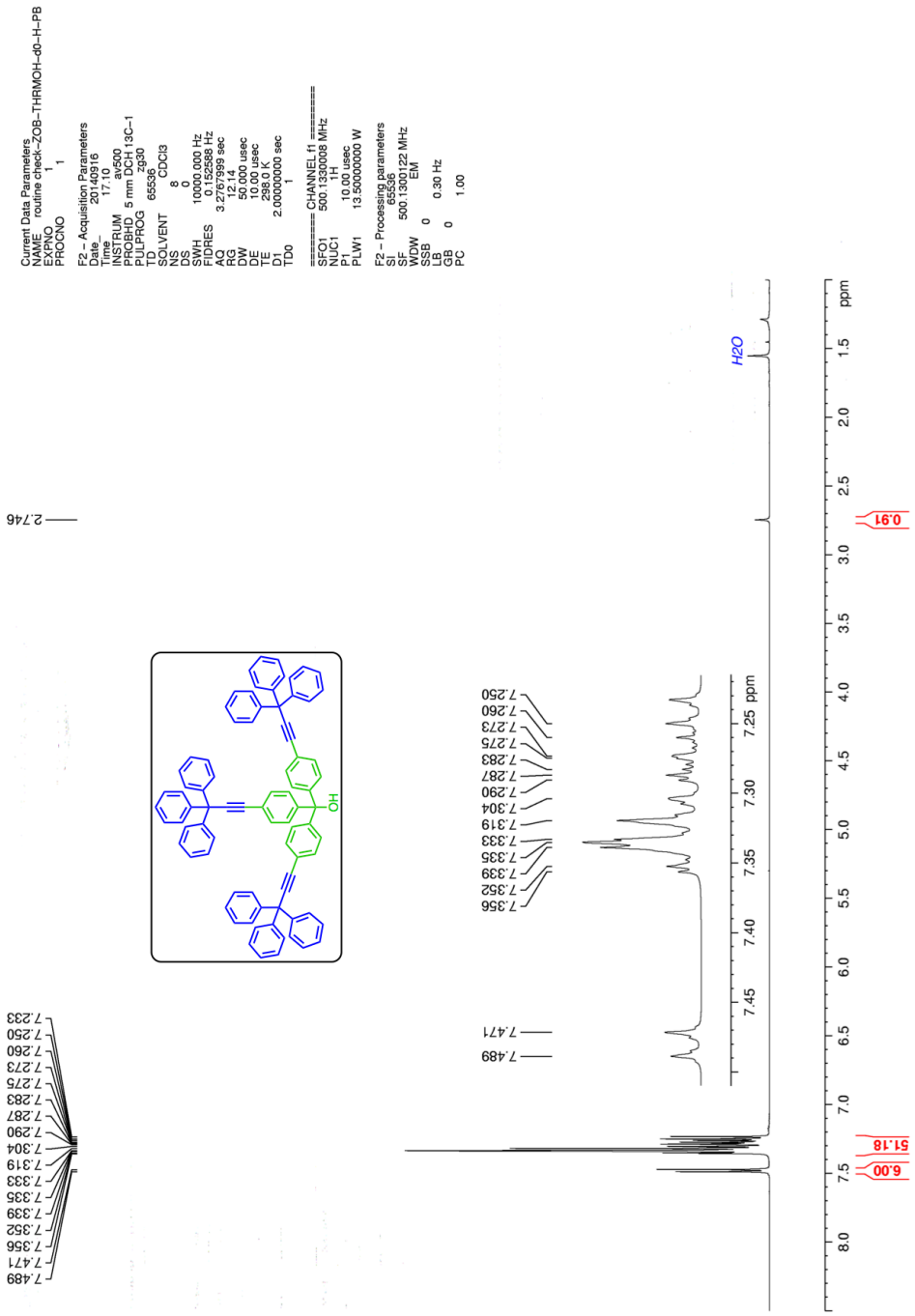

Figure A.2.4. ^{1}H NMR of compound **5** at 500 MHz in $CDCl_3$.

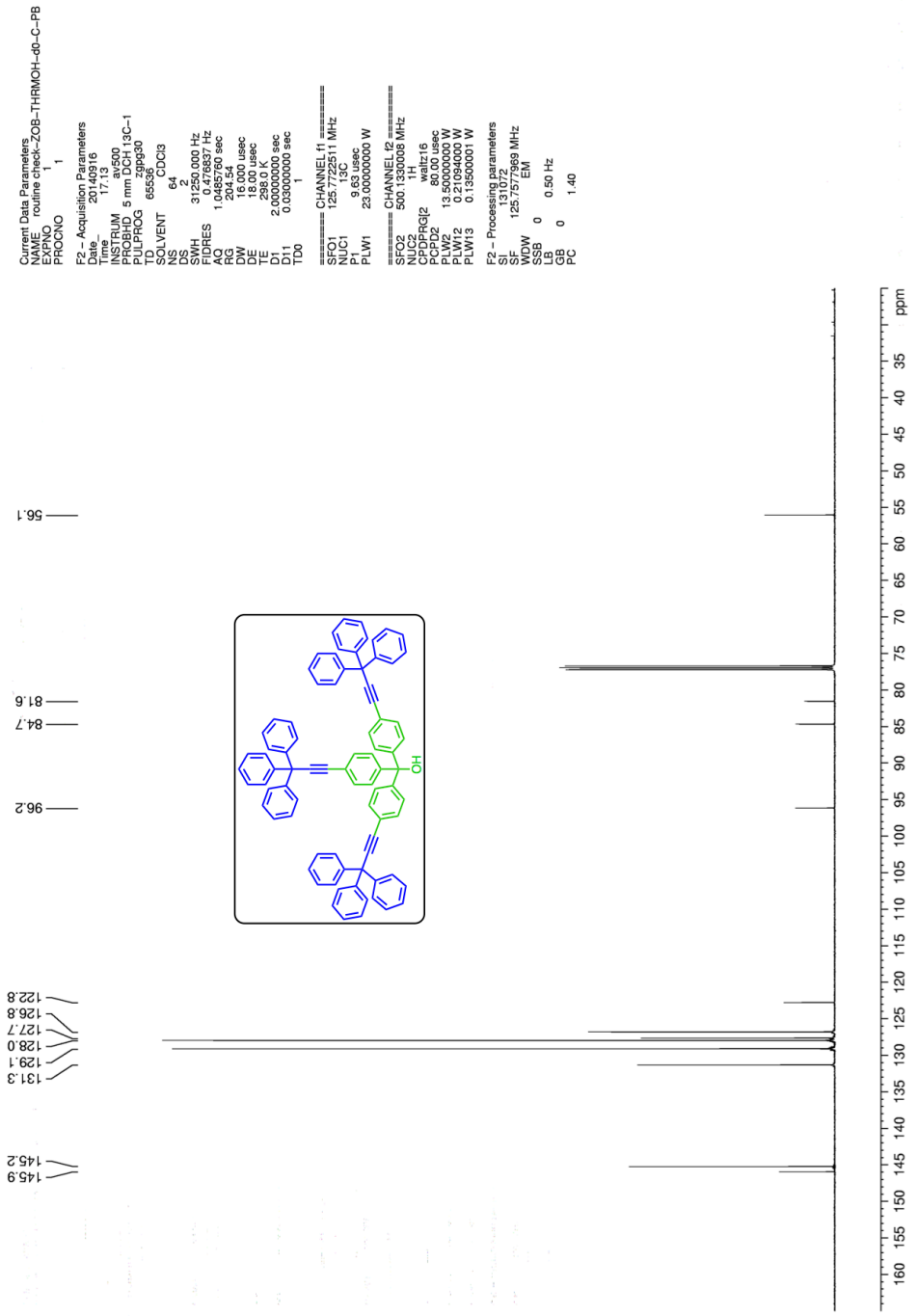

Figure A.2.5. ^{13}C NMR of compound **5** at 125 MHz in $CDCl_3$.

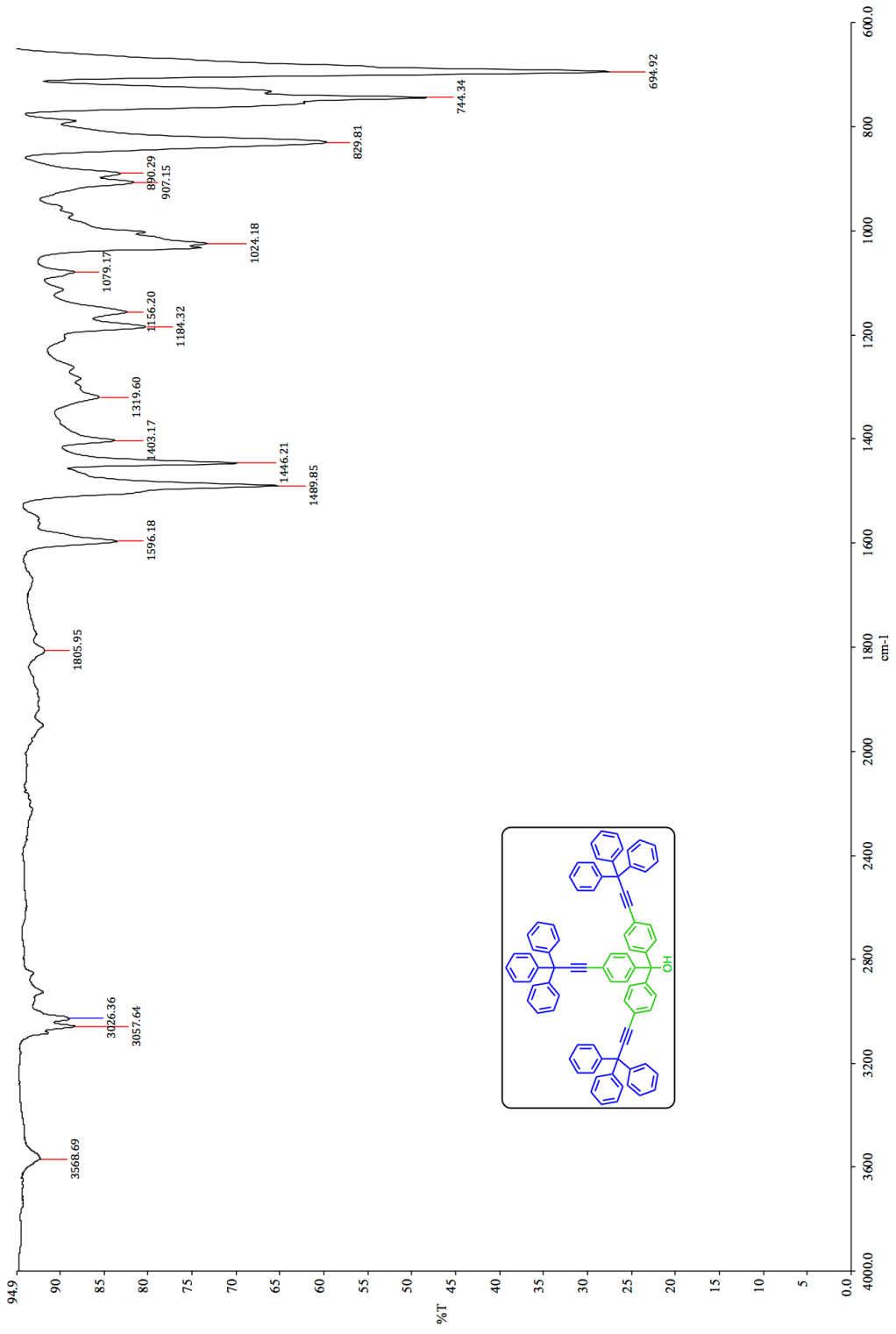

Figure A.2.6. IR of compound **5**.

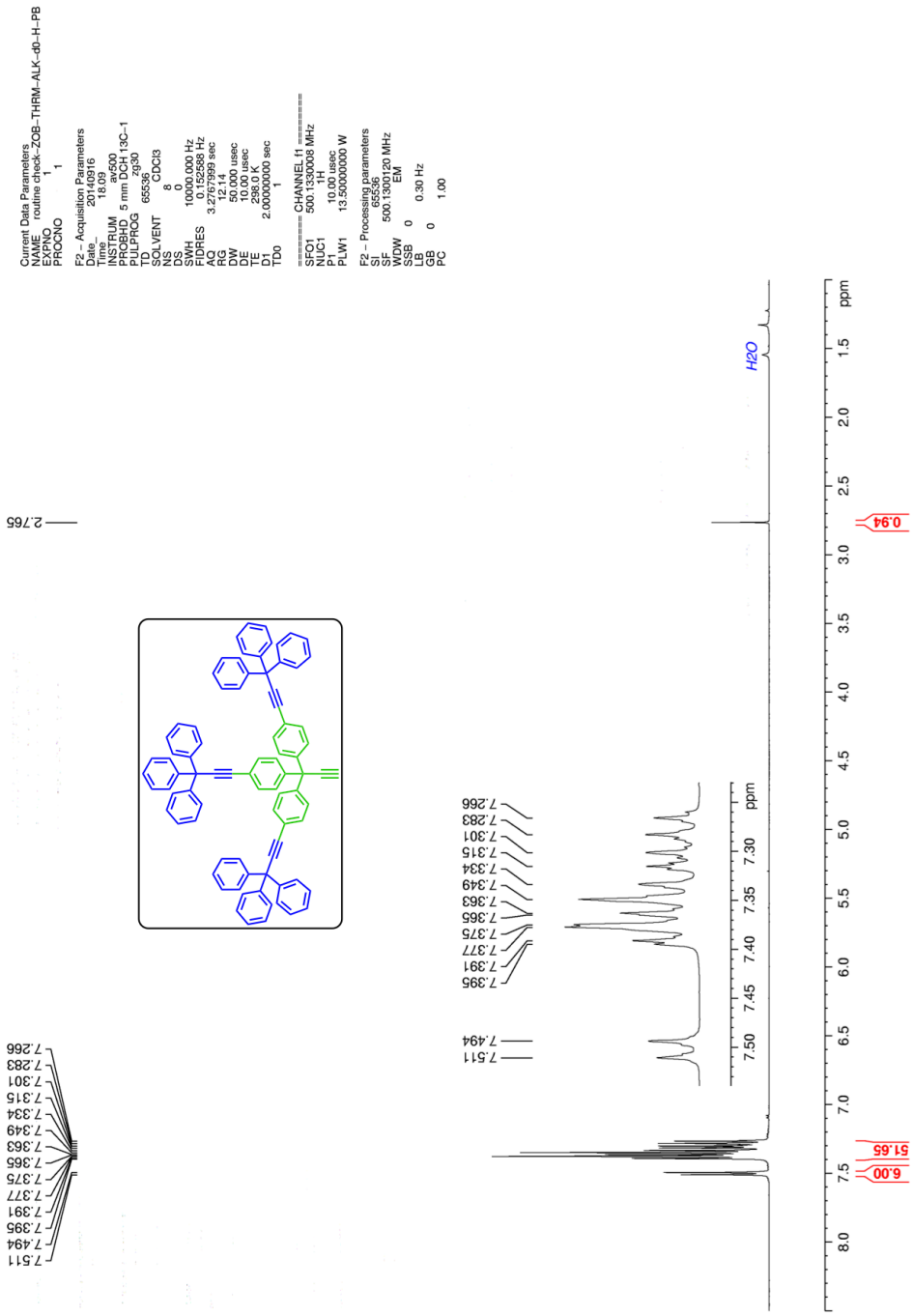

Figure A.2.7. ^{1}H NMR of compound **6** at 500 MHz in $CDCl_3$.

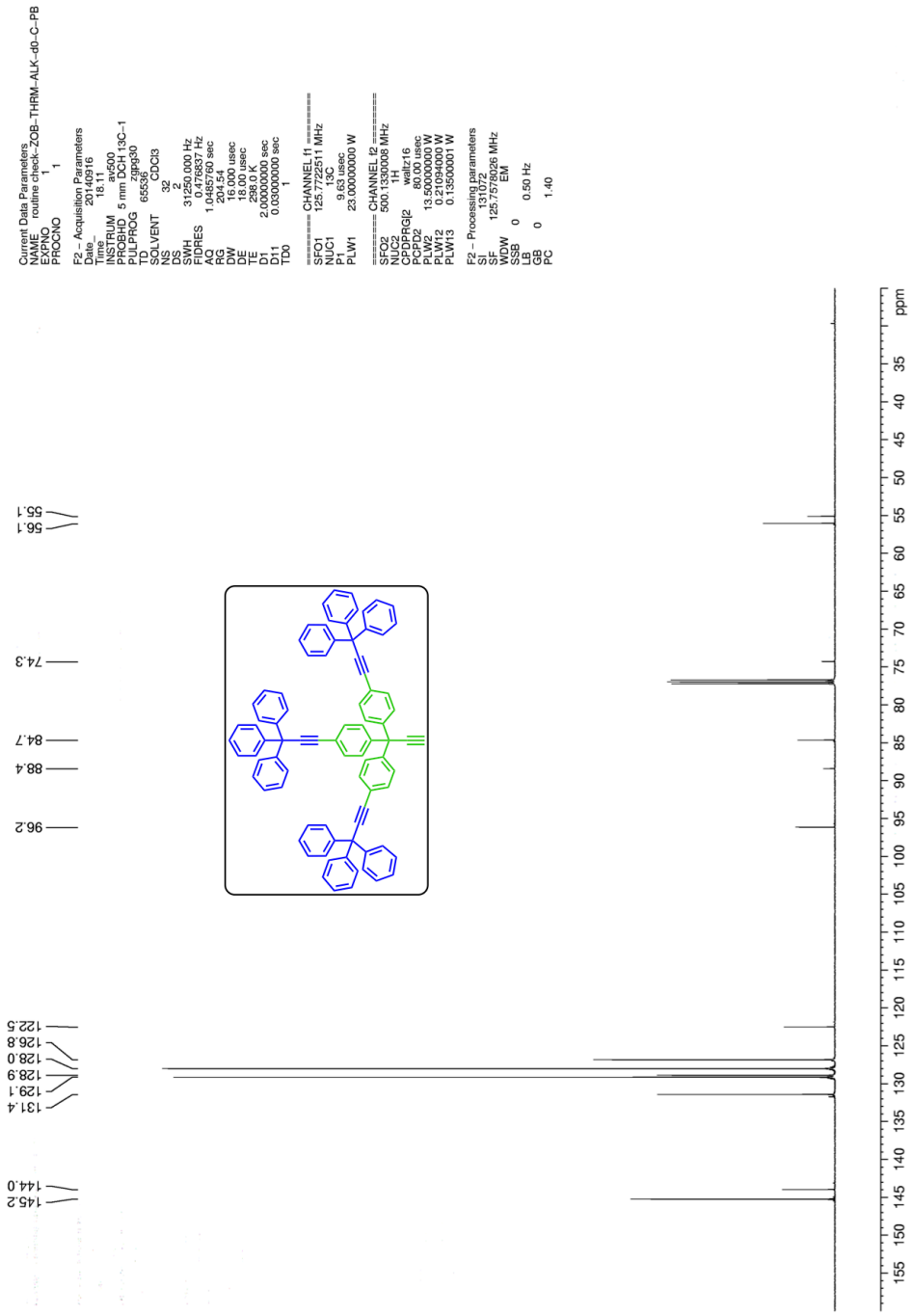

Figure A.2.8. ^{13}C NMR of compound **6** at 125 MHz in $CDCl_3$.

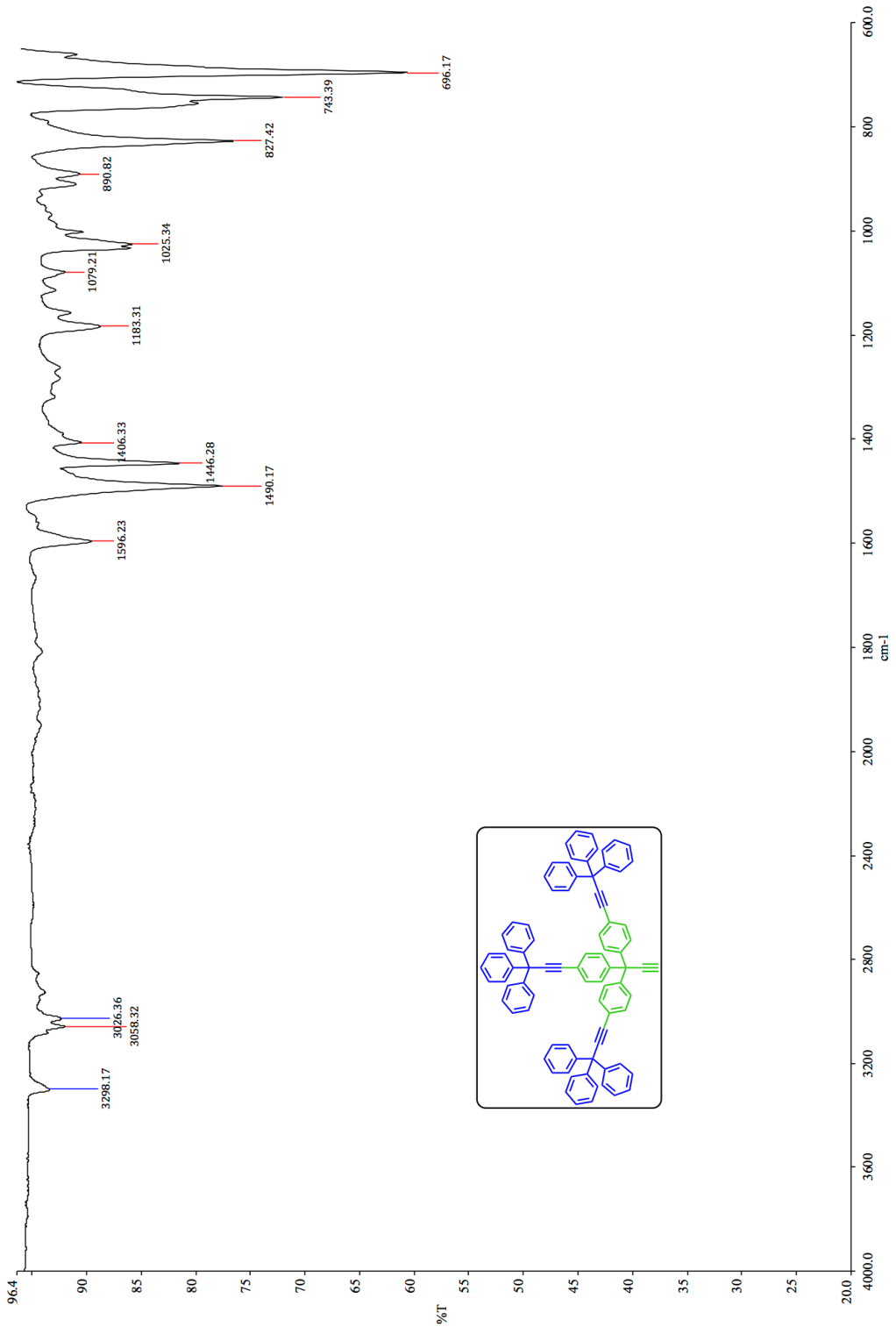

Figure A.2.9. IR of compound **6**.

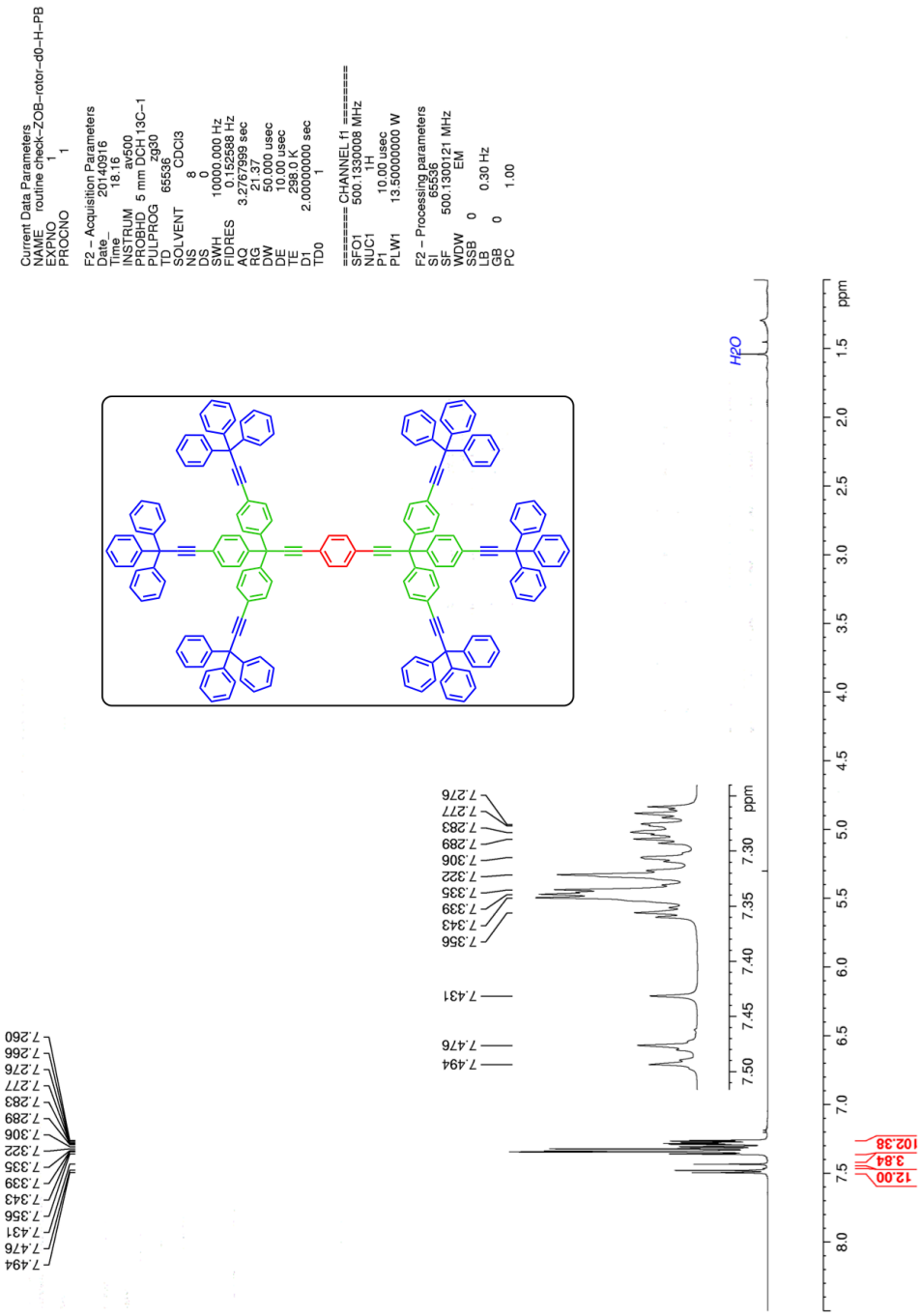

Figure A.2.10. ^{1}H NMR of compound **2** at 500 MHz in $CDCl_3$.

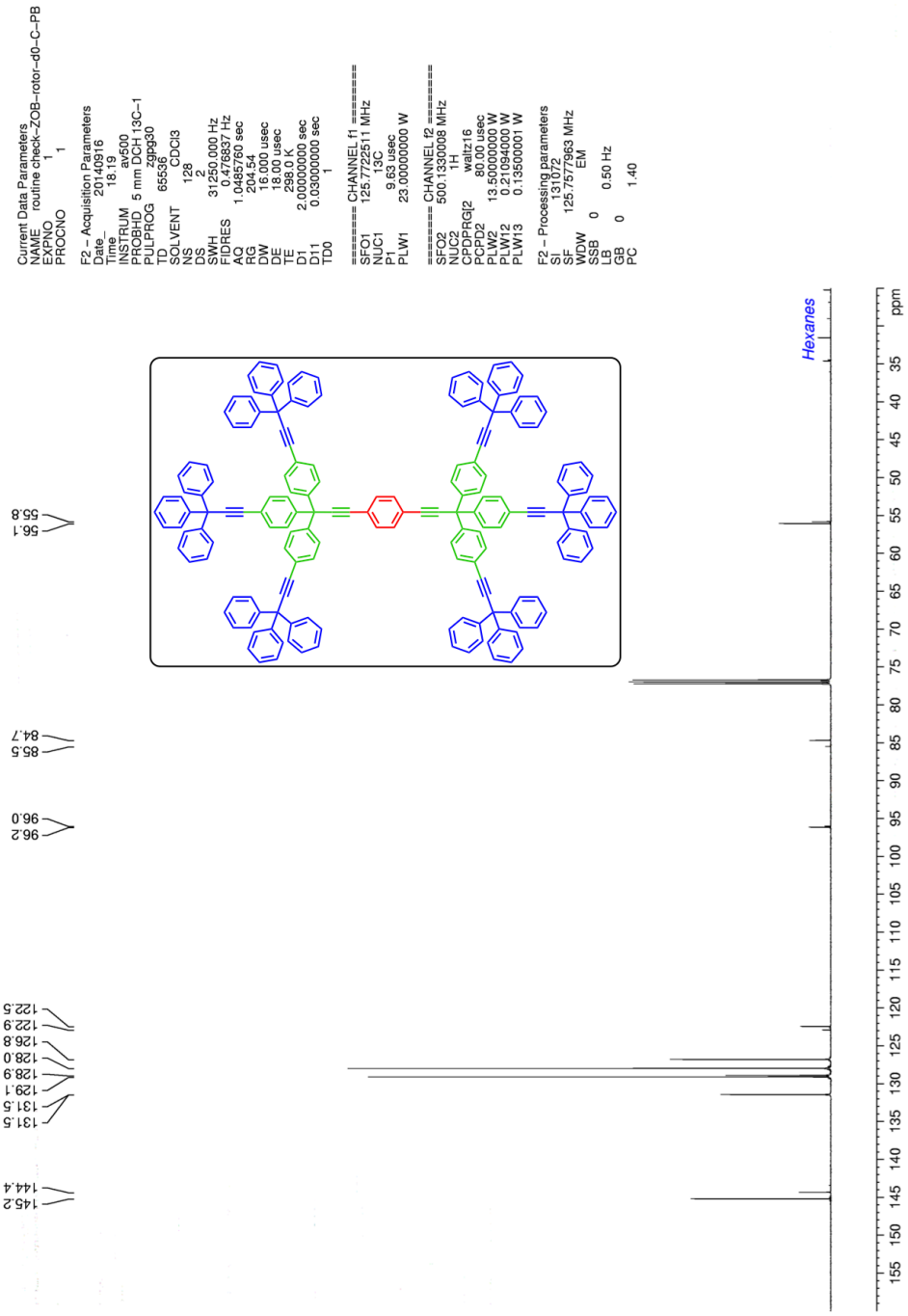

Figure A.2.11. ^{13}C NMR of compound **2** at 125 MHz in $CDCl_3$.

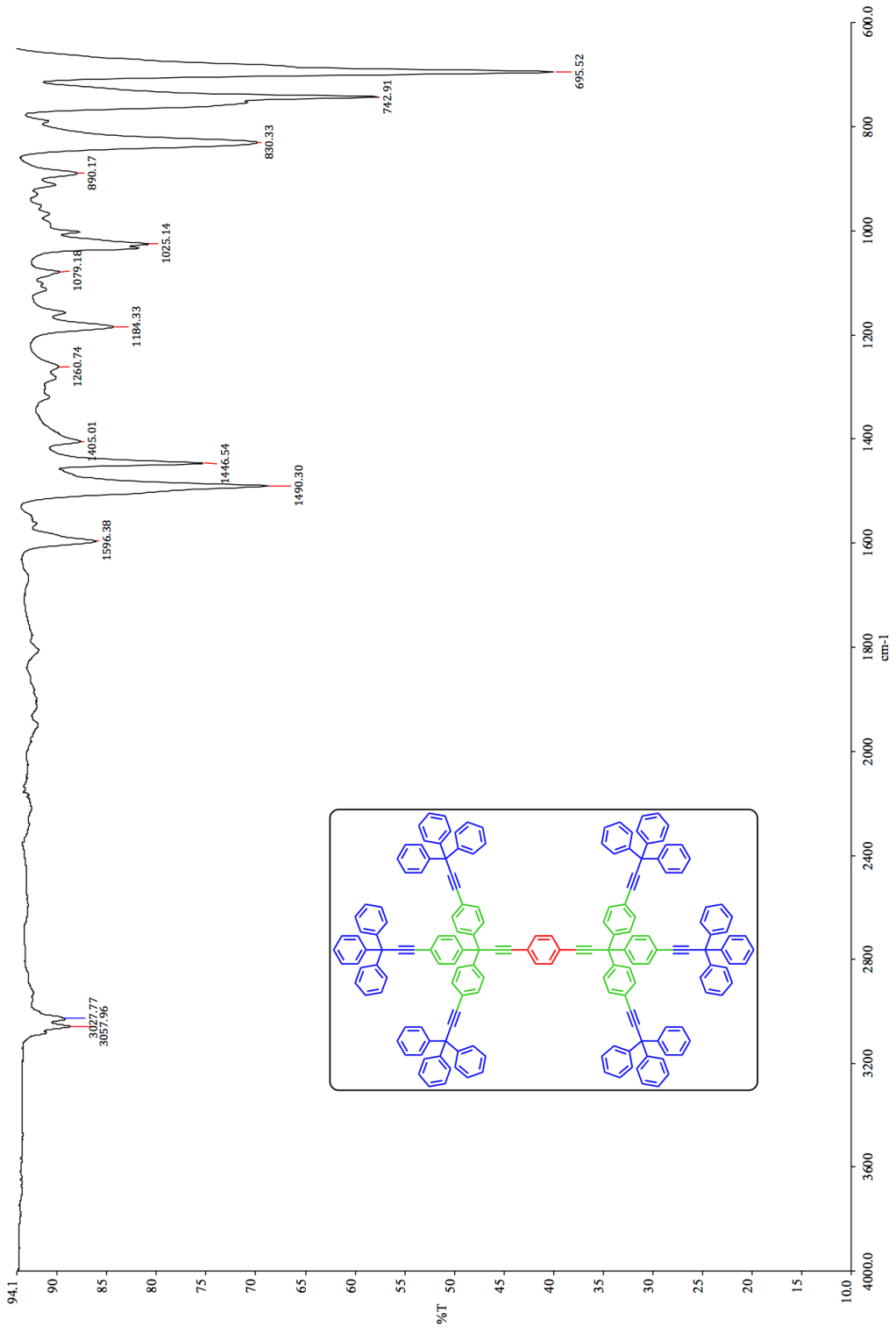

Figure A.2.12. IR of compound **2**.

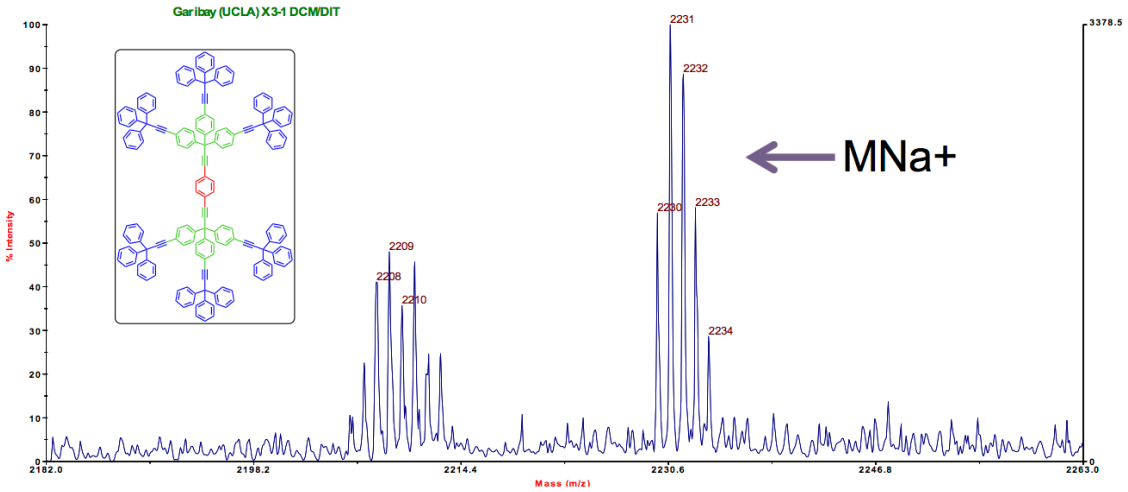

Figure A.2.13. MS (MALDI, TOF) of compound **2** showing the MNa^+ cluster.

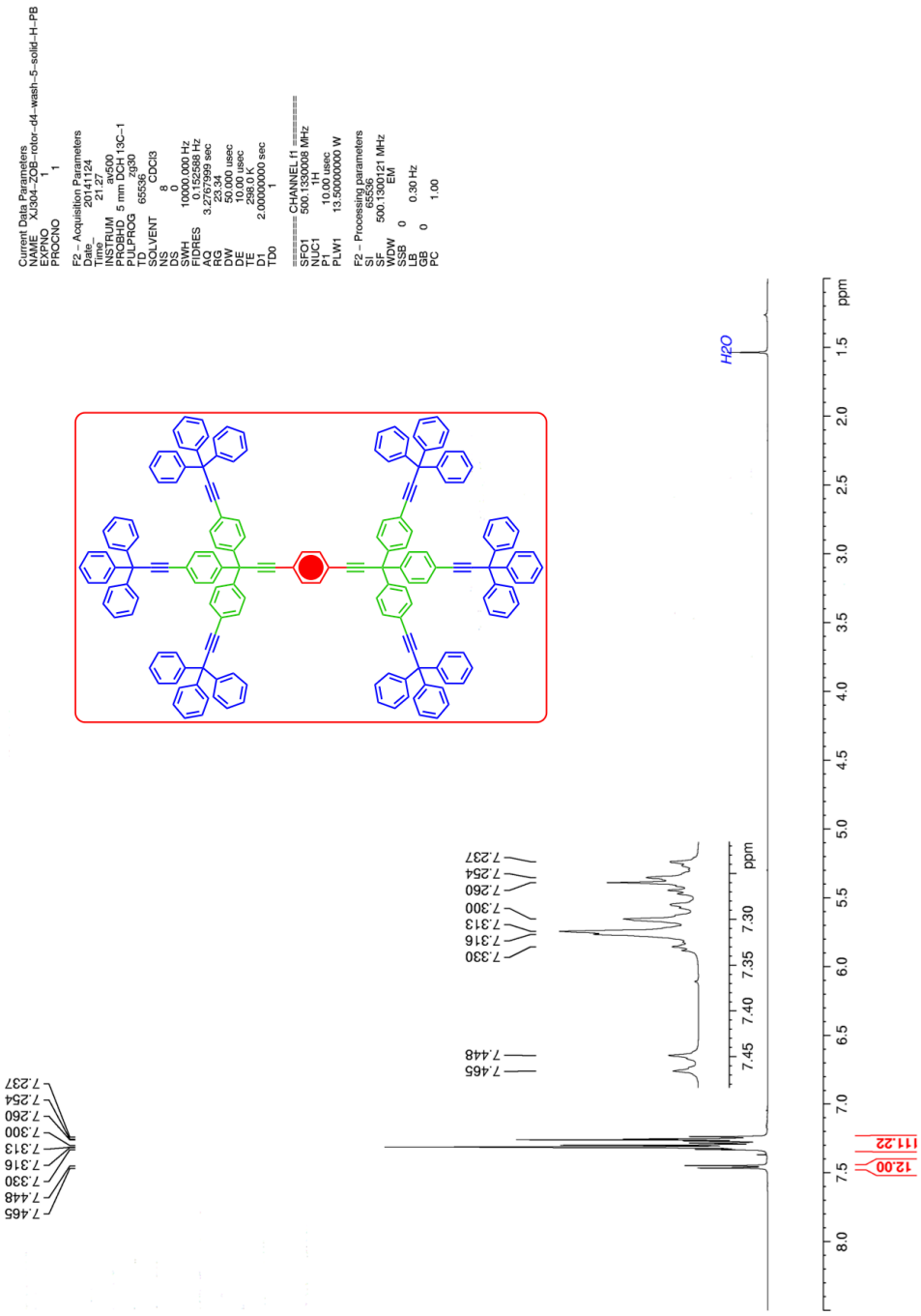

Figure A.2.14. ^{1}H NMR of compound **2**-d_4 at 500 MHz in $CDCl_3$.

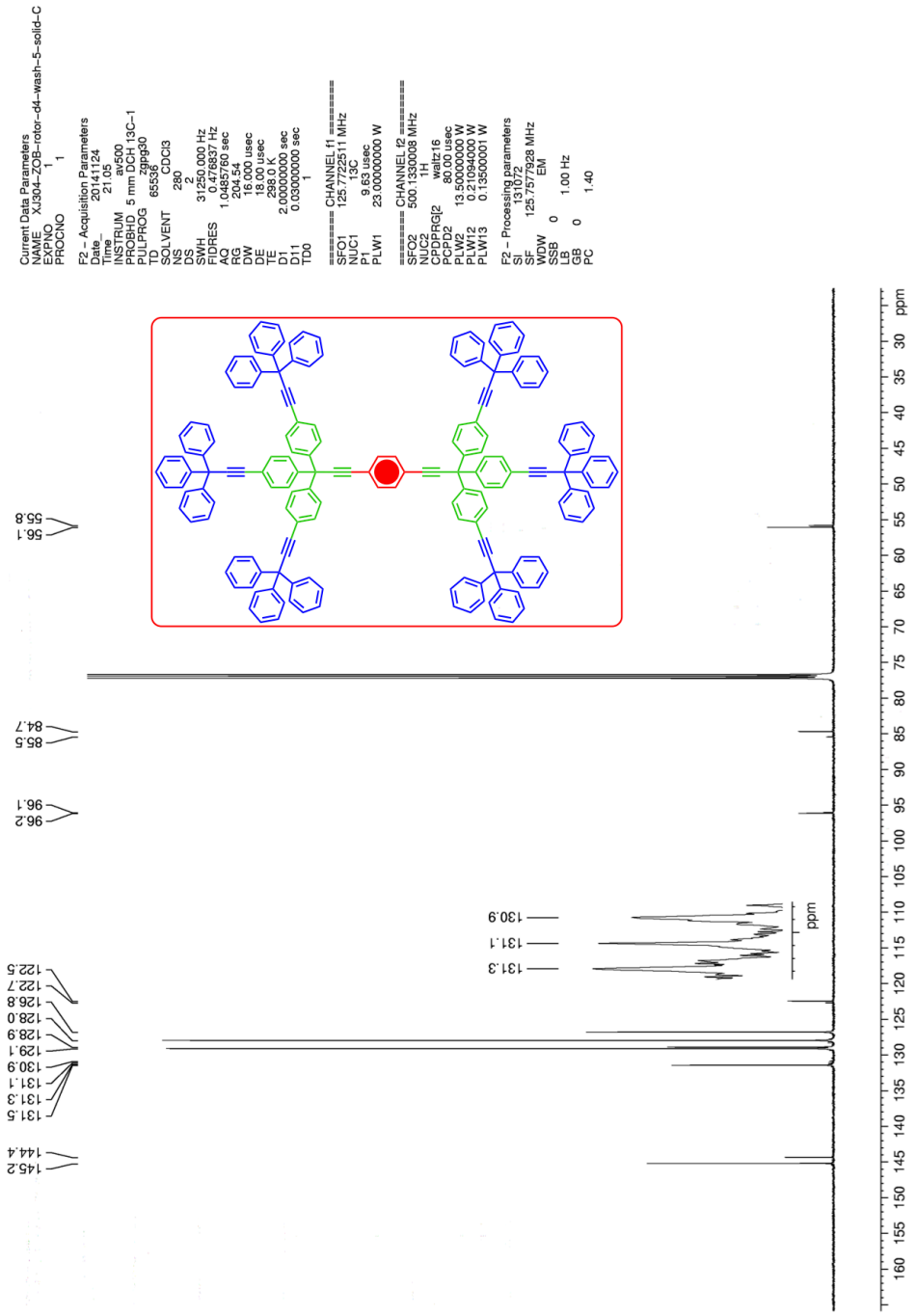

Figure A.2.15. ^{13}C NMR of compound **2**-d_4 at 125 MHz in $CDCl_3$.

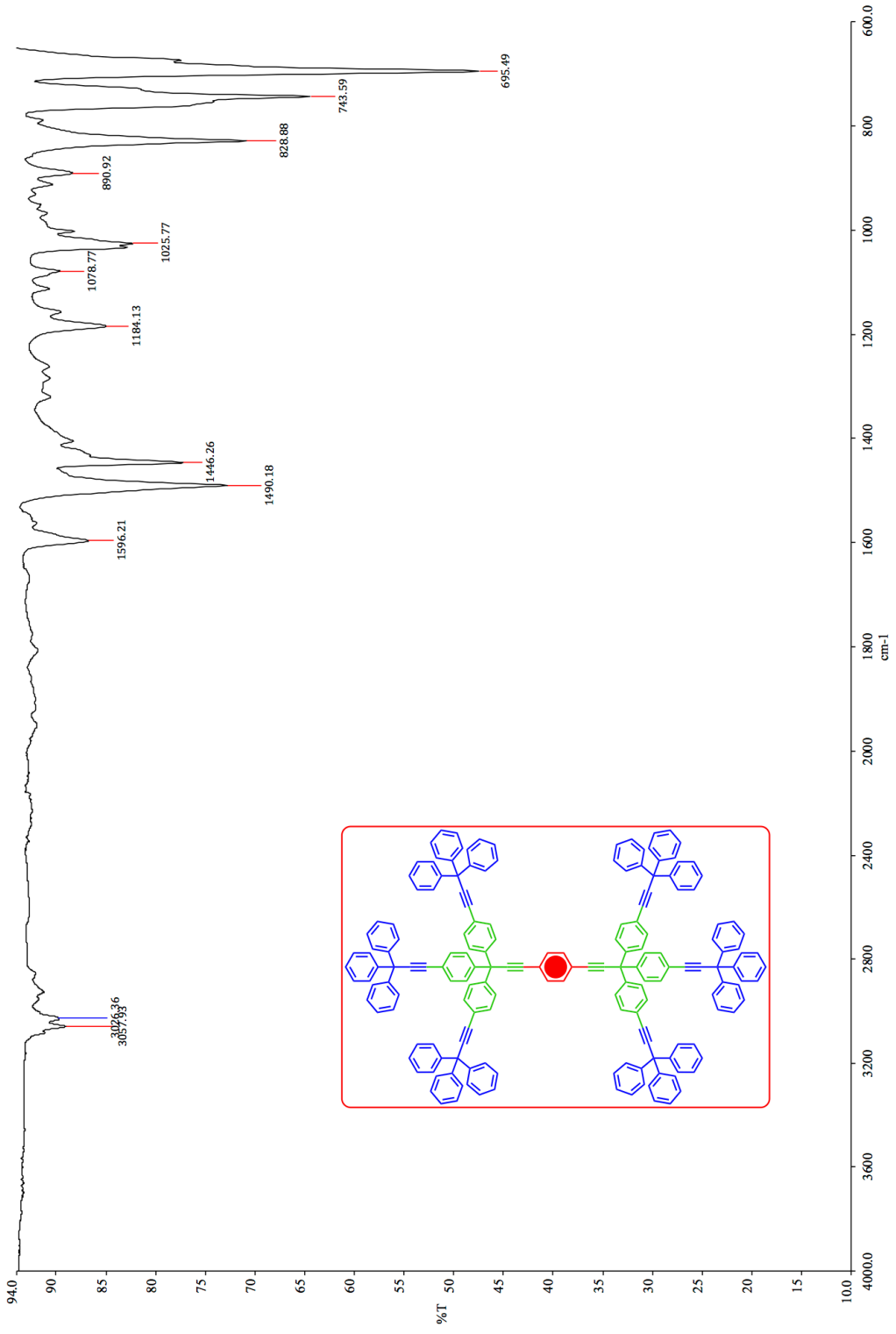

Figure A.2.16. IR of compound **2**-d_4.

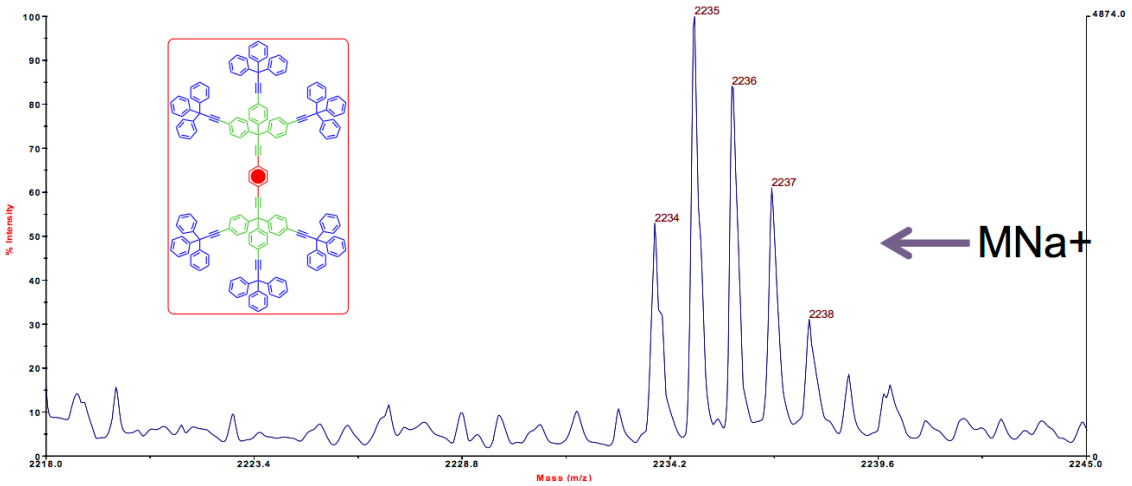

Figure A.2.17. MS (MALDI, TOF) of compound **2**-d_4 showing the MNa^+ cluster.

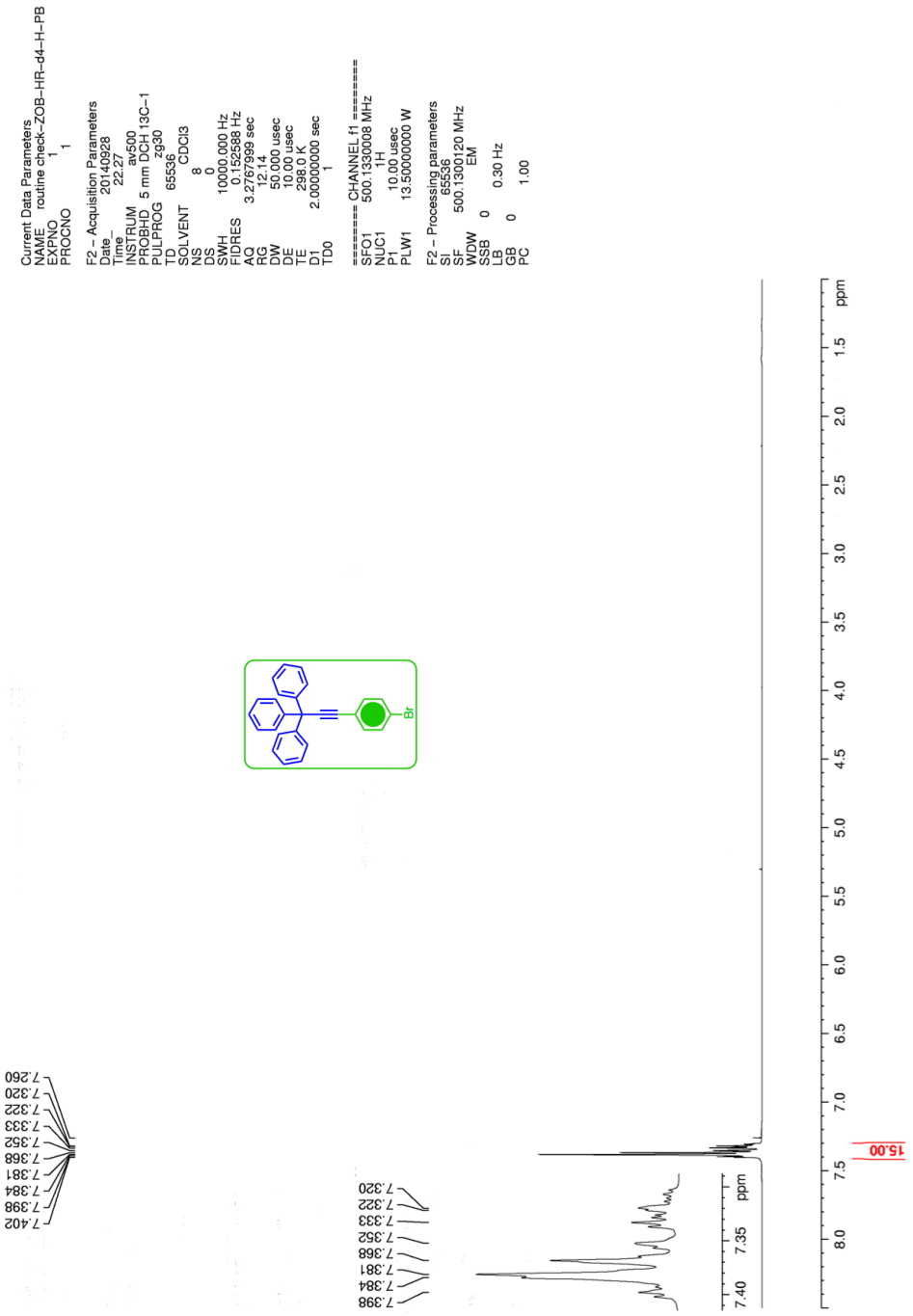

Figure A.2.18. ^{1}H NMR of compound **4**-d_4 at 500 MHz in $CDCl_3$.

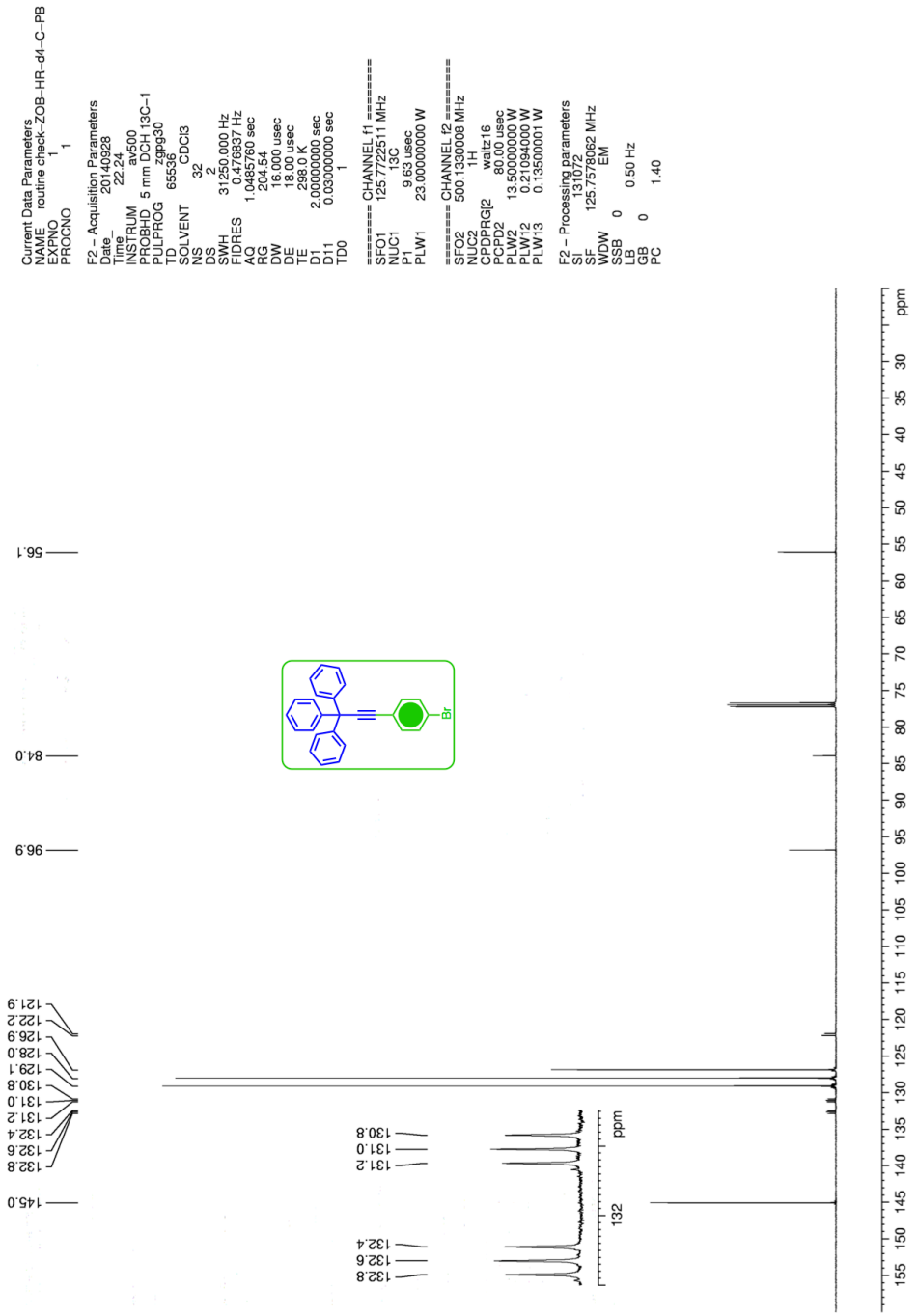

Figure A.2.19. ^{13}C NMR of compound **4**-d_4 at 125 MHz in $CDCl_3$.

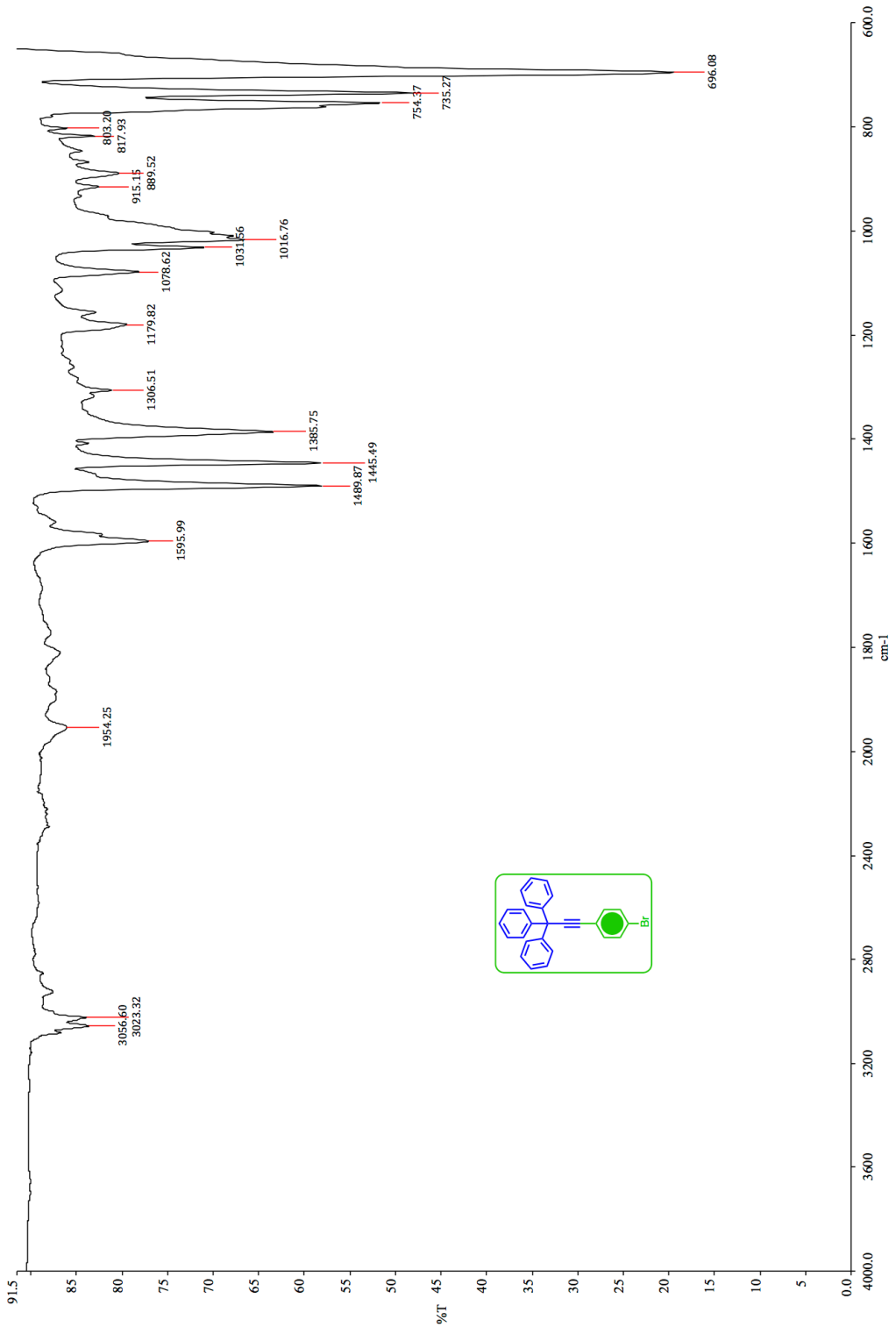

Figure A.2.20. IR of compound **4**-d_4.

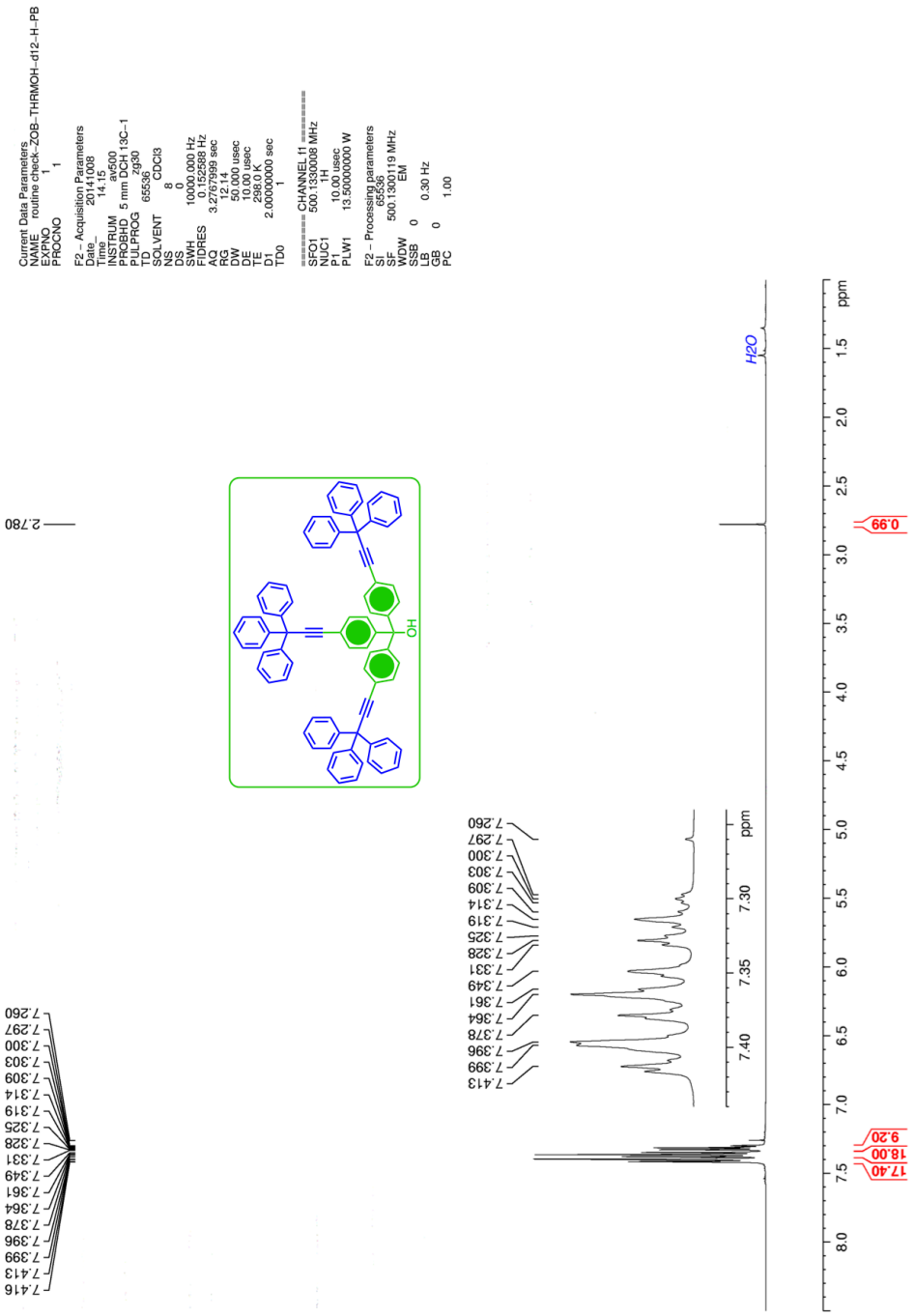

Figure A.2.21. ^{1}H NMR of compound **5**-d_{12} at 500 MHz in $CDCl_3$.

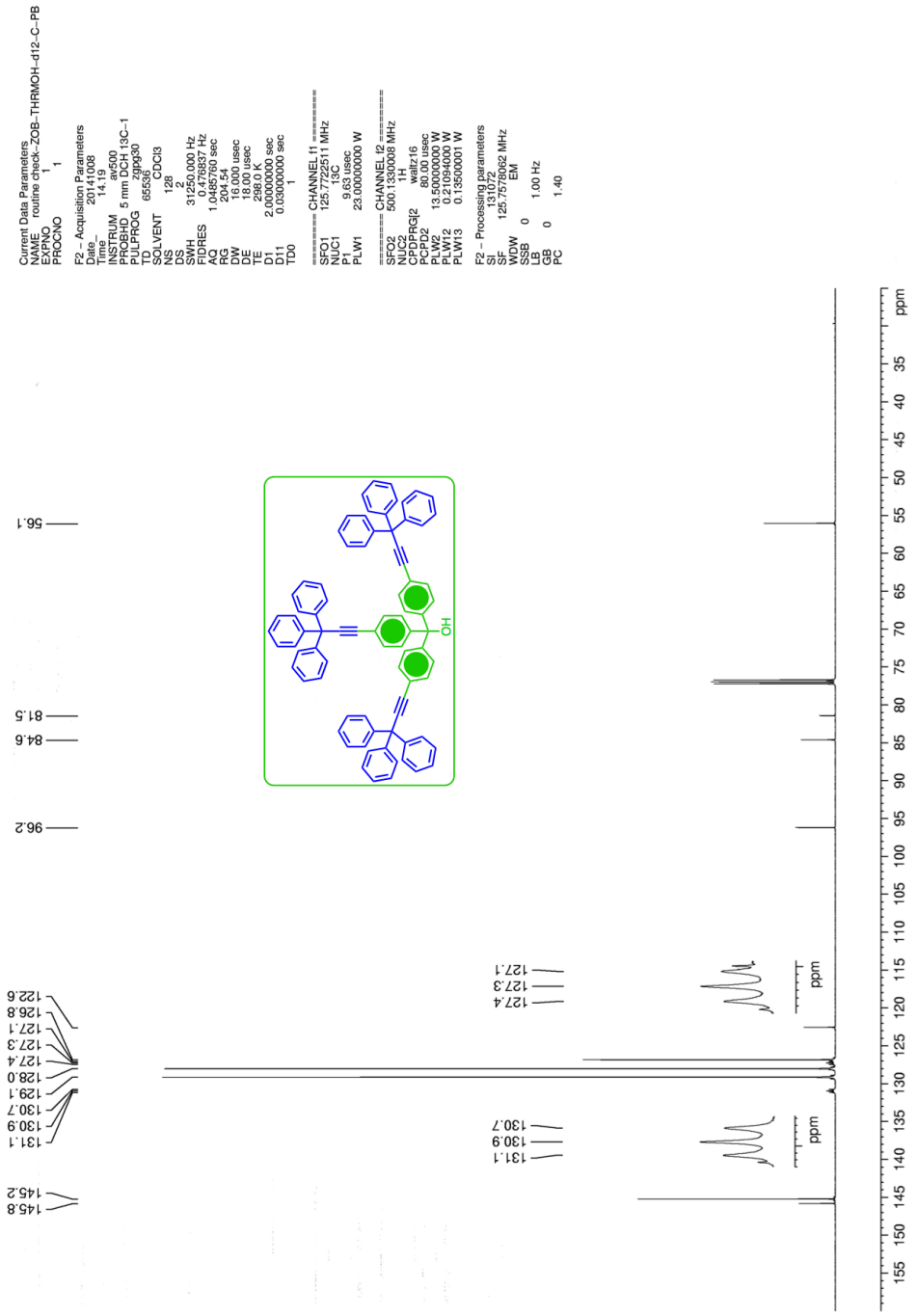

Figure A.2.22. ^{13}C NMR of compound **5**-d_{12} at 125 MHz in $CDCl_3$.

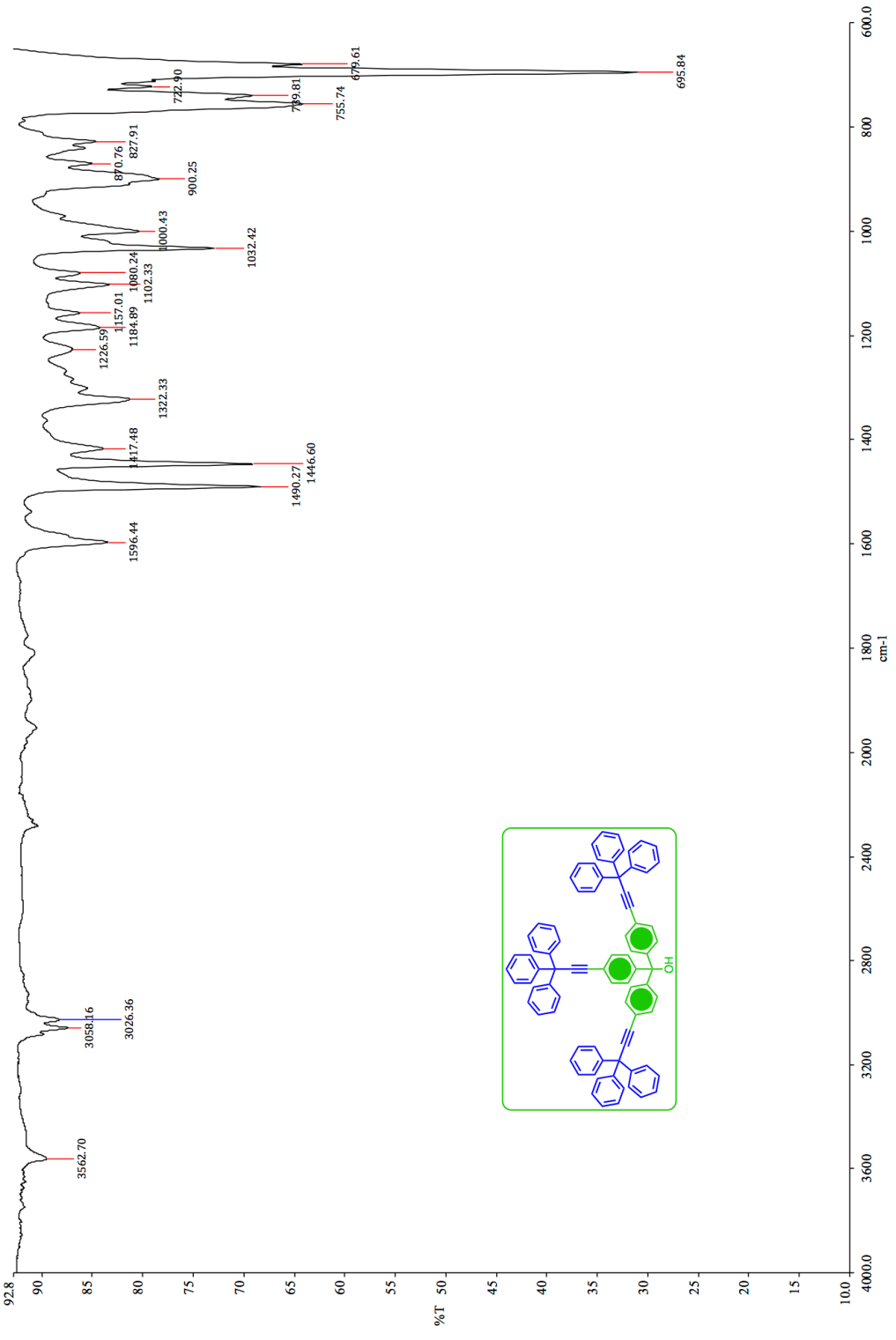

Figure A.2.23. IR of compound **5**-d_{12}.

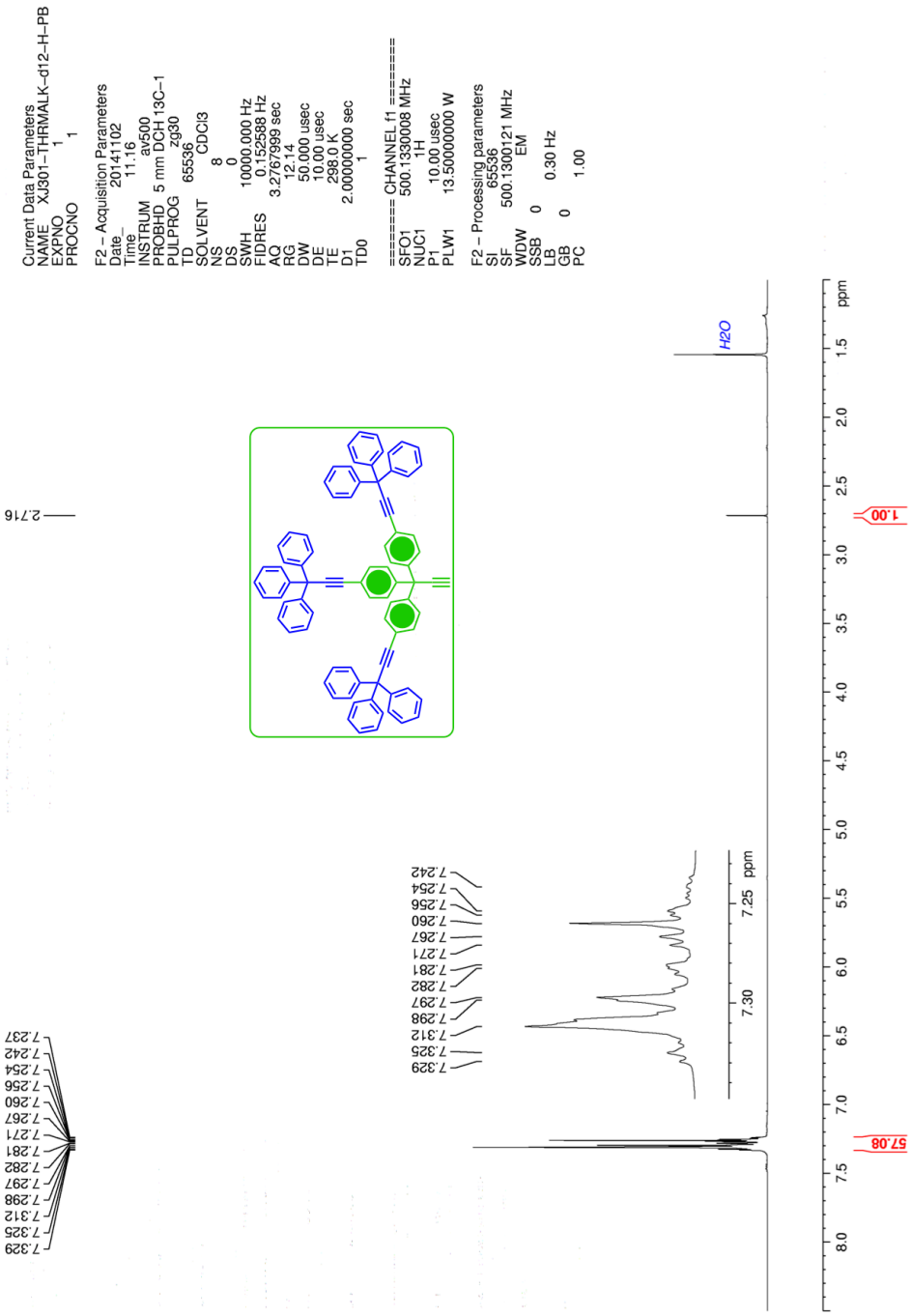

Figure A.2.24. ^{1}H NMR of compound **6**-d_{12} at 500 MHz in $CDCl_3$.

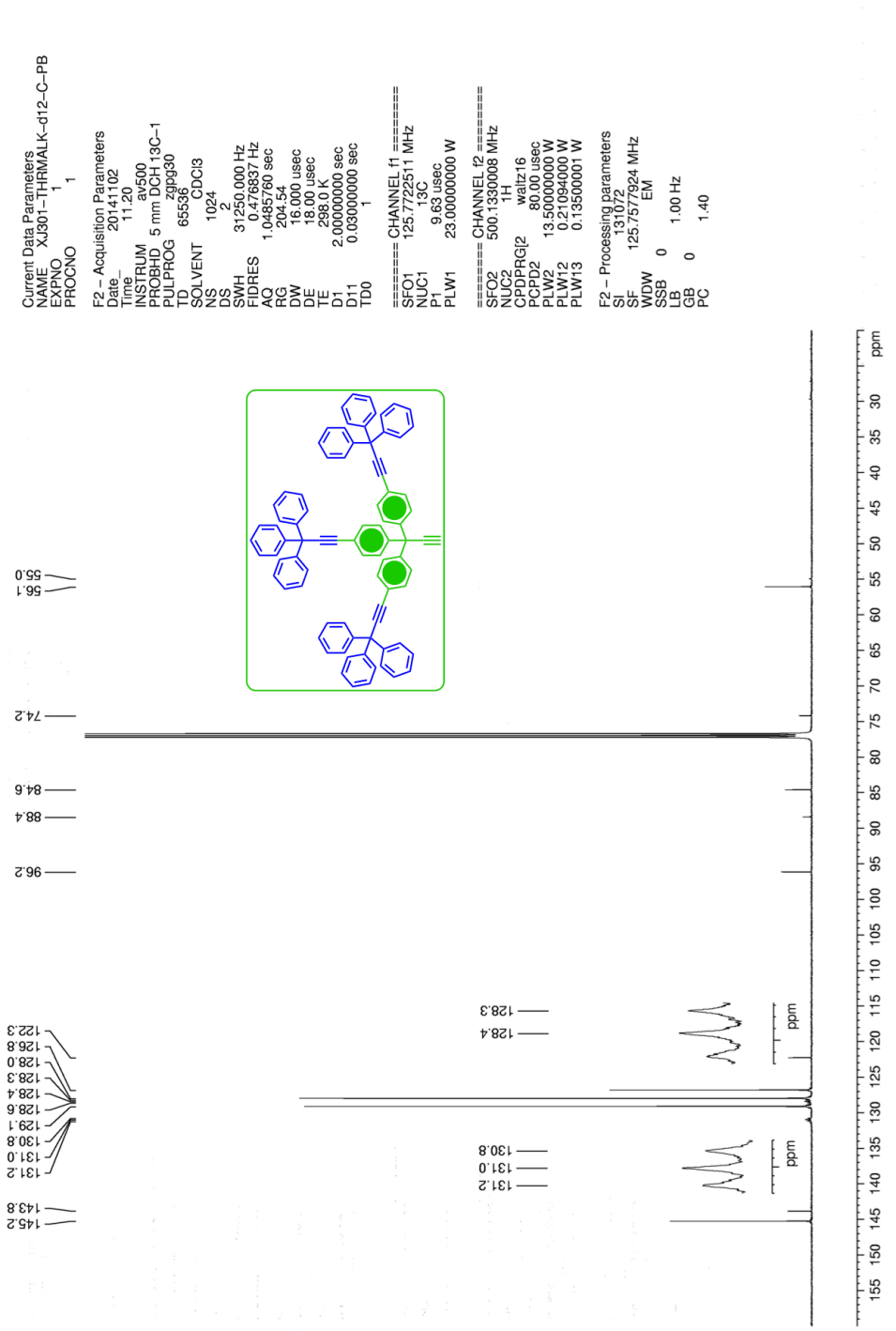

Figure A.2.25. ^{13}C NMR of compound **6**-d_{12} at 125 MHz in $CDCl_3$.

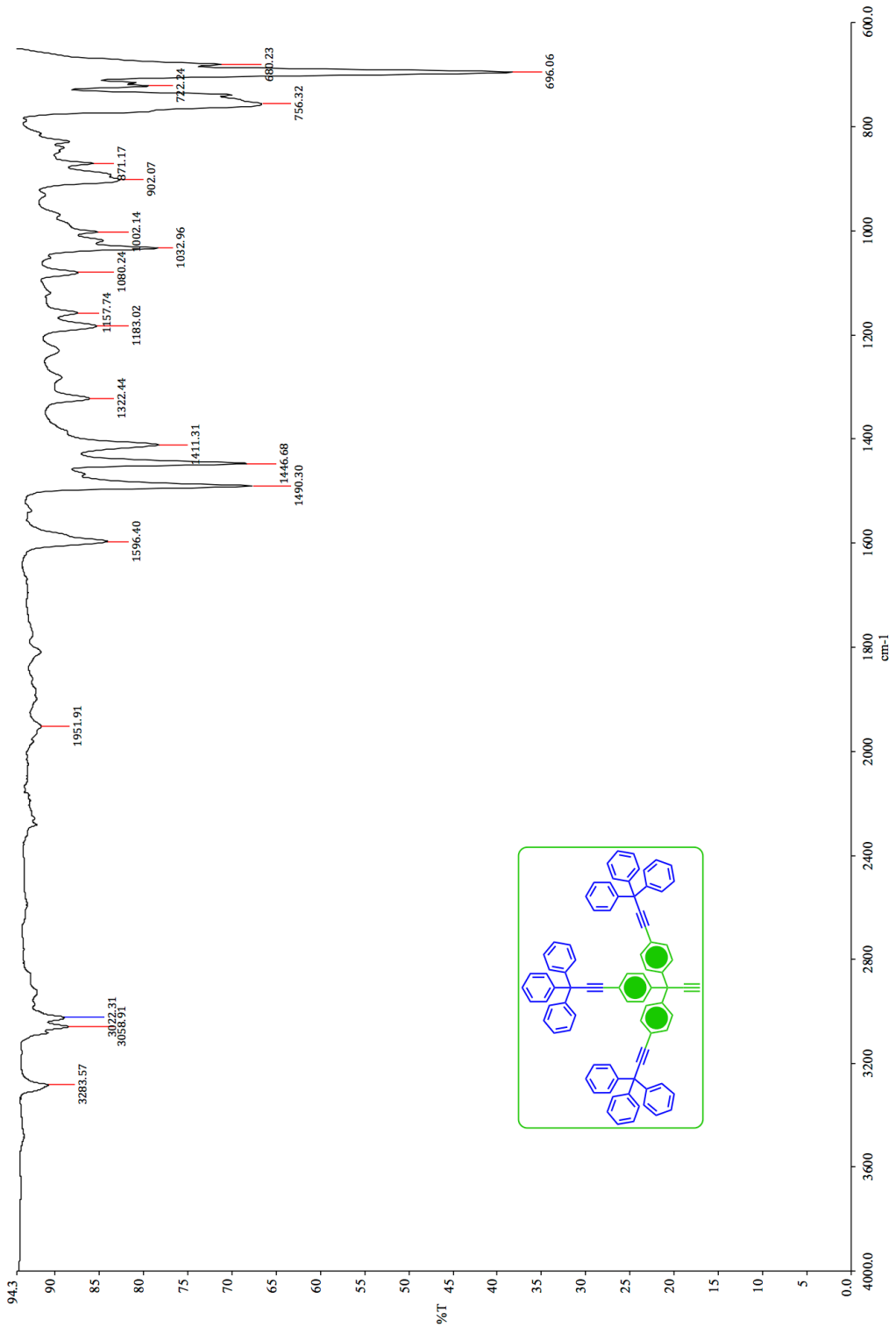

Figure A.2.26. IR of compound **6**-d_{12}.

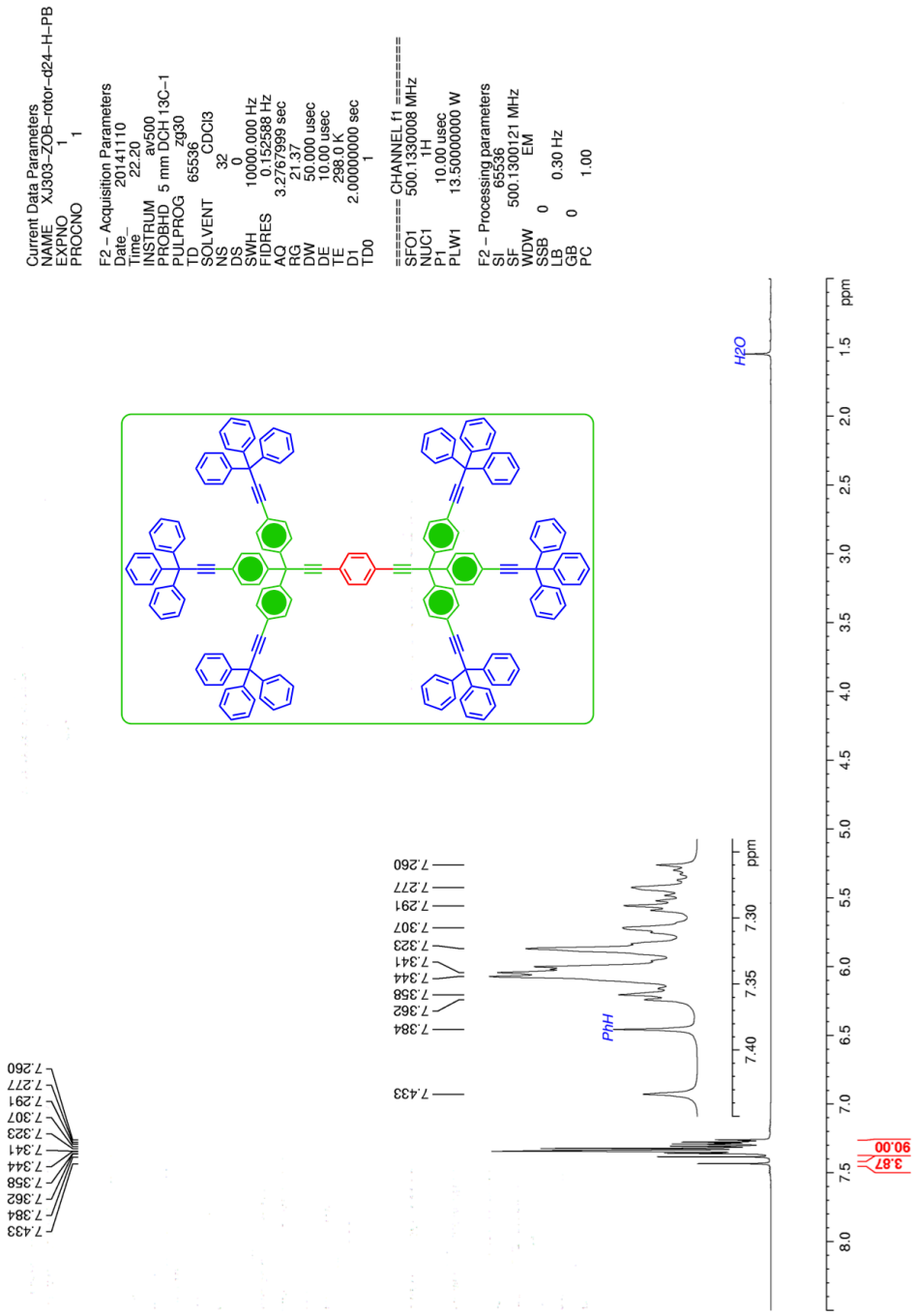

Figure A.2.27. ^{1}H NMR of compound **2**-d_{24} at 500 MHz in $CDCl_3$.

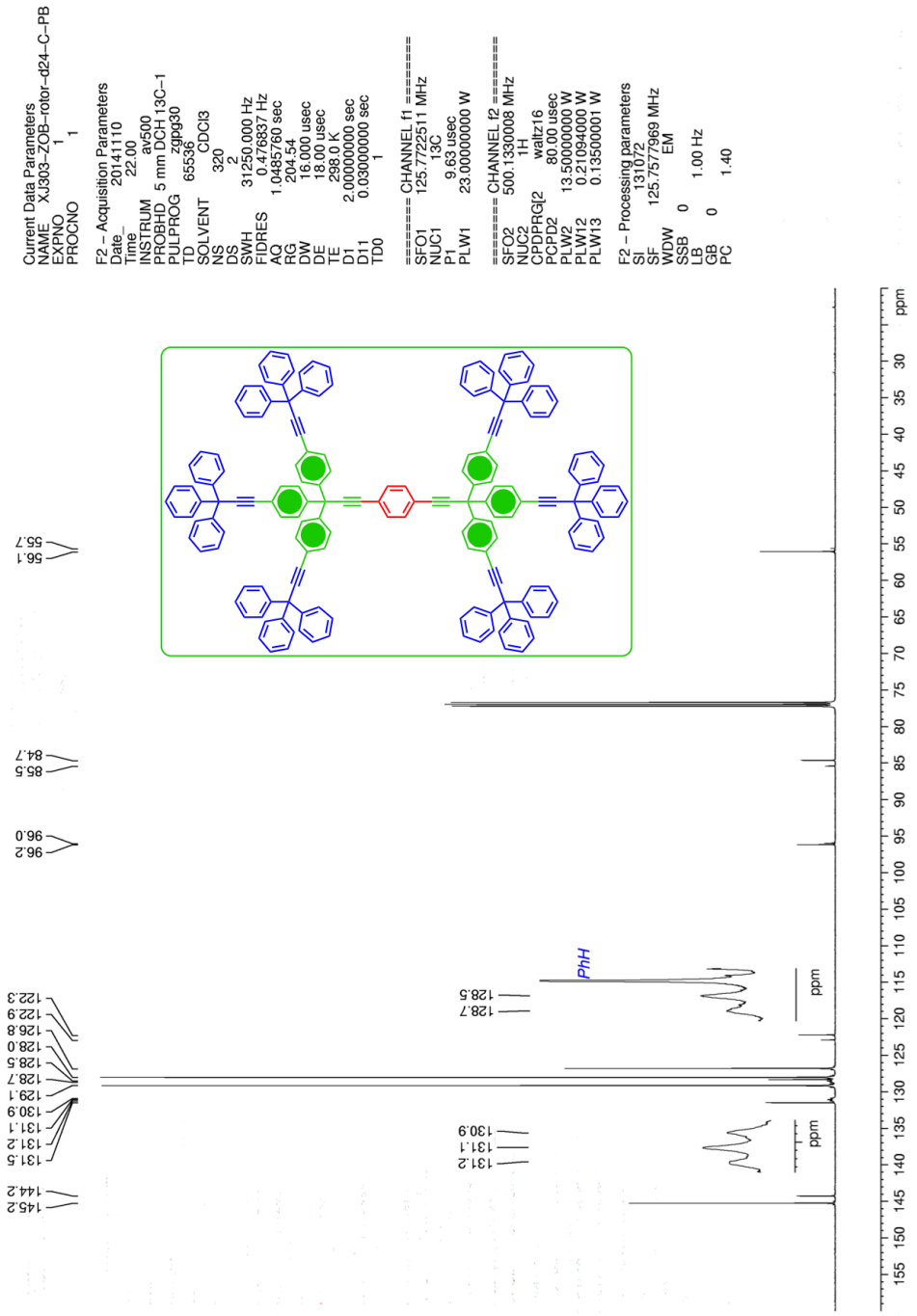

Figure A.2.28. ^{13}C NMR of compound **2**-d_{24} at 125 MHz in $CDCl_3$.

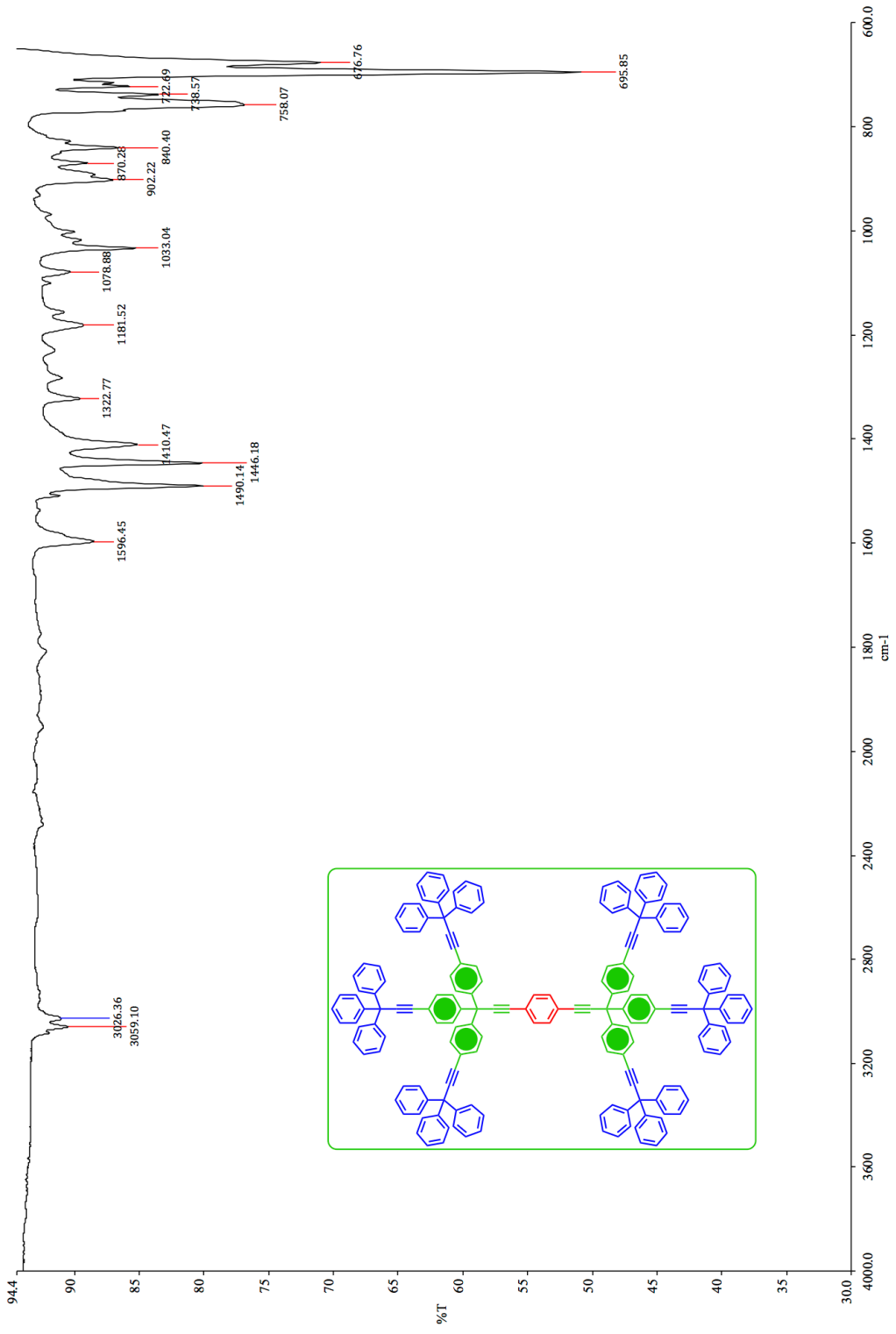

Figure A.2.29. IR of compound **2**-d_{24}.

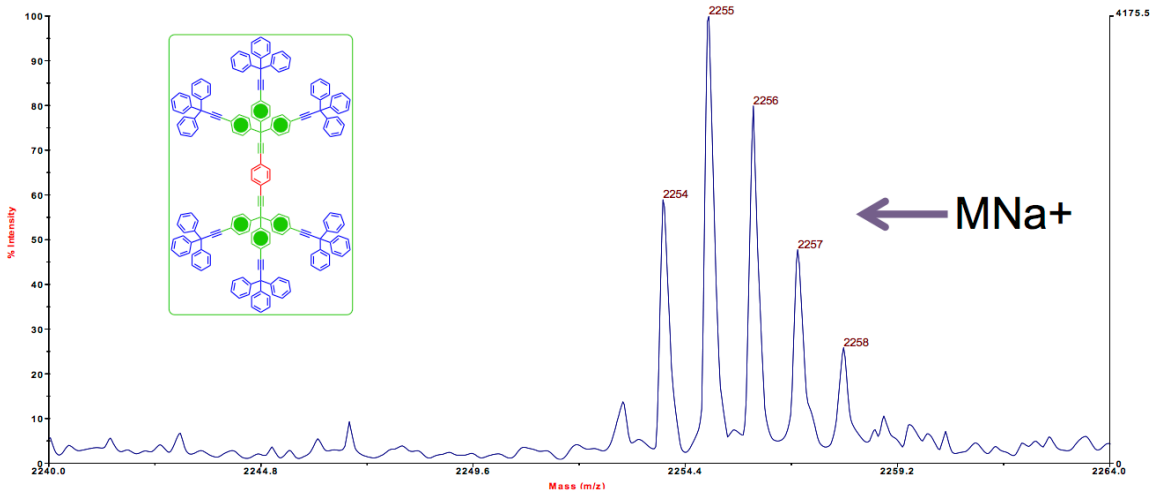

Figure A.2.30. MS (MALDI, TOF) of compound **2**-d_{24} showing the MNa^+ cluster.

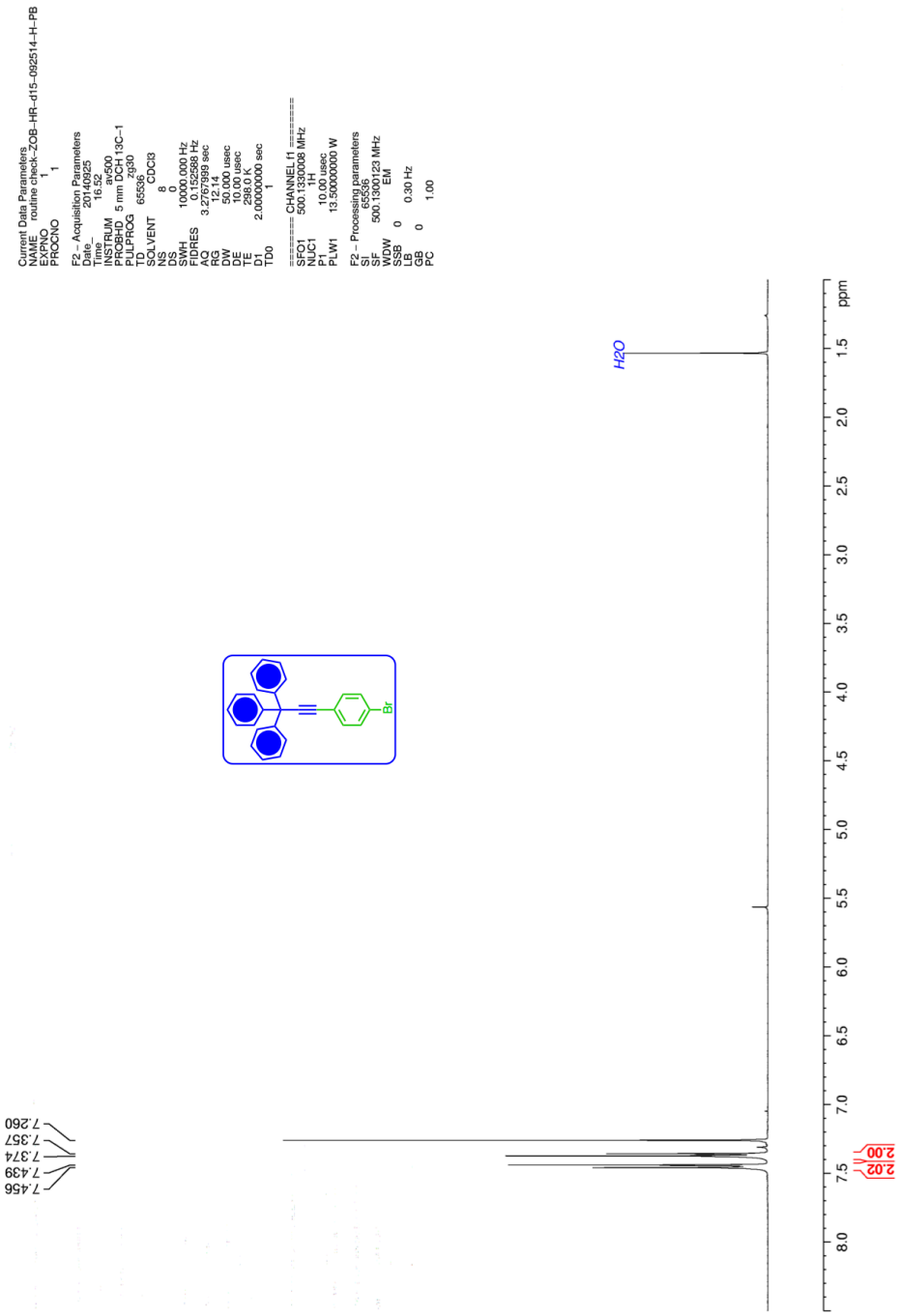

Figure A.2.31. ^{1}H NMR of compound **4**-d_{15} at 500 MHz in $CDCl_3$.

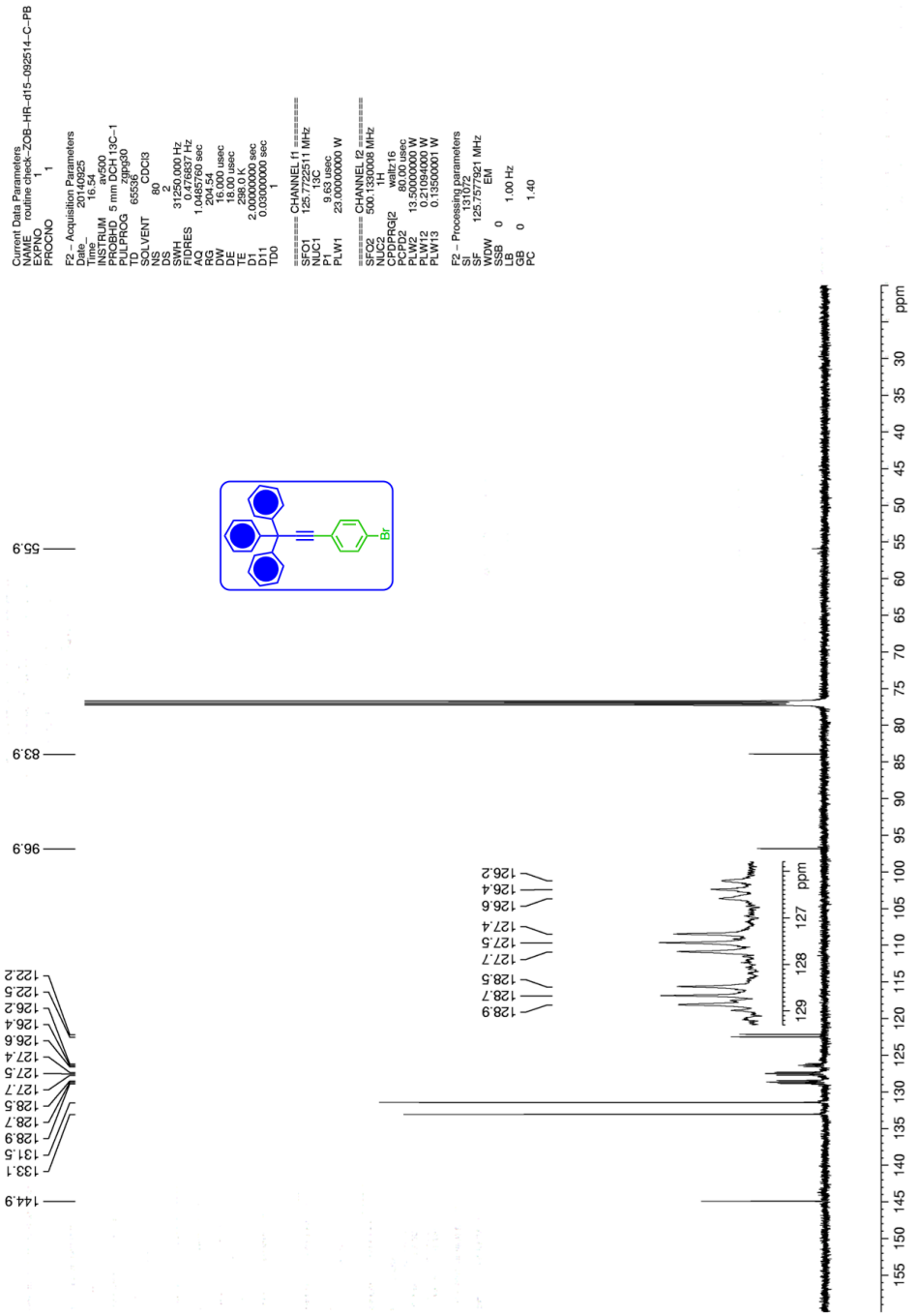

Figure A.2.32. ^{13}C NMR of compound **4**-d_{15} at 125 MHz in $CDCl_3$.

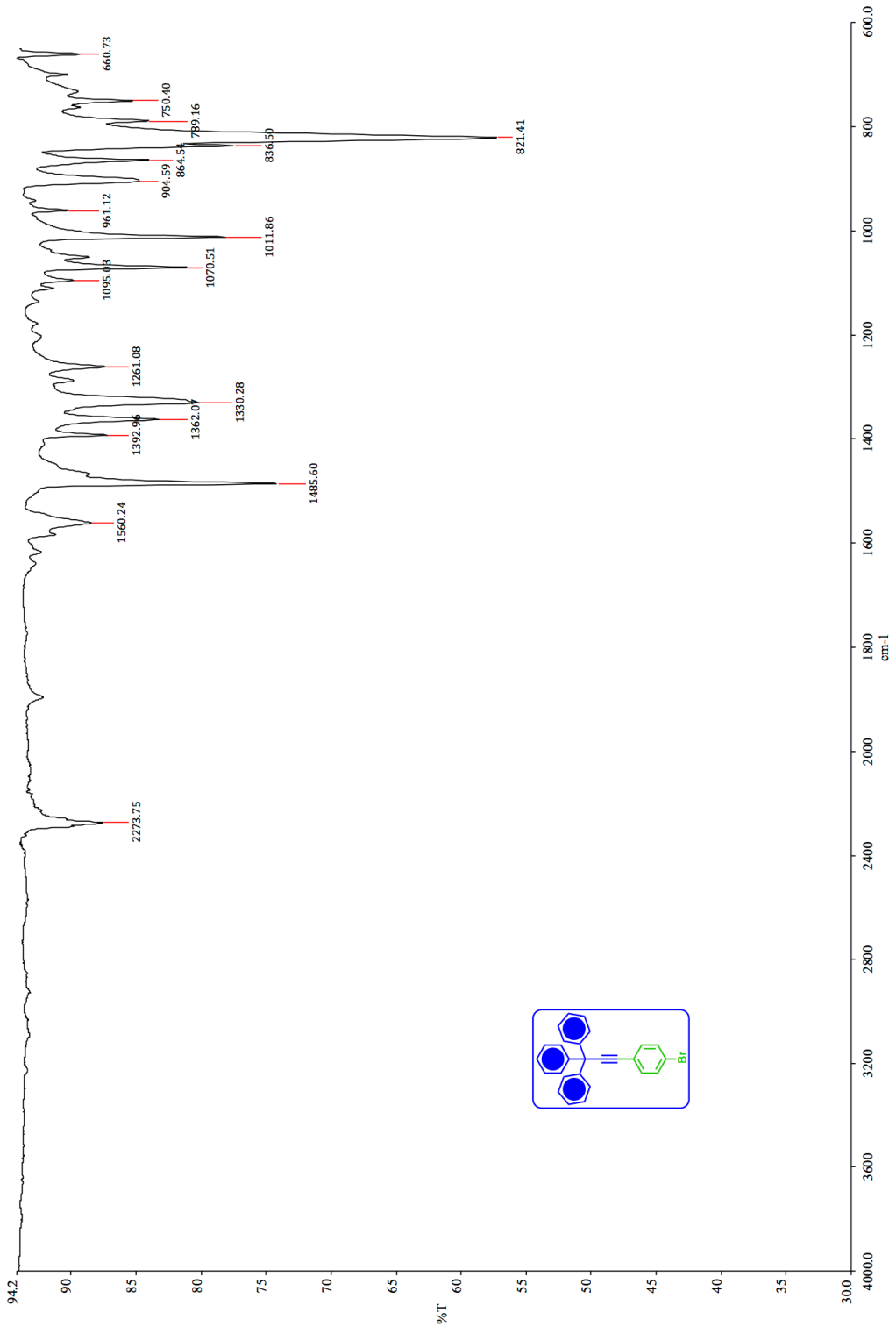

Figure A.2.33. IR of compound **4**-d_{15}.

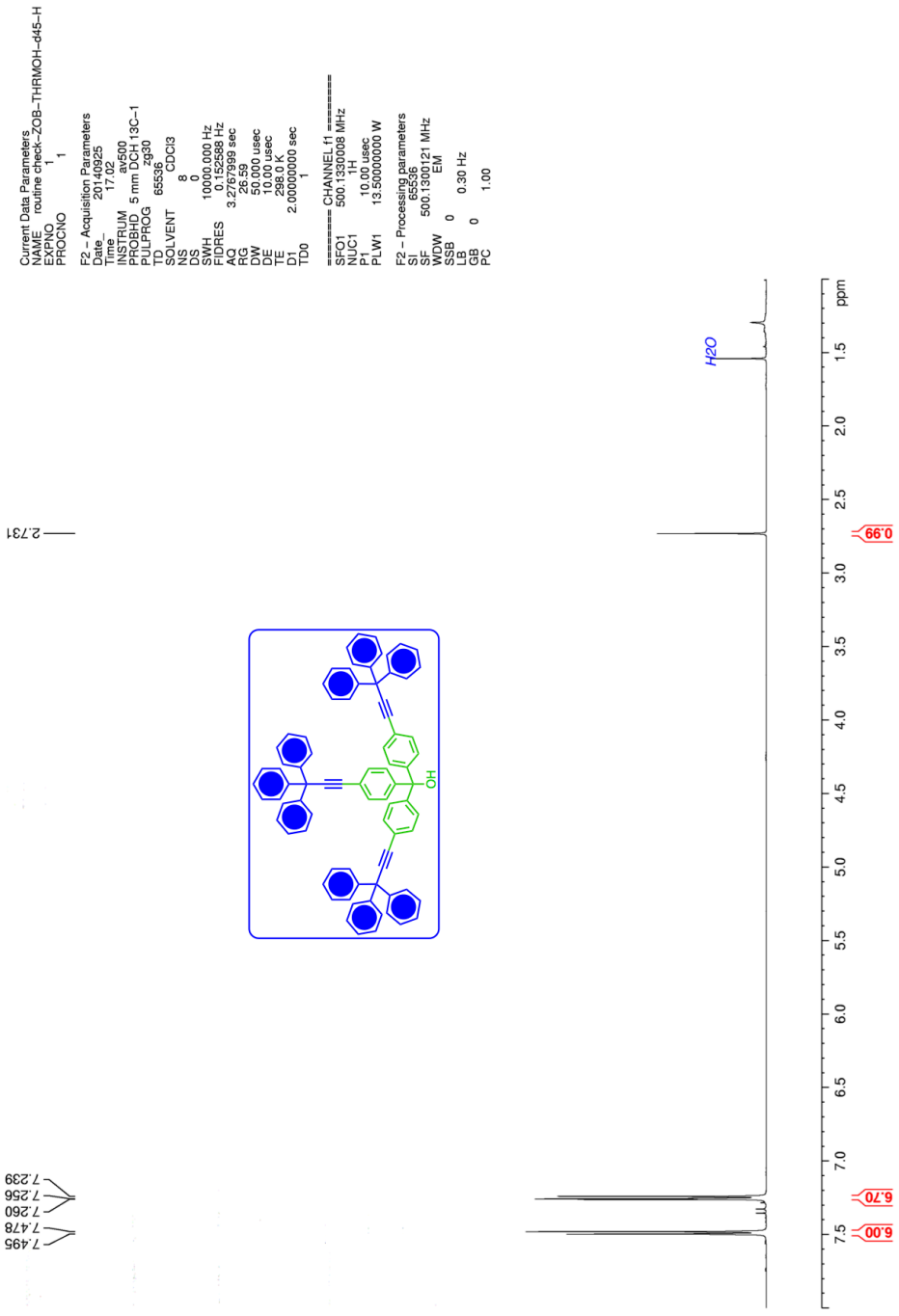

Figure A.2.34. ^{1}H NMR of compound **5**-d_{45} at 500 MHz in $CDCl_3$.

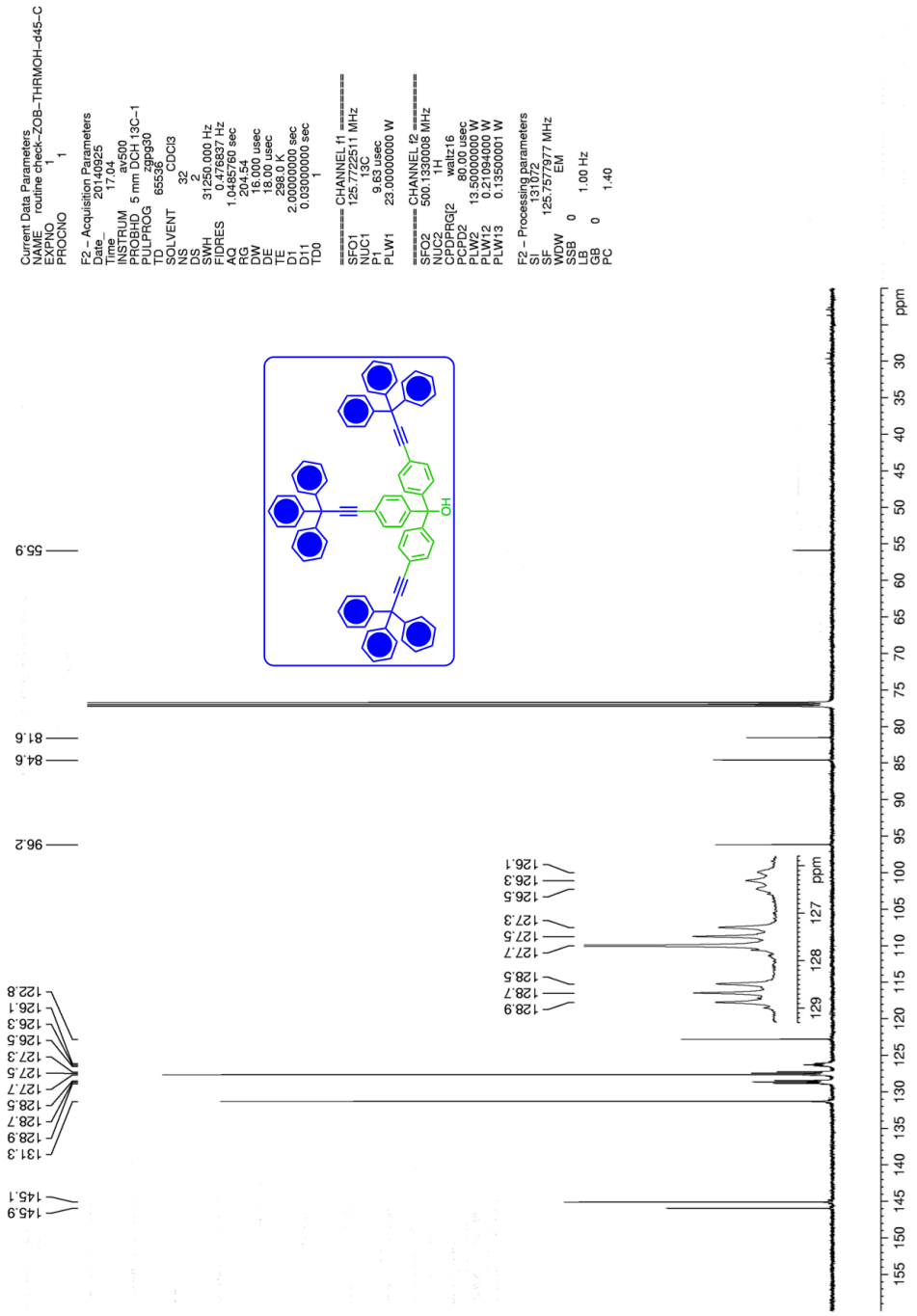

Figure A.2.35. ^{13}C NMR of compound **5**-d_{45} at 125 MHz in $CDCl_3$.

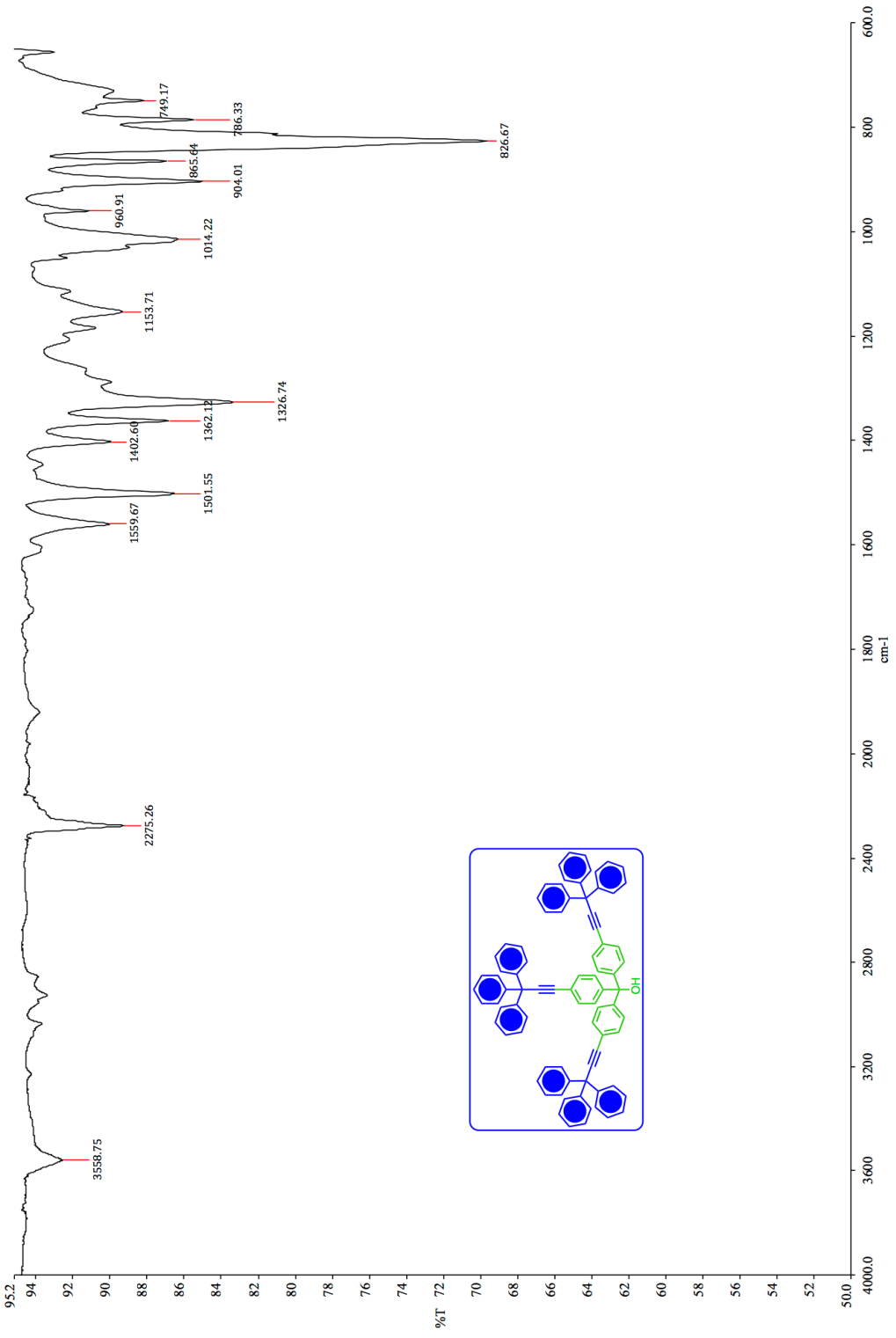

Figure A.2.36. IR of compound **5**-d_{45}.

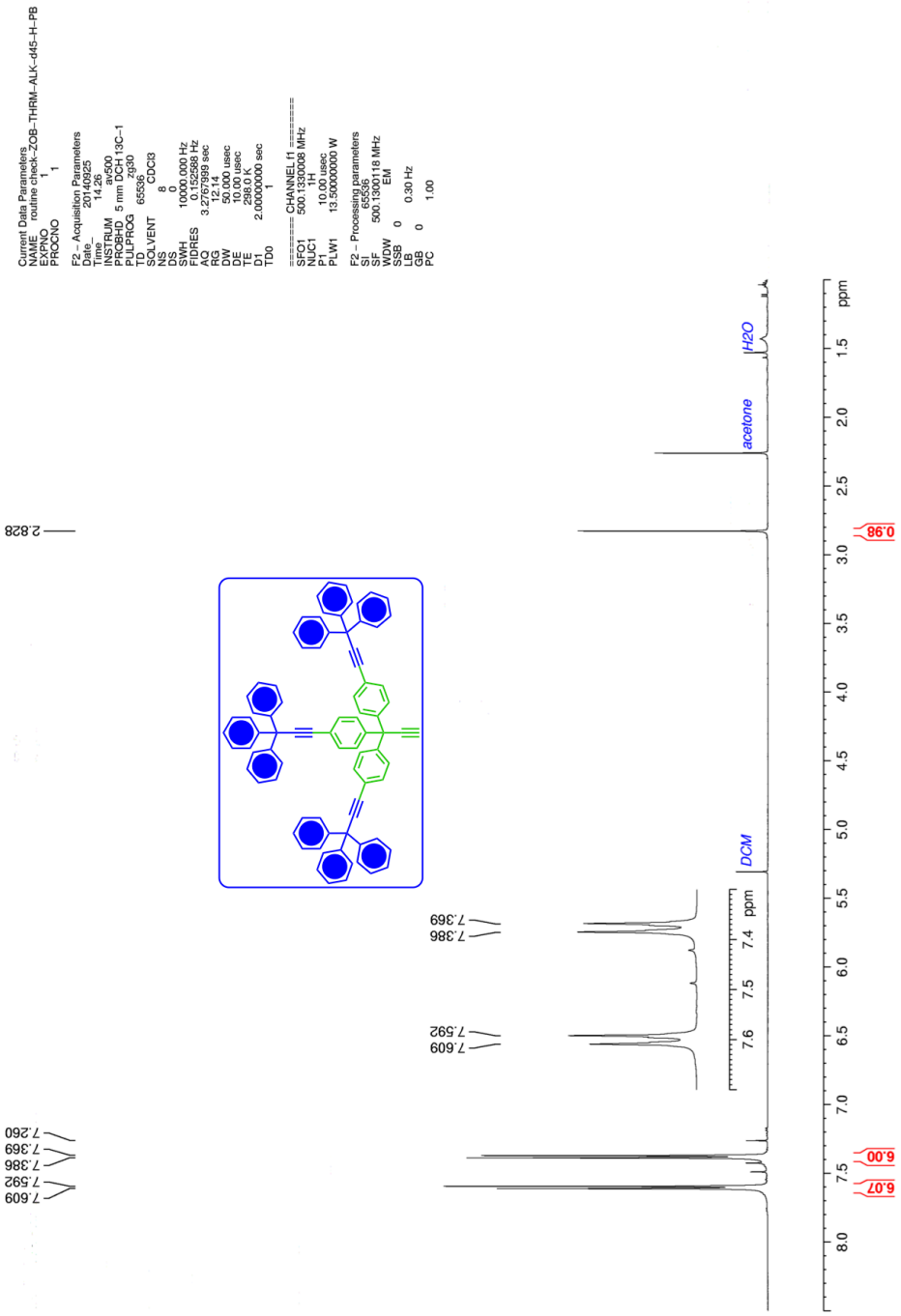

Figure A.2.37. ^{1}H NMR of compound **6**-d_{45} at 500 MHz in $CDCl_3$.

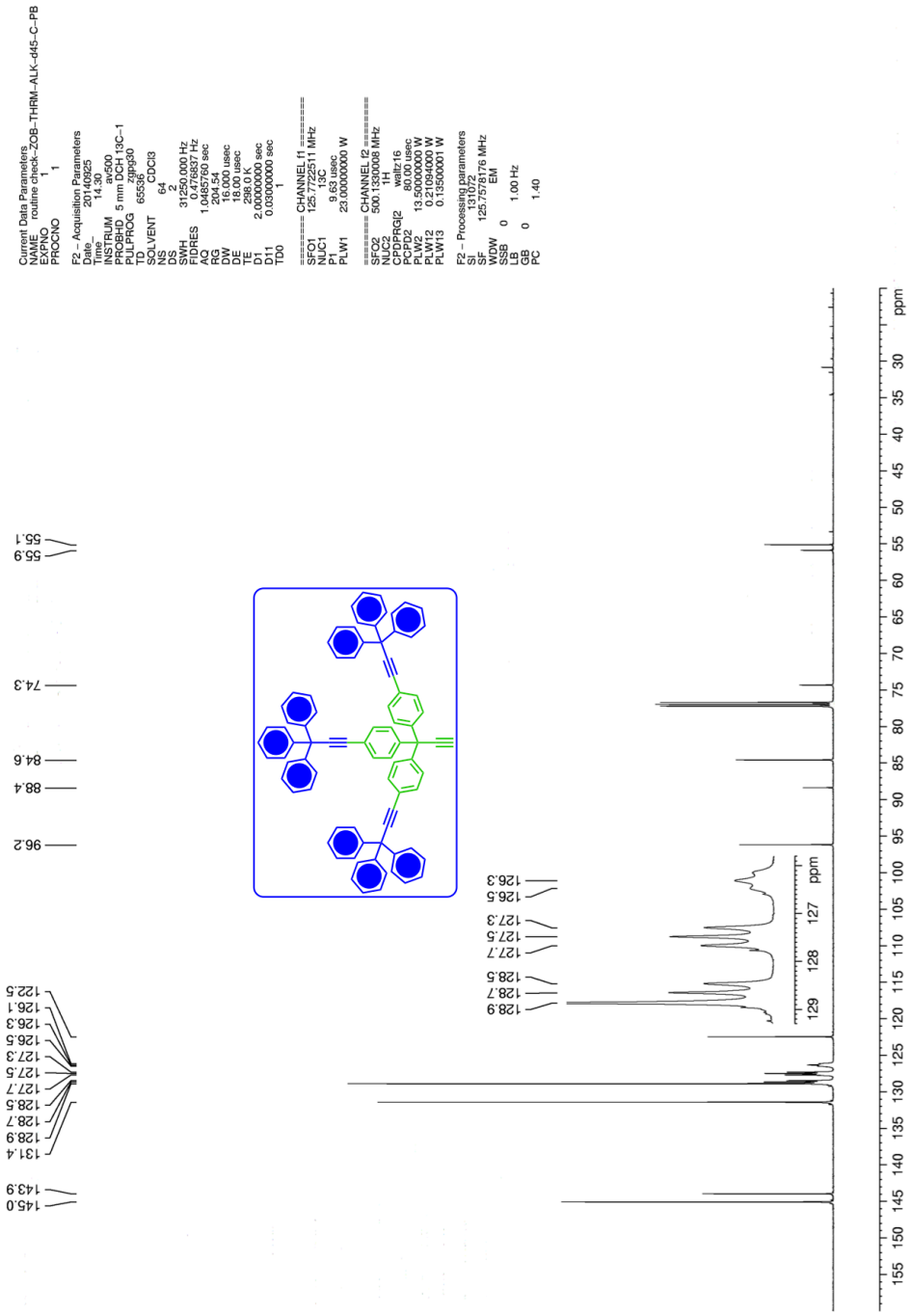

Figure A.2.38. ^{13}C NMR of compound **6**-d_{45} at 125 MHz in $CDCl_3$.

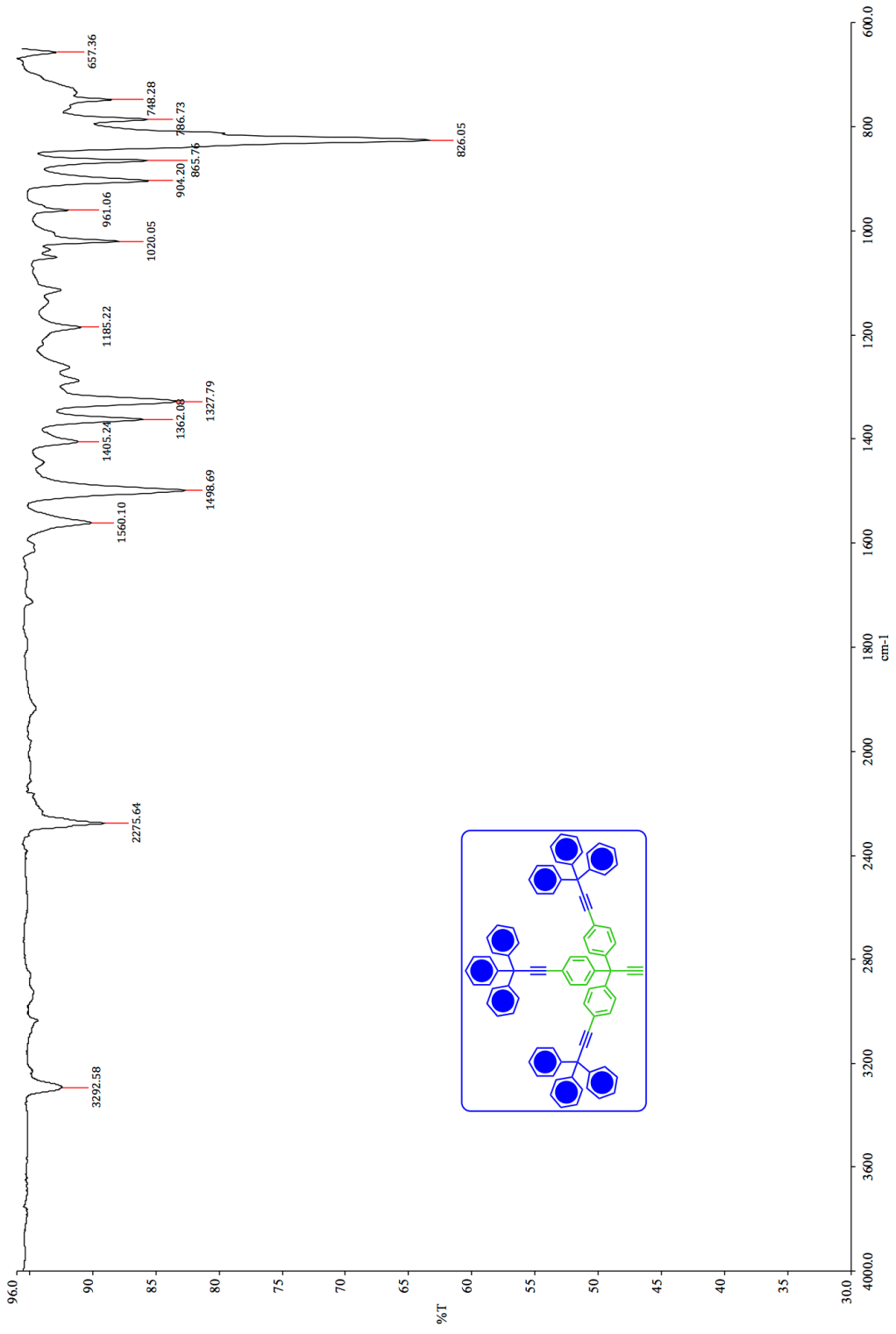

Figure A.2.39. IR of compound **6**-d_{45}.

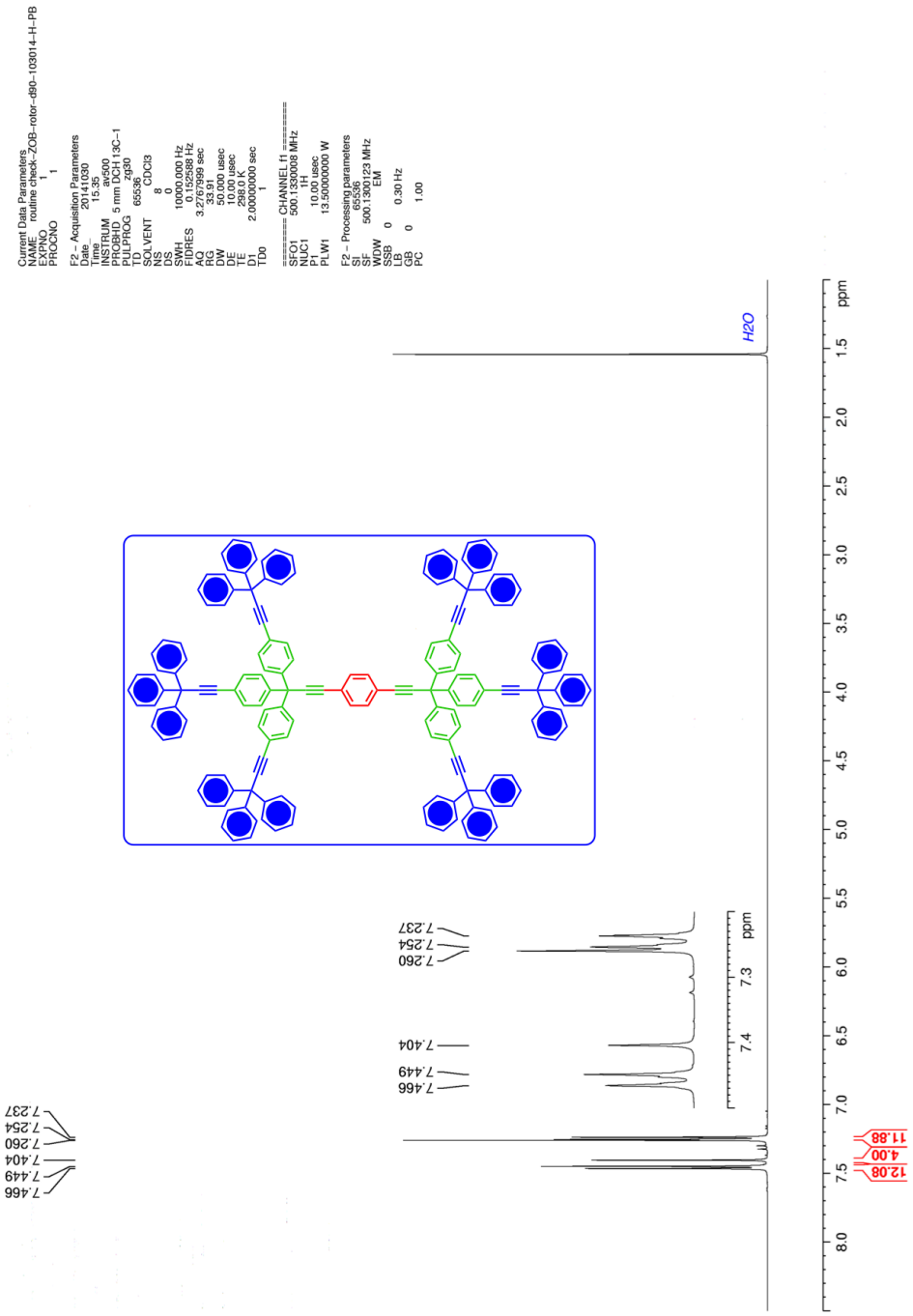

Figure A.2.40. ^{1}H NMR of compound **2**-d_{90} at 500 MHz in $CDCl_3$.

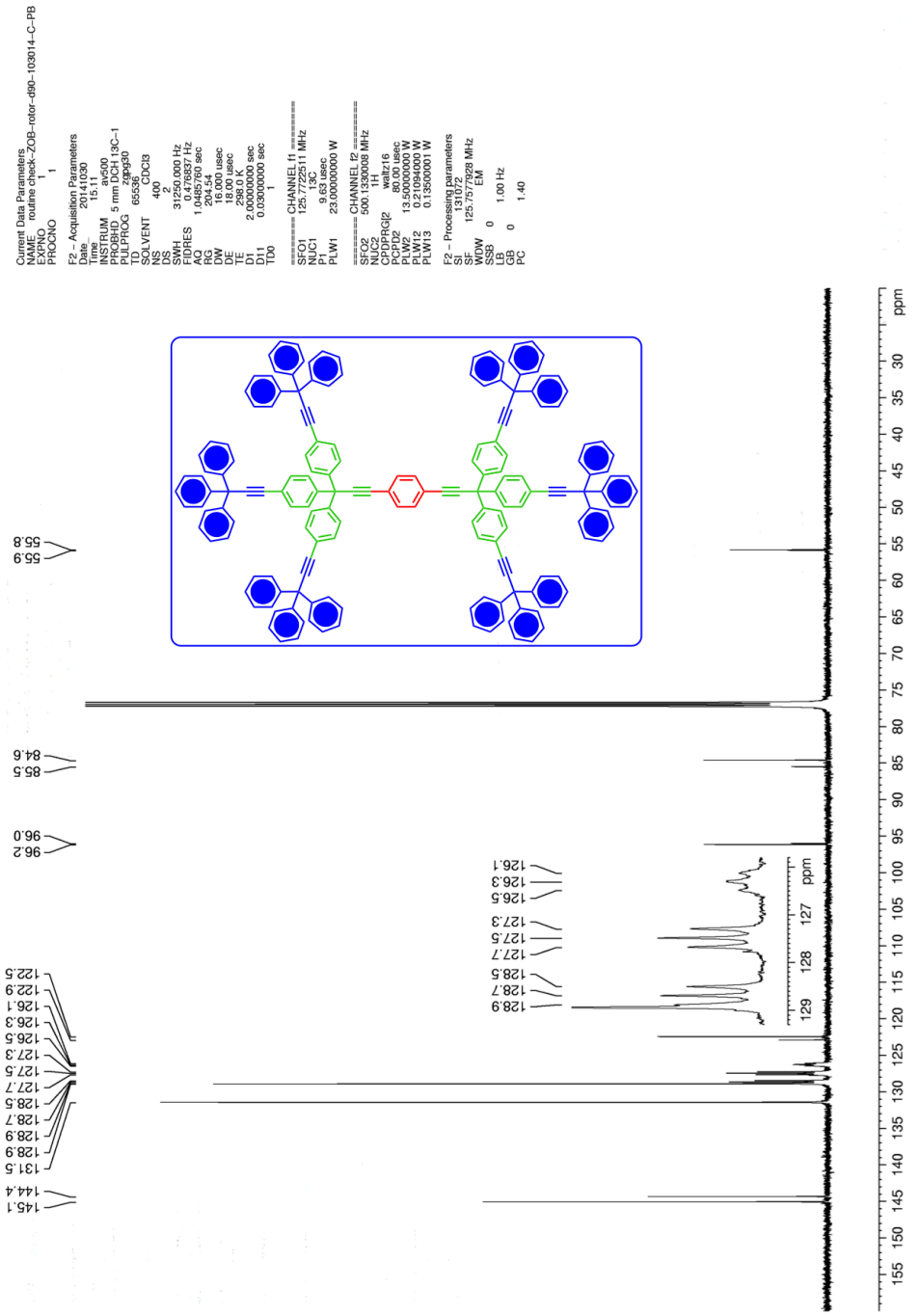

Figure A.2.41. ^{13}C NMR of compound **2**-d_{90} at 125 MHz in $CDCl_3$.

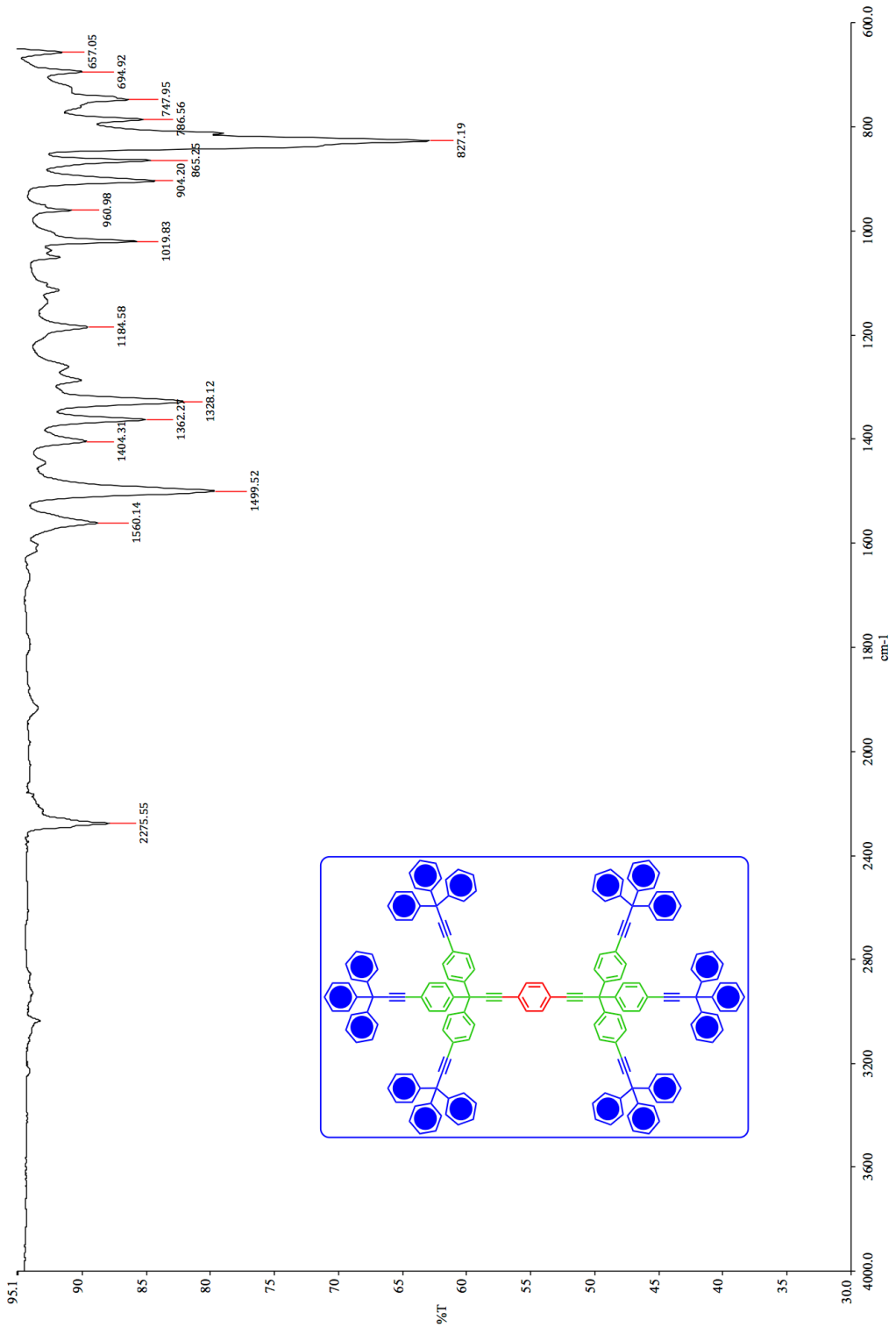

Figure A.2.42. IR of compound **2**-d_{90}.

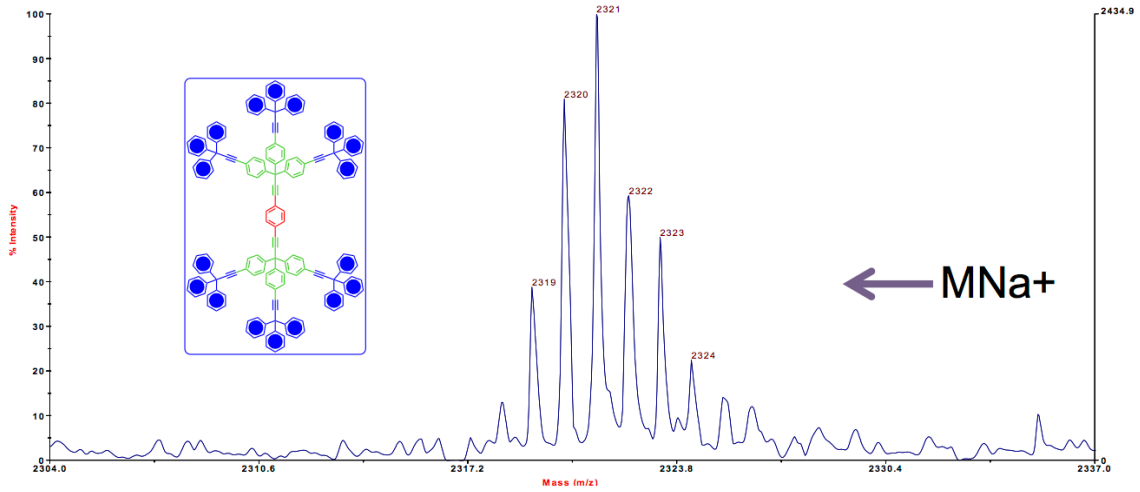

Figure A.2.43. MS (MALDI, TOF) of compound **2**-d_{90} showing the MNa^+ cluster.

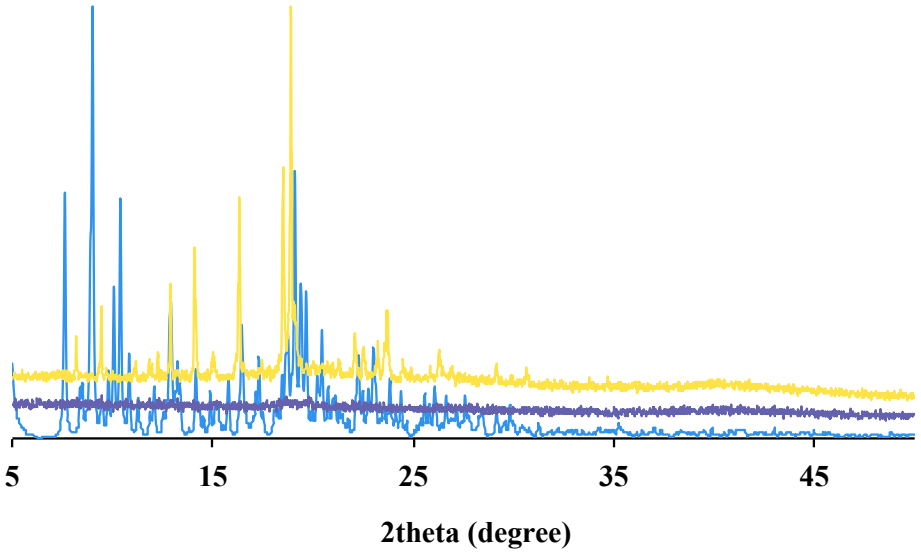

Figure A.2.44. Experimental PXRD patterns obtained for the crystalline (yellow) and the amorphous (purple) sample of **2** and the calculated (blue) pattern.

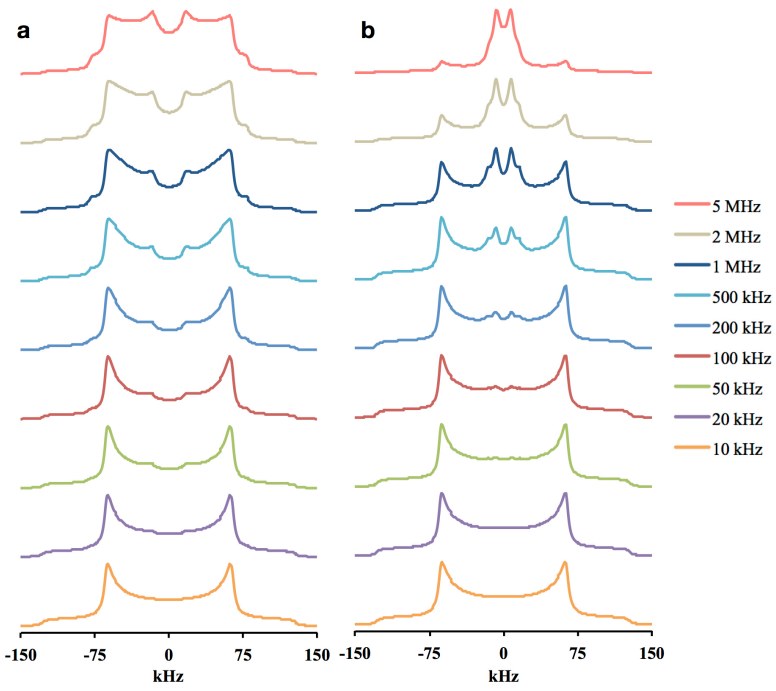

Figure A.2.45. Simulated spectra for rotor **2**-d_{90} with (a) 2-fold and (b) 4-fold rotational modes at various frequencies.

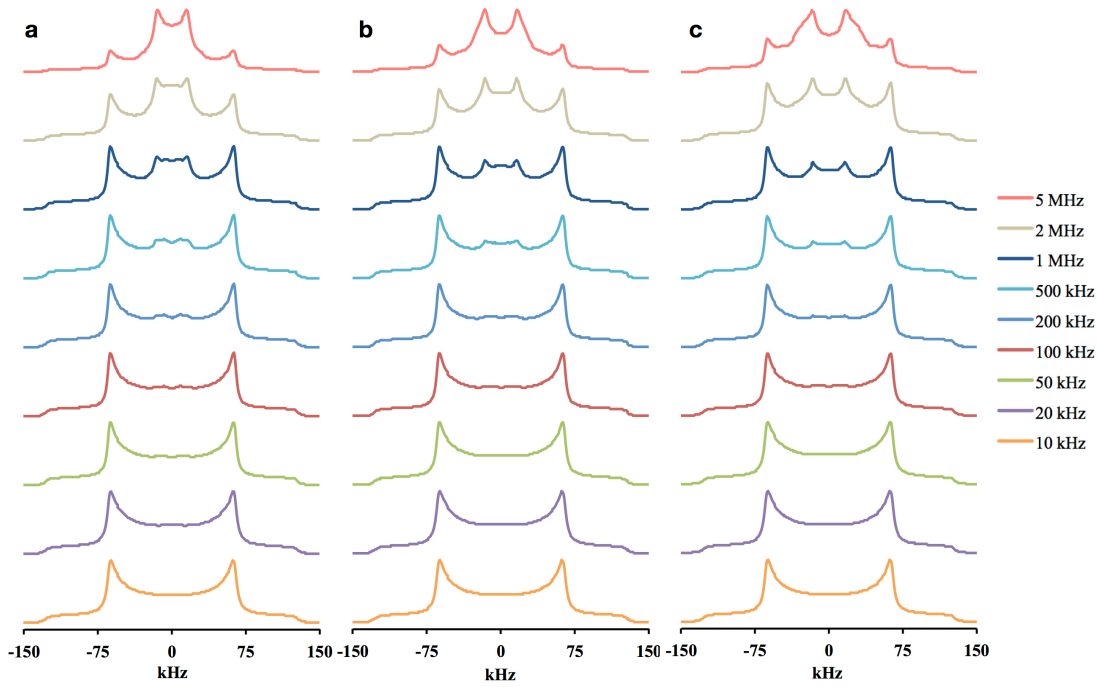

Figure A.2.46. Simulated spectra of 4-fold periphery phenyl rotations of rotor **2**-d_{90} with ratio of occupation at the 4 sites being: (a) 2:1:2:1, (b) 3:1:3:1, and (c) 4:1:4:1.

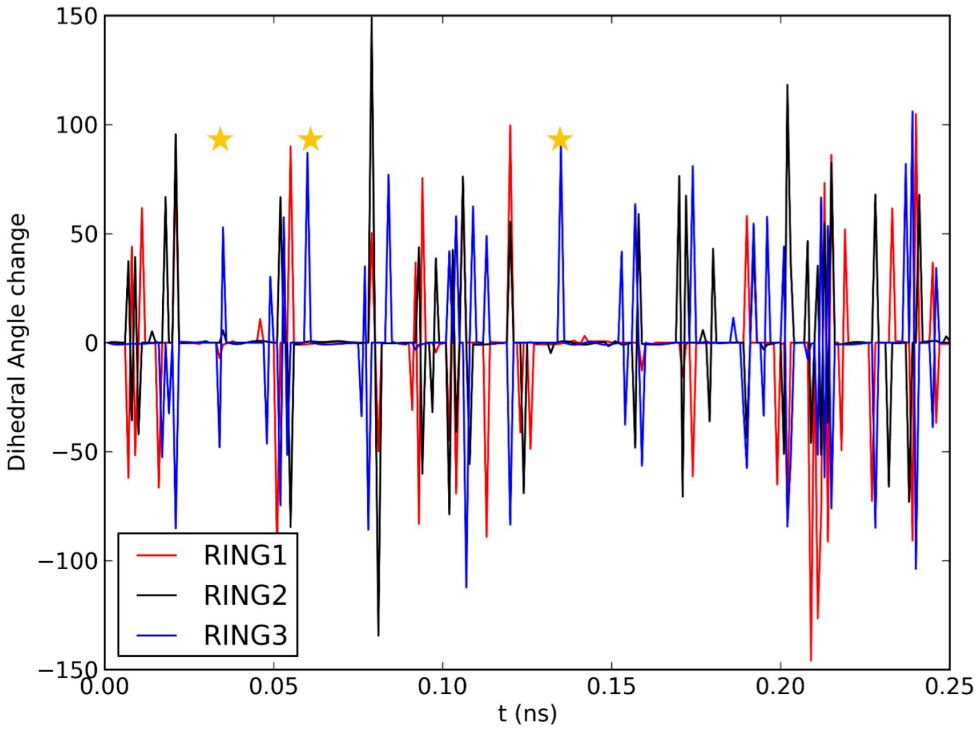

Figure A.2.47. Dihedral angle change of the phenylene groups of one branch trityl group in 250 fs with the independent rotation of one phenylene group labeled with yellow stars.

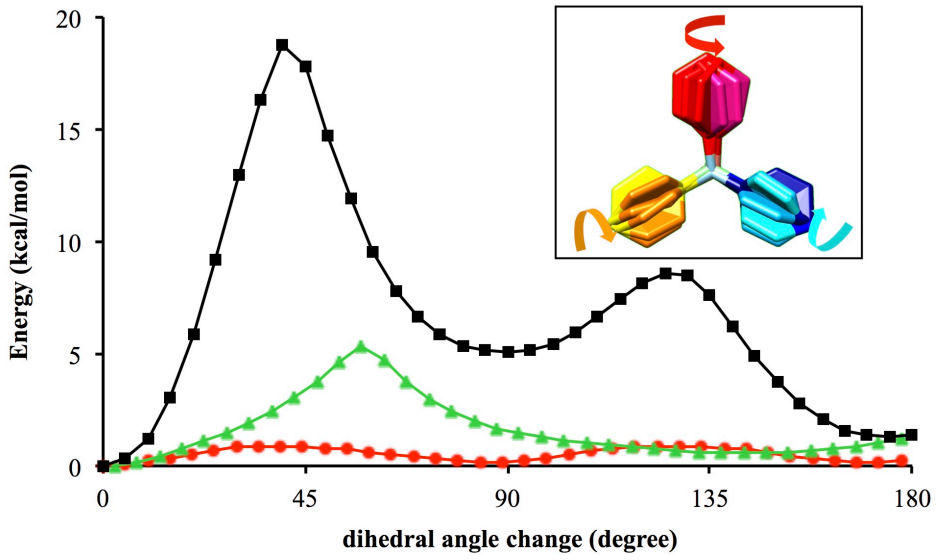

Figure A.2.48. Free energy change of different processes in vacuum including correlated rotation (red circles), isolated rotation with one (green triangles) and two rings restrained (black squares). Insert: trajectories of 90 degree correlated rotation.

Table A.2.1. "Corrected" activation energies of rotation of crystalline samples.

2-d_4		**2**-d_{24}		**2**-d_{90}	
T	E_a/(kcal/mol)	T	E_a/(kcal/mol)	T	E_a/(kcal/mol)
293 K	6.91	293 K	7.38	313 K	8.16
283 K	7.11	283 K	7.91	303 K	8.26
273 K	7.24	273 K	8.15	293 K	8.26
263 K	7.70	263 K	8.25	283 K	8.55
253 K	7.81	253 K	8.58	273 K	8.74
243 K	8.45	-	-	263 K	9.05

2.10. References

1. (a) Abendroth, J. M.; Bushuyev, O. S.; Weiss, P. S.; Barrett, C. J. *ACS Nano* **2015**, *9*, 7746. (b) Erbas-Cakmak, S.; Leigh, D. A.; McTernan, C. T.; Nussbaumer, A. L. *Chem. Rev.* **2015**, *115*, 10081. (c) Coskun, A.; Banaszak, M.; Astumian, R. D.; Stoddart, J. F.; Grzybowski, B. A. *Chem. Soc. Rev.* **2012**, *41*, 19. (d) Kinbara, K.; Aida, T. *Chem. Rev.* **2005**, *105*, 1377. (e) Kottas, G. S.; Clarke, L. I.; Horinek, D.; Michl, J. *Chem. Rev.* **2005**, *105*, 1281.

2. (a) Cheng, C.; McGonigal, P. R.; Schneebeli, S. T.; Li, H.; Vermeulen, N. A.; Ke, C.; Stoddart, J. F. *Nat. Nanotechnol.* **2015**, *10*, 547. (b) Li, Q.; Fuks, G.; Moulin, E.; Maaloum, M.; Rawiso, M.; Kulic, I.; Foy, J. T.; Giuseppone, N. *Nat. Nanotechnol.* **2015**, *10*, 161. (c) Ragazzon, G.; Baroncini, M.; Silvi, S.; Venturi, M.; Credi, A. *Nat. Nanotechnol.* **2015**, *10*, 70. (d) De, S.; Pramanik, S.; Schmittel, M. *Angew. Chem., Int. Ed.* **2014**, *53*, 14255. (e) Conyard, J.; Cnossen, A.; Browne, W. R.; Feringa, B. L.; Meech, S. R. *J. Am. Chem. Soc.* **2014**, *136*, 9692. (f) Lewandowski, B.; De Bo, G.; Ward, J. W.; Papmeyer, M.; Kuschel, S.; Aldegunde, M. J.; Gramlich, P. M. E.; Heckmann, D.; Goldup, S. M.; D'Souza, D. M.; Fernandes, A. E.; Leigh, D. A. *Science* **2013**, *339*, 189. (g) Perera, U. G. E.; Ample, F.; Kersell, H.; Zhang, Y.; Vives, G.; Echeverria, J.; Grisolia, M.; Rapenne, G.; Joachim, C.; Hla, S.-W. *Nat. Nanotechnol.* **2013**, *8*, 46. (h) Thies, S.; Sell, H.; Schütt, C.; Bornholdt, C.; Näther, C.; Tuczek, F.; Herges, R. *J. Am. Chem. Soc.* **2011**, *133*, 16243. (i) Hess, G. D.; Hampel, F.; Gladysz, J. A. *Organometallics* **2007**, *26*, 5129.

3. (a) Vogelsberg, C. S.; Garcia-Garibay, M. A. *Chem. Soc. Rev.* **2012**, *41*, 1892. (b) Khuong, T.-A. V.; Nuñez, J. E.; Godinez, C. E.; Garcia-Garibay, M. A. *Acc. Chem. Res.*

2006, *39*, 413. (c) Garcia-Garibay, M. A. *Proc. Natl. Acad. Sci. U. S. A.* **2005**, *102*, 10771.

4. (a) Pérez-Estrada, S.; Rodríguez-Molina, B.; Xiao, L.; Santillan, R.; Jiménez-Osés, G.; Houk, K. N.; Garcia-Garibay, M. A. *J. Am. Chem. Soc.* **2015**, *137*, 2175. (b) Jiang, X.; Rodríguez-Molina, B.; Nazarian, N.; Garcia-Garibay, M. A. *J. Am. Chem. Soc.* **2014**, *136*, 8871. (c) Commins, P.; Garcia-Garibay, M. A. *J. Org. Chem.* **2014**, *79*, 1611. (d) Rodríguez-Molina, B.; Farfán, N.; Romero, M.; Méndez-Stivalet, M. J.; Santillan, R.; Garcia-Garibay, M. A. *J. Am. Chem. Soc.* **2011**, *133*, 7280. (e) Jarowski, P. D.; Houk, K. N.; Garcia-Garibay, M. A. *J. Am. Chem. Soc.* **2007**, *129*, 3110. (f) Horansky, R. D.; Clarke, L. I.; Price, J. C.; Khuong, T.; Jarowski, P. D.; Garcia-Garibay, M. A. *Phys. Rev. B* **2005**, *72*, 014302.

5. (a) O'Brien, Z. J.; Natarajan, A.; Khan, S.; Garcia-Garibay, M. A. *Cryst. Growth Des.* **2011**, *11*, 2654. (b) Karlen, S. D.; Reyes, H.; Taylor, R. E.; Khan, S. I.; Hawthorne, M. F.; Garcia-Garibay, M. A. *Proc. Natl. Acad. Sci. U. S. A.* **2010**, *107*, 14973. (c) Rodríguez-Molina, B.; Ochoa, M. E.; Farfán, N.; Santillan, R.; Garcia-Garibay, M. A. *J. Org. Chem.* **2009**, *74*, 8554. (d) Khuong, T.-A. V.; Dang, H.; Jarowski, P. D.; Maverick, E. F.; Garcia-Garibay, M. A. *J. Am. Chem. Soc.* **2007**, *129*, 839. (e) Dominguez, Z.; Khuong, T.; Dang, H.; Sanrame, C. N.; Nuñez, J. E.; Garcia-Garibay, M. A. *J. Am. Chem. Soc.* **2003**, *125*, 8827. (f) Dominguez, Z.; Dang, H.; Strouse, M. J.; Garcia-Garibay, M. A. *J. Am. Chem. Soc.* **2002**, *124*, 7719. (g) Dominguez, Z.; Dang, H.; Strouse, M. J.; Garcia-Garibay, M. A. *J. Am. Chem. Soc.* **2002**, *124*, 2398.

6. (a) Harada, J.; Ohtani, M.; Takahashi, Y.; Inabe, T. *J. Am. Chem. Soc.* **2015**, *137*, 4477. (b) Zhu, K.; O'Keefe, C. A.; Vukotic, V. N.; Schurko, R. W.; Loeb, S. J. *Nat.*

Chem. **2015**, *7*, 514. (c) Comotti, A.; Bracco, S.; Yamamoto, A.; Beretta, M.; Hirukawa, T.; Tohnai, N.; Miyata, M.; Sozzani, P. *J. Am. Chem. Soc*. **2014**, *136*, 618. (d) Zhang, Q.-C.; Wu, F.-T.; Hao, H.-M.; Xu, H.; Zhao, H.-X.; Long, L.-S.; Huang, R.-B.; Zheng, L.-S. *Angew. Chem. Int. Ed*. **2013**, *52*, 12602. (e) Setaka, W.; Yamaguchi, K. *J. Am. Chem. Soc*. **2013**, *135*, 14560. (f) Lemouchi, C.; Iliopoulos, K.; Zorina, L.; Simonov, S.; Wzietek, P.; Cauchy, T.; Rodríguez-Fortea, A.; Canadell, E.; Kaleta, J.; Michl, J.; Gindre, D.; Chrysos, M.; Batail, P. *J. Am. Chem. Soc*. **2013**, *135*, 9366. (g) Zhang, Y.; Zhang, W.; Li, S.-H.; Ye, Q.; Cai, H.-L.; Deng, F.; Xiong, R.-G.; Huang, S. D. *J. Am. Chem. Soc*. **2012**, *134*, 11044. (h) Vukotic, V. N.; Harris, K. J.; Zhu, K.; Schurko, R. W.; Loeb, S. J. *Nat. Chem*. **2012**, *4*, 456. (i) Akutagawa, T.; Koshinaka, H.; Sato, D.; Takeda, S.; Noro, S.-I.; Takahashi, H.; Kumai, R.; Tokura, Y.; Nakamura, T. *Nat. Mater*. **2009**, *8*, 342. (j) Jain, P.; Dalal, N. S.; Toby, B. H.; Kroto, H. W.; Cheetham, A. K. *J. Am. Chem. Soc*. **2008**, *130*, 10450.

7. (a) Schliwa, M.; Woehlke, G. *Nature* **2003**, *422*, 759. (b) Piccolino, M. *Nat. Rev. Mol. Cell Biol*. **2000**, *1*, 149.

8. (a) May, R.; Jester, S.-S.; Höger, S. *J. Am. Chem. Soc*. **2014**, *136*, 16732. (b) Shen, X.; Ho, D. M.; Pascal, R. A. *J. Am. Chem. Soc*. **2004**, *126*, 5798.

9. Karlen, S. D.; Garcia-Garibay, M. A. *Chem. Commun*. **2005**, 189.

10. Heck, H. D. A.; Simon, R. L.; Anbar, M. *J. Chromatogr*. **1977**, *133*, 281.

11. Tanaka, N.; Thornton, E. R. *J. Am. Chem. Soc*. **1976**, *98*, 1617.

12. (a) Kondratuk, D. V.; Sprafke, J. K.; O'Sullivan, M. C.; Perdigao, L. M. A.; Saywell, A.; Malfois, M.; O'Shea, J. N.; Beton, P. H.; Thompson, A. L.; Anderson, H. L. *Chem. Eur. J*. **2014**, *20*, 12826. (b) Bauer, R. E.; Enkelmann, V.; Wiesler, U. M.; Berresheim, A.

J.; Müllen, K. *Chem. Eur. J.* **2002**, *8*, 3858. (c) Nielsen, M. B.; Schreiber, M.; Baek, Y. G.; Seiler, P.; Lecomte, S.; Boudon, C.; Tykwinski, R. R.; Gisselbrecht, J.-P.; Gramlich, V.; Skinner, P. J.; Bosshard, C.; Günter, P.; Gross, M.; Diederich, F. *Chem. Eur. J.* **2001**, *7*, 3263. (d) Ipaktschi, J.; Hosseinzadeh, R.; Schlaf, P.; Dreiseidler, E.; Goddard, R. *Helv. Chim. Acta* **1998**, *81*, 1821.

13. Crystals of almost identical cell parameters could be obtained from an *o*-xylene/2,2,4-trimethylpentane mixture with the only differences being the solvent molecules included in the crystals.

14. Spek, A. *Acta Crystallogr. D* **2009**, *65*, 148.

15. The packing coefficient increases to 0.69 when the solvent molecules in the crystal are included. Molecular volumes were calculated using the group increment approach reported in (a) Gavezzotti, A. *J. Am. Chem. Soc.* **1983**, *105*, 5220. (b) Bondi, A. *J. Phys. Chem.* **1964**, *68*, 441. The results agree closely with volumes calculated using (c) Spartan'08 Wavefunction, Inc. Irvine, CA.

16. Dunitz, J. D.; Gavezotti, A. *Acc. Chem. Res.* **1999**, *32*, 677.

17. (a) Schoenborn, B. P.; Garcia, A.; Knott, R. *Prog. Biophys. Mol. Biol.* **1995**, *64*, 105. (b) Richards, F. M. *Annu. Rev. Biophys. Bioeng.* **1977**, *6*, 151.

18. Hansen, M. R.; Graf, R.; Spiess, H. W. *Acc. Chem. Res.* **2013**, *46*, 1996.

19. Macho, V.; Brombacher, L.; Spiess, H. W. *Appl. Magn. Reson.* **2001**, *20*, 405.

20. The SS ^{2}H NMR spectra for the crystalline samples were obtained in the presence of the solvent supernatant to avoid solvent loss and amorphization during the data acquisition. For all the VT experiments, samples were gradually heated or cooled from

293 K to the target temperature. Sample integrity and data reproducibility was analyzed by measuring the 293 K spectra at the end of each experiment.

21. Structurally heterogeneous systems that have a range of activation energies can often be described by a Gaussian distribution centered at E_{a0} with a width σ, which gives rise to a log-Gaussian distribution of rates. Under these conditions, the weight $f(k)$ of a certain rate k to the total is given by a log-Gaussian distribution according to the following equation, where the most probable rate is k_0 and the width of the distribution is given σ,

$$f(x) = \frac{1}{\sigma}\sqrt{\frac{1}{2\pi}}e^{(-\frac{x^2}{2\sigma^2})}$$

with $x = \ln(k / k_0)$.

22. Case, D. A.; Babin, V.; Berryman, J.; Betz, R. M.; Cai, Q.; Cerutti, D. S.; Cheatham III, T. E.; Darden, T. A.; Duke, R. E.; Gohlke, H.; Goetz, A. W.; Gusarov, S.; Homeyer, N.; Janowski, P.; Kaus, J.; Kolossvary, I.; Kovalenko, A.; Lee, T. S.; LeGrand, S.; Luchko, T.; Luó, R.; Madej, B.; Merz, K. M.; Paesani, F.; Roe, D. R.; Roitberg, A.; Sagui, C.; Salomon-Ferrer, R.; Seabra, G.; Simmerling, C. L.; Smith, W.; Swails, J.; Walker, R. C.; Wang, J.; Wolf, R. M.; Wu, X.; Kollman, P. A. *AMBER 14*, 2014.

23. Grossfield, A. Wham: the weighted histogram, analysis method, version 2.0.9, http://membrane.urmc.rochester.edu/content/wham, accessed Jan 27, 2016.

24. Gust, D.; Mislow, K. *J. Am. Chem. Soc.* **1973**, *95*, 1535.

25. Inertial rotational frequency τ_{IR}^{-1} can be estimated from the moment of inertia (I) of a rotator using the equation $\tau_{IR}^{-1} = [(2\pi/9)\ (I/k_BT)^{1/2}]^{-1}$, where I is moment of inertia measured along the rotational axis. Please see: Kawski, A. *Crit. Rev. Anal. Chem.* **1993**, *23*, 459.

26. Vogelsberg, C. S.; Bracco, S.; Beretta, M.; Comotti, A.; Sozzani, P.; Garcia-Garibay, M. A. *J. Phys. Chem. B* **2012**, *116*, 1623.

Chapter Three

Rotation of a Bulky Triptycene in the Solid State:

Toward Engineered Nanoscale Artificial Molecular Machines

3.1. Introduction

The development of artificial molecular machines represents a significant challenge in current science as it demands a deep understanding of the relationship between structure and dynamics, so that both characteristics can be combined to control mechanical functions resulting from molecular and supramolecular design.[1,2] Pioneering research by Mislow and coworkers in the 1980s analyzed the correlated motions of triarylmethanes and triptycene gears in solution,[3] laying the ground for the development of molecular rotors[4] capable of undergoing mechanical processes and switching functions controlled by physical and chemical stimuli.

Considering that many macroscopic and biomolecular machines feature dense, multicomponent structures, we and others have explored some of the structural factors that enable molecular rotation in the solid state.[5,6] It is known that globular methyl groups, with a small moment of inertia and a very small van de Waals contact area, are able to undergo Brownian rotation in the GHz to THz regimes in most solids.[7] By contrast, solid-state rotation of phenylene and bicyclo[2.2.2]octylidene groups, with larger van de Waals surfaces and more steric interactions, is not common, but it can be strongly facilitated in structures akin to macroscopic gyroscopes[5,8] with two shielding groups coaxially linked by triple bonds to the central rotator,[9] as shown in Figure 3.1a. Isomorphous crystals of molecular rotor **1** and **2** with triphenylsilyl stators were shown to display Brownian rotation with ambient-temperature site exchange frequencies of 9 and 110 MHz, corresponding to activation energies of 8.5 and 3.5 kcal/mol, respectively.[8] Experimental observations indicate that the size, shape, and symmetry of the rotator play very important roles in their thermal motion, pointing out that structural factors must be

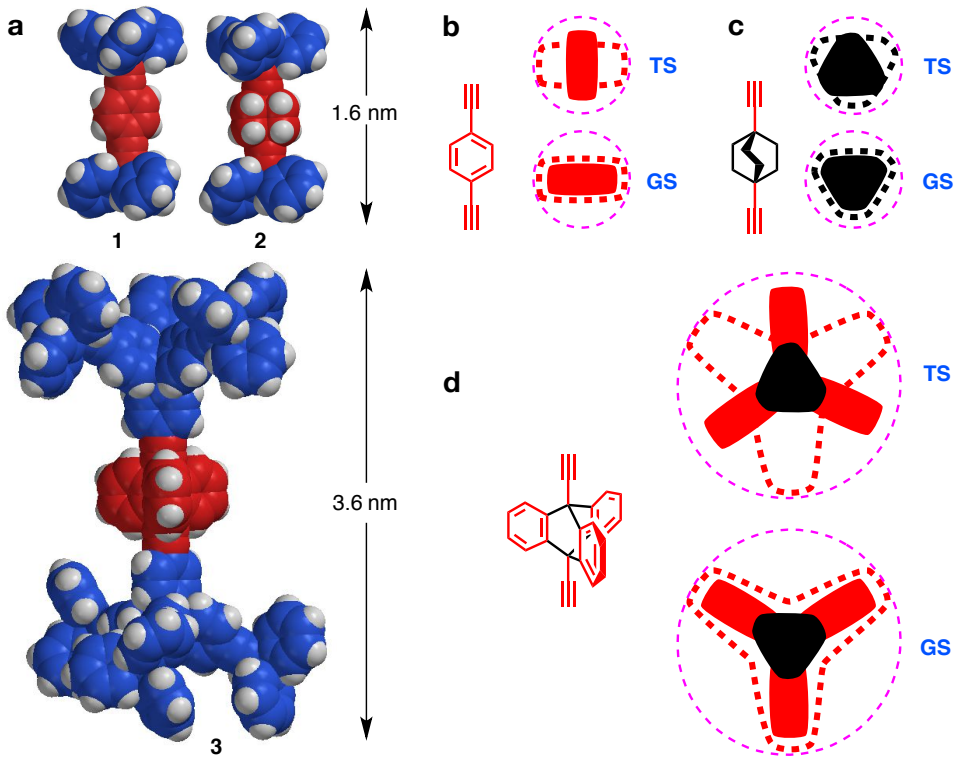

Figure 3.1. (a) Space-filling models of molecular rotors **1**, **2** and **3** with 1,4-phenylene, 1,4-bicyclo[2.2.2]octylidene, and 9,10-triptycylidene rotators. The cross sections of the three rotators, of their reaction cavities, and of their volumes of revolution are represented with a filled shape, a heavy dashed line, and a thin dashed circle for (b) 1,4-phenylene, (c) 1,4-bicyclo[2.2.2]octylidene, and (d) 9,10-triptycylidene, at the ground state (GS) and rotational transition state (TS).

considered for the design of nanoscale rotors such as **3**, which may be viewed as an entry toward the design of structures of the size and complexity of ATP synthase. Thus, the different dynamics of the rotators in Figure 3.1 depend on the extent of the mismatch between their shapes and those of their crystal cavities at the rotational transition states (TSs). Key structural differences arise from the cross sections of the rotators, shown with filled shapes in Figure 3.1b–d, and those of their ground-state (GS) crystal cavities (heavy dashed lines) and volumes of revolution (thin dashed circles). While the crystal

cavity is defined as the volume enclosed by the boundary formed by close neighbors,[10] the volume of revolution corresponds to the empty space that would be needed for unhindered rotation. Also shown in the Figure 3.1 is the mismatch that occurs between the crystal cavity and the shape of the rotator at the TS.[11] Based on computer generated models, the diameter required for unhindered rotation of a triptycene group, ca. 10.7 Å, is approximately twice as large as the one needed for rotation of a phenylene or a bicyclo[2.2.2]octane, ca. 5.6 Å. It is also worth noting that the moments of inertia along their principal rotational axis for a methyl (3.3 $g \cdot mol^{-1} \cdot Å^2$), phenylene (89 $g \cdot mol^{-1} \cdot Å^2$) and a bicyclo[2.2.2]octane (207 $g \cdot mol^{-1} \cdot Å^2$) are three to one order of magnitude smaller than that of triptycene (1838 $g \cdot mol^{-1} \cdot Å^2$).[12] In order to accommodate the larger rotator, we selected the relatively large, shape- and volume-persistent stator of molecular rotor **3**, which is viewed as a higher generation dendron[13] of the stator used for **1** and **2**. We confirmed the success of this design by measuring its solid-state rotational dynamics by ^2H NMR spectroscopy.

3.2. Synthesis and Characterization

Molecular rotor **3** and its deuterated analog **3**-d_8 were synthesized as outlined in Scheme 3.1 using a divergent modular synthesis with three key building blocks consisting of 9,10-diethynyl triptycenes **6** and **6**-d_8 for the rotator and dendrimeric core, 4-iodo-4′,4″,4‴-tribromo-tetraphenylmethane **7** as the first generation branch, and 3,3,3-triphenylpropyne as the surface group. Although the yields for the synthesis of intermediates **6** and **8** were modest (30% and 43%, respectively), the final coupling

reaction carried out with an excess of 3,3,3-triphenylpropyne occurred in a nearly quantitative yield. All the steps indicated in Scheme 3.1 and the characterization of all the compounds are described in detail in the experimental section.

Scheme 3.1. Synthesis of molecular rotor **3** and **3**-d_8.[#]

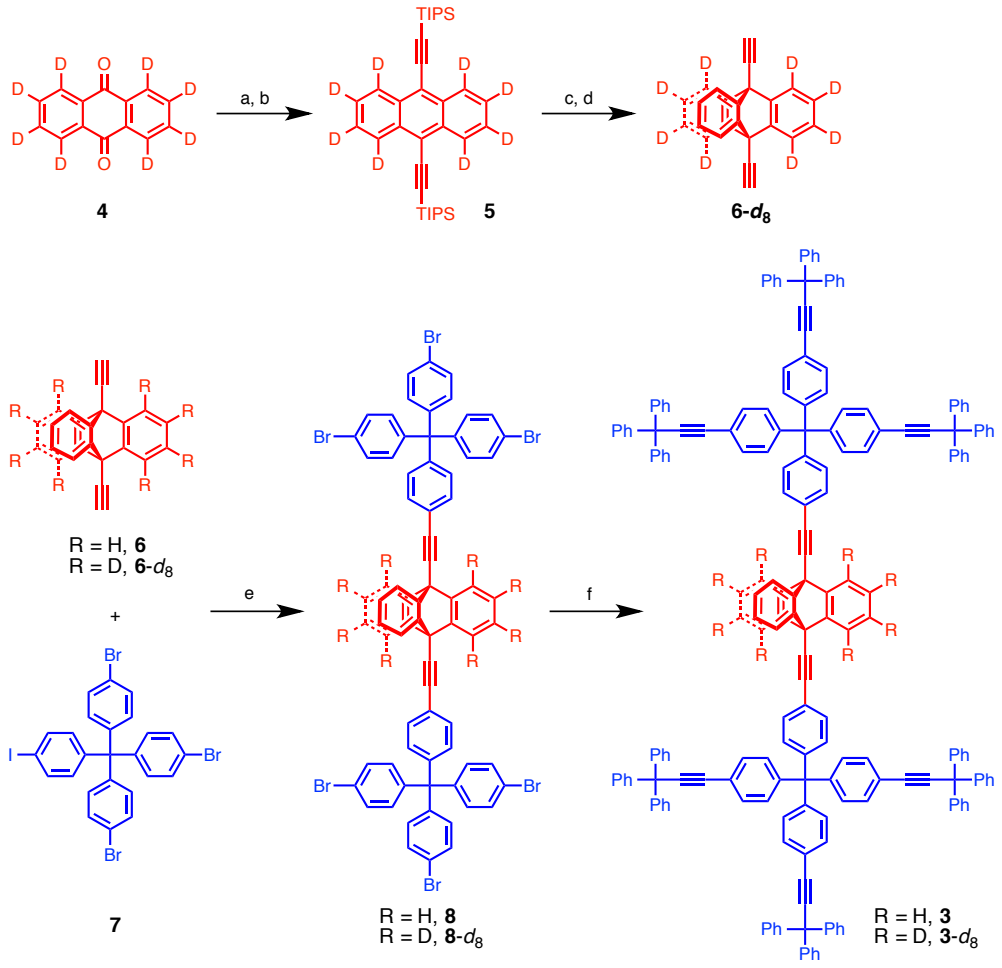

[#]Reagents and conditions: (a) TIPS acetylene, *n*-BuLi, THF, –78 °C; (b) $SnCl_2$, AcOH, EtOH, 67 % over two steps; (c) anthranilic acid, *i*-amyl nitrite, dioxane, reflux; (d) TBAF, THF, 0 °C, 45 % over two steps; (e) $PdCl_2(PPh_3)_2$, CuI, *i*-Pr_2NH, THF, reflux, 43 %; (f) $PdCl_2(PPh_3)_2$, CuI, 3,3,3-triphenylpropyne, *i*-Pr_2NH, THF, reflux, 99 %.

Crystallization of molecular rotor **3** by slow evaporation from several solvents led to the formation of needles with a tendency to splinter and turning opaque. Optical microscopic analysis under cross polarizers showed the initially crystalline specimens to lose their birefringence, and scanning electron microscopy (SEM) revealed a spontaneous splintering process (Figure 3.2). Powder X-ray diffraction (PXRD) of the resulting solids in the range of 4 –50° (2θ) displayed sharp peaks at 6°, 12°, and 19° (2θ) and a broad signal spanning from 3° to 33°, suggesting ordered and amorphous regions. They were shown to be stable up to 573 K by differential scanning calorimetric (DSC) and thermal gravimetric analysis (TGA), making it possible to explore the rotation of the triptycene rotator using high-temperature quadrupolar echo solid-state ^{2}H NMR spectroscopy.[14]

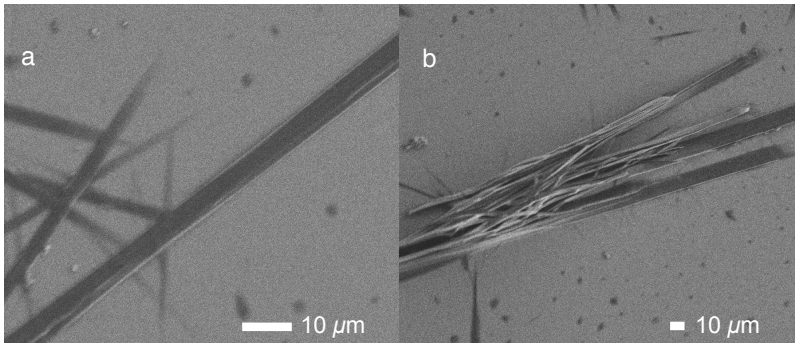

Figure 3.2. Scanning electron micrographs (SEM) of (a) the initial crystalline needles of **3**, which subsequently splinter into (b) fine semi-amorphous fibers.

3.3. Solid-State Quadrupolar Echo ^{2}H NMR Spectroscopy

The use of ^{2}H NMR for the determination of dynamic processes in solid-state materials relies on the predictable changes in the spectrum caused by the orientation-dependent interaction of the nuclear spin and electric quadrupole moment at the

nucleus.[14] Thus, rapid (ca. 10^3–10^8 s^{-1}) variations in the orientation of the C–D bond vector with respect to the external magnetic field result in spectral changes that depend on their trajectories and frequencies. For aromatic groups undergoing axial rotation, the key parameters are the angle made between the C–D bond, the axis of rotation (cone angle), and the amplitude of the displacement between sites. As a result, the ^{2}H NMR spectrum of the partially deuterated triptycene rotator is expected to have contributions from two components, assuming a 3-fold rotational potential with 120° jumps between sites (Figure 3.3). The deuterium atoms at the α-carbons with a C–D bond parallel to the rotational axis (cone angle 0°) do not experience any change in the ^{2}H NMR spectroscopy, and their contribution to the line-shape remains unchanged as a broad Pake pattern with two sharp maxima and two shoulders (Figure 3.3b), regardless of the rotational rate. By contrast, deuterium atoms connected to the triptycene β-carbons make a 60° cone angle, and their contributions to the ^{2}H NMR spectrum line-shape will change as a function of rotational frequency. As shown in Figure 3.3c, the spectrum of deuterium atoms on β-carbons evolves from a broad Pake pattern at low temperatures, where rotational exchange rates are lower than ca. 10 kHz, to a relatively narrow pattern that changes from four to two signals as the temperature increases and the site exchange frequency approaches motion in the fast limit at ca. 10 MHz.

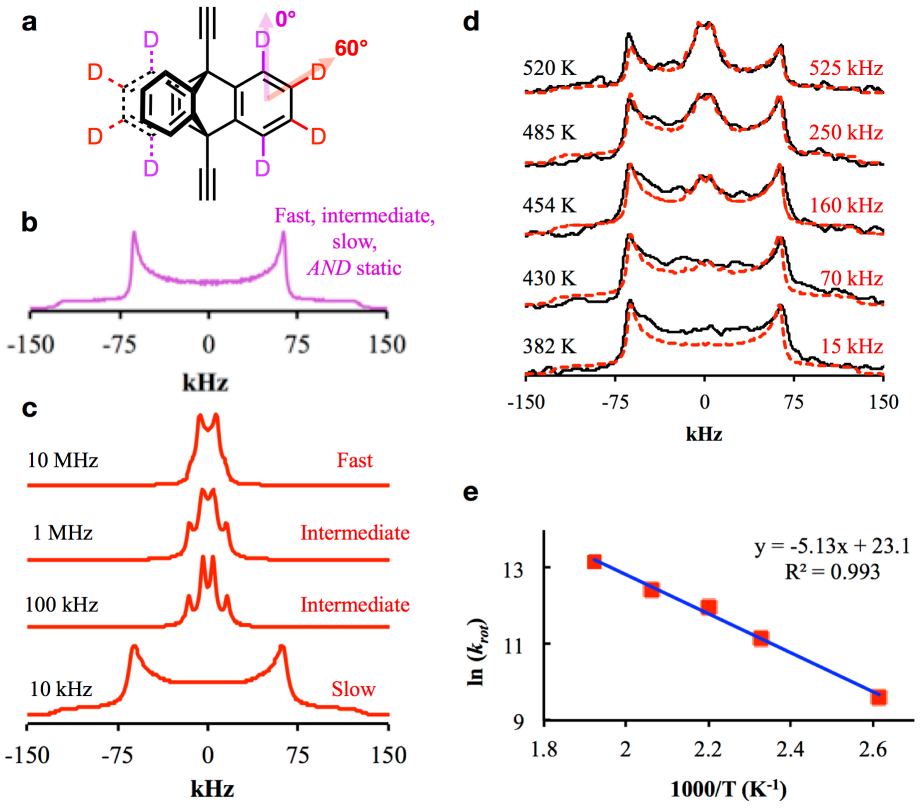

Figure 3.3. (a) Cone angles experienced by the tritycene C–D bonds at the α- and β-positions highlighted in purple and red, respectively. Simulated 2H NMR spectra for (b) the α-C–D bonds at all exchange frequencies and (c) the β-C–D bonds assuming a three-fold symmetric rotation. (d) Superposition of experimental (black solid spectra) and simulated (red dashed spectra) ^{2}H NMR line shapes of rotor **3**-d_8 and (e) Arrhenius plot for the three-fold site exchange of rotor **3**-d_8.

The ambient-temperature experimental spectrum was very similar to that of a static triptycene, indicating a rotational frequency that is no more than 10 kHz. However, as shown in Figure 3.3d (solid spectra), spectral changes were observed upon heating, with a signal developing at the center of the spectrum at ca. 430–454 K. Further heating up to 520 K, which is the limit of our solid-state NMR instrument, revealed two intense central peaks separated by 7 kHz.

Although the axial symmetry of the triptycene-d_8 rotator suggests a 3-fold site exchange, the overall axial symmetry of the stators (rigorous or approxi mate C_3, S_3, or S_6) indicates that symmetric or unsymmetric 6-fold site exchange could also account for the rotational dynamics. A simulation of symmetric 3-fold rotation with an exchange frequency of 525 kHz matched the experimental spectrum at 520 K best (Figure 3.3d, top spectrum). Considering the partially crystalline and amorphous nature of the sample, a log-Gaussian distribution of exchange rates, which corresponds to a Gaussian distribution of activation energies was used for the simulation with a $\sigma = 3$ value for the width of the barrier.[15] The same procedure was applied to the simulations of the experimental spectra obtained from 485 K to 382 K and rotational frequencies were identified as 250 kHz, 160 kHz, 70 kHz, and 15 kHz, respectively. Spectral simulations with different σ values and 6-fold site exchange models were explored but they all failed to describe the experimental line shapes with the agreement observed with the 3-fold site model described above.

Using the simulation-derived rotational exchange frequencies, k_{rot}, and the experimental temperatures we built an Arrhenius plot that resulted in a good linear relationship ($R^2 = 0.993$). The slope and intercept correspond to an averaged activation energy of 10.2 kcal/mol and pre-exponential factor of ca. 1.1×10^{10} s^{-1}, respectively (Figure 3.3e). It should be noted that the experimental pre-exponential factor is about an order of magnitude smaller than the value expected for rotational inertia, 5.6×10^{11} s^{-1},[12] as observed for solids with limited long-range order. These activation parameters indicate that triptycene rotation at ambient temperature (300 K) should occur with a frequency of 4.6 kHz, which corresponds to jumps between sites every 220 μs. It is notable that,

despite the many conformations that could be adopted by the stator to make a more complex rotational potential, the ^{2}H NMR spectroscopy simulations clearly indicate a three-fold symmetric potential. We interpret this as an indication that the potential energy profile is primarily determined by the relatively larger triptycene rotator.

3.4. Conclusions

In conclusion, an expanded triptycene rotator can be rendered functional in the context of a volume-conserving system by using a stator that consists of shape- and volume-persistent dendrons. A very efficient divergent and modular strategy was successfully implemented in order to overcome the challenges involved in the direct coupling of bulky stator groups onto the central triptycene rotator. Using variable temperature solid-state ^{2}H NMR spin-echo experiments and line shape analysis we showed that rotation in the intermediate exchange regime occurs in the range of 382–520 K with an average activation energy of 10.2 kcal/mol and a pre-exponential factor of 1.1×10^{10} s^{-1}. These results confirm that mechanical functions in solids can be attained for larger molecules by suitable molecular design and bode well for in the nascent field of crystalline molecular machines. The success reported herein with a star-shaped rotator suggests structural strategies for the design of gearing motions in condensed solid phases.[16]

3.5. Experimental

3.5.1. General Methods

Commercially available compounds were used without further purification unless otherwise notified. [Tris(4-bromophenyl)](4-iodophenyl) methane,[17] 9,10-diethynyl-triptycene,[18] and anthraquinone-d_8[19] were synthesized as reported previously in the literature. Pre-coated thin-layer chromatography (TLC) plates with Silica Gel 60 F_{254} and silica gel (230–400 mesh) were used and the spots on TLC plates were visualized by using a UV lamp. Tetrahydrofuran (THF) was distilled from sodium-benzophenone in a continuous still under an atmosphere of argon. Melting points of solids were measured without calibration. ^{1}H NMR, ^{2}H NMR, and ^{13}C NMR in solution were recorded at 500 MHz, 77 MHz, and 125 MHz, respectively. Chemical shifts are reported in ppm and the residual solvent signals of $CDCl_3$ (^{1}H NMR: δ 7.26 ppm; ^{13}C NMR: δ 77.16 ppm), $CHCl_3$ (^{2}H NMR: δ 7.26 ppm) were used as reference. Multiplicities of the peaks are reported as broad (br), singlet (s), doublet (d), triplet (t), or multiplet (m). The coupling constants *J* are reported in Hz. Infrared spectra (IR) were obtained with a HATR-FTIR instrument. Mass spectra were acquired on a MALDI-TOF and a LIFDI-TOF instrument.

3.5.2. Synthesis and Characterization

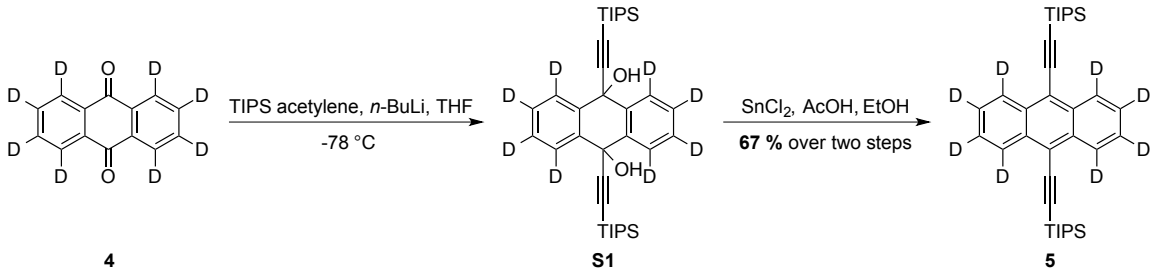

In a flame-dried flask with a rubber stopper was added TIPS acetylene (720 mg, 3.95 mmol) and anhydrous THF (10 mL) under Argon and the reaction flask was cooled down to –78 °C using an acetone-dry ice bath. To the reaction flask was slowly added *n*-BuLi (1.6 M solution in hexanes, 2.4 mL) and the reaction mixture was stirred in the chilling bath for 30 min before it was cannulated into a solution of anthraquinone-d_8 **4** in anhydrous THF (10 mL) at –78 °C. The reaction was allowed to slowly warm up to room temperature and was quenched with water. The product was extracted with ethyl acetate (50 mL) twice. The combined organic layers were washed with brine, and dried over anhydrous Na_2SO_4. The solvent was removed *in vacuo* and the crude product was used in the next step without further purification.

The white crude from the previous reaction was dissolved in ethanol (10 mL) and the resulting solution was treated with a solution of $SnCl_2 \cdot 2H_2O$ (887 mg, 3.93 mmol) in 50 % acetic acid (10 mL) at 50 °C. The reaction was stirred for 30 min and a yellow precipitate was obtained by filtration. The solid was washed with water (10 mL) and ethanol (10 mL). Gravity column chromatography with hexanes as the eluent provided the desired product **5** (481 mg, 67 %).

5: Yellow Solid, m.p. 203–205 °C; ^{1}H NMR (500 MHz, $CDCl_3$, ppm): δ 1.27 (d, J = 5.0 Hz, 36H), 1.28 (septet, J = 5.0 Hz, 6H); ^{2}H NMR (77 MHz, $CHCl_3$, ppm): δ 7.69,

8.74; ^{13}C NMR (125 MHz, $CDCl_3$, ppm): δ 11.7, 19.0, 103.5, 104.8, 118.8, 126.2–127.3(m), 132.5; IR (powder, cm^{-1}): ν 659, 674, 768, 802, 882, 919, 997, 1013, 1072, 1232, 1358, 1382, 1459, 1531, 1585, 1601, 2130, 2289, 2863, 2888, 2941; HRMS (ESI/APCI, TOF): m/z calculated for $C_{36}H_{43}D_8Si_2$ (MH^+): 547.4026, found: 547.4033.

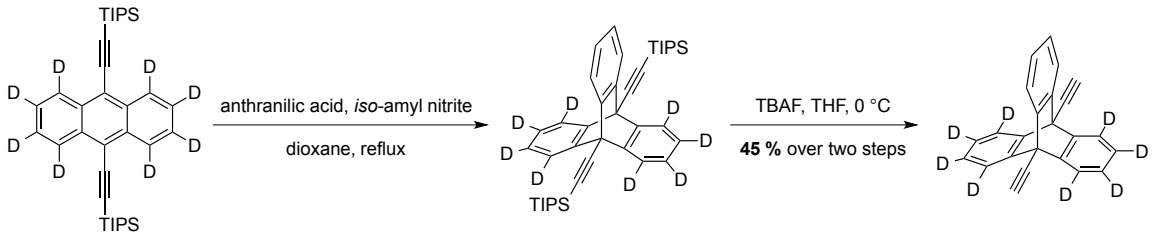

9,10-Bis(tri-*iso*-propylsilylethynyl)-anthracene-d_8 **5** (450 mg, 0.823 mmol) was dissolved in anhydrous 1,4-dioxane (12 mL) in a 3-neck flask under Argon atmosphere. The solution was heated to reflux and then a solution of anthranilic acid (1.127 g, 8.23 mmol) in anhydrous dioxane (12 mL) and a solution of *iso*-amyl nitrite (962 mg, 8.22 mmol) in anhydrous dioxane (12 mL) were simultaneously added in via additional funnels over a period of 4 h. The reaction mixture was refluxed for another 12 h before it was allowed to cool down to room temperature. The solvent was evaporated *in vacuo*. The residue was flashed through a short plug of silica gel and the crude obtained was used directly in the next reaction.

The crude product obtained from the previous reaction was dissolved in THF (10 mL) at 0 °C and TBAF (1.0 M solution in THF, 6.0 mL) was added into the reaction flask slowly. The reaction was stirred in an ice-water bath at 0 °C for 30 min before a saturated NH_4Cl solution was added in to quench the reaction. The product was extracted with ether (50 mL) twice. The combined organic layers were washed with brine, dried

over anhydrous Na_2SO_4, and concentrated under vacuum to give a pale yellow residue. Flash column chromatography of the residue using hexanes as the eluent provided the desired product **6**-d_8 (114 mg, 45 %).

6-d_8: White Solid, m.p. 306–307 °C; ^{1}H NMR (500 MHz, $CDCl_3$, ppm): δ 3.01 (s, 2H), 7.12 (dd, J = 5.5, 3.0 Hz, 2H), 7.77 (dd, J = 5.5, 3.0 Hz, 2H); ^{2}H NMR (77 MHz, $CHCl_3$, ppm): δ 7.17, 7.82; ^{13}C NMR (125 MHz, $CDCl_3$, ppm): δ 52.3, 78.2, 81.0, 121.9 (t, J = 25 Hz), 122.3, 125.5 (t, J = 25 Hz), 126.0, 143.0, 143.1; IR (powder, cm^{-1}): ν 621, 643, 656, 670, 680, 746, 813, 883, 1049, 1161, 1225, 1288, 1308, 1359, 1389, 1452, 1469, 1553, 1577, 1600, 1932, 2277, 3069, 3284, 3297; HRMS (ESI/APCI, TOF): m/z calculated for $C_{24}H_7D_8$ (MH^+): 311.1670, found: 311.1681.

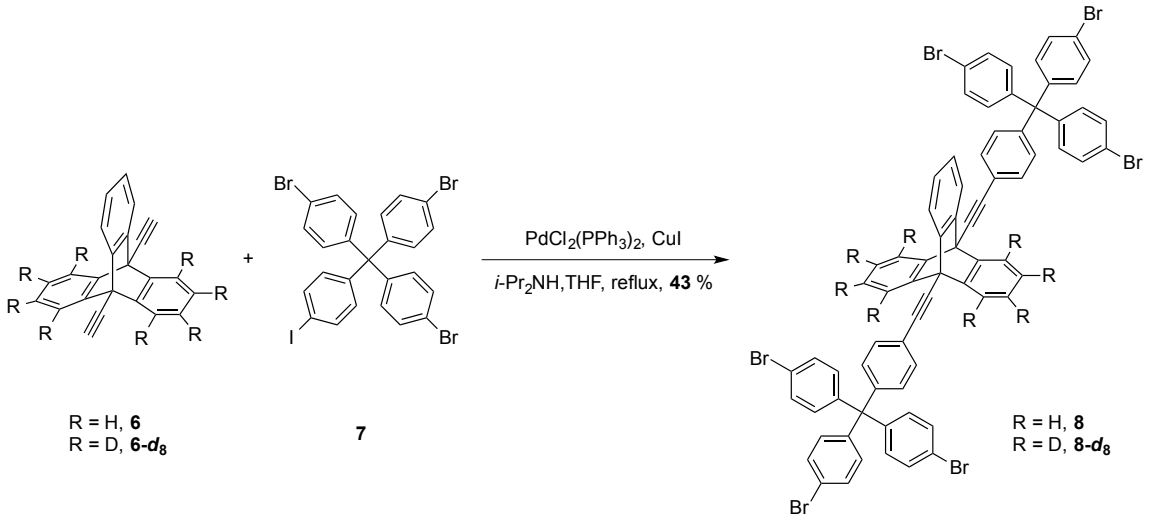

(The same procedures were used for the syntheses of **8** and **8**-d_8.) Tris(4-bromophenyl)-4-iodophenyl methane **7** (171 mg, 0.25 mmol), **6** or **6**-d_8 (0.099 mmol), CuI (1 mg, 0.005 mmol), and $Pd(PPh_3)_2Cl_2$ (4 mg, 0.006 mmol) were added to a degased mixture of anhydrous THF (25 mL) and diisopropylamine (25 mL) and the reaction mixture was stirred at room temperature for 4 h and at 50 °C for 10 h. Saturated NH_4Cl

solution and DCM were added to the reaction flask, and the organic layer was separated. The aqueous layer was extracted again with DCM (100 mL) and the organic layers were combined, washed with brine (100 mL) and dried over anhydrous Na_2SO_4. The solvent was removed *in vacuo* and a white crude was obtained. Flash column chromatography a hexanes-DCM mixture (3:1, v/v) provided the desired product (0.042 mmol, 43 %).

8: White Solid, decomposes over 280 °C; ^{1}H NMR (500 MHz, $CDCl_3$, ppm): δ 7.11 (app. d, J = 8.5 Hz, 12H), 7.11 (dd, J = 5.5, 3.5 Hz, 6H), 7.28 (app. d, J = 8.5 Hz, 4H), 7.44 (app. d, J = 8.5 Hz, 12H), 7.74 (app. d, J = 8.5 Hz, 4H), 7.81 (dd, J = 5.5, 3.5 Hz, 6H); ^{13}C NMR (125 MHz, $CDCl_3$, ppm): δ 53.0, 64.2, 84.1, 92.7, 121.0, 121.2, 122.5, 125.9, 131.0, 131.3, 131.9, 132.6, 143.7, 144.7, 146.3; IR (powder, cm^{-1}): ν 751, 806, 817, 842, 911, 1008, 1034, 1077, 1186, 1263, 1397, 1454, 1482, 1608, 1909, 2852, 2925, 2949, 3067; MS (LIFDI, TOF): m/z calculated for $C_{74}H_{44}Br_6$ (M^+): 1405.8, found: 1406.

8-d_8: White Solid, decomposes over 280 °C; ^{1}H NMR (500 MHz, $CDCl_3$, ppm): δ 7.11 (app. d, J = 8.5 Hz, 12H), 7.11 (dd, J = 5.5, 3.5 Hz, 6H), 7.27 (app. d, J = 8.5 Hz, 4H), 7.44 (app. d, J = 8.5 Hz, 12H), 7.74 (app. d, J = 8.5 Hz, 4H), 7.81 (dd, J = 5.5, 3.5 Hz, 6H); ^{13}C NMR (125 MHz, $CDCl_3$, ppm): δ 52.9, 64.2, 84.2, 92.6, 121.0, 121.3 122.5, 125.9, 131.0, 131.3, 131.9, 132.6, 143.6, 143.7, 144.7, 146.3; IR (powder, cm^{-1}): ν 747, 799, 809, 881, 911, 1008, 1077, 1188, 1263, 1362, 1394, 1484, 1570, 1909, 2280, 2852, 2922, 3059; MS (MALDI, TOF): m/z calculated for $C_{74}H_{37}D_8Br_6$ (MH^+): 1420.9, found: 1421.

*Note: It was observed that sometimes the terminal alkyne **6** or **6**-d_8 would react with the phenyl bromide moiety instead of the desired phenyl iodide moiety of tris(4-*

bromophenyl)-4-iodophenyl methane in the Sonogashira reaction. This would not affect the following transformation so systematic optimization to avoid the side reaction has yet been performed.

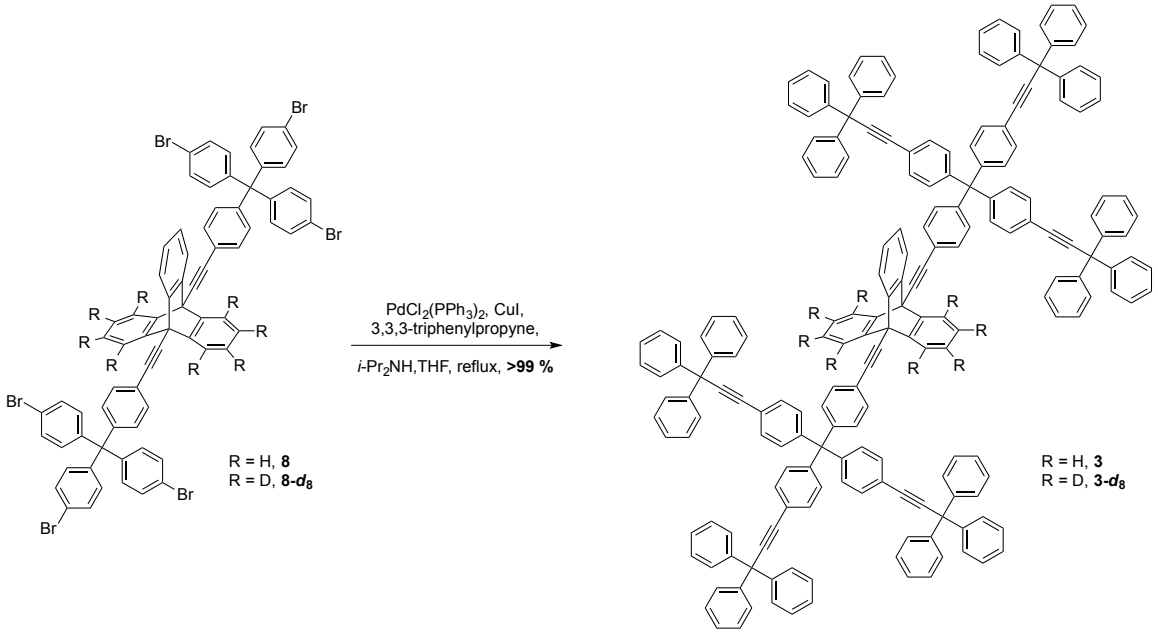

(The same procedures were used for the syntheses of **3** and **3**-d_8.) Tritylacetylene (537 mg, 2.00 mmol), **8** or **8**-d_8 (0.042 mmol), CuI (4 mg, 0.02 mmol), and $Pd(PPh_3)_2Cl_2$ (15 mg, 0.02 mmol) were added to a degased mixture of anhydrous THF (10 mL) and diisopropylamine (5 mL) and the reaction mixture was refluxed overnight before NH_4Cl solution and DCM was added to the reaction flask. The organic layer was separated and the aqueous layer was extracted with DCM (100 mL). The organic layers were combined, washed with NH_4Cl (100 mL) and brine (100 mL) consecutively and dried over anhydrous Na_2SO_4. The solvent was removed *in vacuo* and a white solid was obtained. Flash column chromatography of the crude using a hexanes-DCM mixture (2:1, v/v) as the eluent provided the desired product (0.042 mmol, > 99 %).

3: white solid, decompose over 320 °C; ^{1}H NMR (500 MHz, $CDCl_3$, ppm): δ 7.12 (dd, J = 5.3, 3.3 Hz, 6 H), 7.20–7.38 (m, 106H), 7.46 (app. d, J = 8.5 Hz, 12H), 7.72 (app. d, J = 8.5 Hz, 4H), 7.81 (dd, J = 5.3, 3.3 Hz, 6 H); ^{13}C NMR (125 MHz, $CDCl_3$, ppm): δ 53.0, 56.3, 65.0, 83.9, 84.9, 92.9, 96.3, 120.9, 121.8, 122.5, 125.9, 127.0, 128.2, 129.3, 130.8, 131.1, 131.3, 131.8, 143.7, 145.4, 145.9, 146.8; IR (powder, cm^{-1}): ν 695, 744, 824, 891, 913, 1002, 1032, 1079, 1114, 1157, 1186, 1320, 1404, 1446, 1490, 1596, 1806, 3030, 3058; MS (MALDI, TOF): m/z calculated for $C_{200}H_{135}$ (MH^+): 2535.0, found: 2535.

3-d_8: white solid, decompose over 320 °C; ^{1}H NMR (500 MHz, $CDCl_3$, ppm): δ 7.10 (dd, J = 5.3, 3.3 Hz, 2 H), 7.20–7.37 (m, 106H), 7.45 (app. d, J = 8.5 Hz, 12H), 7.71 (app. d, J = 8.5 Hz, 4H), 7.80 (dd, J = 5.3, 3.3 Hz, 2 H); ^{13}C NMR (125 MHz, $CDCl_3$, ppm): δ 52.9, 56.3, 65.0, 83.9, 84.9, 92.8, 96.3, 120.9, 121.8, 122.1(br), 122.5, 125.4(br), 125.9, 127.0, 128.2, 129.3, 130.8, 131.1, 131.3, 131.8, 143.7, 143.7, 145.4, 145.9, 146.8; IR (powder, cm^{-1}): ν 696, 744, 823, 889, 1026, 1066, 1187, 1361, 1403, 1447, 1490, 1597, 3026, 3057; MS (MALDI, TOF): m/z calculated for $C_{200}H_{127}D_8$ (MH^+): 2546.1, found: 2546.

3.5.3. Thermal Analysis

Differential Scanning Calorimetry (DSC) and Thermal Gravimetric Analysis (TGA) measurements were carried out on a Mettler-Toledo DSC 821e and TGA/SDTA 851e thermoanalyzer. Solid samples were ground with a mortar and a pestle in order to have a homogeneous powder and they were placed inside aluminum pans during the analysis. Differential scanning calorimetry experiments were carried out on a DSC

analyzer under nitrogen atmosphere, using a heating ramp from 25 to 350 °C with a heating rate of 10 °C/min. Thermogravimmetric analyses were obtained on a thermoanalyzer under argon atmosphere using a temperature interval from 25 to 350 °C with a heating rate of 10 °C/min.

3.5.4. Powder X-ray Diffraction

PXRD Analyses were carried out using Cu-$K_{\alpha 1}$ = 1.5406 Å radiation. Data were collected at room temperature in the range of 2θ = 3–50° (step of 0.016°, step time 75 s).

3.5.5. Solid-State ^{2}H NMR Spin-Echo Experiments

For the ^{2}H NMR spin-echo experiments, a quadrupolar-echo sequence with phase cycling to suppress undesired single- and double-quantum coherence-transfer artifacts was used in the wide-line ^{2}H data acquisition. The spectra were obtained on a spectrometer operating at ^{2}H frequency of 46.07 MHz. A pulse spacing of 50 μs with a refocusing delay of 42 μs was used in the quadrupolar-echo sequence. The spectrometer produced 2.5-μs 2H $\pi/2$ pulses at 46 MHz with a recycle delay of 20 s between pulses. Variable temperature experiments were performed between 296 K and 473 K. For these experiments, ca. 45 mg of the solid sample was placed inside a borosilicate glass NMR tube between two glass rods and sealed with Teflon tape. The spectra were acquired by averaging 2000 scans at room temperature and up to 4000 scans at high temperature. The data was processed using a line broadening of 3 kHz. The spectrometer temperature was calibrated with ^{207}Pb NMR of a static lead nitrate sample at variable temperatures.

3.6. Appendix

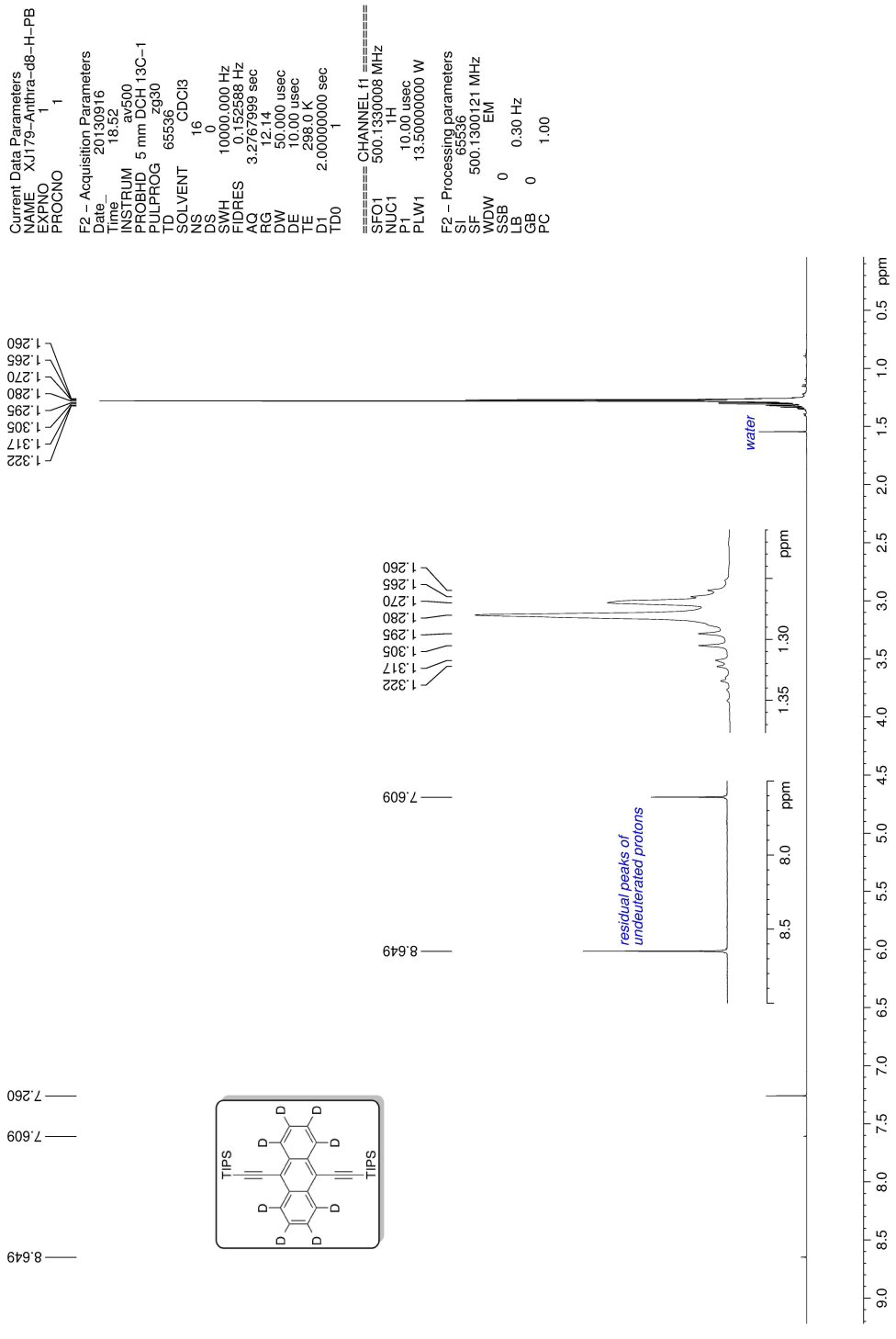

Figure A.3.1. ^{1}H NMR of compound **5** at 500 MHz in $CDCl_3$.

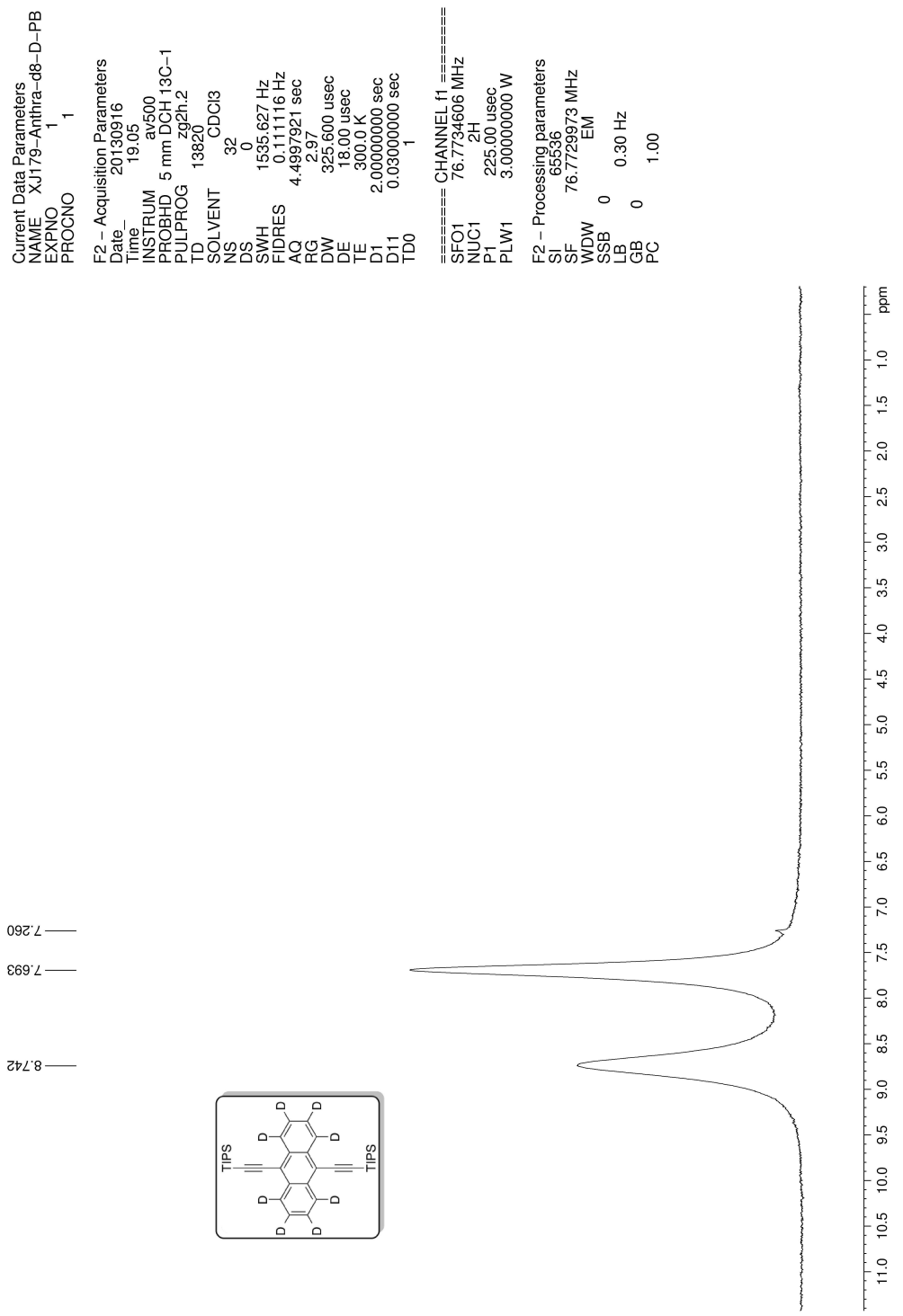

Figure A.3.2. ^{2}H NMR of compound **5** at 77 MHz in $CHCl_3$.

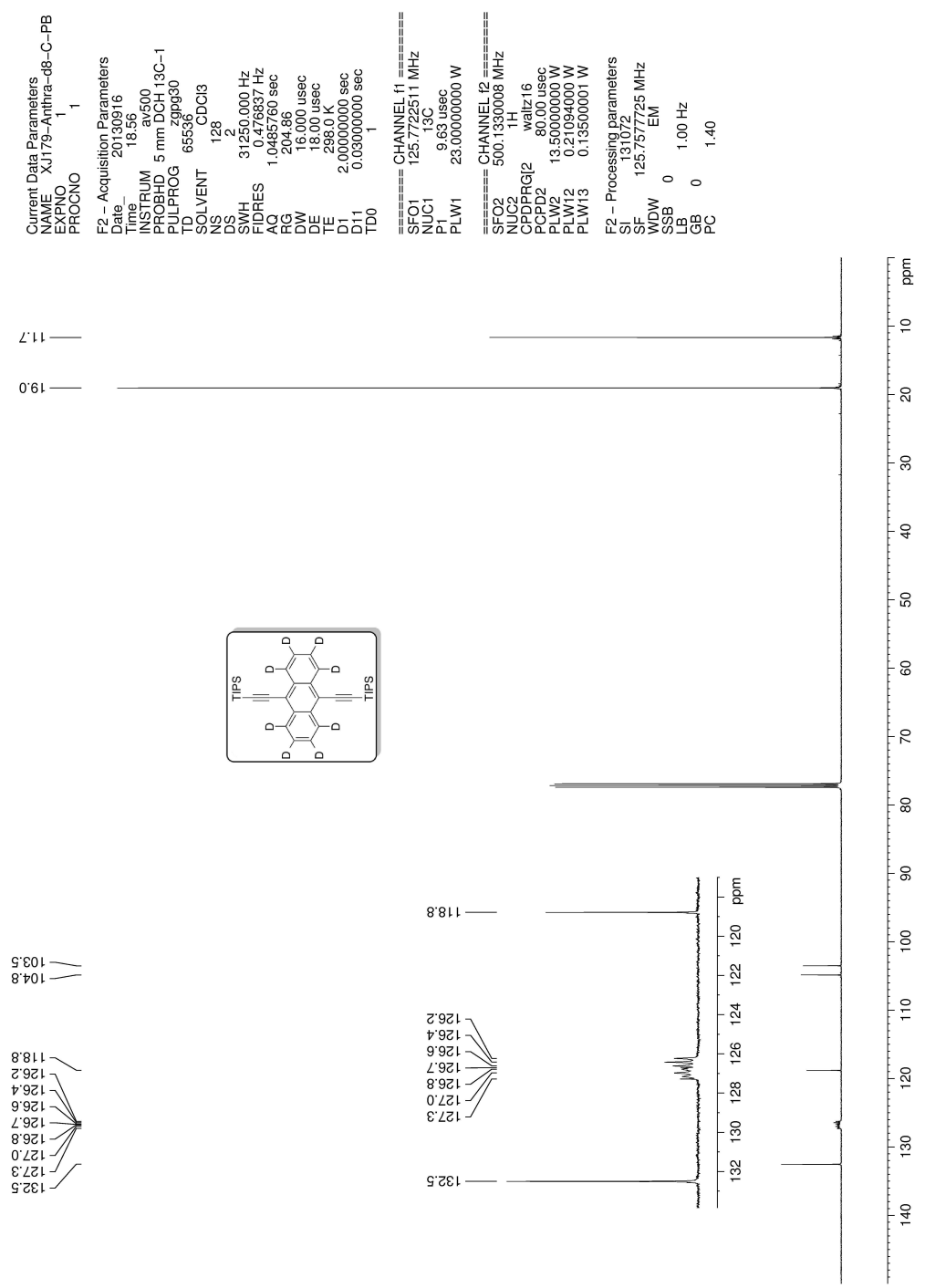

Figure A.3.3. ^{13}C NMR of compound **5** at 125 MHz in $CDCl_3$.

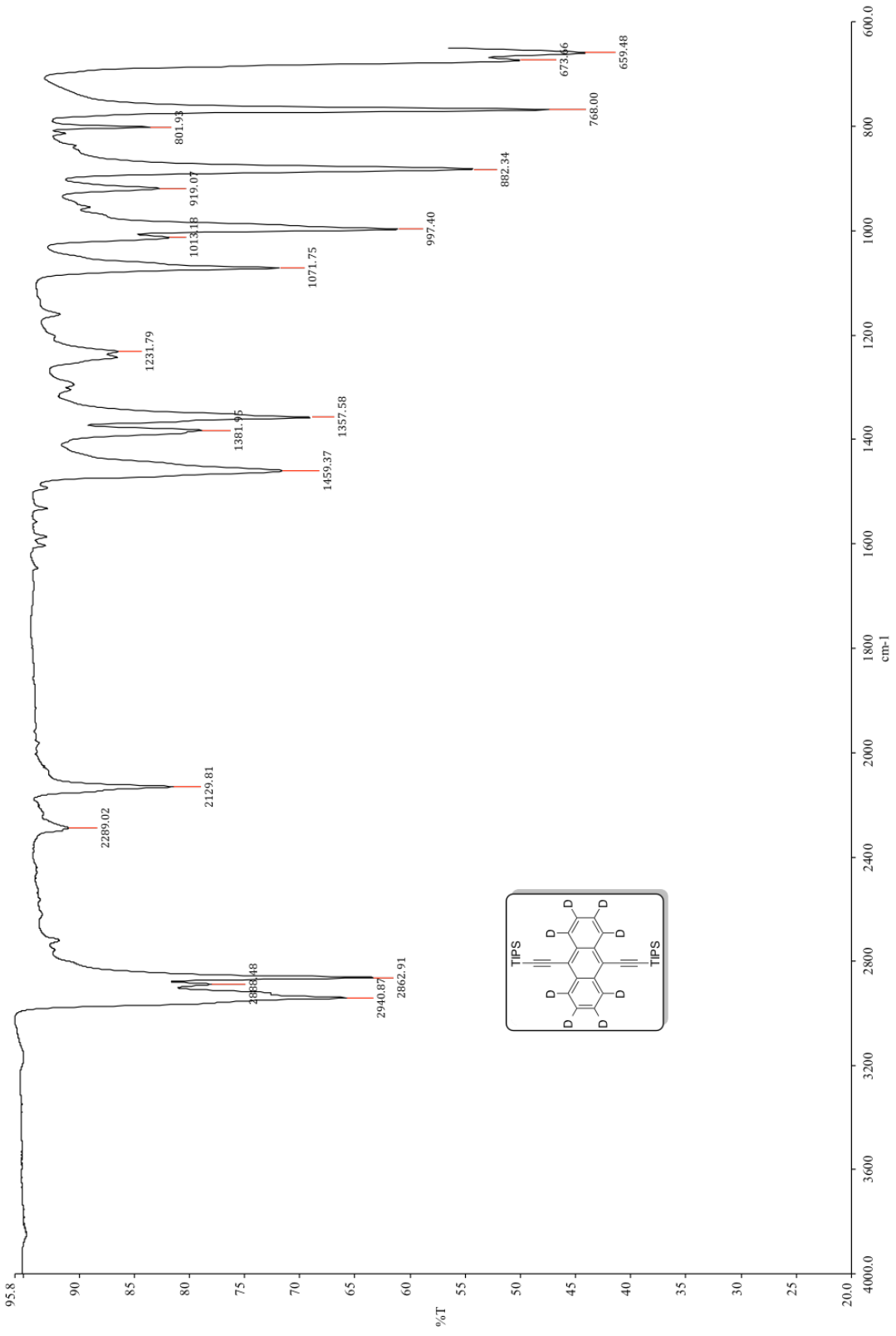

Figure A.3.4. FTIR of compound **5**.

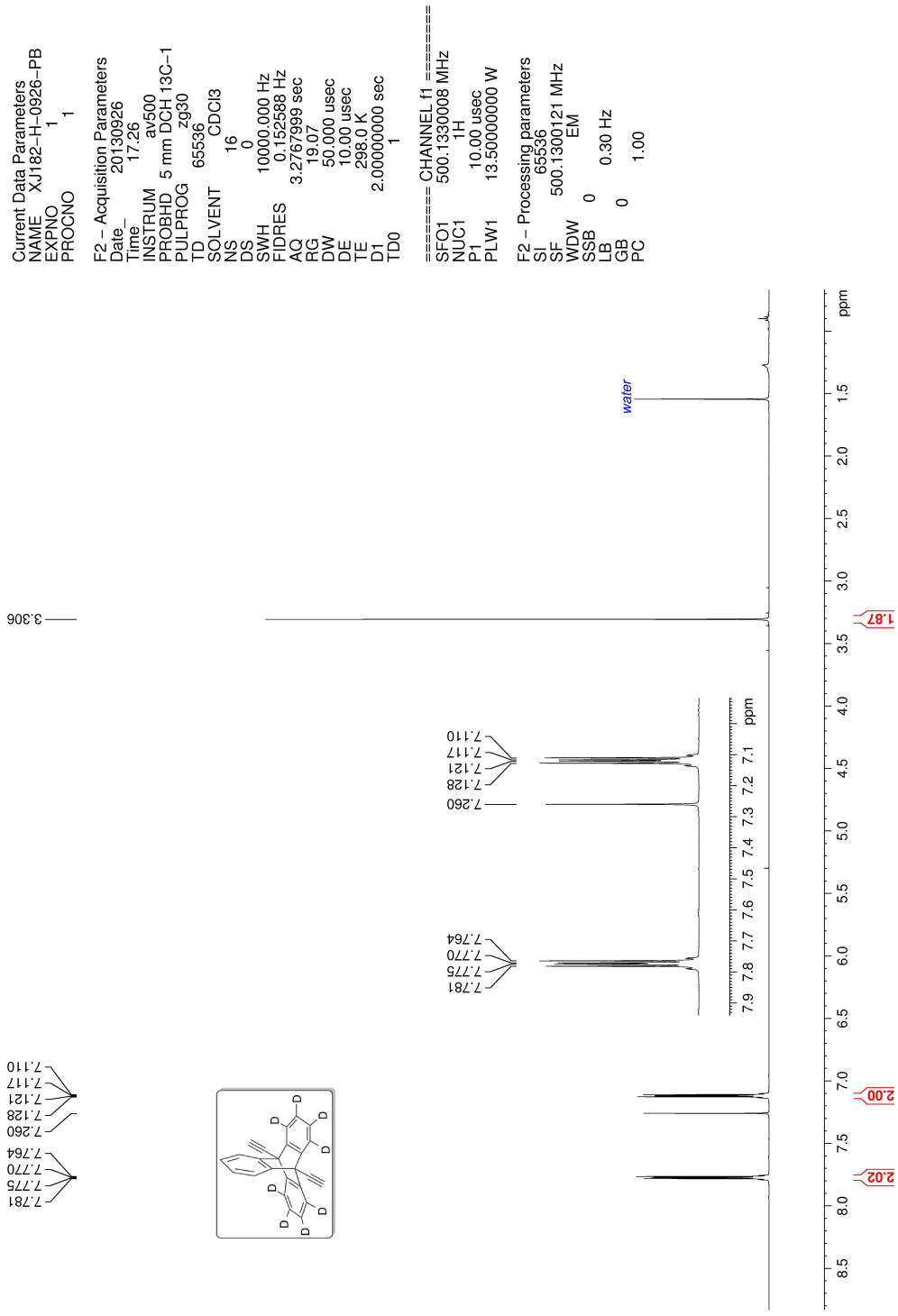

Figure A.3.5. ^{1}H NMR of compound **6**-d_8 at 500 MHz in $CDCl_3$.

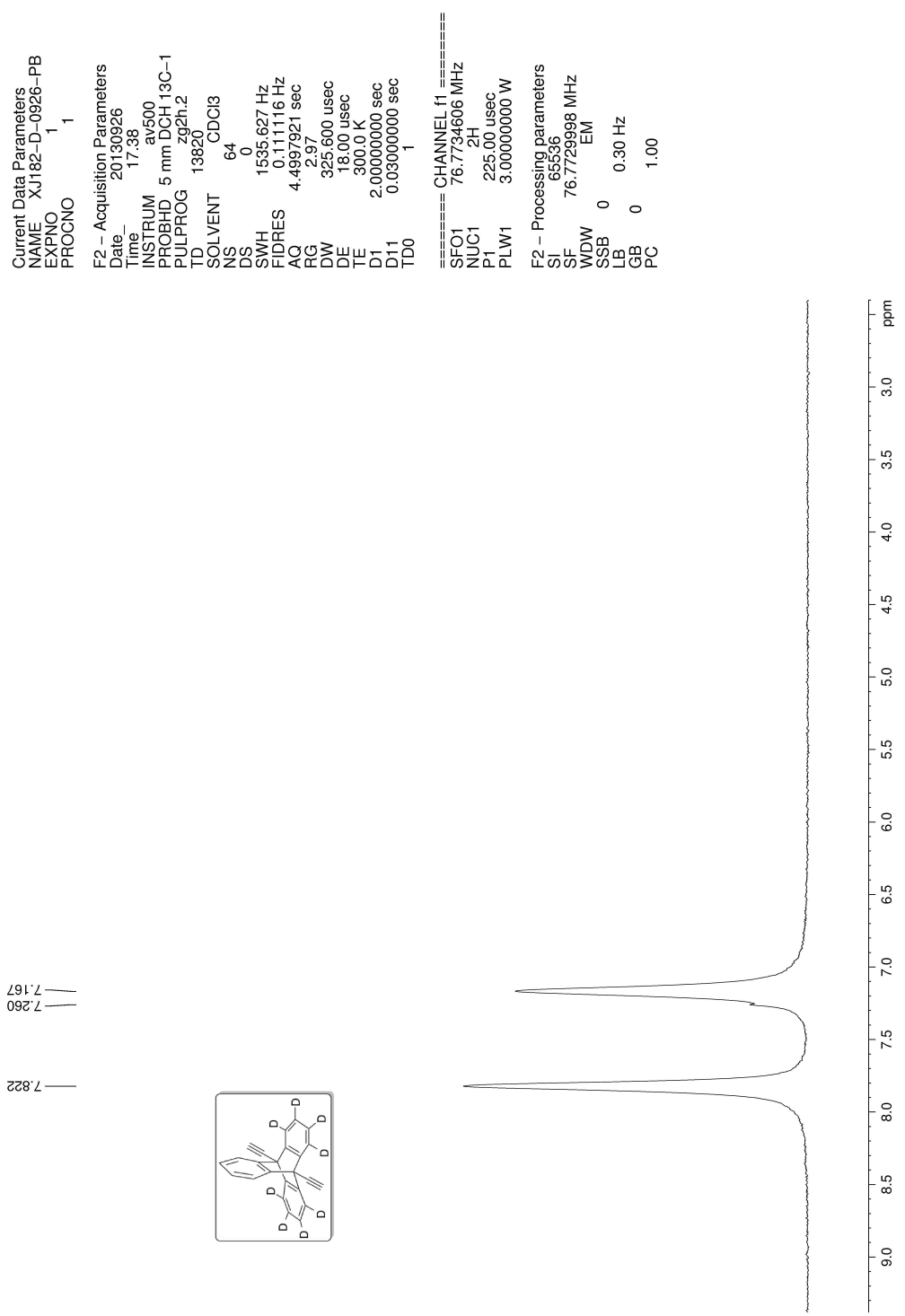

Figure A.3.6. ^{2}H NMR of compound **6**-d_8 at 77 MHz in $CHCl_3$.

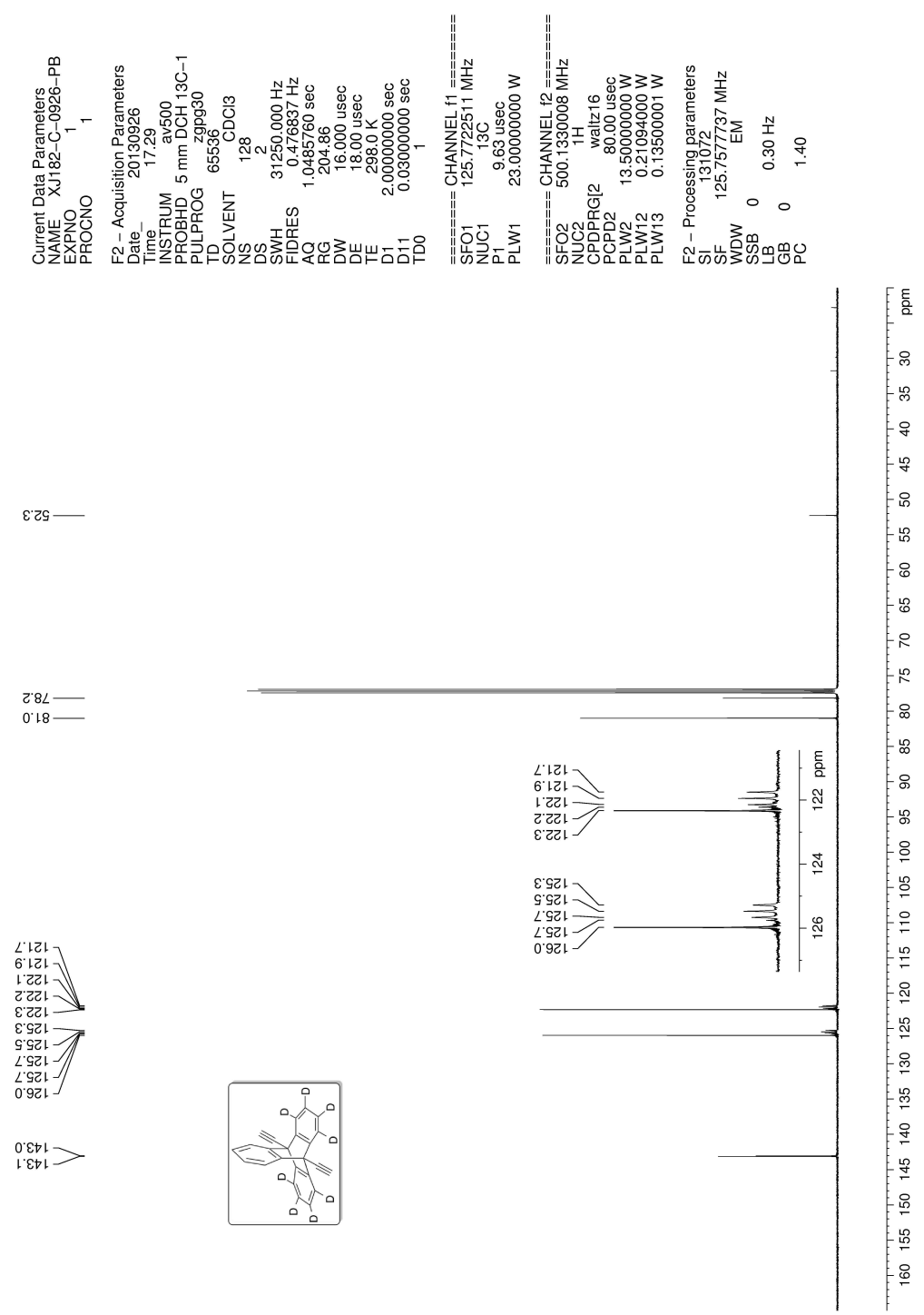

Figure A.3.7. ^{13}C NMR of compound **6**-d_8 at 125 MHz in $CDCl_3$.

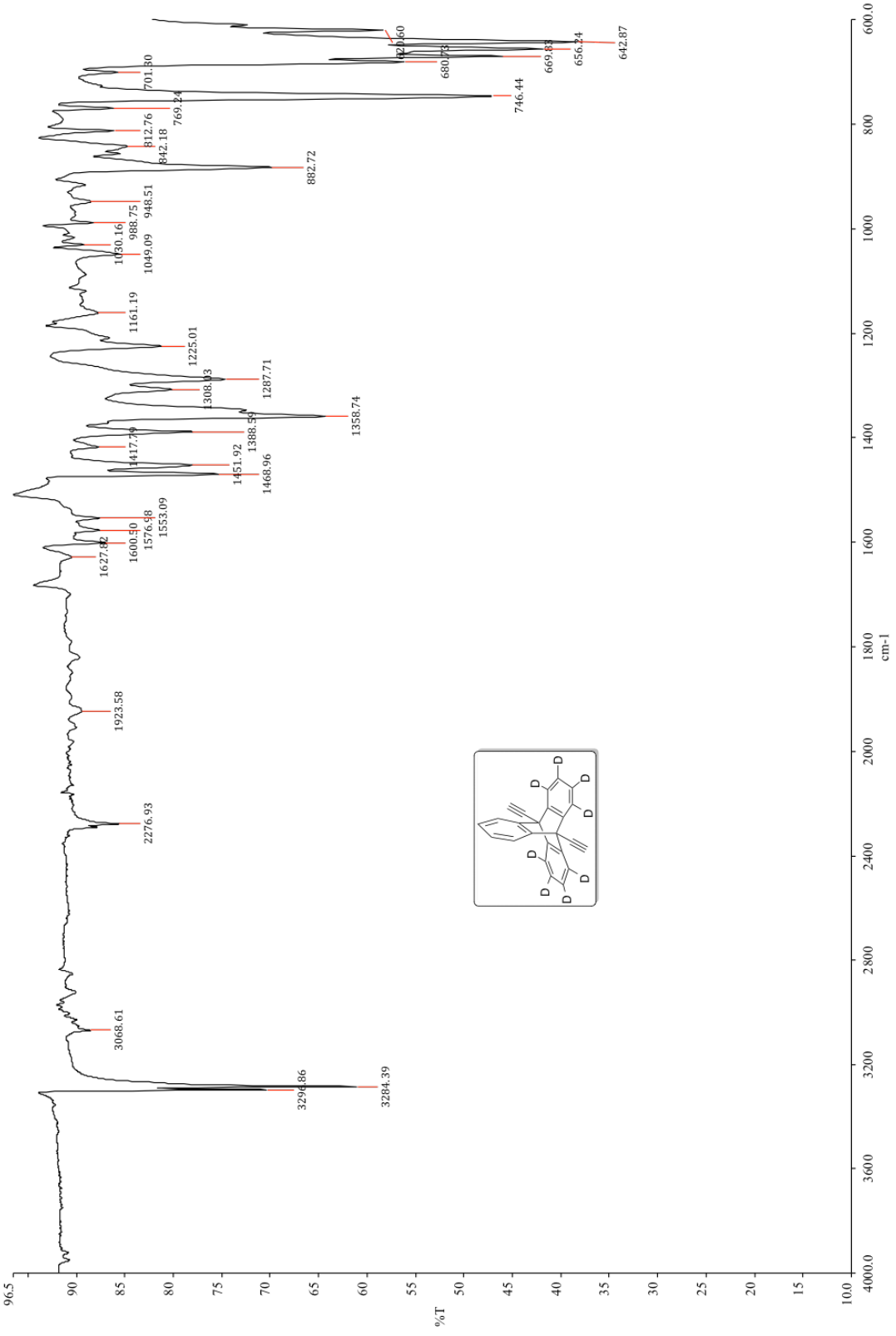

Figure A.3.8. FTIR of compound **6**-d_8.

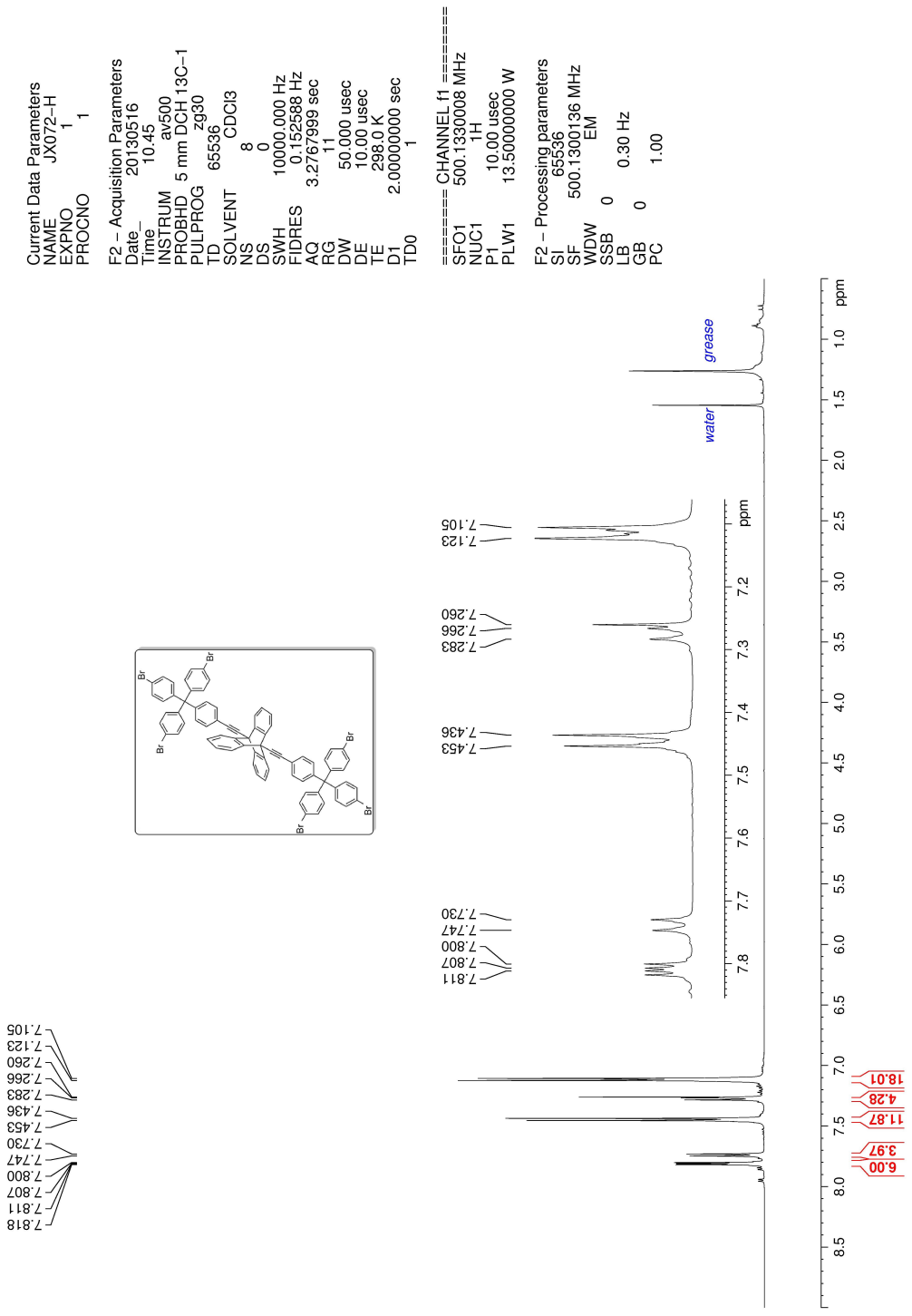

Figure A.3.9. ^{1}H NMR of compound **8** at 500 MHz in $CDCl_3$.

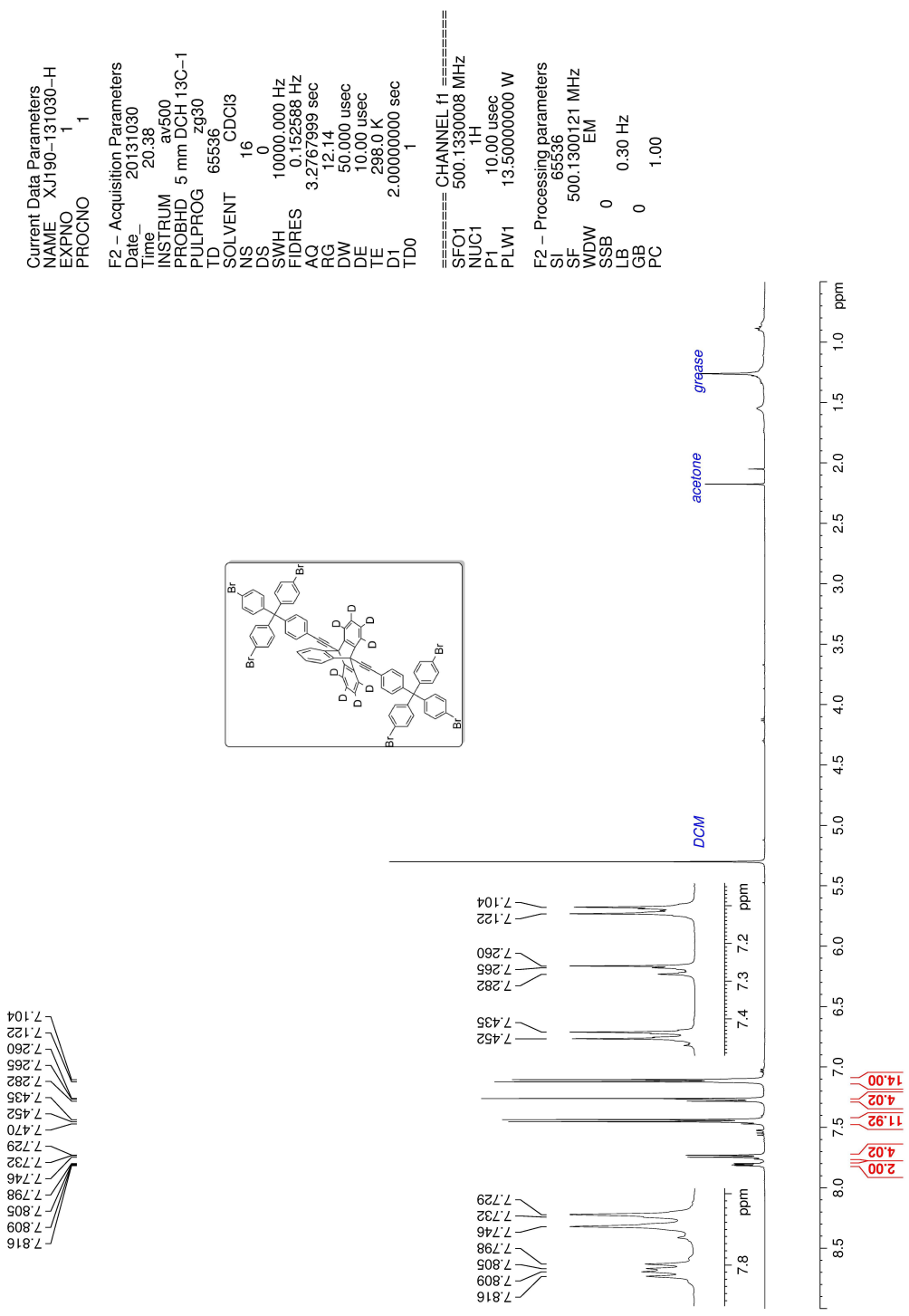

Figure A.3.10. ^{1}H NMR of compound **8**-d_8 at 500 MHz in $CDCl_3$.

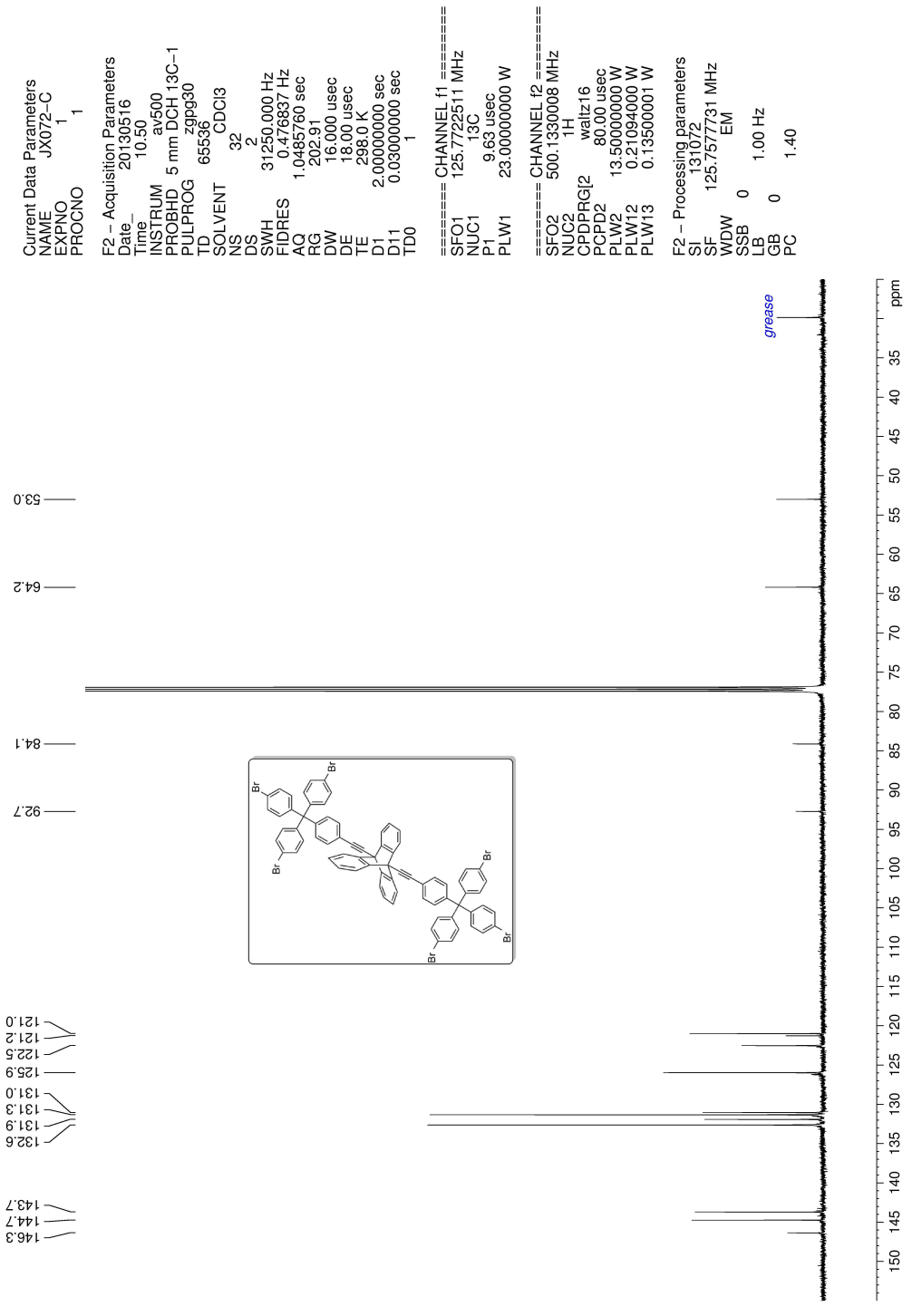

Figure A.3.11. ^{13}C NMR of compound **8** at 125 MHz in $CDCl_3$.

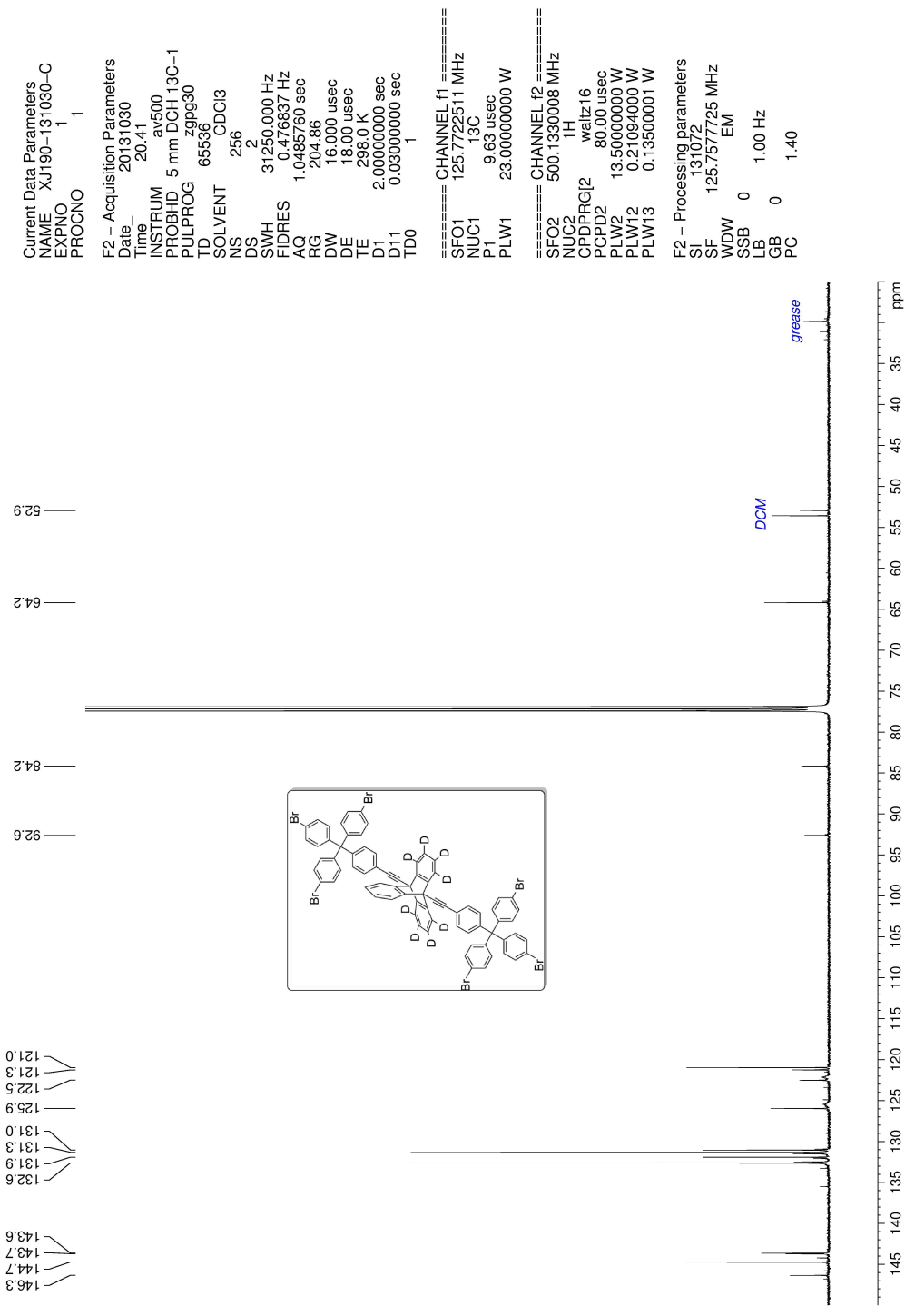

Figure A.3.12. ^{13}C NMR of compound **8**-d_8 at 125 MHz in $CDCl_3$.

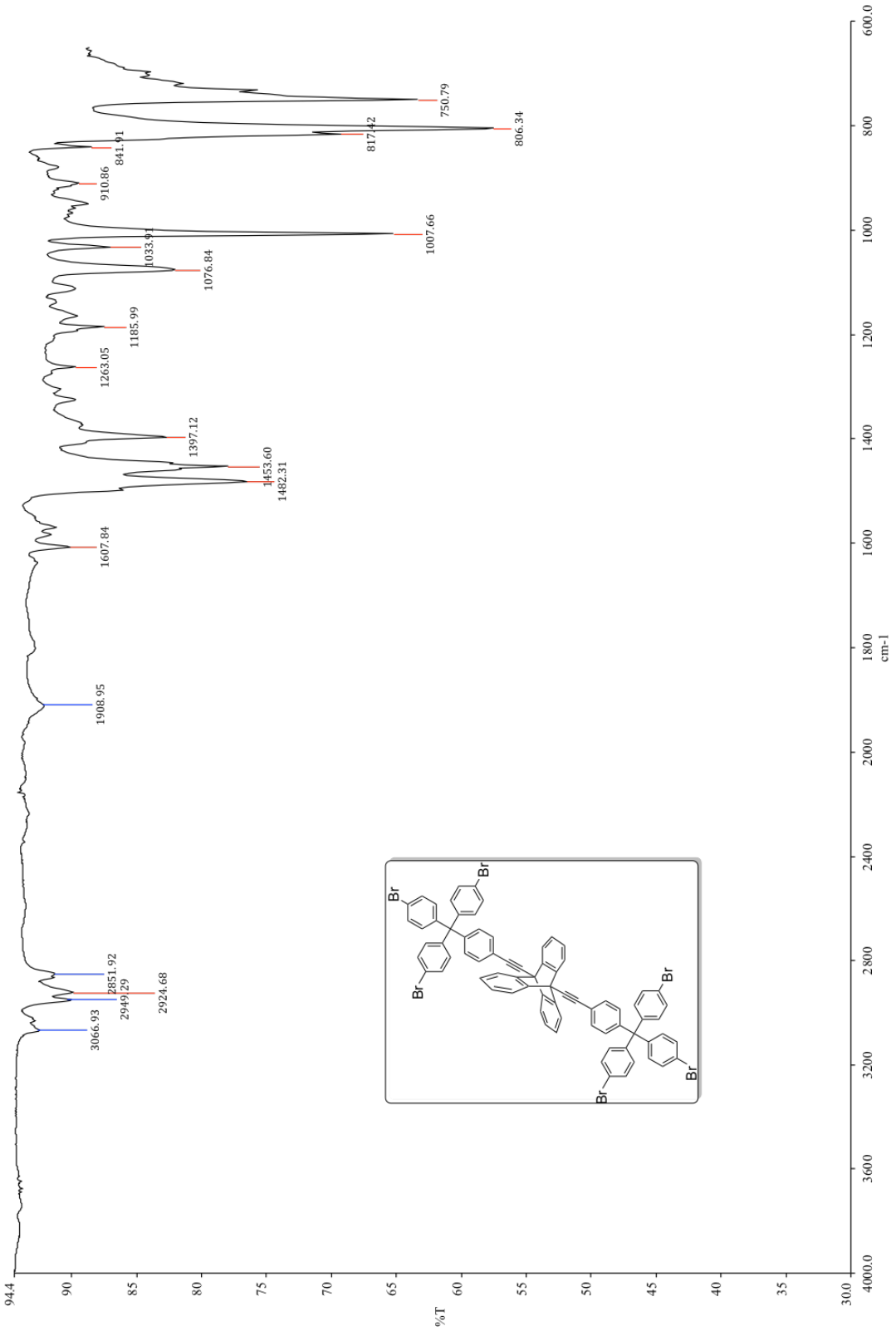

Figure A.3.13. FTIR of compound **8**.

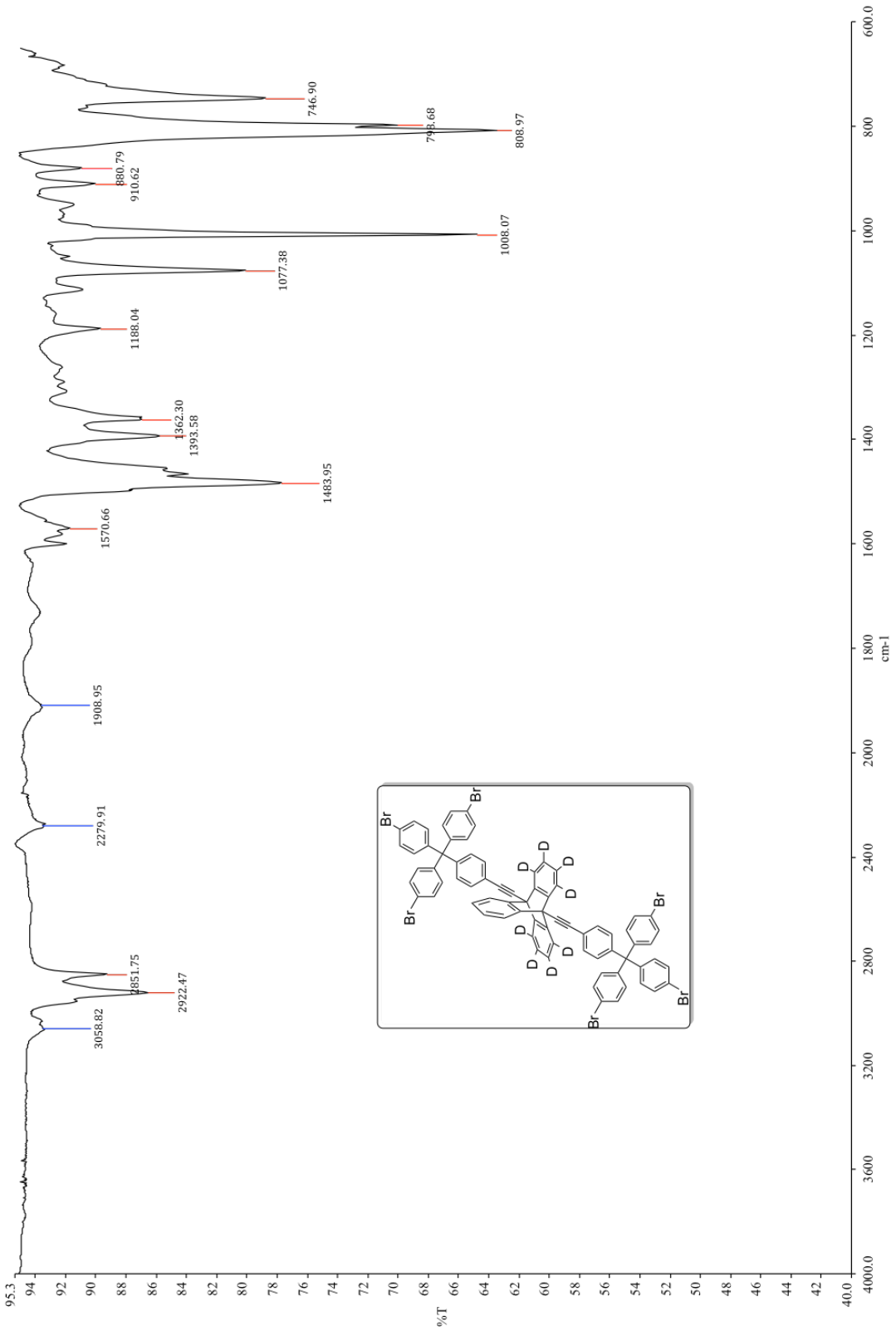

Figure A.3.14. FTIR of compound **8**-d_8.

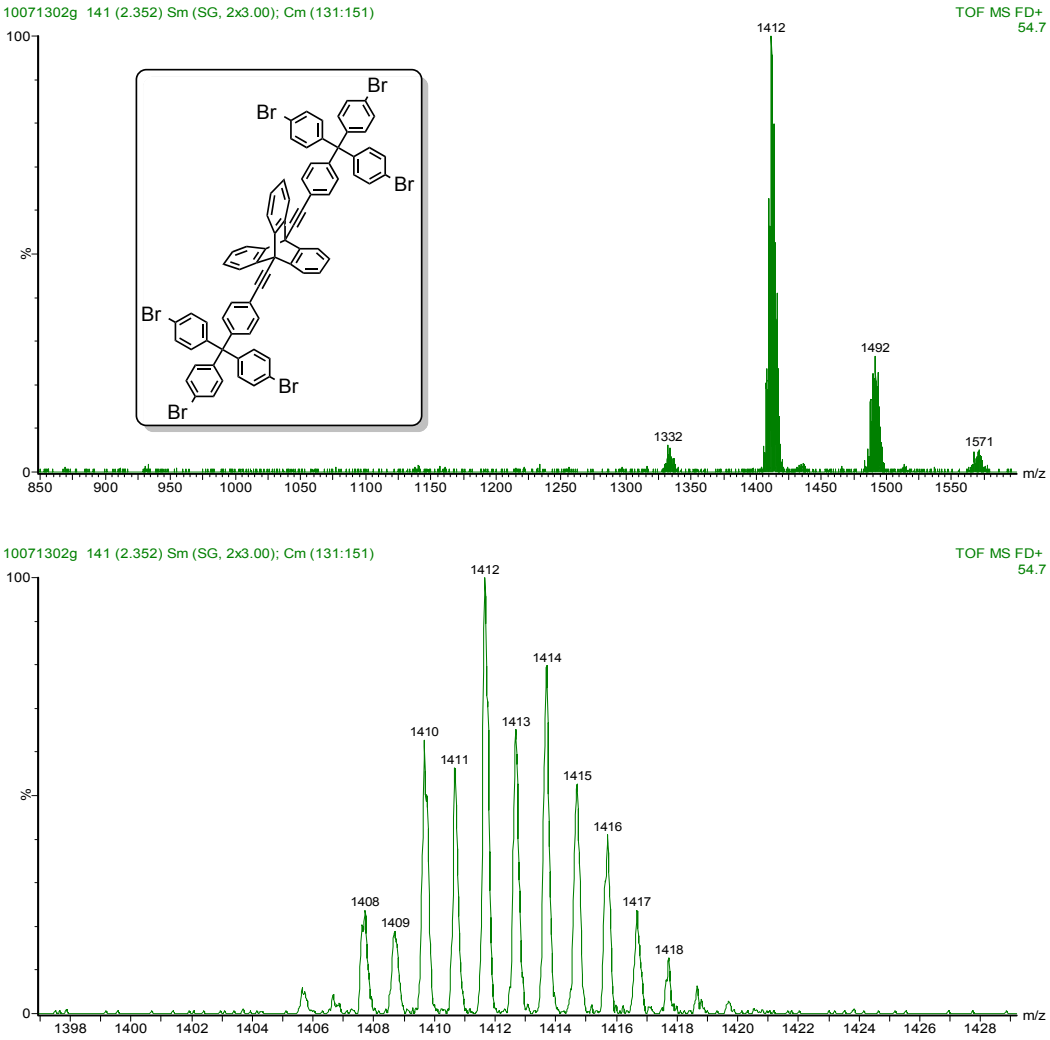

Figure A.3.15. MS (MALDI, TOF) of compound **8** showing M^+ cluster.

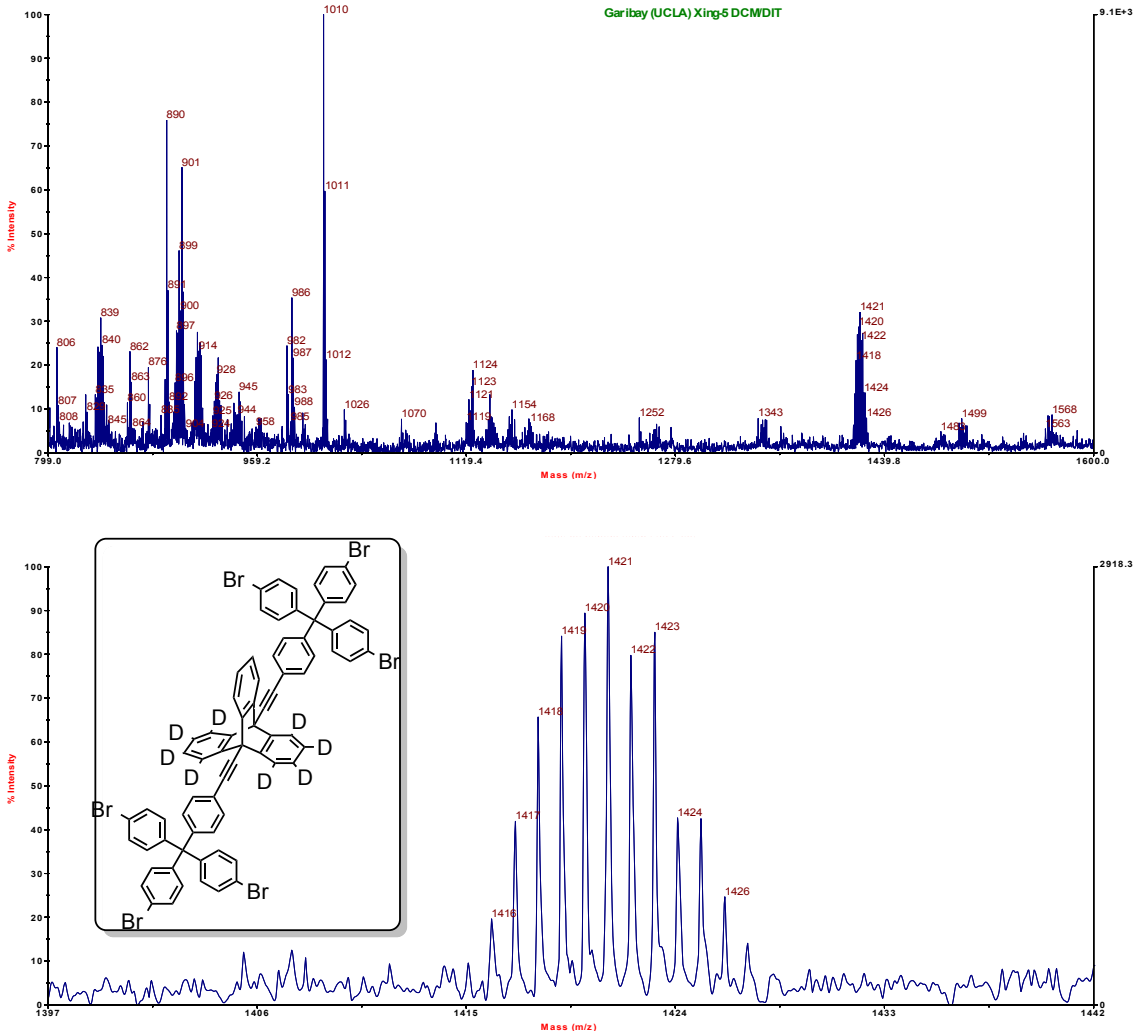

Figure A.3.16. MS (MALDI, TOF) of compound **8**-d_8 showing MH^+ cluster.

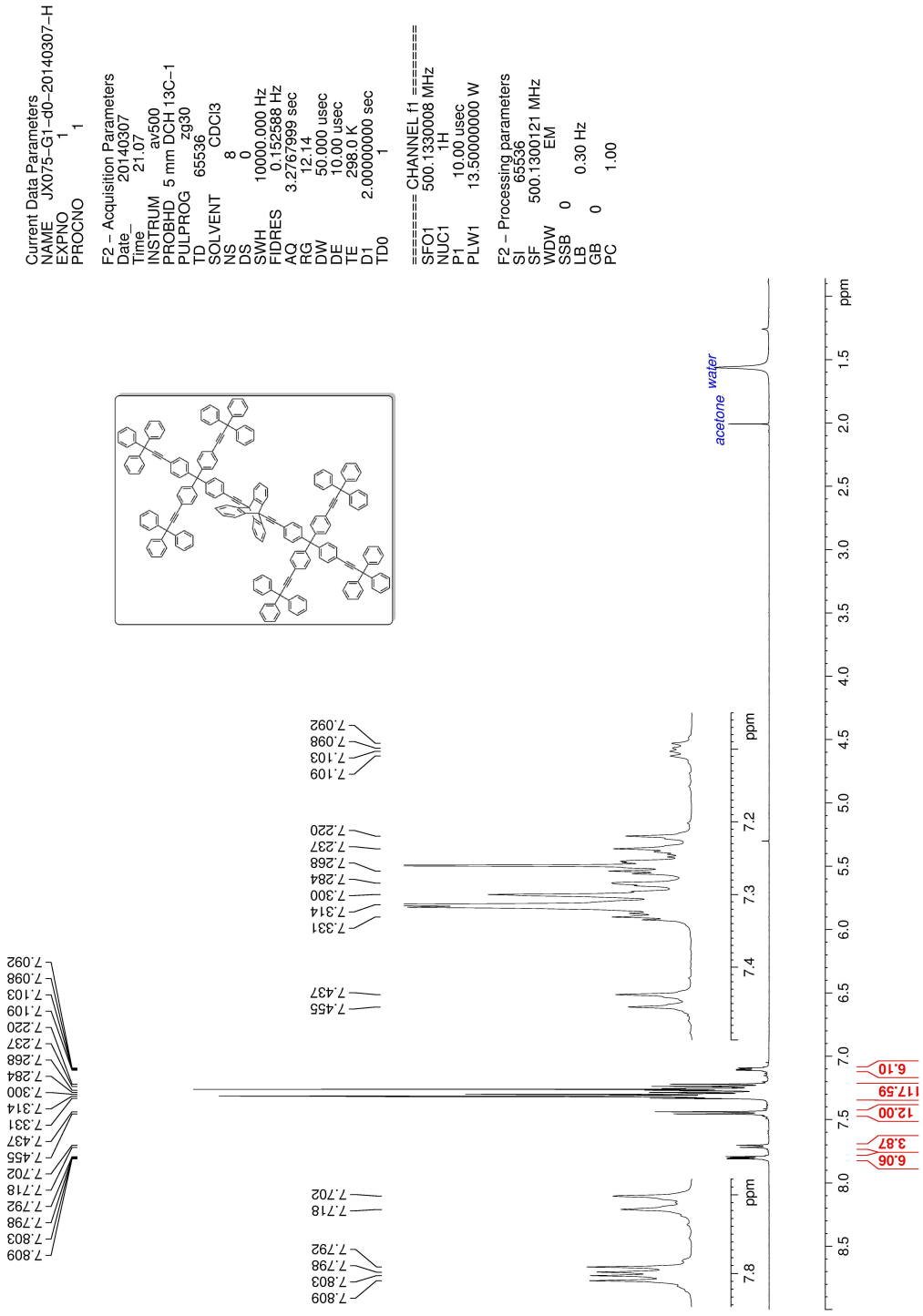

Figure A.3.17. ^{1}H NMR of compound **3** at 500 MHz in $CDCl_3$.

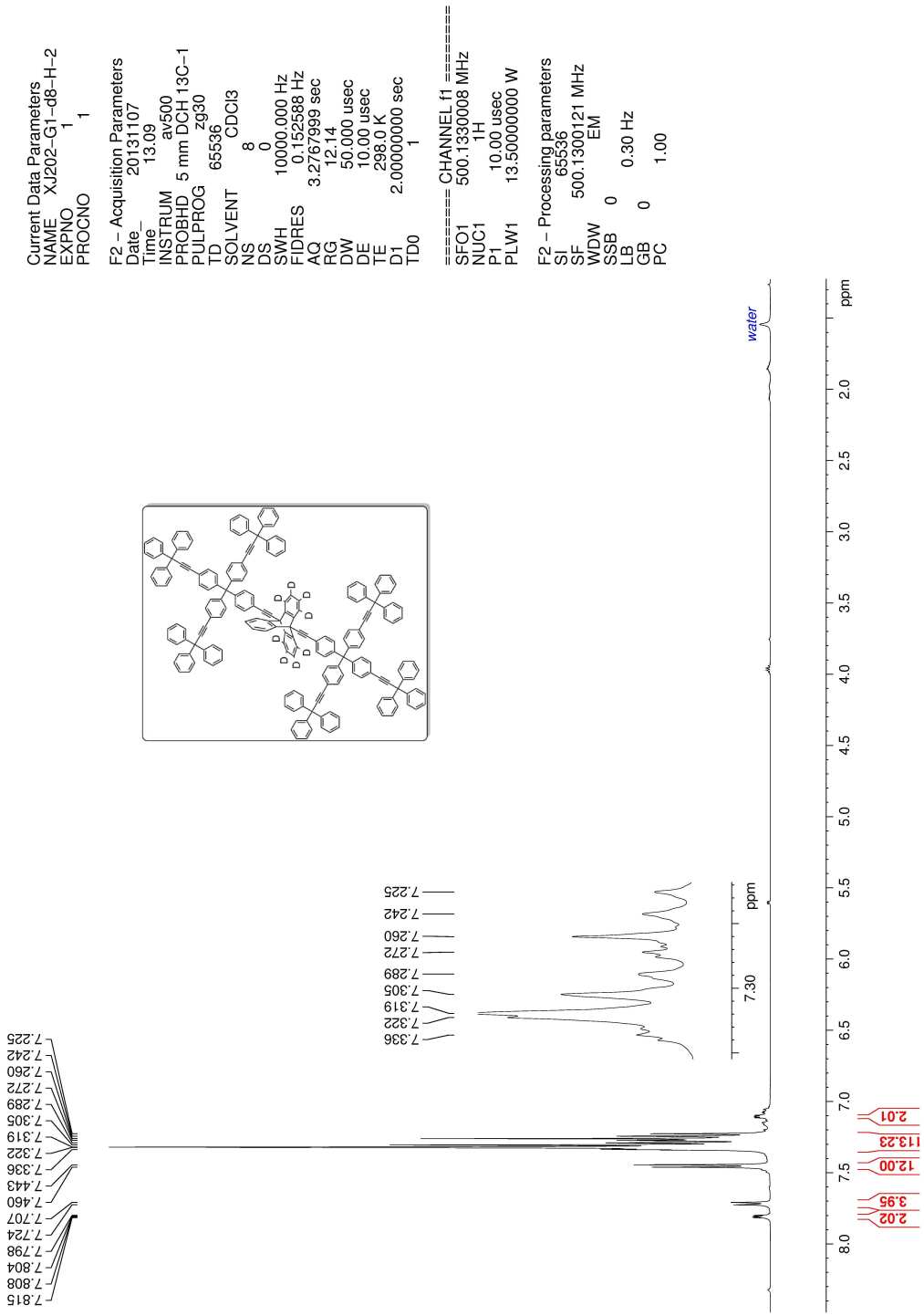

Figure A.3.18. ^{1}H NMR of compound **3**-d_8 at 500 MHz in $CDCl_3$.

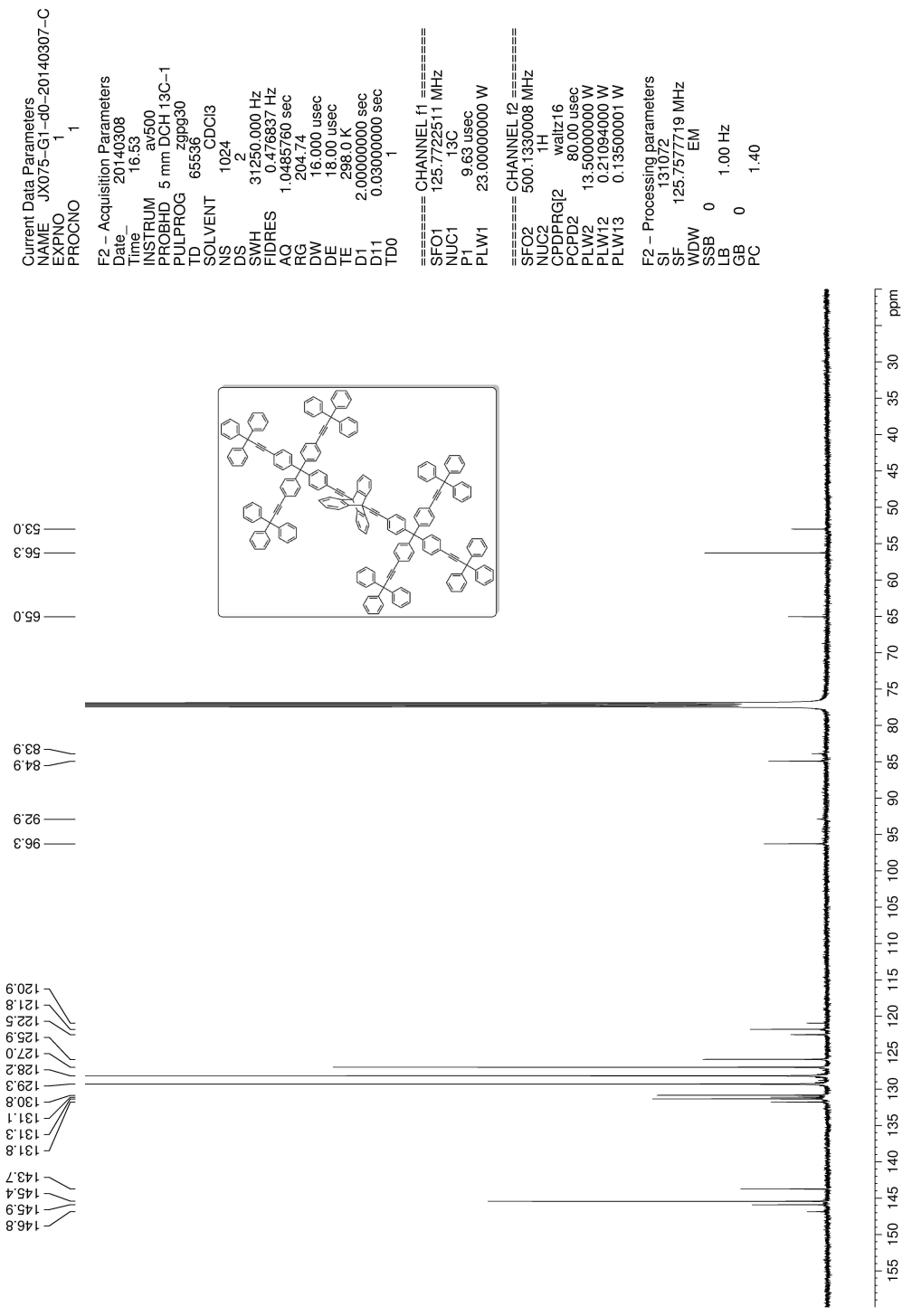

Figure A.3.19. ^{13}C NMR of compound **3** at 125 MHz in $CDCl_3$.

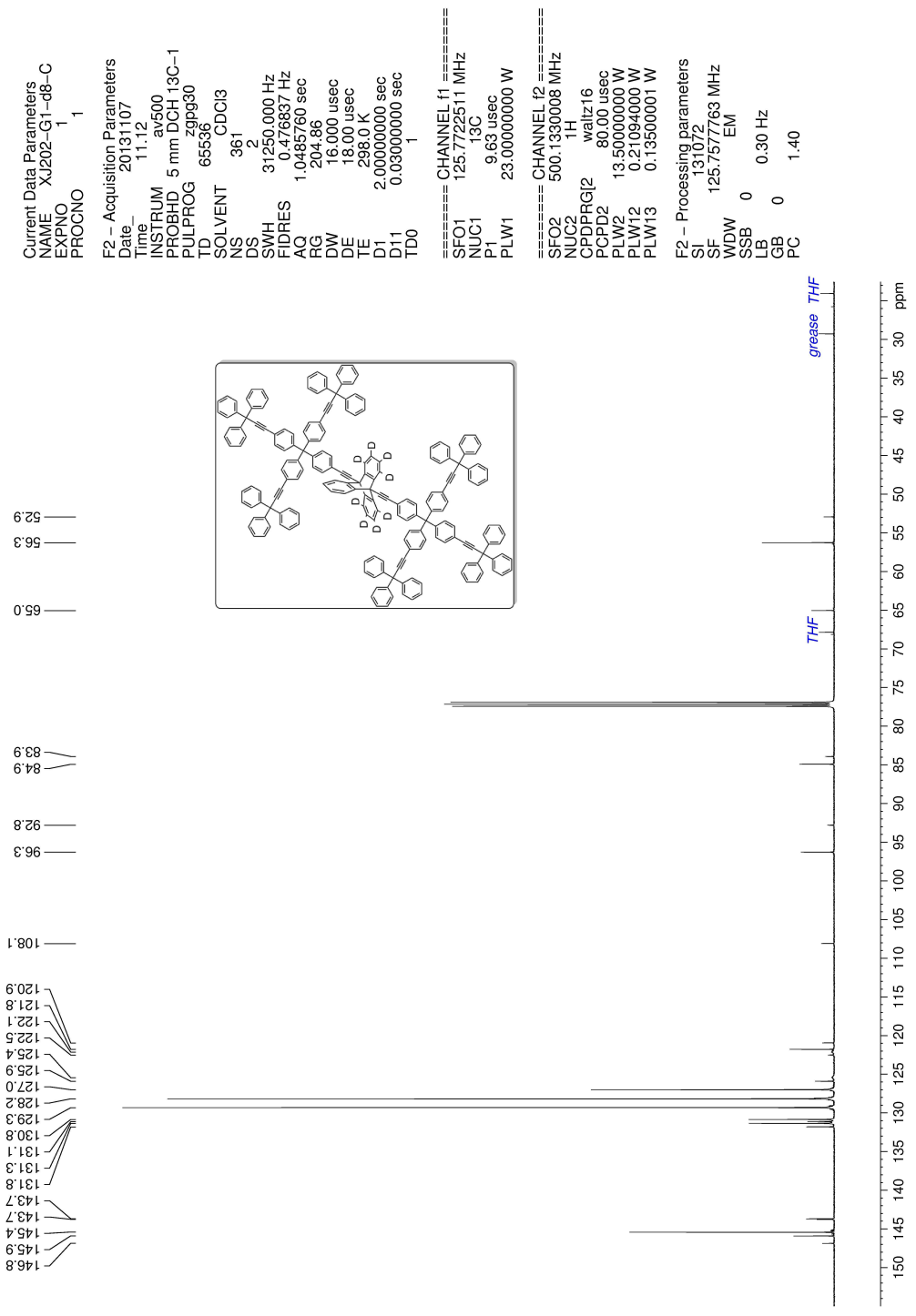

Figure A.3.20. ^{13}C NMR of compound **3**-d_8 at 125 MHz in $CDCl_3$.

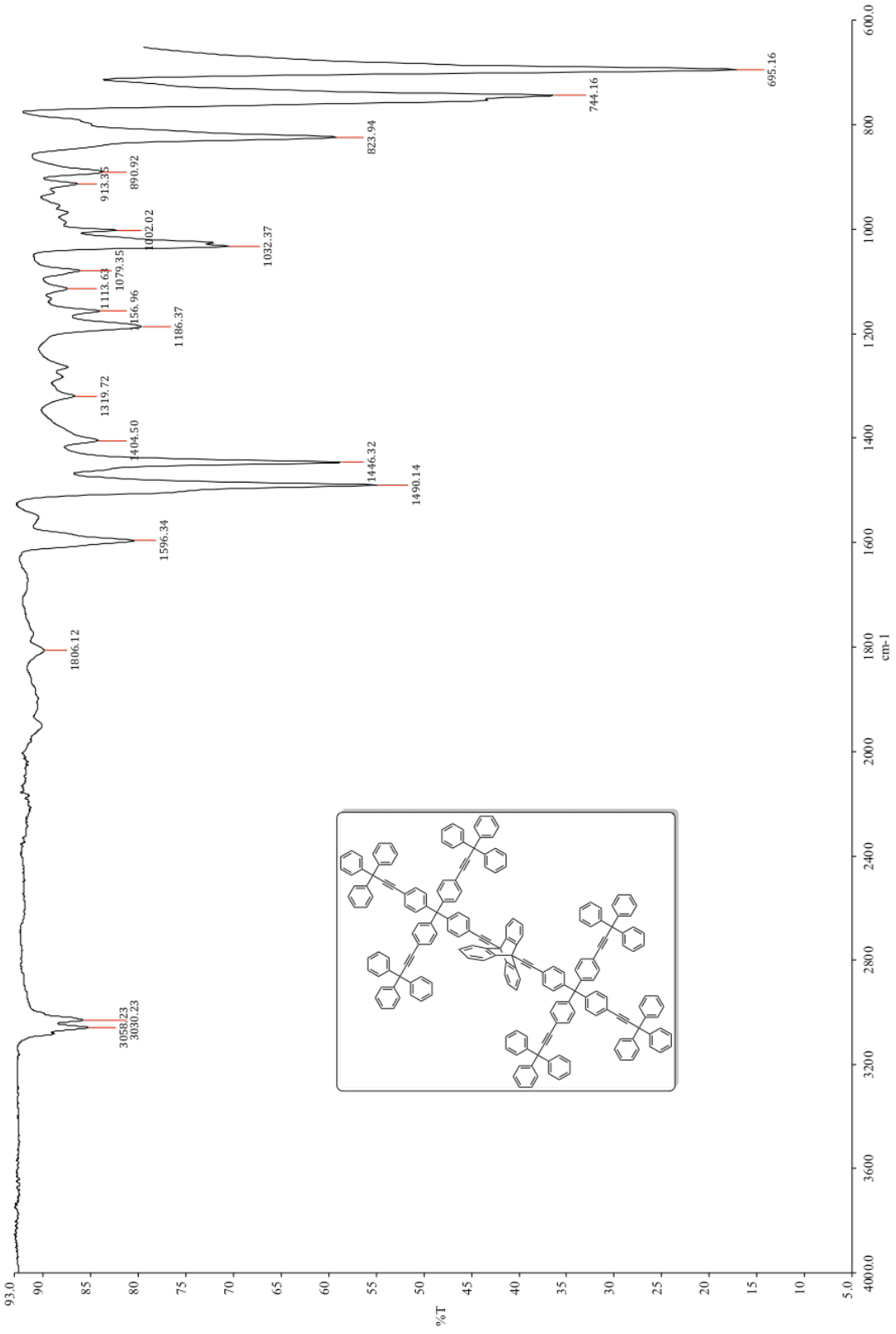

Figure A.3.21. FTIR of compound **3**.

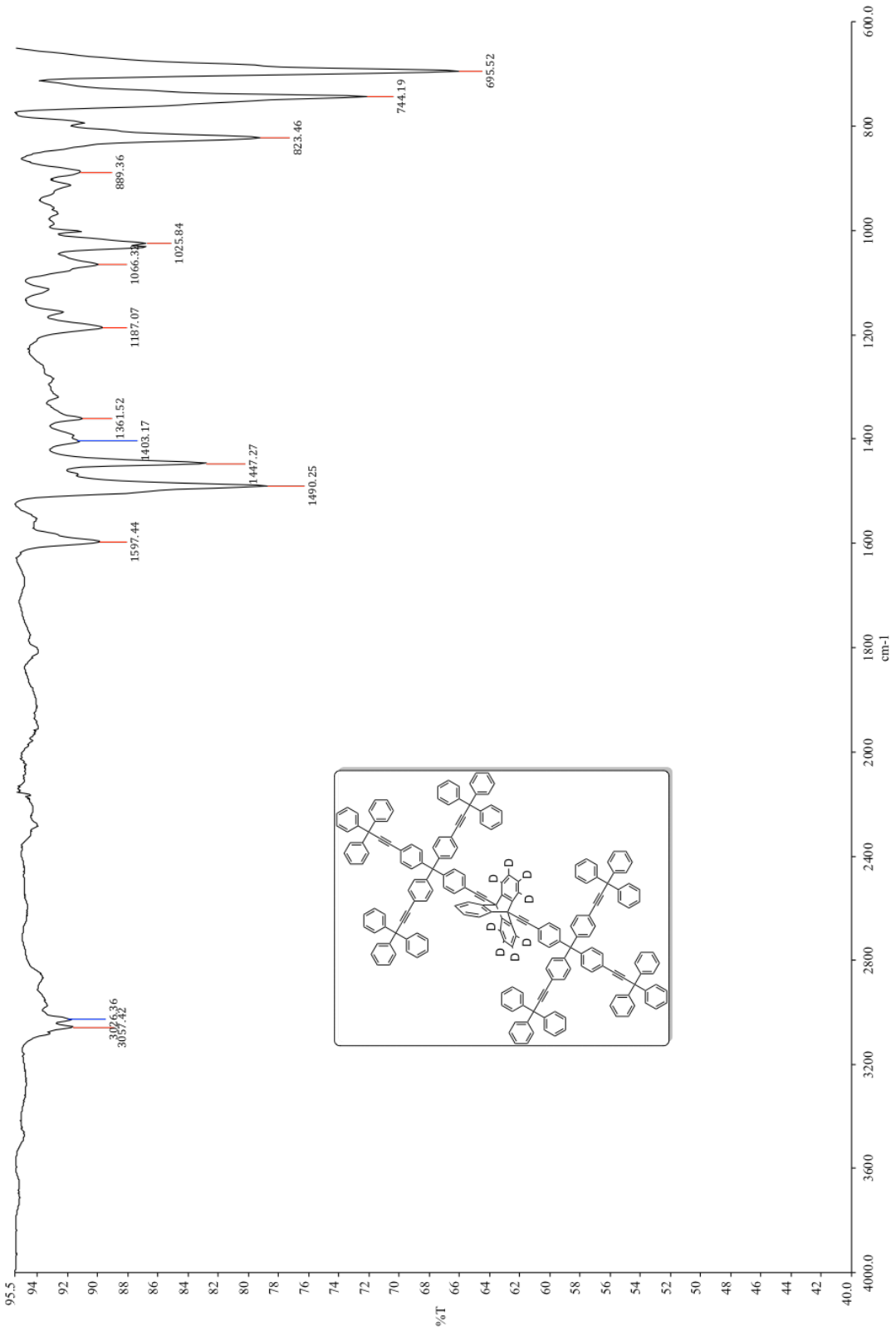

Figure A.3.22. FTIR of compound **3**-d_8.

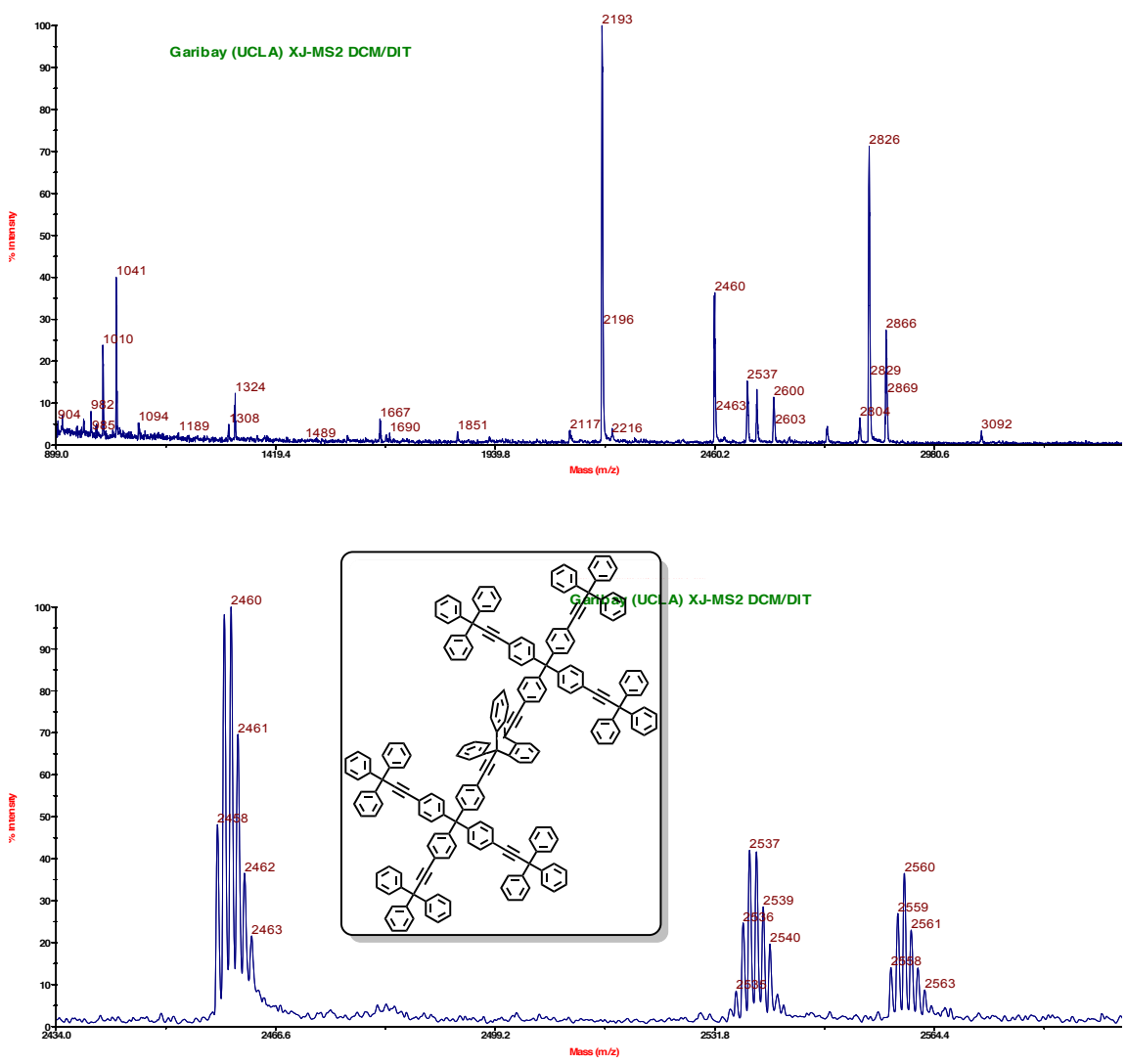

Figure A.3.23. MS (MALDI, TOF) of compound **3** showing MH^+ cluster.

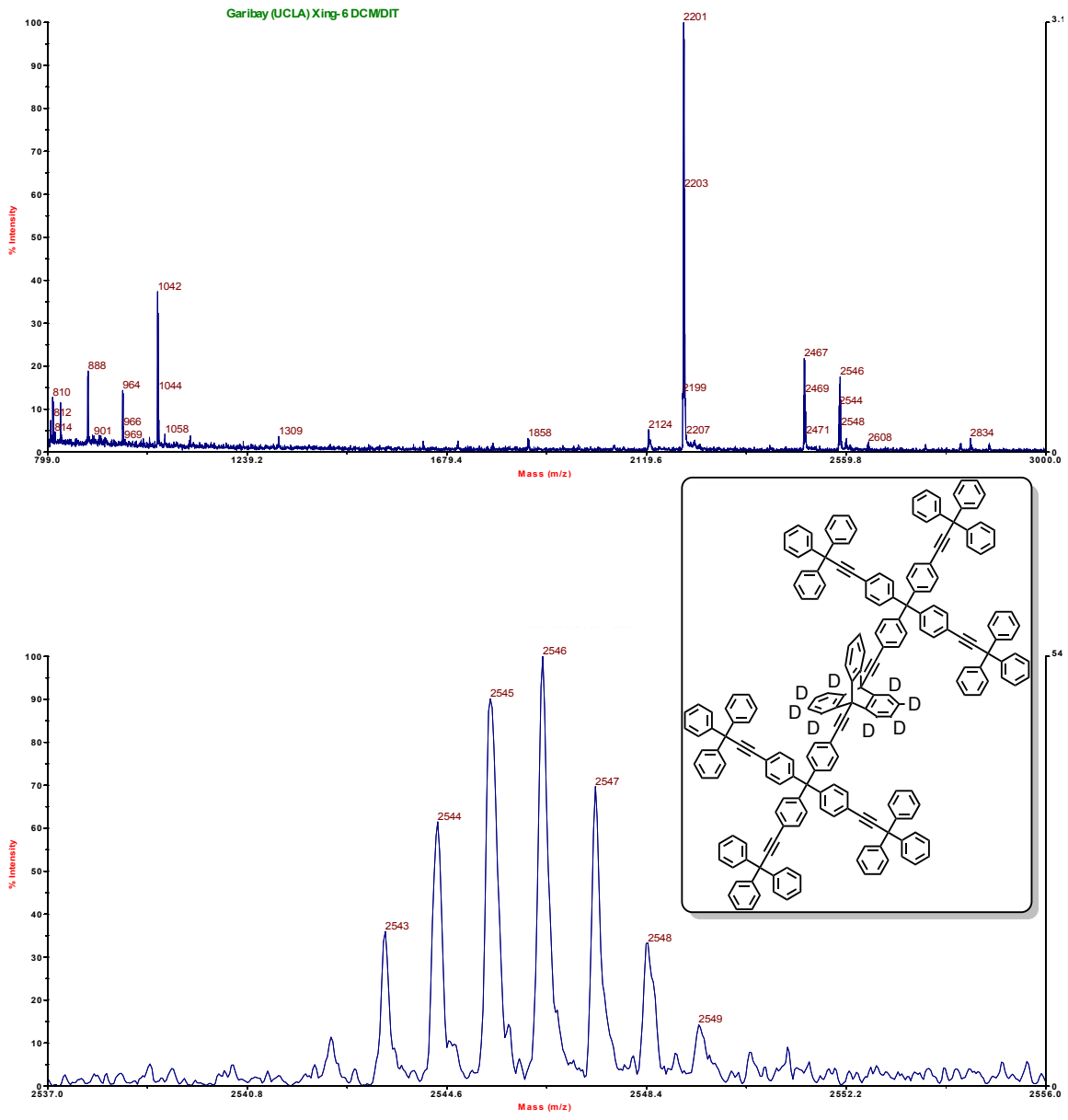

Figure A.3.24. MS (MALDI, TOF) of compound **3**-d_8 showing MH^+ cluster.

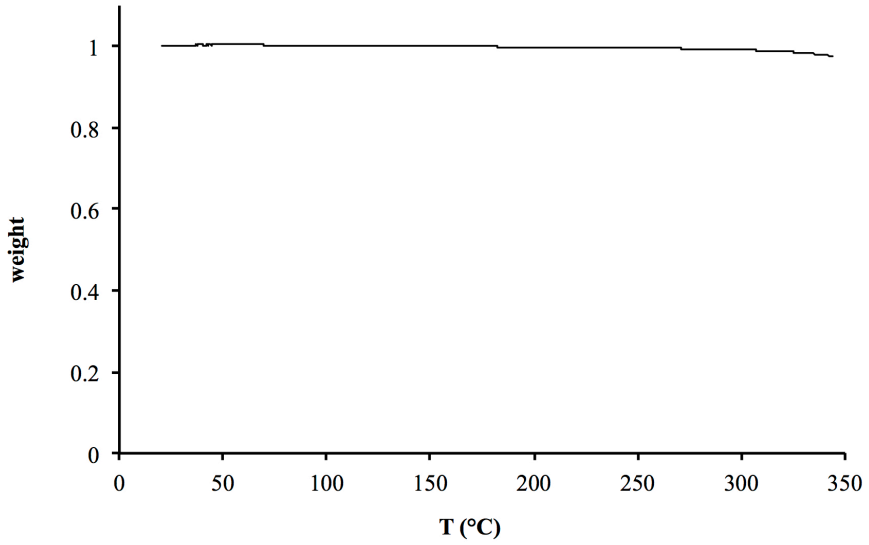

Figure A.3.25. TGA of rotor **3** with little weight loss when heated to 350 ˚C.

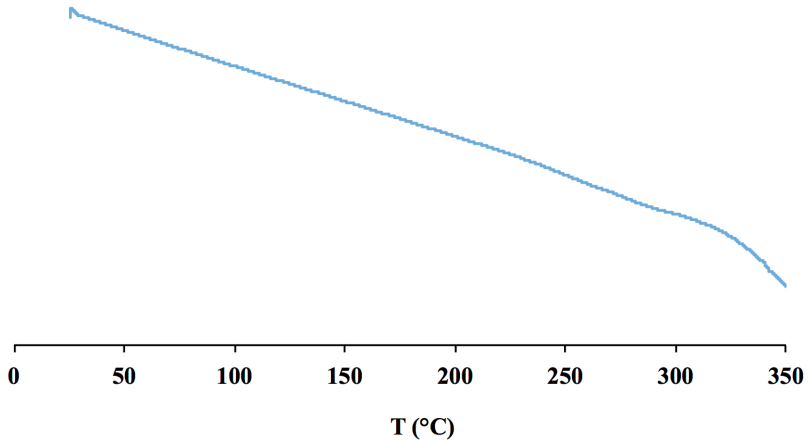

Figure A.3.26. DSC trace of rotor **3** from 25 to 350 ˚C with no first order transition before 300 ˚C.

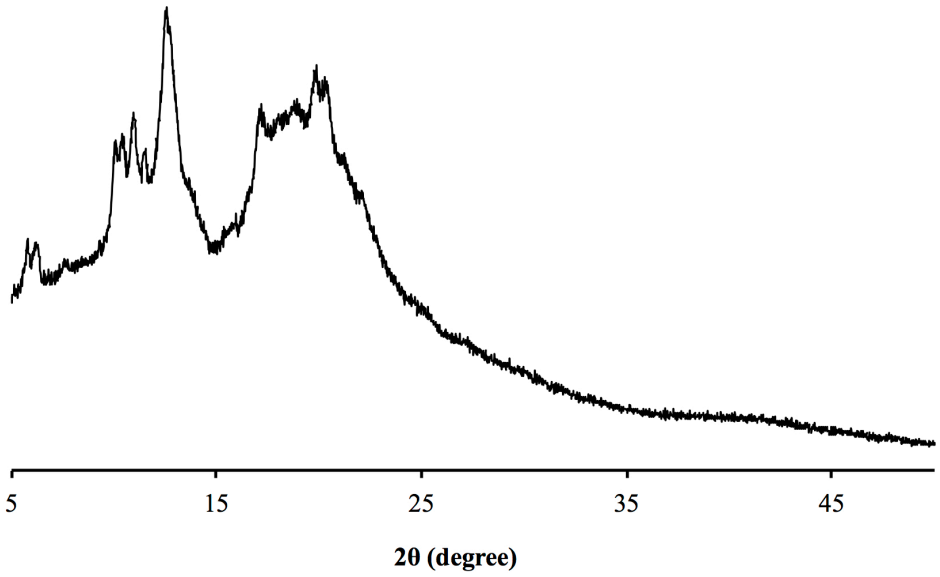

Figure A.3.27. PXRD of the solid sample of **3**.

3.7. References

1. (a) Coskun, A.; Banaszak, M.; Astumian, R. D.; Stoddart, J. F.; Grzybowski, B. A. *Chem. Soc. Rev.* **2012**, *41*, 19. (b) Kay, E.; Leigh, D.; Zerbetto, F. *Angew. Chem., Int. Ed.* **2007**, *46*, 72. (c) Balzani, V.; Credi, A.; Raymo, F.; Stoddart, J. *Angew. Chem., Int. Ed.* **2000**, *39*, 3348.

2. (a) Lewandowski, B.; De Bo, G.; Ward, J. W.; Papmeyer, M.; Kuschel, S.; Aldegunde, M. J.; Gramlich, P. M. E.; Heckmann, D.; Goldup, S. M.; D'Souza, D. M.; Fernandes, A. E.; Leigh, D. A. *Science* **2013**, *339*, 189. (b) Perera, U. G. E.; Ample, F.; Kersell, H.; Zhang, Y.; Vives, G.; Echeverria, J.; Grisolia, M.; Rapenne, G.; Joachim, C.; Hla, S.-W. *Nat. Nanotechnol.* **2013**, *8*, 46. (c) Nguyen, T.-T.-T.; Türp, D.; Wagner, M.; Müllen, K. *Angew. Chem., Int. Ed.* **2013**, *52*, 669. (d) Schmittel, M.; De, S.; Pramanik, S. *Angew. Chem., Int. Ed.* **2012**, *51*, 3832. (e) Carroll, G. T.; Pollard, M. M.; van Delden, R.; Feringa, B. L. *Chem. Sci.* **2010**, *1*, 97. (f) Silvi, S.; Arduini, A.; Pochini, A.; Secchi, A.; Tomasulo, M.; Raymo, F. M.; Baroncini, M.; Credi, A. *J. Am. Chem. Soc.* **2007**, *129*, 13378. (g) Muraoka, T.; Kinbara, K.; Aida, T. *Nature* **2006**, *440*, 512.

3. Iwamura, H.; Mislow, K. *Acc. Chem. Res.* **1988**, *21*, 175.

4. (a) Comotti, A.; Bracco, S.; Ben, T.; Qiu, S.; Sozzani, P. *Angew. Chem., Int. Ed.* **2014**, *53*, 1043. (b) Tierney, H. L.; Murphy, C. J.; Jewell, A. D.; Baber, A. E.; Iski, E. V.; Khodaverdian, H. Y.; McGuire, A. F.; Klebanov, N.; Sykes, E. C. H. *Nat. Nanotechnol.* **2011**, *6*, 625. (c) Akutagawa, T.; Endo, D.; Kudo, F.; Noro, S.; Takeda, S.; Cronin, L.; Nakamura, T. *Cryst. Growth Des.* **2008**, *8*, 812. (d) Nawara, A. J.; Shima, T.; Hampel, F.; Gladysz, J. A. *J. Am. Chem. Soc.* **2006**, *128*, 4962. (e) Kottas, G. S.; Clarke, L. I.;

Horinek, D.; Michl, J. *Chem. Rev.* **2005**, *105*, 1281. (f) Hiraoka, S.; Shiro, M.; Shionoya, M. *J. Am. Chem. Soc.* **2004**, *126*, 1214.

5. (a) Vogelsberg, C. S.; Garcia-Garibay, M. A. *Chem. Soc. Rev.* **2012**, *41*, 1892. (b) Khuong, T.-A. V.; Nuñez, J. E.; Godinez, C. E.; Garcia-Garibay, M. A. *Acc. Chem. Res.* **2006**, *39*, 413.

6. (a) Setaka, W.; Yamaguchi, K. *J. Am. Chem. Soc.* **2013**, *135*, 14560. (b) Akutagawa, T.; Shitagami, K.; Nishihara, S.; Takeda, S.; Hasegawa, T.; Nakamura, T.; Hosokoshi, Y.; Inoue, K.; Ikeuchi, S.; Miyazaki, Y.; Saito, K. *J. Am. Chem. Soc.* **2005**, *127*, 4397.

7. (a) Wang, X.; Beckmann, P. A.; Mallory, C. W.; Rheingold, A. L.; DiPasquale, A. G.; Carroll, P. J.; Mallory, F. B. *J. Org. Chem.* **2011**, *76*, 5170. (b) van der Putten, D.; Diezman, G.; Fujara, F.; Hartmann, K.; Silescu, H. *J. Chem. Phys.* **1992**, *96*, 1748. (c) Rodríguez-Molina, B.; Pérez-Estrada, S.; Garcia-Garibay, M. A. *J. Am. Chem. Soc.* **2013**, *135*, 10388.

8. Karlen, S. D.; Reyes, H.; Taylor, R. E.; Khan, S. I.; Hawthorne, M. F.; Garcia-Garibay, M. A. *Proc. Natl. Acad. Sci. U. S. A.* **2010**, *107*, 14973.

9. As proposed in ref. 4c, we use the word "rotor" to describe the entire molecular assembly, and "rotator" and "stator" to denote the rotary units and the static component, respectively.

10. Cohen, M. D. *Angew. Chem., Int. Ed.* **1975**, *14*, 386.

11. Khuong, T.-A. V.; Dang, H.; Jarowski, P. D.; Maverick, E. F.; Garcia-Garibay, M. A. *J. Am. Chem. Soc.* **2007**, *129*, 839.

12 . (a) Moments inertia were determined on minimized structures using the ChemPropStd function in SC ChemDraw 3D Pro. (b) A inertial rotational frequency τ_{IR}^{-1}

can be estimated from the moment of inertia (I) of a rotator using the equation $\tau_{IR}^{-1} = [(2\pi/9)(I/k_BT)^{1/2}]^{-1}$. The values for methyl, phenylene, byclo[2.2.2]octane, and triptycene groups are, 1.3×10^{13} s^{-1}, 2.4×10^{12} s^{-1}, 1.6×10^{12} s^{-1} and 5.6×10^{11} s^{-1}, respectively. Please see: Kawski, A., *Crit. Rev. Anal. Chem.* **1993**, *23*, 459.

13. (a) Bauer, R. E.; Grimsdale, A. C.; Müllen, K. *Top. Curr. Chem.* **2005**, *245*, 253. (b) Moore, J. S. *Acc. Chem. Res.* **1997**, *30*, 402.

14. Macho, V.; Brombacher, L.; Spiess, H. W. *Appl. Magn. Reson.* **2001**, *20*, 405.

15. (a) Schmidt, C.; Kuhn, J.; Spiess, H. W. *Progr. Colloid Polymer Sci.* **1985**, *71*, 71. (b) Fischer, E. W. Hellmann, G. P.; Spiess, H. W.; Hörth, F. J.; Gearius, U.; Wehrle, M. *Makromol. Chem. Suppl.* **1985**, *12*, 189.

16. For a recent example of geared motion in the solid state, see: Lemouchi, C.; Iliopoulos, K.; Zorina, L.; Simonov, S.; Wzietek, P.; Cauchy, T.; Rodríguez-Fortea, A.; Canadell, E.; Kaleta, J.; Michl, J.; Gindre, D.; Chrysos, M.; Batail, P. *J. Am. Chem. Soc.* **2013**, *135*, 9366.

17. Ie, Y.; Hirose, T.; Nakamura, H.; Kiguchi, M.; Takagi, N.; Kawai, M.; Aso, Y. *J. Am. Chem. Soc.* **2011**, *133*, 3014.

18. Goldsmith, R. H.; Vura-Weis, J.; Scott, A. M.; Borkar, S.; Sen, A.; Ratner, M. A.; Wasielewski, M. R. *J. Am. Chem. Soc.* **2008**, *130*, 7659.

19. Heimer, N. E.; Mattern, D. L. *J. Am. Chem. Soc.* **1993**, *115*, 2217.

Chapter Four

Diffusion-Controlled Rotation of a Crystalline Triptycene MOF Determined by the Hydrodynamics of a Confined Liquid

4.1. Introduction

The design of usable artificial molecular machines will require the input of a broad range of physical and material scientists. However, it will be up to chemists to develop the structural platforms needed to realize their functions.[1,2] Early work on artificial molecular machinery was guided by the structural and dynamic analogies between macroscopic objects and small molecules in solution.[3] In recent years, alternative approaches have been inspired by the design and function of biomolecular machines such as ATP synthase, the bacterial flagellum, and the skeletal muscle.[4] These structures highlight the importance of biased Brownian motion under conditions where inertial forces are orders of magnitude smaller than viscous forces,[1c] and suggest the advantage of using nanometer size units that become part of higher assemblies.

With the objective of exploring structures that display those characteristics, we suggested that artificial molecular machinery based on the design of molecules that are capable of performing dynamic processes in the crystalline state, such that their molecular level operation can be determined by external control in the macroscopic world.[5] The number of so-called "amphidynamic" crystals built with static and dynamic elements has increased over the last few years.[6] Motion in solids has been reliably engineered using molecules with conformationally flexible bulky groups acting as a stator, covalently linked to a central group that acts as the rotator, such as bicyclo[2.2.2]octane in **1**[7] (Figure 4.1a). It has been shown that low packing densities and conformational degrees of freedom allow for volume fluctuations[6a,f] that play a role analogous to that of viscous forces in liquids and can be used in simple scaling strategies to prepare molecular solids to support the dynamics of significantly larger rotators. For

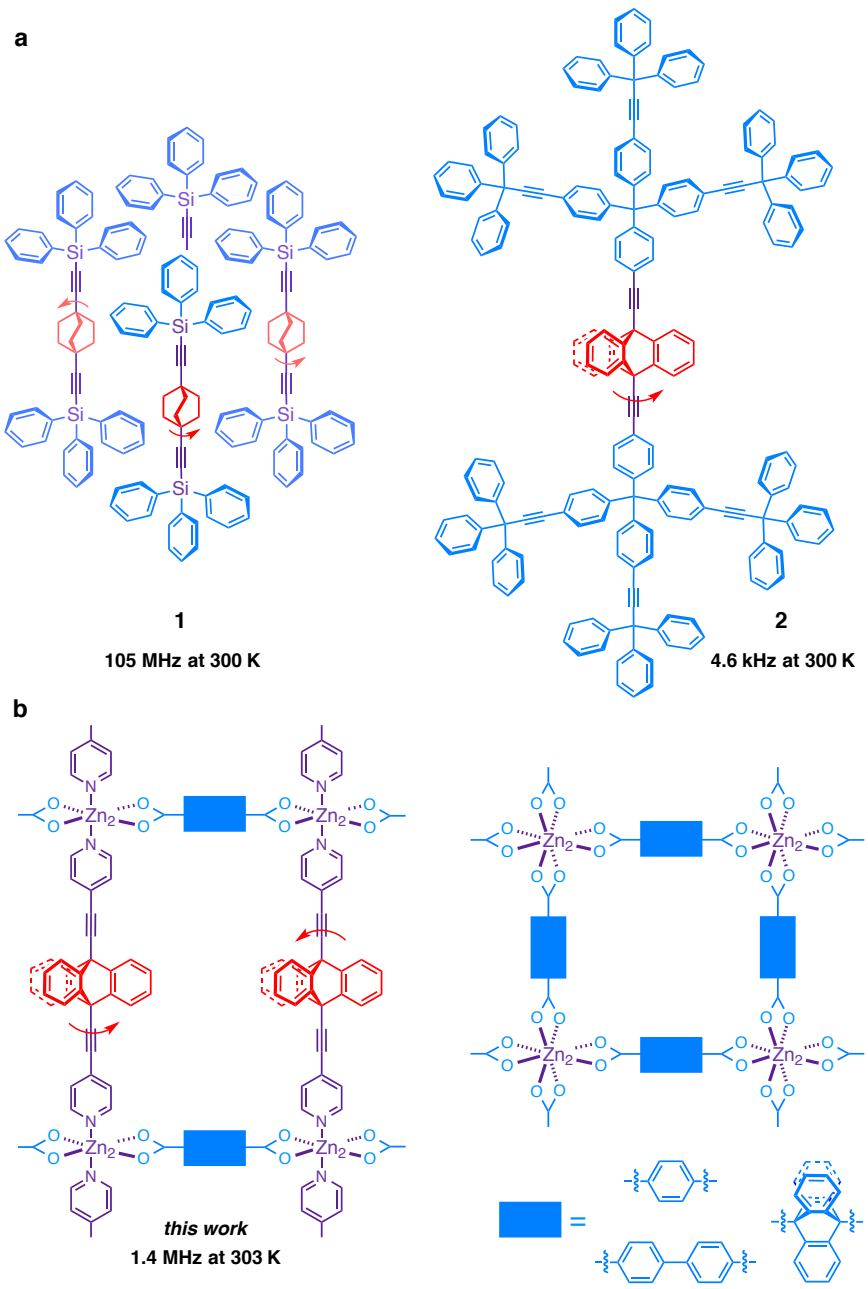

Figure 4.1. (a) Chemical structures of the molecular rotor **1** illustrating a packing structure that supports the rotation of a compact bicyclo[2.2.2]octane rotator and molecular rotor **2** with a larger triptycene rotator. (b) Pillar ligand 9,10-bis(4-pyridylethynyl)triptycene **3** with triptycene moieties coordinates to bimetallic nodes, connecting the 2D grid formed by the bimetallic nodes and dicarboxylates including terephthalate (**UCLA-R1**), biphenyl-4,4′-dicaboxylate (**UCLA-R2**), and triptycene-9,10-dicarboxylate (**UCLA-R3**).

example, line shape analysis of solid state ^{2}H NMR spectra showed the deuterium-labeled triptycene in **2**-d_8 to have a 3-fold energy potential with 4600 jumps per second at 300 K.[8] Although these have been important steps forward in efforts to expand the scale of crystalline molecular rotors and explore the role of random forces in the dynamics of condensed phase media, one can appreciate that a simple scaling strategy drastically reduces the density of rotators in the lattice and increases the distance between them, neither is desirable if one envisions molecular machines that can take advantage of dipole-dipole interactions or mechanical gearing. A promising strategy for the construction of a dense array of larger molecular rotators while removing close contacts with the lattice is given by the use of metal-organic frameworks (MOFs).[9] It seemed that by taking advantage of different carboxylate and amine linkers, one should be able to fine-tune the structures of pillared paddlewheel MOFs to provide an optimized spatial arrangement of molecular rotators and functional groups.[10] Herein, we report the preparation of three pillared paddlewheel MOFs, **UCLA-R1**, **UCLA-R2**, and **UCLA-R3**, and the remarkable rotational dynamics of triptycene groups in **UCLA-R3**. As shown in Figure 4.1b, ligand **3** with a triptycene rotator covalently linked by triple bonds to two pyridine moieties makes up a pillar and connects the square 2D grids formed by bimetallic zinc nodes and dicarboxylate linkers. Three different dicaboxylates (terephthalate, biphenyl-4,4′-dicarboxylate, and triptycene-9,10-dicaboxylate) were used to adjust the distances between the neighboring triptycene rotators as well as the degree of catenation, defined as the interpenetration of two or more identical and independent frameworks.[10a] Taking advantage of triptycene-d_8 labeled frameworks, we used solid-state ^{2}H NMR line-shape analysis to demonstrate that rotation of triptycenes is only possible in

the catenation-free **UCLA-R3**, which displays three-fold jumps with frequencies in the MHz (10^6 s^{-1}) regime near ambient temperatures. Notably, the temperature dependence of the rotational frequencies revealed a dynamic behavior that results from interactions between the rotator and solvent molecules confined in the crystal. With no steric or intrinsic barriers in the structure, the rotation of the triptycene group in **UCLA-R3** constitutes a diffusion-controlled process.

4.2. Synthesis and Characterization

Samples of ligand 9,10-bis(4-pyridylethynyl)triptycene **3** and its isotopologue **3**-d_8 were prepared by Sonagashira reactions between 4-bromopyridine and 9,10-diethynyl-triptycene and 9,10-diethynyltriptycene-d_8, respectively.[8] The detailed synthetic procedure is included in the experimental section. MOFs **UCLA-R1**–**R3** were prepared by solvothermal synthesis from a mixture of zinc nitrate hexahydrate, the carboxylic acids, and pillaring ligand **3** in DMF. Single crystals were picked up from the vials in the presence of DMF and used for X-ray diffraction immediately as irreversible phase transitions and structure collapse were shown to occur when the samples were exposed to air and the solvent escaped. As a result, all characterizations were performed on solvent-saturated samples.

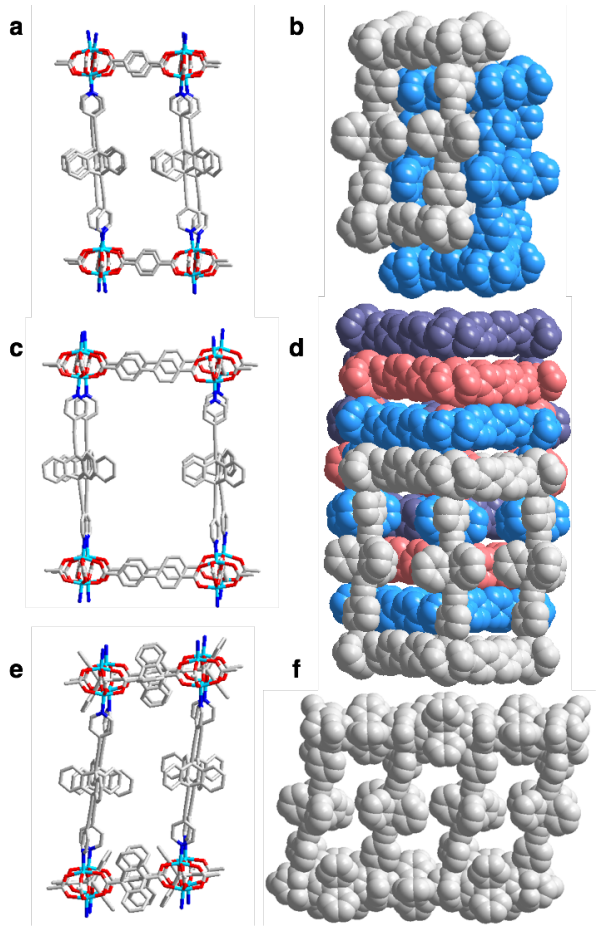

Figure 4.2. Crystal structures of MOFs **UCLA-R1** (a,b), **UCLA-R2** (c,d), **UCLA-R3** (e,f) showing cube-like cages after a partial expansion. Solvent molecules (DMF) and hydrogen atoms are removed for clarity. The space-filling representations are colored to show the 2-fold (b) and 4-fold catenated (d) structures. For the capped stick models (a,c,e), the color code is designated: Zn: cyan; N: blue; O: red; C: silver.

The single crystal structures of MOFs **UCLA-R1**–**R3** obtained at 100 K are illustrated in Figure 4.2. The expected paddle wheel architectures with dimetallic zinc nodes connected by dicaboxylates and ligand **3** were obtained as expected for all three frameworks. Samples of **UCLA-R1** crystalized in the space group P-1 with an asymmetric unit consisting of two binuclear zinc units, four terephthalates, and two molecules of **3**. The 2-fold catenated structure observed for **UCLA-R1** with the pillar

distorted to accommodate the catenation is shown in Figure 4.2a and the constituting lattices shown in grey and blue in Figure 4.2b. A structural feature resulting from the interpenetration was the close π-π stacking between the triptycene rotators in one pillar and the pyridine groups of the adjacent ones, as shown in the space-filling model. This close contact, together with the relatively short distances between triptycenes within the same network (8.1 Å, distance between bridge head carbons), makes it difficult for the triptycene to rotate. A higher ordered catenation was observed in the crystal structure of **UCLA-R2**, which was solved in the space group $P2_1/c$. Since the voids in the 2D grids formed by zinc nodes and biphenyl-4,4′-dicarboxylates are larger than those in **UCLA-R1**, a 4-fold interdigitated structure was observed. Two pyridines from the neighboring networks are consequently placed in between the blades of each triptycene in the pillar, leaving little room for any motion of those groups. The crystal structure of **UCLA-R3** was solved in the monoclinic space group C2/c. In this case, the presence of sterically demanding triptycene-9,10-dicarboxylate linkers led to the formation of densely packed layer structures and prevented catenation. While the triptycene groups in the layer structure are expected to be static as all of their blades are meshed with each other, the ones in the pillar structures have contacts only with the DMF molecules and might be able to undergo fast dynamics. A close inspection of neighboring rotators (Figure 4.3) reveals a distance of 10.3 Å between their rotational axes, which is almost twice the radius of their volume of revolution.[8,11] The closest distance of approach between hydrogen atoms in adjacent rotators occurs away from their crystallographic positions, at which they are 2.9 Å away from each other, suggesting the lack of significant rotator–rotator interactions. In fact, as shown in Figure 4.3b, only solvent molecules

could be observed in the proximity of the triptycene rotator in the structure obtained at 100 K.

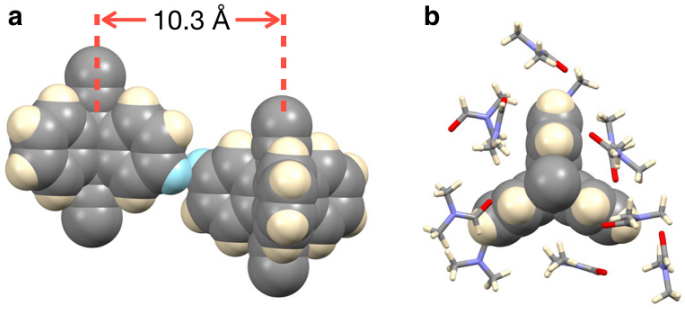

Figure 4.3. (a) The distances between the rotational axes of neighboring triptycene rotators are 10.3 Å, which is close to twice the radius of the volume of revolution of a triptycene rotator. Only two hydrogen atoms highlighted in cyan are relatively close to each other at a distance of 2.9 Å, which is longer than the sum of their van der Waals radii (2.4 Å). (b) DMF molecules are the only ones making van der Waals contacts with the triptycene rotator in the crystal.

4.3. Solid-State ^{2}H NMR Analysis

The rotational dynamics of triptycene rotators in the pillars were analyzed by solid-state ^{2}H NMR spin echo experiments (SS ^{2}H NMR) using solvent-containing polycrystalline (powder) samples of **UCLA-R1**-d_8, **UCLA-R2**-d_8, and **UCLA-R3**-d_8 with partially deuterated triptycene rotators. Qualitatively, the SS ^{2}H NMR method takes advantage of changes in the line shape of the spectrum resulting from the dynamic modulation of the C–D bond vectors with respect to the direction of the external magnetic field.[12] The lineshape is sensitive to motions ranging from the kilohertz to tens of megahertz (ca. 10^3–10^7 Hz). Samples with groups bearing solely static C–D bonds are characterized by a very broad symmetric spectrum with two shoulders and two peaks,

known as a Pake, or powder pattern, which extends for *ca*. 260 kHz. Similarly, C–D bond vectors aligned with the rotational axis (cone angle 0°) do not change their orientation with the external field as a function of rotation and give raise to the same Pake pattern, as shown by the purple spectra assigned to the α-deuterons in Figure 4.4b. By contrast, the C–D vector of the β-deuterons (shown in red in Figure 4.4a) makes a 60° degree angle with the rotational axis and changes its orientation with respect to the external magnetic field. With this difference in mind, we were able to simulate the experimental spectra by assuming that the triptycene rotator undergoes a degenerate 3-fold rotation about the alkyne axis, and that the overall spectrum is a weighted sum of two profiles.[13] As shown by spectral simulations in Figure 4.4b, when the simulated frequency of rotation is low (10 kHz), the β-deuteron spectrum is almost identical to the static pattern; however, its relative intensity is lower than that of α-deuterons because of a reduction factor of 0.17, reflecting a frequency-dependent echo-damping effect in two-pulse solid echo experiments.[14] As the rotation gets faster (500 kHz), the spectrum of the β-deuterons features a set of peaks at the center of the spectrum. Because of a smaller reduction factor (0.05), the central peaks only account for a small fraction of the overall simulated spectrum. Lastly, when the simulated rate of rotation reaches 10 MHz, the central peaks coalesce into two peaks separated by about 13 kHz. With a relatively large reduction factor of 0.68 and narrow spectrum width, the central peaks become the most dominant feature of the overall spectrum.

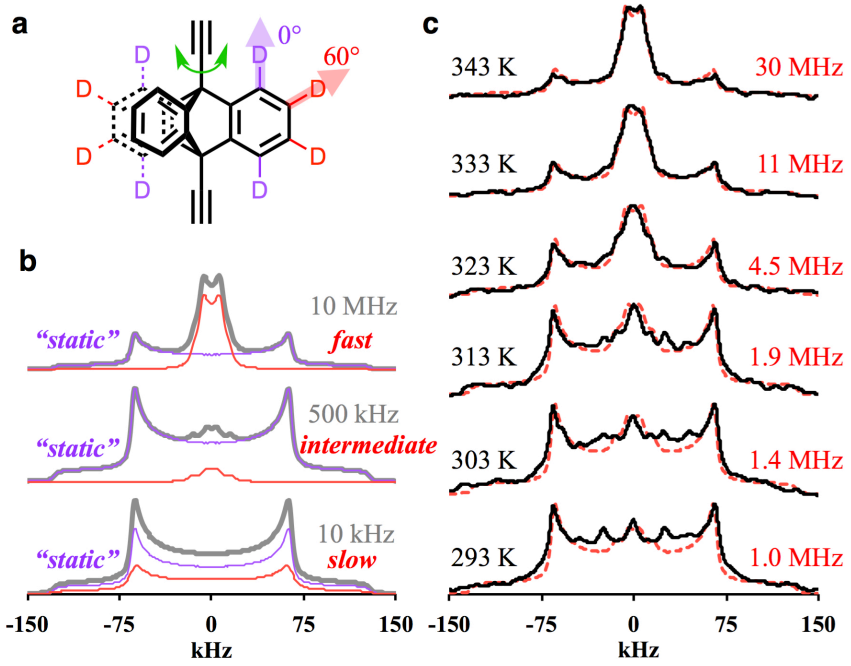

Figure 4.4. (a) Chemical structure of the partially deuterated triptycene rotator highlighting α- and β-deuteriums. (b) Simulated ^{2}H NMR spectra (shown in grey) with various rotational frequencies are composed of spectra reflecting "static" α-deuteriums (purple) and dynamic β-deuteriums (red). (c) Experimental (black solid curves) and simulated (red dashed curves) ^{2}H NMR spectra of **UCLA-R3**-d_8.

Both samples of **UCLA-R1**-d_8 and **UCLA-R2**-d_8 showed spectra with line-shape of static rotators at 303 K, and the spectra remained the same when the samples were heated to 373 K, which was close to the upper limit of temperature we could apply before significant solvent evaporation and decomposition (Figure A.4.8). These results indicated that the triptycene groups of **UCLA-R1**-d_8 and **UCLA-R2**-d_8 are static, as suggested by their crystal structures. The solvated sample of **UCLA-R3**-d_8, to our delight, displayed a spectrum with some features at the center at 293 K (Figure 4.4c). As the sample was gradually heated to 343 K, the intensity of the central peaks increased while the intensity of the side peaks decreased. The observed spectra could be reproduced with the simple 3-

fold site exchange model previously discussed. The rate of exchange at 293, 303, 313, 323, 333, and 343 K were estimated to be 1.0, 1.4, 1.9, 4.5, 11, and 30 MHz, with the latter being an estimate, as indicated by the large error bar in Figure 4.5.

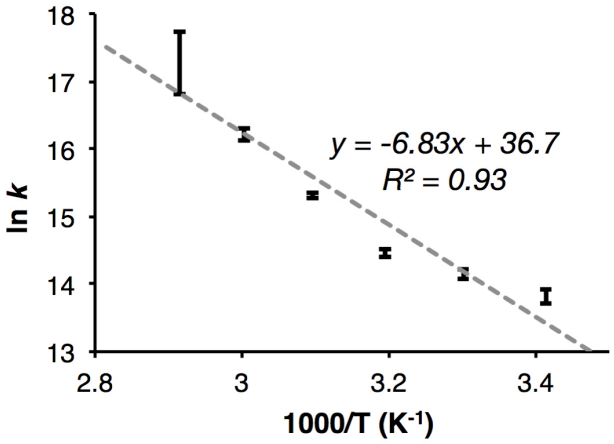

Figure 4.5. An Arrhenius plot shown by the dashed line highlighting the large deviation of the data points from the expected linearity. The value of the intercept from the linear fitting would be too large to be correctly interpreted as an elementary process associated with an attempt frequency.

An Arrhenius plot of the variable temperature data shown in Figure 4.5 is strongly non-linear with an upward curvature in the range of temperatures explored in our experiments. The best linear fit suggests an activation energy of ca. 13.5 kcal/mol and a pre-exponential factor of 8.7×10^{15} s^{-1}. Considering the large deviation from linearity and the fact that the expected pre-exponential factor for a triptycene rotator should be ca. 4 orders of magnitude smaller (*ca*. 5×10^{11} s^{-1}),[15] one would come to the conclusion that the temperature-dependence of the rotational frequency does not reflect an energy potential from permanent structural features in the crystal.[6a,16] Knowing that gas phase rotation of the triptycene rotator about the two triple bond axle should be essentially

free,[17] hindrance must arise from interactions between triptycene and the solvent molecules in the crystal. Interestingly, spin-lattice relaxation studies carried out at ambient temperature in liquid $CHCl_3$ have shown that the correlation time for the rotation of triptycene about its 3-fold axis (50 ps) is about three times longer than the one for rotation about the perpendicular 2-fold axes (16 ps), despite the fact that their moments of inertia are in opposite order.[18] This suggests that solvent molecules fill the space between the three blades and slow down the rotation along the 3-fold axis, which is also suggested by the solid-state structural features shown in Figure 4.3b. Assuming that hydrodynamic theory can describe the behavior of a pinned molecular rotor in a strictly confined liquid, using a calculated molecular volume for triptycene of $V_{mol} = 2.3 \times 10^{-28}$ m^3, and considering that it has a rotational correlation time of ca. $\tau_{rot} = 714$ ns at 303 K (from $\tau_{rot} = 1/ k_{rot} = 1/ 1.4 \times 10^6$ s^{-1}, Figure 4.4), we can estimate the dynamic viscosity η of the MOF-confined DMF to be,

$$\eta_{MOF\text{-}DMF} = \tau_{rot}\, k_B T / V_{mol} = 13.3 \text{ N·s/m}^2 \text{ (or, Pa·s)},$$

which is similar to that of honey, and about 4 orders of magnitude greater than the dynamic viscosity of bulk DMF at the same temperature, $\eta_{Liq\text{-}DMF} = 8.2 \times 10^{-4}$ N·s/m^2.[19]

A diffusion-controlled mechanism implies that the large activation energy and pre-exponential factor in the case of **UCLA-R3** reflect changes in the viscosity of the local environment as a function of temperature where the effect of solvent confinement is manifested in terms of an apparent activation energy that changes from 1.79 kcal/mol in the bulk liquid[19] to 13.5 kcal/mol in the MOF cavity.[20]

4.4. Conclusions

We have shown that a simple modular approach leads to the successful preparation of a homologous set of paddle-wheel amphidynamic metal organic frameworks with a relatively large 9,10-*bis*(pyridylethtnyl)triptycene acting as a pillar and molecular rotor, complemented by dicarboxylate linkers of varying lengths and steric bulk. Single crystals obtained from DMF by changing the linker from terephthalate (**UCLA-R1**), biphenyl-4,4′-dicarboxylate (**UCLA-R2**), and triptycene-9,10-dicarboxylate (**UCLA-R3**) display 2-fold, 4-fold, and no catenation, respectively, reflecting the amount of space available in their corresponding frames. While the two catenated structures display a tight packing environment with inter-lattice contacts, the noncatenated crystals of **UCLA-R3** have no contacts between pillars and linkers in lattice. Rotation by a Brownian three-fold jumping mechanism was determined by line shape analysis of solid-state ^{2}H NMR data obtained with tritptycene-d_8 labeled samples. Having a barrierless alkyne linkage and no steric interaction, it was shown that the rotation of the triptycene group in **UCLA-R3** is determined by interactions with the confined DMF molecules in the lattice. Assuming a hydrodynamic model one can estimate the viscosity of MOF-confined DMF to be about four orders of magnitude greater than the one in the liquid. An abnormal temperature dependence of the rotational motion with very high apparent activation energy and pre-exponential factor is interpreted in terms of viscosity changes, suggesting an opportunity to analyze the dynamics of fluids under tight confinement. The results reported here prove the robust nature of molecular and crystal design and reveal new strategies to control the dynamics of crystalline rotators.

4.5. Experimental

4.5.1. General Methods

Unless otherwise notified all commercially available compounds were used as received without further purification. 9,10-Diethynyltriptycene **1S** [21], 9,10-diethynyltriptycene-d_8 **1S**-d_8 [8], and triptycene-9,10-dicarboxylic acid[22] were prepared as reported in the literature. Thin-layer chromatography (TLC) plates pre-coated with silica gel 60 F_{254} were purchased and they were visualized using a UV lamp. Flash column chromatography was performed using silica gel (230–400 mesh) as the stationary phase. Anhydrous tetrahydrofuran (THF) was distilled from sodium-benzophenone in a continuous still under an atmosphere of argon. Melting points of solids were measured without calibration of the apparatus. ^{1}H NMR and ^{13}C NMR spectra in solution were recorded at 500 MHz and 125 MHz, respectively. Chemical shifts are reported in ppm and the (residual) solvent signals of $CDCl_3$ (^{1}H NMR: δ 7.26 ppm; ^{13}C NMR: δ 77.0 ppm) were used as reference. Multiplicities of the peaks are reported as singlet (s), doublet (d), triplet (t), or multiplet (m). The coupling constants J are reported in Hz. Infrared spectra (IR) were recorded with a HATR-FTIR instrument. High-resolution mass spectra were acquired using ESI/APCI ionization methods and the signal was detected with a TOF detector. Reported yield for MOF synthesis is based on the weight of the sample after partial solvent removal and is thus only an estimation of the real yield.

4.5.2. Synthesis and Characterization

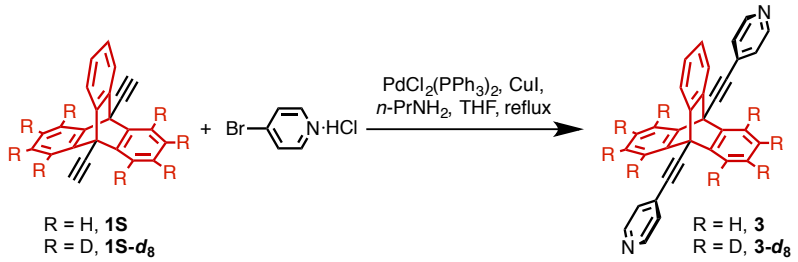

To a 100 mL 2-neck flask equipped with stir bar and condenser were added 9,10-diethynyltriptycene **1S** (135 mg, 0.446 mmol), 4-bromopyridine hydrochloride (260 mg, 1.34 mmol), propylamine (10 mL), and anhydrous THF (10 mL) under Argon. The resulting mixture was degased for 20 min before catalysts palladium bis(triphenylphosphine) dichloride (28 mg, 0.040 mmol) and copper iodide (7.6 mg, 0.040 mmol) were added into the flask. The reaction mixture was degased for another 5 min and refluxed for 6 hours before it was allowed to cool down to room temperature. Saturated NH_4Cl solution (50 mL) was added into the flask, and the mixture was extracted with DCM (30 mL) twice. The combined organic layers were then washed with brine and dried over anhydrous Na_2SO_4. The solvent was removed *in vacuo* and the residue was purified by flash column chromatography (dry loading) using 1 % MeOH solution in DCM as eluent to provide the desired compound **3** (201 mg, 99 %). **3**-d_8 was prepared from **1S**-d_8 with the same procedures for ligand **3**.

3: White solid, m.p. > 240 °C (dec); ^{1}H NMR (500 MHz, $CDCl_3$, ppm): δ 7.16 (dd, J = 5.5, 3.2 Hz, 6H), 7.69–7.73 (m, 4H), 7.79 (dd, J = 5.5, 3.2 Hz, 6H), 8.77 (d, J = 5.0 Hz, 4H); ^{13}C NMR (125 MHz, $CDCl_3$, ppm): δ 52.8, 88.5, 90.5, 122.3, 126.1, 126.2, 131.0, 142.9, 149.9; IR (powder, cm^{-1}): ν 638(s), 751(s), 820(s), 875(w), 948(w), 989(w), 1030(w), 1067(w), 1178(w), 1217(m), 1323(w), 1407(m), 1454(m), 1489(w), 1540(w),

1591(s), 2244(w), 3070(w); HRMS (ESI/APCI, TOF): m/z calculated for $C_{34}H_{21}N_2$ (MH^+): 457.1699, found: 457.1707.

3-d_8: White solid, m.p. > 240 °C (dec); ^{1}H NMR (500 MHz, $CDCl_3$, ppm): δ 7.16 (dd, J = 5.5, 3.2 Hz, 2H), 7.68–7.73 (m, 4H), 7.80 (dd, J = 5.5, 3.2 Hz, 2H), 8.77 (d, J = 5.1 Hz, 4H); ^{13}C NMR (125 MHz, $CDCl_3$, ppm): δ 52.7, 88.4, 90.4, 121.9 (t, J = 23.3 Hz), 122.3, 125.5 (t, J = 23.5 Hz), 126.1, 126.2, 130.9, 142.9, 142.9, 150.0; IR (powder, cm^{-1}): ν 620(m), 747(s), 809(m), 820(s), 881(w), 992(w), 1050(w), 1067(w), 1182(w), 1217(m), 1291(w), 1361(m), 1393(w), 1407(m), 1455(w), 1490(w), 1540(w), 1591(s), 2243(w), 2276(w), 3042(w); HRMS (ESI/APCI, TOF): m/z calculated for $C_{34}H_{21}N_2$ (MH^+): 465.2201, found: 465.2211.

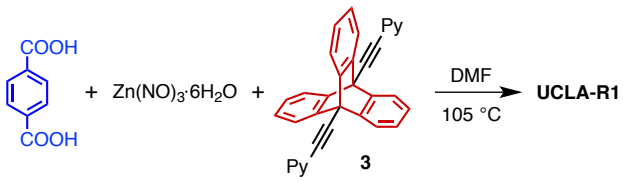

To a vial were added terephthalic acid (16.6 mg, 0.10 mmol), zinc nitrate hexahydrate (29.8 mg, 0.10 mmol), ligand **3** (22.8 mg, 0.050 mmol), and anhydrous DMF (2 mL). The vial was sealed and heated to 105 °C in an oven overnight before it was allowed to cool back to room temperature. The solution was decanted and the crystals at the bottom of the vial were washed with anhydrous DMF twice. The crystals would lose solvent and undergo an irreversible phase transition when exposed to air at ambient temperature. As a result, the crystal structure was determined by diffraction of a single crystal at 100 K immediately after it was picked up from the solvent. The yield (46.1 mg, 84 %) of the synthesis could only be estimated by removing the surface solvent in

vacuum and weighing the partially desolvated sample. **UCLA-R1**-d_8 was prepared using ligand **3**-d_8 in the same manner.

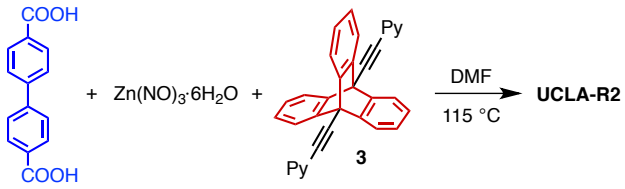

To a vial were added biphenyl-4,4'-dicarboxylic acid (24.2 mg, 0.10 mmol), zinc nitrate hexahydrate (29.8 mg, 0.10 mmol), ligand **3** (22.8 mg, 0.050 mmol), and anhydrous DMF (2 mL). The vial was sealed and heated to 115 °C in an oven overnight before it was allowed to cool back to room temperature. The brownish solution was decanted and the crystals obtained were washed with fresh anhydrous DMF twice. The crystals would lose solvent and undergo an irreversible phase transition when exposed to air at ambient temperature. As a result, the diffraction data was collected immediately at 100 K after it was picked up from the solvent and mounted on the diffractometer. The yield (55.3 mg, 94 %) of the synthesis could only be estimated by removing the surface solvent in vacuum and weighing the partially desolvated sample. **UCLA-R2**-d_8 was prepared using ligand **3**-d_8 in the same manner.

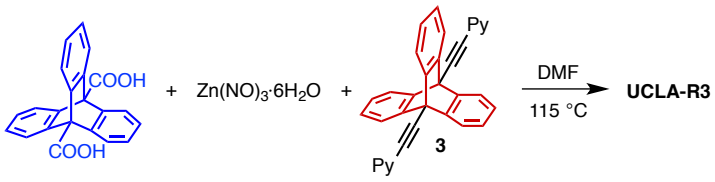

To a vial were added triptycene-9,10-dicarboxylic acid (34.2 mg, 0.10 mmol), zinc nitrate hexahydrate (29.8 mg, 0.10 mmol), ligand **3** (22.8 mg, 0.050 mmol), and

anhydrous DMF (2 mL). The vial was capped and heated to 115 °C in an oven overnight before it was allowed to cool back to room temperature. The solution was decanted and the crystals at the bottom of the vial were washed with fresh anhydrous DMF twice. The crystals would lose solvent and undergo an irreversible phase transition when exposed to air at ambient temperature. As a result, the crystal structure was determined by diffraction of a single crystal at 100 K immediately after it was picked up from the solvent. The yield (86.7 mg, 87 %) of the synthesis could only be estimated by removing the surface solvent in vacuum and weighing the partially desolvated sample. **UCLA-R3**-d_8 was prepared using ligand **3**-d_8 in the same manner.

4.5.3 Single Crystal X-Ray Diffraction

For structural determination, a colorless prism was picked out from the mother liquor and mounted on the diffractometer immediately for data collection. The diffractometer was equipped with Mo-K_α radiation (λ = 0.71073 Å) and an area detector. Diffraction was collected at 100 K and the structures were solved and refined with the SHELXTL program. All heavy atoms were refined anisotropically while the hydrogen atoms were placed at the calculated positions.

4.5.4 Powder X-Ray Diffraction Analysis of Bulk Samples

The PXRD analyses were carried out with Cu-$K_{\alpha1}$ radiation (1.5406 Å) and samples were placed on a zero-background plate at a fixed stage with a drop of DMF to prevent undesired solvent loss and phase transition. Data was collected from 5 to 50

degrees at room temperature. The step width was 0.016 degree with acquisition time being approximately 10 s each step.

4.5.5 Solid-State ^{2}H NMR Spin-Echo Experiments

The solid-state ^{2}H NMR (SS ^{2}H NMR) spin-echo experiments in this work were performed on a Bruker DRX300 instrument at 46.07 MHz (deuterium resonance frequency) with a 4 mm wide-line probe and 90-degree pulse of 2.5 μs. To suppress the undesired artifacts, a quadrupolar-echo sequence with phase recycling was used. An echo delay of 50 μs was used after the refocusing delay of 42 μs, and the recycle delay between pulses was 20 s. In the experiment, about 50 mg of sample was placed in a short borosilicate glass NMR tube with an excess of solvent to prevent the undesired phase transition. Approximately 400 scans were acquired for the crystalline samples, and more than 2000 scans were necessary to achieve reasonable a reasonable signal-to-noise ratio for the samples after solvent removal. All spectra in this work were obtained using a line broadening of 5 kHz in data processing. For variable temperature experiments, the spectrum was obtained again after the sample cooled down to the starting temperature (293 or 303 K) to make sure no irreversible phase transition happened during the experiment.

SS ^{2}H NMR spectra were also obtained for the **UCLA-R3**-d_8 after solvent removal by heating the sample to 110 ˚C for one hour under vacuum. In the experiment, the sample was heated gradually from 303 K all the way to 443 K before it was cooled down to 383 K and eventually back to 303 K. A noticeable abnormity was observed during the variable temperature experiments, suggesting phase transitions possibly due to

the lack of a stable solvent-free state for **UCLA-R3**-d_8. As shown in Figure A.4.9, the spectrum obtained at 383 K was almost identical to the one obtained 423K. Consequently, the obtained spectra were documented without further analysis.

To obtain information about the dynamics of solvent molecules trapped in MOF **UCLA-R3**, SS ^{2}H NMR spectra of a sample of the natural abundance framework and deuterated solvent DMF-*d* were also obtained and analyzed. We chose to work with DMF-*d* with partial deuteration instead of fully deuterated DMF-d_7 since it is known that methyl groups would undergo fast dynamics even in closely packed crystals because of their globular shape. Since it is necessary to have an excess of solvent to prevent phase transitions, the isotropic peak corresponding to free solvent molecules dominated the spectrum and made it difficult to draw any direct conclusion on the solvent dynamics. But it was clear that, other than the isotropic peak, the obtained spectra featured a temperature-dependent second component (Figure A.4.10). Attempts to subtract the isotropic component led, with low level of confidence, to spectra corresponding to the motion of trapped DMF-*d* molecules. The broadening of these spectra is in agreement with the slower solvent and triptycene rotator dynamics at lower temperatures.

4.6. Appendix

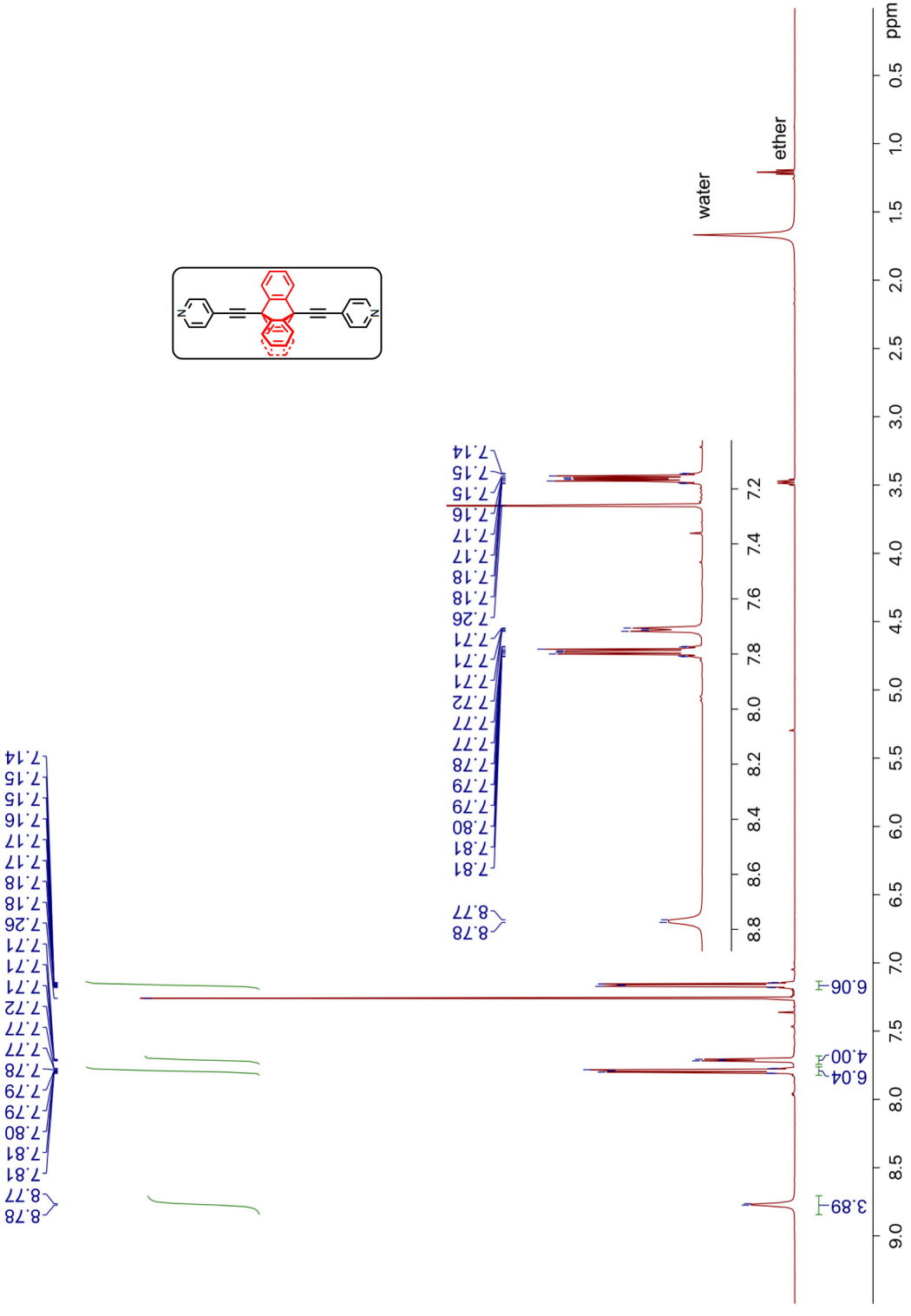

Figure A.4.1. ^{1}H NMR spectra of compound **3** at 500 MHz in $CDCl_3$.

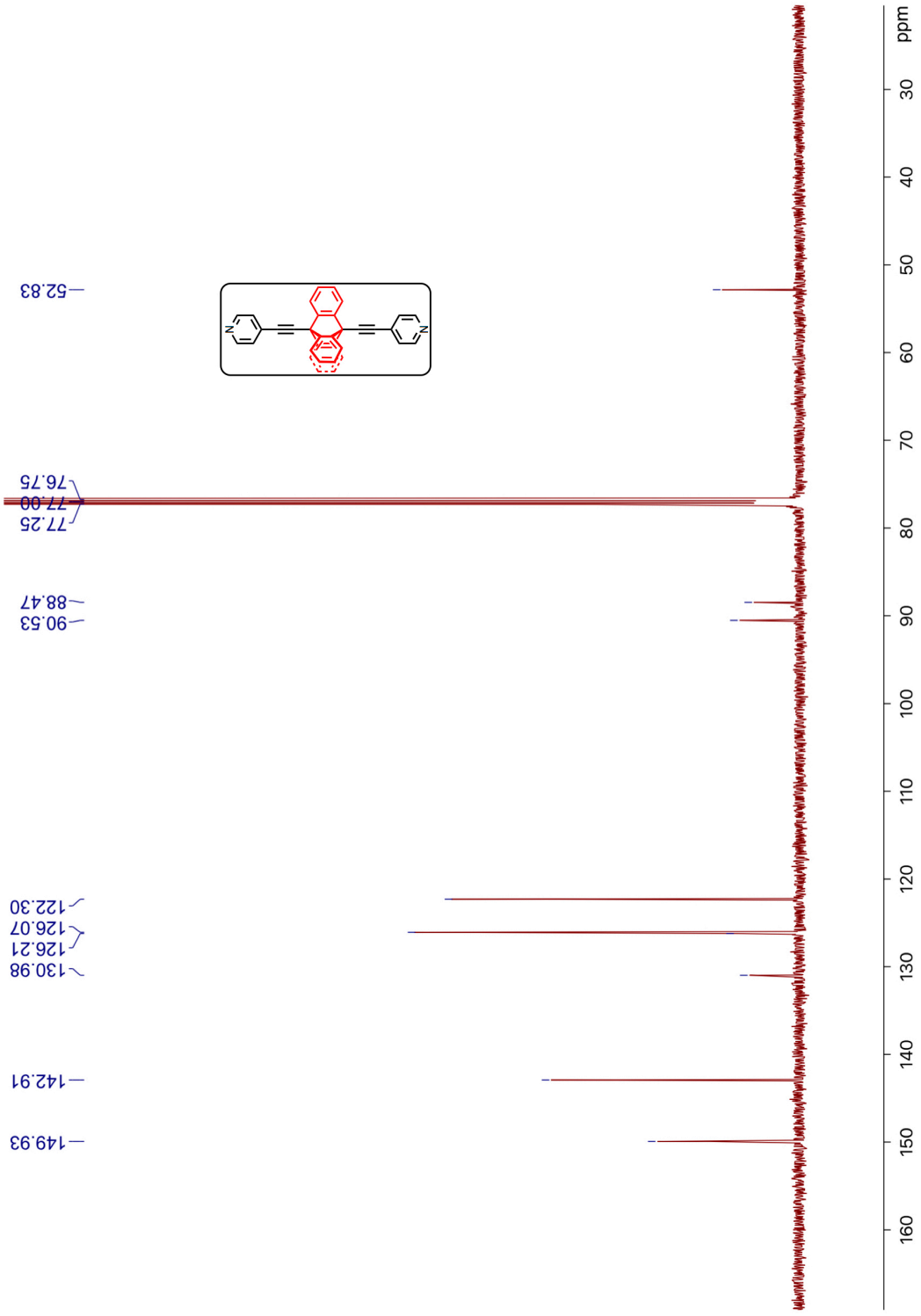

Figure A.4.2. ^{13}C NMR spectra of compound **3** at 125 MHz in $CDCl_3$.

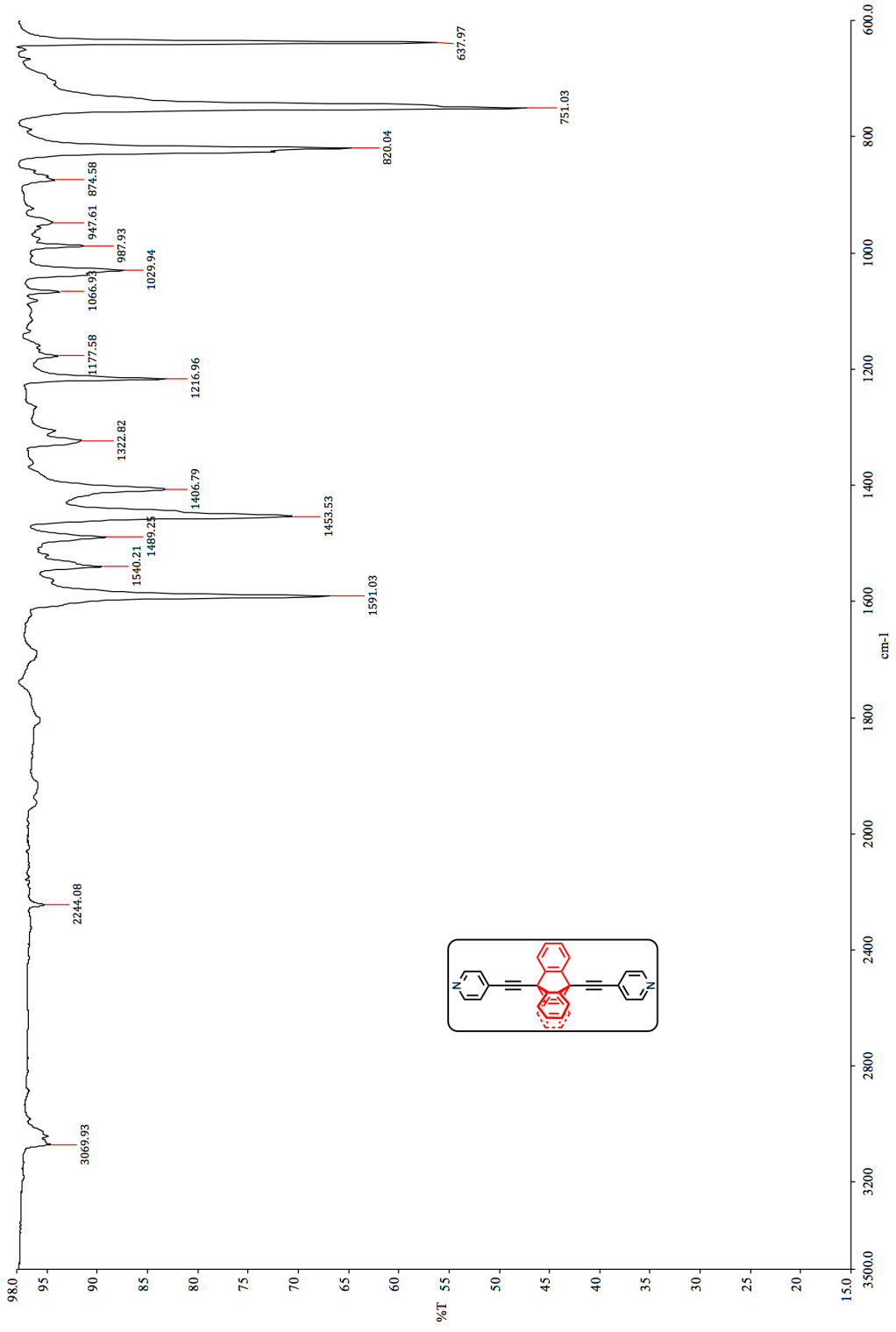

Figure A.4.3. IR of compound **3**.

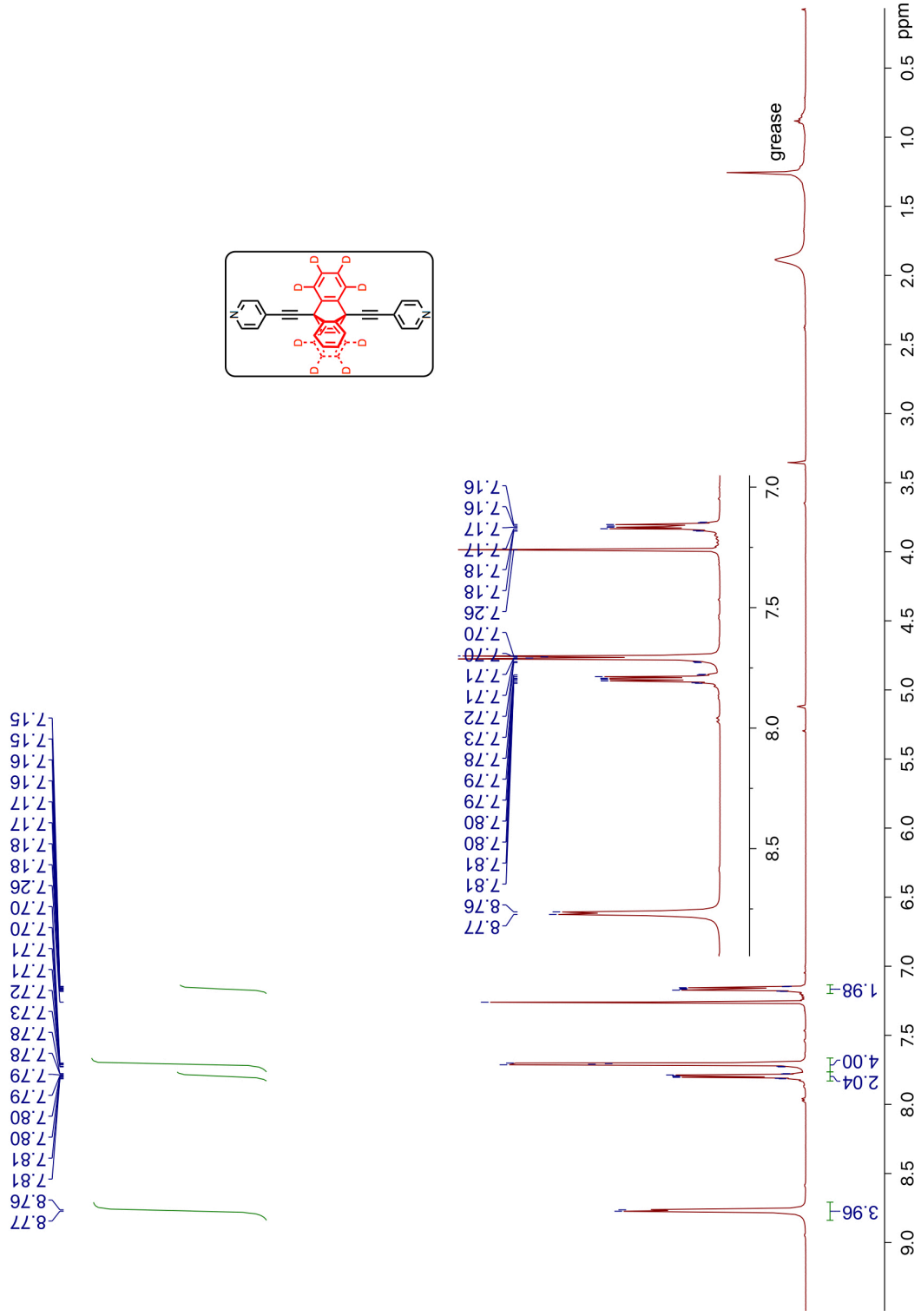

Figure A.4.4. ^{1}H NMR spectra of compound **3**-d_8 at 500 MHz in $CDCl_3$.

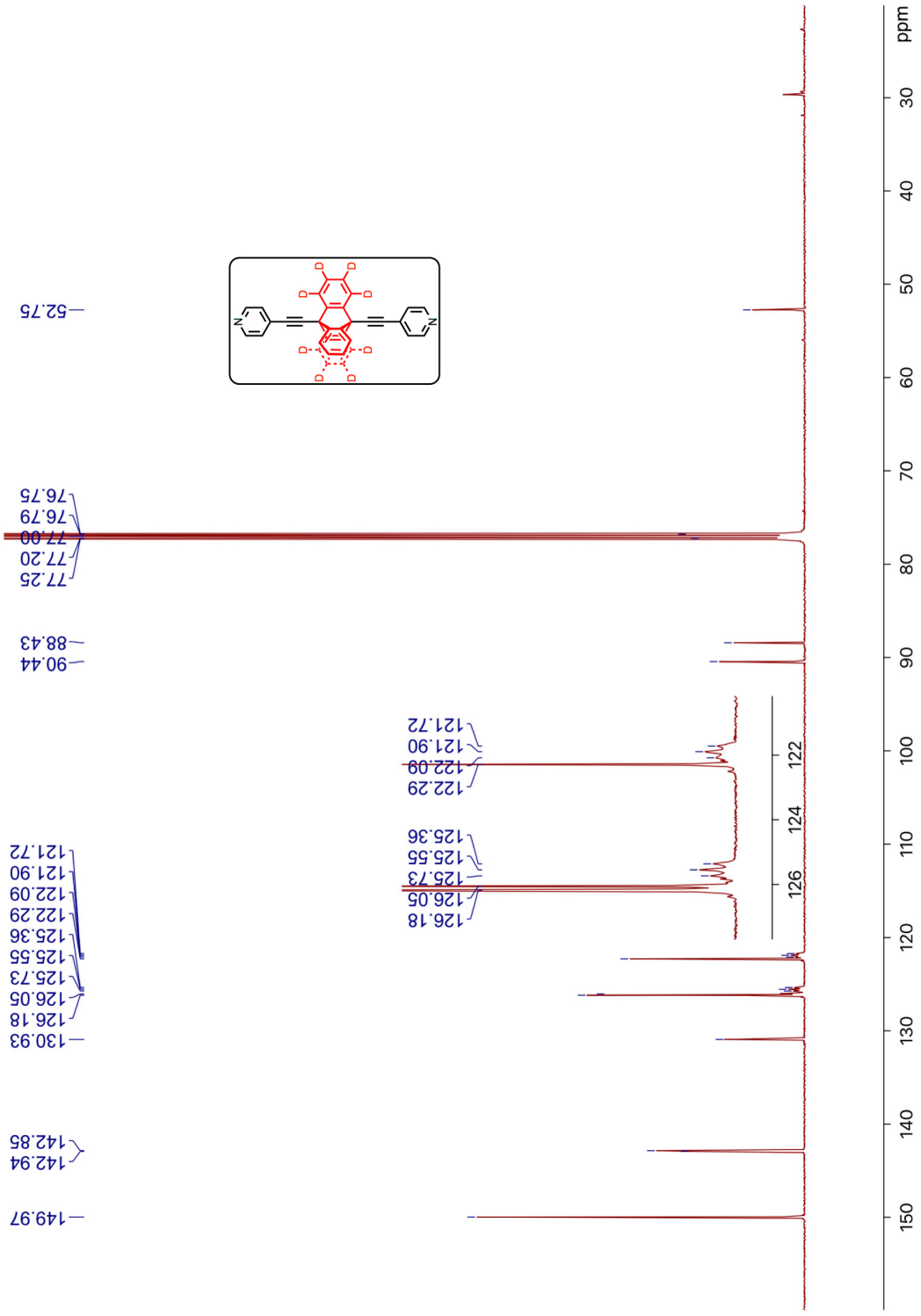

Figure A.4.5. ^{13}C NMR spectra of compound **3**-d_8 at 125 MHz in $CDCl_3$.

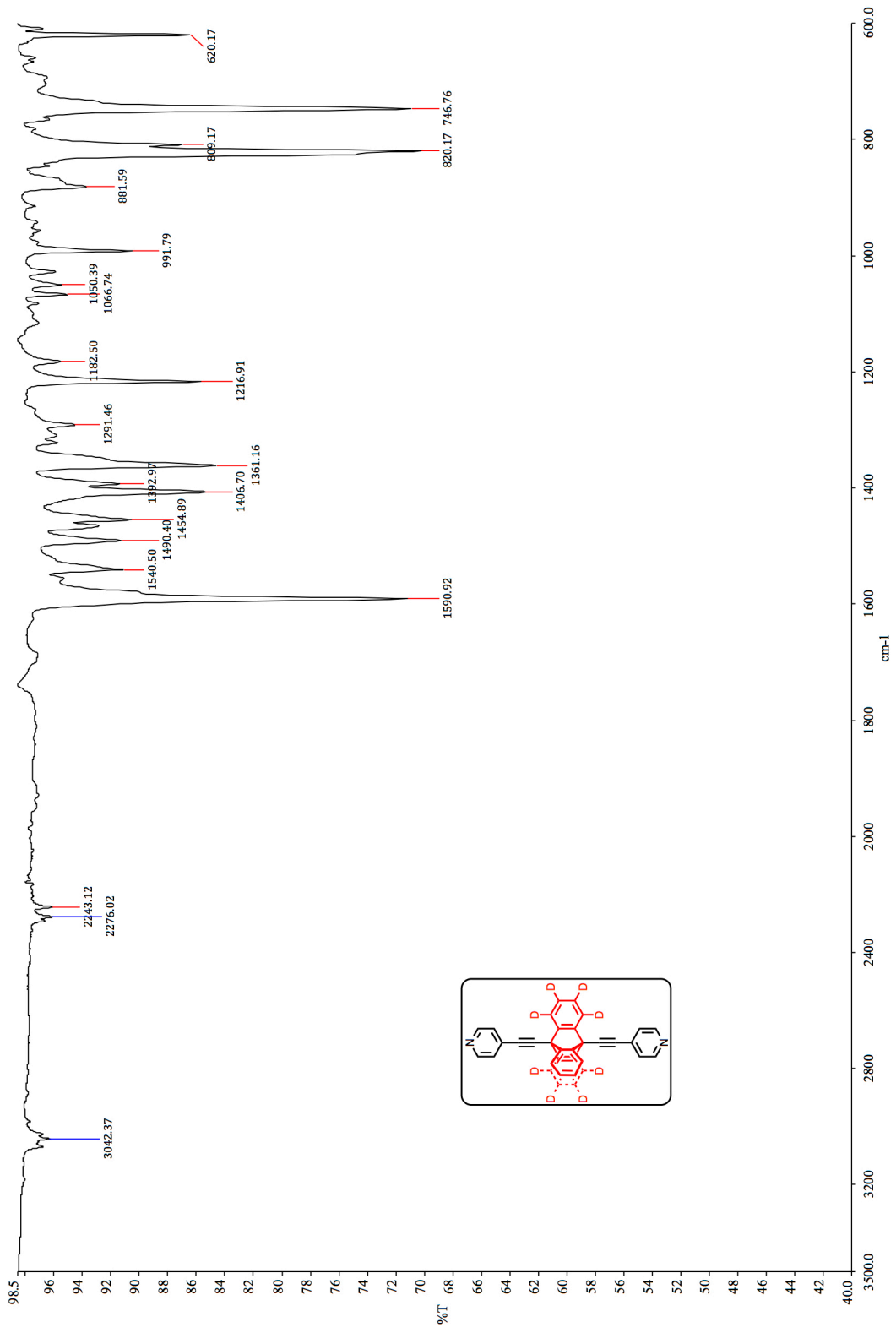

Figure A.4.6. IR of compound **3**-d_8.

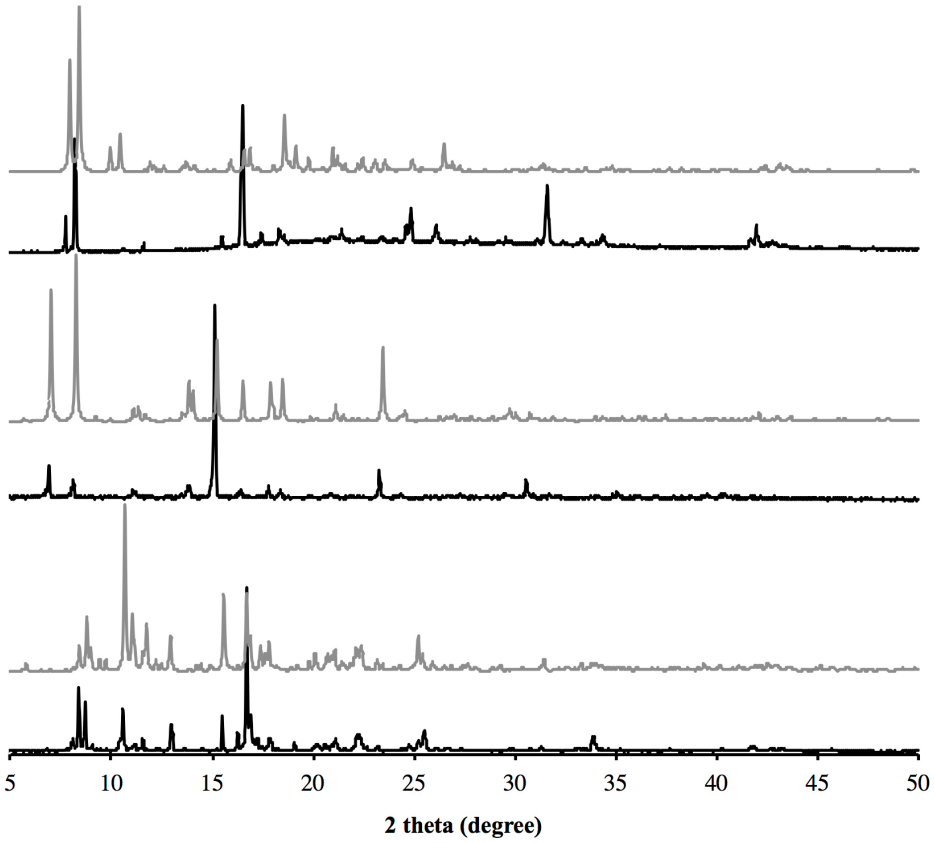

Figure A.4.7. Experimental (shown in black) and calculated (shown in grey) PXRD patterns of **UCLA-R1** (lower), **UCLA-R2** (middle), and **UCLA-R3** (upper).

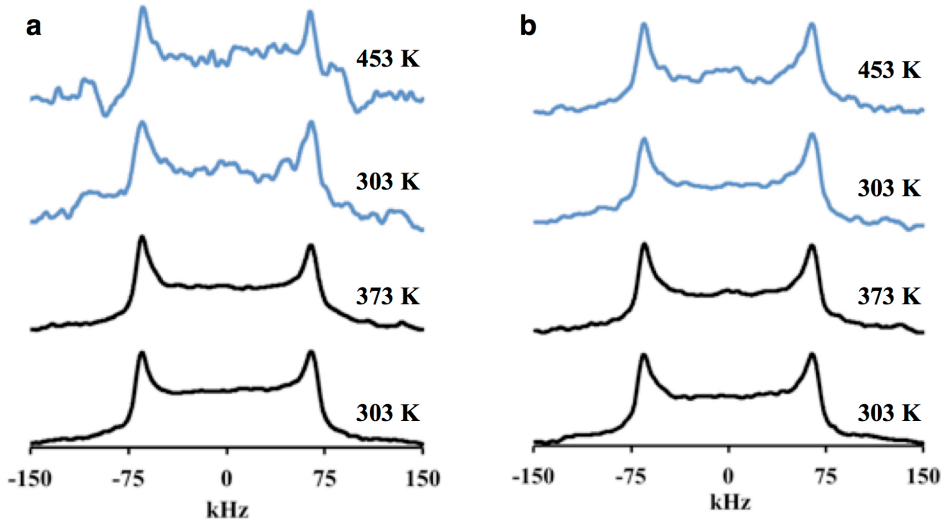

Figure A.4.8. SS ^{2}H NMR Spectra of (a) **UCLA-R1**-d_8 and (b) **UCLA-R2**-d_8 before (shown in black) and after (shown in blue) solvent removal.

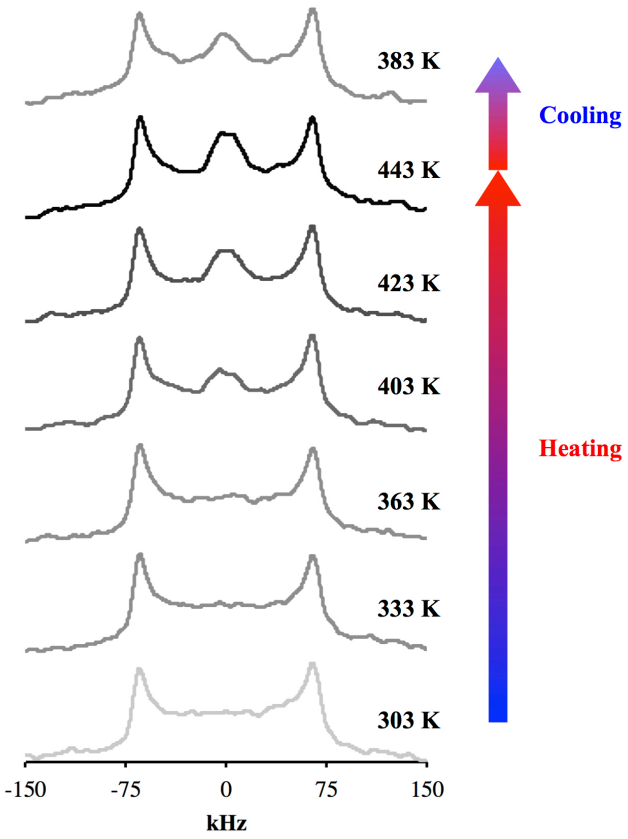

Figure A.4.9. SS ^{2}H NMR spectra of a desolvated sample of **UCLA-R3**-d_8. As indicated, the sample was gradually heated up to 443 K and then cooled to 383 K.

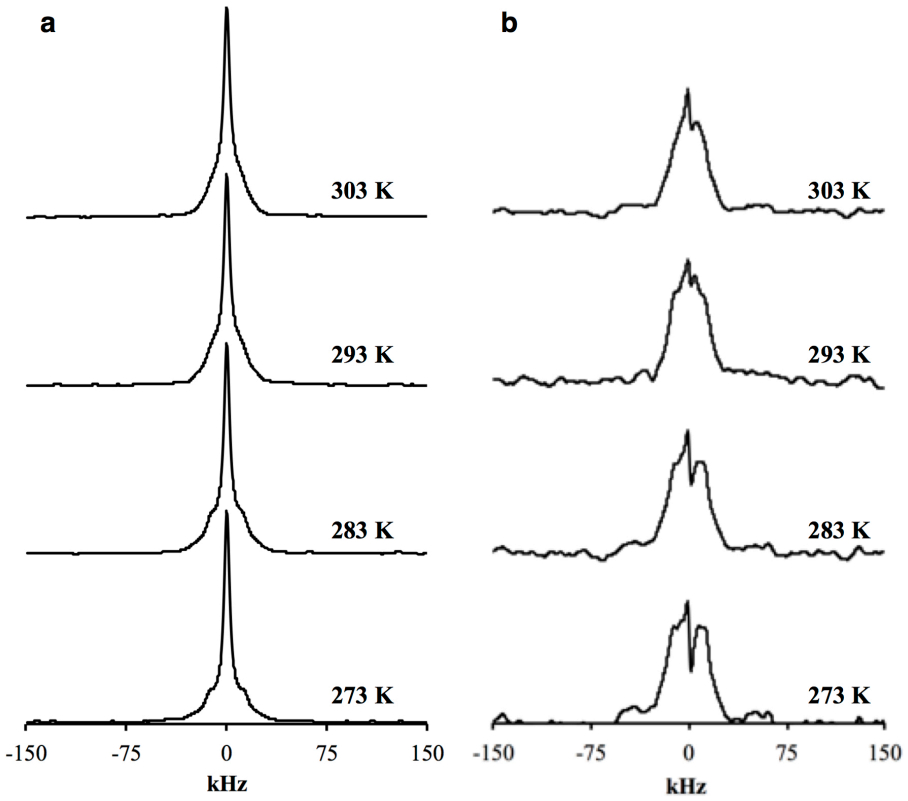

Figure A.4.10. (a) VT SS ^{2}H NMR spectra of a sample of MOF **UCLA-R3** and DMF-*d* showing an isotropic component and a second component which broadened at lower temperatures. Subtracting the isotropic component revealed (b) the shape of the second component.

Table A.4.1. Summary of crystal structure data of **UCLA R1–3**.

Frameworks	**UCLA-R1**	**UCLA-R2**	**UCLA-R3**
molecular formula	$[Zn_2(pdc)_2(\mathbf{3})]_2(DMF)_5$	$[Zn_2(bpdc)_2(\mathbf{3})]_2(DMF)_3$	$[Zn_2(tdc)_2(\mathbf{3})]_{0.5}(DMF)_5$
	$C_{115}H_{88}N_9O_{21}Zn_4$	$C_{133}H_{93}N_7O_{19}Zn_4$	$C_{54}H_{57}N_6O_9Zn$
crystal system	triclinic	monoclinic	monoclinic
space group	P-1	P 2_1/c	C 2/c
a/Å	13.798	15.639	44.263
b/Å	16.605	21.426	15.016
c/Å	24.133	15.998	14.974
α/(°)	106.906	90	90
β/(°)	99.469	94.589	94.012
γ/(°)	90.184	90	90
V/Å^3	5210.6	5343.5	9927.4
Z	2	2	8
Z'	0	0	0
ϱ_{calcd}/(g·cm^{-3})	1.398	1.463	1.350
μ/(mm^{-1})	0.986	0.965	0.560
reflections measured	65235	68154	63422
independent reflections (R_{int})	24492 (0.0309)	13150 (0.0386)	12613 (0.0842)
T_{max}/T_{min}	0.74/0.62	0.74/0.70	0.97/0.96
restraint/para-meters	415/1499	8/732	206/662
GOF	0.977	1.094	1.033
R_1, wR_2 [$F^2 > 2\sigma(F^2)$]	0.0485, 0.1163	0.0470, 0.1086	0.0790, 0.1974
R_1, wR_2 (all data)	0.0721, 0. 1280	0.0658, 0.1148	0.1390, 0.2278
$\Delta\varrho_{max}$/(e·Å^{-3})	1.228	1.586	2.702
$\Delta\varrho_{min}$/(e·Å^{-3})	-0.778	-0.785	-1.025
T/K	100	100	100

4.7. References

1. (a) Abendroth, J. M.; Bushuyev, O. S.; Weiss, P. S.; Barrett, C. J. *ACS Nano* **2015**, *9*, 7746. (b) Erbas-Cakmak, S.; Leigh, D. A.; McTernan, C. T.; Nussbaumer, A. L. *Chem. Rev.* **2015**, *115*, 10081. (c) Coskun, A.; Banaszak, M.; Astumian, R. D.; Stoddart, J. F.; Grzybowski, B. A. *Chem. Soc. Rev.* **2012**, *41*, 19.

2. (a) Cheng, C.; McGonigal, P. R.; Schneebeli, S. T.; Li, H.; Vermeulen, N. A.; Ke, C.; Stoddart, J. F. *Nat. Nanotechnol.* **2015**, *10*, 547. (b) Li, Q.; Fuks, G.; Moulin, E.; Maaloum, M.; Rawiso, M.; Kulic, I.; Foy, J. T.; Giuseppone, N. *Nat. Nanotechnol.* **2015**, *10*, 161. (c) Velema, W. A.; van der Berg, J. P.; Hansen, M. J.; Szymanski, W.; Driessen, A. J. M.; Feringa, B. L. *Nat. Chem.* **2013**, *5*, 924 (d) Lewandowski, B.; De Bo, G.; Ward, J. W.; Papmeyer, M.; Kuschel, S.; Aldegunde, M. J.; Gramlich, P. M. E.; Heckmann, D.; Goldup, S. M.; D'Souza, D. M.; Fernandes, A. E.; Leigh, D. A. *Science* **2013**, *339*, 189. (e) Perera, U. G. E.; Ample, F.; Kersell, H.; Zhang, Y.; Vives, G.; Echeverria, J.; Grisolia, M.; Rapenne, G.; Joachim, C.; Hla, S.-W. *Nat. Nanotechnol.* **2013**, *8*, 46.

3. Iwamura, H.; Mislow, K. *Acc. Chem. Res.* **1988**, *21*, 175.

4. Goodsell, D. S. *The Machinery of Life*.; 2nd ed.; Springer: New York, **2009**.

5. (a) Vogelsberg, C. S.; Garcia-Garibay, M. A. *Chem. Soc. Rev.* **2012**, *41*, 1892. (b) Khuong, T.-A. V.; Nuñez, J. E.; Godinez, C. E.; Garcia-Garibay, M. A. *Acc. Chem. Res.* **2006**, *39*, 413.

6. (a) Jiang, X.; O'brien, Z. J.; Yang, S.; Lai, L. H.; Buenaflor, J.; Tan, C.; Khan, S.; Houk, K. N.; Garcia-Garibay, M. A. *J. Am. Chem. Soc.* **2016**, *138*, 4650. (b) Harada, J.; Ohtani, M.; Takahashi, Y.; Inabe, T. *J. Am. Chem. Soc.* **2015**, *137*, 4477. (c) Setaka, W.; Yamaguchi, K. *J. Am. Chem. Soc.* **2013**, *135*, 14560. (d) Lemouchi, C.; Iliopoulos, K.;

Zorina, L.; Simonov, S.; Wzietek, P.; Cauchy, T.; Rodríguez-Fortea, A.; Canadell, E.; Kaleta, J.; Michl, J.; Gindre, D.; Chrysos, M.; Batail, P. *J. Am. Chem. Soc.* **2013**, *135*, 9366. (e) Akutagawa, T.; Koshinaka, H.; Sato, D.; Takeda, S.; Noro, S.-I.; Takahashi, H.; Kumai, R.; Tokura, Y.; Nakamura, T. *Nat. Mater.* **2009**, *8*, 342. (f) Jarowski, P. D.; Houk, K. N.; Garcia-Garibay, M. A. *J. Am. Chem. Soc.* **2007**, *129*, 3110.

7. Karlen, S. D.; Reyes, H.; Taylor, R. E.; Khan, S. I.; Hawthorne, M. F.; Garcia-Garibay, M. A. *Proc. Natl. Acad. Sci. U. S. A.* **2010**, *107*, 14973.

8. Jiang, X.; Rodríguez-Molina, B.; Nazarian, N.; Garcia-Garibay, M. A. *J. Am. Chem. Soc.* **2014**, *136*, 8871.

9. (a) Inukai, M.; Fukushima, T.; Hijikata, Y.; Ogiwara, N.; Horike, S.; Kitagawa, S. *J. Am. Chem. Soc.* **2015**, *137*, 12183. (b) Zhu, K.; O'Keefe, C. A.; Vukotic, V. N.; Schurko, R. W.; Loeb, S. J. *Nat. Chem.* **2015**, *7*, 514. (c) Murdock, C. R.; McNutt, N. W.; Keffer, D. J.; Jenkins, D. M. *J. Am. Chem. Soc.* **2014**, *136*, 671. (d) Shustova, N. B.; Cozzolino, A. F.; Reineke, S.; Baldo, M.; Dincă, M. *J. Am. Chem. Soc.* **2013**, *135*, 13326. (e) Vukotic, V. N.; Harris, K. J.; Zhu, K.; Schurko, R. W.; Loeb, S. J. *Nat. Chem.* **2012**, *4*, 456. (f) Gould, S. L.; Tranchemontagne, D.; Yaghi, O. M.; Garcia-Garibay, M. A. *J. Am. Chem. Soc.* **2008**, *130*, 3246.

10. (a) Farha, O. K.; Malliakas, C. D.; Kanatzidis, M. G.; Hupp, J. T. *J. Am. Chem. Soc.* **2010**, *132*, 950. (b) Vagin, S. I.; Ott, A. K.; Hoffmann, S. D.; Lanzinger, D.; Rieger, B. *Chem. Eur. J.* **2009**, *15*, 5845. (c) Shekhah, O.; Wang, H.; Paradinas, M.; Ocal, C.; Schüpbach, B.; Terfort, A.; Zacher, D.; Fischer, R. A.; Wöll, C. *Nat. Mater.* **2009**, *8*, 481. (d) Dybtsev, D. N.; Chun, H.; Kim, K. *Angew. Chem., Int. Ed.* **2004**, *43*, 5033.

11. Frantz, D. K.; Linden, A.; Baldridge, K. K.; Siegel, J. S. *J. Am. Chem. Soc.* **2012**, *134*, 1528.

12. Hansen, M. R.; Graf, R.; Spiess, H. W. *Acc. Chem. Res.* **2013**, *46*, 1996.

13. Macho, V.; Brombacher, L.; Spiess, H. W. *Appl. Magn. Reson.* **2001**, *20*, 405.

14. Wittebort, R. J.; Olejniczak, E. T.; Griffin, R. G. *J. Chem. Phys.* **1987**, *86*, 5441.

15. Inertial rotation of triptycene was obatined from a calculated moment of inertia, I = 1838 g mol^{-1}Å^{-1}, as indicated in: Kawski, A. *Crit. Rev. Anal. Chem.* **1993**, *23*, 459.

16. Vogelsberg, C. S.; Bracco, S.; Beretta, M.; Comotti, C.; Sozzani, P.; Garcia-Garibay, M. A. *J. Phys. Chem. B* **2012**, *116*, 1623.

17. Harris, R. K.; Newman, R. H. *Mol. Phys.* **1979**, *38*, 1315.

18. (a) Sipachev, V. A.; Khaikin, L. S.; Grikina, O. E.; Nikitin, V. S.; Traettberg, M. J. *Mol. Struct.* **2000**, *523*, 1. (b) Saebø, S.; Almolöf, J.; Boggs, J. E.; Stark, J. G. *J. Mol. Struct.:THEOCHEM* **1989**, *200*, 361. (c) Abramenkov, A. V.; Almenningen, A.; Cyvin, B. N.; Cyvin, S. J.; Jonvik, T.; Khaikin, L. S.; Rommingin, C.; Vilkov, L. V. *Acta Chem. Scand.* **1988**, *42A*, 674.

19. Bernal-García, J. M.; Guzmán-López, A.; Cabrales-Torre, A.; Estrada-Baltazar, A.; Iglesias-Silva, G. A. *J. Chem. Eng. Data* **2008**, *53*, 1024.

20. It is well known that confined liquids have greatly enhanced viscosities, e.g., Bell, R. C.; Wang, H.; Iedema, M. J.; Cowin, J. P. *J. Am. Chem. Soc.* **2003**, *125*, 5176.

21. Goldsmith, R. H.; Vura-Weis, J.; Scott, A. M.; Borkar, S.; Sen, A.; Ratner, M. A.; Wasielewski, M. R. *J. Am. Chem. Soc.* **2008**, *130*, 7659.

22. Klanderman, B. H.; Faber, J. W. H. *J. Polym. Sci., Part A1* **1968**, *6*, 2955.